FLUORESCENCE PROBING OF COMPLEX SOLVENT ENVIRONMENTS: POLYMERIC NANOCARRIER AGGREGATES AND RILPIVIRINE

BY KAREN ELIZABETH STEEGE

A dissertation submitted to the

Graduate School—New Brunswick

Rutgers, The State University of New Jersey

in partial fulfillment of the requirements

for the degree of

Doctor of Philosophy

Graduate Program in Chemistry and Chemical Biology

written under the direction of

Edward W. Castner Jr.

and approved by

_____

_____

_____

_____

New Brunswick, New Jersey

May, 2008

ABSTRACT OF THE DISSERTATION

Fluorescence Probing of Complex Solvent Environments: Polymeric Nanocarrier Aggregates and Rilpivirine

by Karen Elizabeth Steege

Dissertation Director: Edward W. Castner Jr.

The local environment of a drug molecule in polymeric drug nanocarrier solutions impacts the bioavailability of the drug and its ability to reach its target in the biological system. The local environment and aggregation properties of small, hydrophobic molecules in aqueous polymeric micelles and nanocarrier aggregates are explored using fluorescence spectroscopy for the purpose of characterizing drug delivery formulations on molecular length scales. The fluorescence properties of seven coumarin dyes in A-B-A triblock copolymer unimer, micelle, and gel solutions respond to changes in local solvent environment. The A-B-A copolymer is used as a model for the encapsulation properties of three novel amphiphilic polymers designed for hydrophobic drug delivery. Rilpivirine, a novel HIV inhibitor shows solvatochromic fluorescence spectral response due to a large charge transfer between the ground and electronic excited states. The fluorescence of rilpivirine in A-B-A triblock copolymer is investigated as a method to differentiate between the aggregated and unimer forms of the solubilized drug.

Acknowledgements

I would like to acknowledge the support of a wonderful group of scientists, coworkers, friends, and family. Thank you to Professor Ed Castner whose discussions on science and life I have enjoyed greatly. Thank you for being my teacher. Also, thanks to the faculty, staff and students of the Rutgers Department of Chemistry and Chemical Biology, especially my esteemed Ph.D. committee whom I respect and regard as a great contingent of scientists and minds. Thank you to Dr. Anthony, Prof. Moghe, and the IGERT program. I am grateful for the opportunity to interact with and learn from an exceptional group of leaders. To my family who has always supported me and believed I could do anything I aspired to do. Thank you to my Nejeda family, whose support I am eternally lucky to have throughout life. To Erin and Alycia, I have great admiration for the strength in both of you, especially during these past few years. We will continue to live 'hardcore.' To Mike, whose faith in me has never faltered. I could not have done this with out you. I love you.

Table of Contents

List of Tables

List of Figures

Chapter 1

Introduction

1.1 Overview

The local environment of a drug molecule in aqueous polymeric nanocarriers has an impact on the delivery of that drug to biological systems.[1, 2, 3, 4, 5, 6, 7, 8, 9, 10, 11] Fluorescence spectroscopy is able to study the local environment of materials from molecular length scales to microns.[12] The properties of drug molecules themselves, polymeric micelles that act as drug delivery vehicles, and the interface between the two are of importance in the fields of biomaterials and drug formulation development. While pharmaceutical companies screen many potential molecules for drug activity per year, some drug candidates are eliminated form the development pipeline due to insolubility, a cause of poor bioavailability.[1] This dissertation reports work on the measurement of local environment a small hydrophobic molecule is experiencing when solubilized inside a nanocarrier designed to dissolve it.

Chapter 2 describes the experimental methods used to characterize amphiphilic polymer solutions and fluorophores such as coumarin solvatochromic probes and rilpivirine, an HIV inhibitor. Steady-state and time-resolved fluorescence spectroscopy techniques are described with analysis methods for the chemical systems under investigation. Thermal analysis, particle size measurements, and electronic structure calculations are also key tools used for the physical characterizations described.

In Chapter 3, a class of HIV non-nucleoside reverse transcriptase inhibitors (NNRTIs) called diarylpyrimidines (DAPYs), presents the opportunity to look at drug encapsulation from molecules that are self-reporting of their environments. Rilpivirine (R278474, TMC278 Janssen Pharmaceutica) a DAPY which is entering FDA Phase III trials as an effective HIV treatment, is the focus of a fluorescence study presented in

this dissertation. Since rilpivirine is a fluorescent molecule, a study is presented of its spectral response to solvent polarity, viscosity, and nanoscale transitions in these two properties. The behavior of rilpivirine spectroscopy lays a basis for the use of rilpivirine fluorescence to report on the drug's own local environment. Electronic structure calculations in the form of ZINDO calculations are performed to aid in the explanation of rilpivirine fluorescence and absorption spectroscopy. The environments presented here include a range of solvent polarities and delivery solutions, including aqueous polymer micelles and the rilpivirine molecule in both unimer and aggregate form.

In Chapter 4, the known fluorescence behavior of coumarin 153 is used to study novel polymers called amphiphilic star-like macromolecules (ASMs) and amphiphilic scorpion-like macromolecules (AScMs) and the differences in the hydrophobic cores in aggregates of both molecules in solution. Fluorescence spectroscopy in the steady-state and time domain gives information about the polarity and friction of the local environment of an encapsulated coumarin dye.

In Chapter 5, a common amphiphilic A-B-A triblock copolymer, poly(ethylene oxide)$_{109}$ - poly(propylene oxide)$_{41}$ - poly(ethylene oxide)$_{109}$ is used as a control system to observe seven fluorescent dye molecules of similar structure and varying in solubility and polarity. Seven coumarin dyes of various solubility properties are used to probe multiple and select regions of the polymeric micelles, including the hydrophobic micelle core, the hydrophilic micelle corona, the bulk water region outside the micelles, and the interfacial regions between each of these local environments. The coumarin fluorophores act as models for drug molecules encapsulated in various amphiphilic polymer solutions.

Chapter 6 of this dissertation will summarize the key findings described here and suggest some possibilities for future directions of this research.

1.2 Discussion

Objectives of Research:

- Investigation of local solvent environments of small fluorescent molecules such as hydrophobic drugs
- Systematic characterization of the spectroscopy of rilpivirine, an anti-HIV drug, in various solvent environments, including solutions of aqueous A-B-A triblock copolymer micelles that act as drug nanocarriers
- Use of coumarin 153 fluorescence for investigation and comparison of core characteristics of amphiphilic macromolecules designed for hydrophobic drug encapsulation and delivery
- Characterization of multiple local environments in A-B-A triblock copolymer micelles on molecular length scales using seven coumarin solvatochromic fluorescence probe molecules of various solubility properties

This dissertation will focus on several objectives. The first aim is the systematic characterization of the spectroscopy of rilpivirine, an anti-HIV drug, in various solvent environments, including solutions of aqueous A-B-A triblock copolymer micelles that act as drug nanocarriers. The second endeavor of this work is the characterization of various drug nanocarriers themselves using the solvatochromic fluorescence properties of coumarin dyes as model drug molecules. The comparison is between three amphiphilic macromolecules specifically designed for hydrophobic drug encapsulation and delivery. Seven coumarin dye molecules of various solubility properties are then used in a similar way to describe the various local environments in A-B-A triblock copolymer micelles on molecular length scales. These objectives address the need for the characterization of the local environment polarity and microviscosity of small molecules in polymeric micelle solutions and apply the methods developed to characterize the potent, but insoluble HIV inhibitor, rilpivirine, as well as three novel polymeric drug nanocarriers.

1.2.1 Local Environments of Drugs in Solution

There are several requirements for a drug molecule to efficiently be delivered to its target biological system.[1, 5] Drugs are usually small molecules that have molecular

weights under 500 g/mol, water/octanol partition coefficients (clogP) values of under 5, have no more than 5 hydrogen bond donors and have no more than 10 hydrogen bond acceptors.[1] These general guidelines are known as "Lipinski's Rule of 5" and pharmaceutical companies often screen potential drug candidate molecules using them.[1, 13, 14] Many molecules are rejected early if one or more of these rules are broken. Unfortunately, there are some molecules that are highly potent against their target diseases, but are too hydrophobic and therefore insoluble in aqueous environments (biological environments) to be delivered efficiently.

There is a widely used application of polymer materials to encapsulate drug molecules in solution and improve the solubility and release profiles of drugs in biological systems. Polymeric micelles, vesicles, liposomes, and other aggregated nanocarriers are finding an advantage in the fact that polymers can be tailored to specific solubility needs. In other words, block copolymers can be designed with variations in the length and composition of each polymer block making up the delivery vehicle.[8, 5]

1.2.2 Rilpivirine, a Non-Nucleoside Reverse Transcriptase Inhibitor and Fluorescence Dye

The rilpivirine molecule is of great interest on account of its potent activity as a non-nucleoside reverse transcriptase inhibitor (NNRTI) of the human immunodeficiency virus, (HIV).[15, 16] Rilpivirine (CAS number [500287-72-9], 4-[[4-[[4-[(1E)-2-cyanoethenyl]-2,6-dimethylphenyl]amino]-2- pyrimidinyl]amino]benzonitrile) is also called R278474 or TMC278.[15] This drug is part of a group of NNRTIs with a diarylpyrimidine structure called DAPYs. Like rilpivirine, a number of DAPYs have been found to bind to reverse transcriptases (RTs). Crystal structures of DAPY molecules bound to the hydrophobic binding pocket of RTs show that the DAPYs adopt a butterfly conformation.[15, 17] The binding of rilpivirine to RTs inhibits transcription of the retroviral RNA to the DNA of the infected cell.[15, 16, 18]. DAPYs fit loosely into the RT binding pocket, giving this class of drugs high resistance to viral mutations.[15, 17] In vitro studies have shown that rilpivirine may be even more effective in stopping HIV replication than another recently FDA-approved DAPY drug (etravirine, TMC 125).[15]

Rilpivirine structure and solvent environment are described using electronic structure calculations and optical spectroscopy methods. ZINDO calculations are performed for four conformations. These include an anhydrous crystal structure conformation of rilpivirine, the conformation of rilpivirine co-crystalized with DMSO solvent in a 1:2 ratio, and the conformation of rilpivirine taken from the crystal structure of the drug bound in the hydrophobic binding site of the 52A mutant of HIV-RT.[19]

The predicted energy differences between the electronic ground state, or highest occupied molecular orbital (HOMO) and the first Franck-Condon excited state or lowest unoccupied molecular orbital (LUMO) by ZINDO methods are compared to experimental results from measured absorbance spectra and fluorescence excitation spectra. Rilpivirine solutions for a selection of solvents varying in dielectric, viscosity, and polarity and the local environment of rilpivirine are reported using the fluorescence spectrum, lifetime and reorientational behavior of the drug. The spectral properties of rilpivirine are compared to each of these solvent properties to show how spectroscopy is used to characterize the local environment of rilpivirine in solution.

Rilpivirine has a clogP value of 5.8, making the delivery of the drug to aqueous biological environments a challenge.[16] Because rilpivirine is a potent inhibitor of HIV replication but is very hydrophobic, the delivery of this drug molecule has a need for vast improvement. Rilpivirine has been found to be present in both unimer and aggregate forms in some solvents, as demonstrated in recent publications.[15, 16] Rilpivirine aggregates have been found to form in aqueous buffer solutions, and while the theoretical EC_{50} of rilpivirine is less than 0.1 nM, the EC_{50} found in cellular uptake studies is approximately 5 times this value.[15] The proposed theory is that rilpivirine is absorbed by cells at all because of the formation of nanoparticle aggregates. Scanning electron micrographs and dynamic light scattering measurements of rilpivirine aggregates in buffer solution co-solvated with tylaxopol surfactant show the average diameter of the drug nanoparticles to be approximately 58 nm.[15, 16] In Chapter 3, rilpivirine is dissolved in solutions of A-B-A triblock copolymer poly(ethylene oxide)$_{109}$ - poly(propylene oxide)$_{41}$ - poly(ethylene oxide)$_{109}$ unimers, micelles, and gels. The solvent environment and aggregation properties are studied using fluorescence spectral

shifts, time constants, and reorientational dynamics from polarization anisotropy measurements. The concentration and temperature dependence of rilpivirine in 25 w/v% amphiphilic polymer solutions is investigated, as well as the direct link between aggregation state and emission wavelength as measured by fluorescence dynamics and polarization anisotropy. Fluorescence spectroscopy is shown as a sensitive and useful tool for the characterization of aggregate and unimer rilpivirine in solution.

1.2.3 Coumarin Fluorescent Dye Molecules

Seven coumarin fluorescence dyes are used to study multiple regions of A-B-A triblock copolymers in solution.

These coumarin dyes have been chosen because of the range in solubility of the seven molecules while maintaining the same relative size, shape, and core molecular structure. Because of the variations in the solubility of each coumarin, each dye is expected to localize in a different region or range of regions within an aqueous solution of polymeric micelles including hydrophobic core, hydrophilic corona, and interfacial polymer and water regions of the aggregate solution. We measure the solubility of the coumarin dyes with calculated water-octanol partition coefficients, or clogP values.[1] Coumarins do not aggregate at dilute concentrations such as used for the fluorescence measurements described here. The peak excitation and emission energies for these seven coumarin dyes fall within the range of experimental practicality for the time-resolved fluorescence anisotropy measurements using the second harmonic generation frequency of a tunable Ti-sapphire laser as an excitation source. Previous studies of 7-aminocoumarin dyes have shown that the dipole moment of a coumarin dye increases dramatically from the electronic ground state to the excited state.[20, 21] This characteristic makes coumarin dyes positively solvatochromic and good candidates for measuring local changes in polarity in a nanophase transition such as micellization or differences in local polarity.[22]

1.2.4 Amphiphilic Star-Like Macromolecules and Amphiphilic Scorpion-Like Macromolecules

A number of amphiphilic polymers have been designed to solubilize hydrophilic molecules for applications in drug delivery.[8, 5, 23, 24] Because poly (ethylene glycol) (PEG) is highly water-soluble, it is ubiquitous in these synthetic copolymers.[25] PEG and its conjugates are widely used in the areas of small-molecule encapsulation, drug formulation, modification of proteins and pharmaceutical molecules, cosmetics, biomedical coatings, and other surface modifications.[25, 8, 5, 24, 23, 26] The hydrophilic, non-toxic, biocompatible, biodegradable nature has led to the use of PEG in amphiphilic polymers for encapsulation of hydrophobic drugs.[8, 5] Many molecules considered as drug candidates are insufficiently water-soluble to be absorbed effectively into biological systems and one must take into account the solubility and biological interactions of both the drug and its delivery media.[5] Such delivery media must be biocompatible, non-toxic, and able to solubilize but not inhibit the drug molecule. Each of these attributes depends on appropriate selection of the PEG functionality.[25, 27, 5, 7] Another goal of drug delivery systems is to simultaneously increase the circulation time while decreasing the dosage.[8] This can enable a reduction of cytotoxicity, such as for chemotherapy drugs.[8]

Amphiphilic polymers with PEG hydrophilic blocks have been used for increased solubility of hydrophobic molecules.[8, 5, 24, 23] Here, three such amphiphilic polymers are examined with the coumarin 153 (C153) fluorescence probe encapsulated as a reporter of local environment within the core of each of three polymer solutions. The three amphiphilic polymers, designed by the Uhrich group at Rutgers University are M12P5, NC12P5, and NC6P5. M12P5 is a molecule containing an acylated mucic acid core and a PEG tail, giving it a shape resembling a scorpion. The group to which M12P5 belongs is aptly named AScMs or amphiphilic scorpion-like macromolecules. NC12P5 and NC6P5, also designed and synthesized by the Uhrich group, are similar in molecular makeup, but have four acylated mucic acid groups covalently tethered to make a hydrophobic core, with four PEG chains forming a hydrophilic shell on the outside of

the macromolecule. These are called amphiphilic star-like macromolecules (ASMs) and NC6P5 and NC12P5 differ only by the number of carbons in the alkyl chains of the core structure. C153 is used as a hydrophobic drug model for observation of the local friction and local solvent polarity in the core of each nanocarrier.[28, 29, 21, 30, 31]

C153 is a well-characterized solvatochromic fluorescence probe that has a hydrophobic clogP value of 4.08.[32] By measuring the steady-state fluorescence emission, time-dependent polarization anisotropy, and reorientation time constants of C153, it is possible to clearly distinguish between a flexible, polar, water-like environment and a more rigid, non-polar environment of the dye molecule.[33, 34]

1.2.5 A-B-A Triblock Copolymer PEO_{109}-PPO_{41}-PEO_{109}

Triblock copolymers are utilized in various fields including pharmaceuticals, personal hygiene, water purification, and other areas that require the uptake and improved solubility of small molecules.[5, 8, 7] A-B-A triblock polymers have three components consisting of two A-blocks of the same repeating monomer and a center B-block consisting of a second type of repeat unit. When the two A-blocks have one type of solubility and the B-block has a different solubility, the A-B-A triblock copolymers are referred to as amphiphilic. The amphiphilic nature of A-B-A triblock copolymers has been previously used as a means of encapsulating insoluble molecules and making them miscible in a preferred solvent.[25] The solubility properties of A-B-A triblock copolymers may be used to separate impurities in solution, aid in chromatographic processes, and improve the delivery of pharmaceutical ingredients.[5, 8, 7, 35, 2, 36]

Small molecules may be dissolved in a solvent in which the A-blocks are soluble and the B-block is not because upon dissolution of the polymer, the hydrophobic effect causes the B-blocks of the polymer to aggregate and form various structures in solution.[37] The hydrophobic effect occurs when polar and non-polar molecules separate. This can be explained most often by thermodynamic driving forces such as enthalpy and entropy to decrease solvation free energy between molecules. These driving forces depend on properties such as solute and solvent size (surface area), van der Waals interactions, hydrogen bonding, and temperature.[37, 25] In the solvation free

energy ($\triangle G_{solvation} = \triangle H_{solvation}$ - $T\triangle S_{solvation}$) there are enthalpic and entropic components that differ with every system.[37] In the case of A-B-A triblock copolymers in a solvent miscible with the A-block, aggregation of the B-blocks occurs and micelles are formed. An increase in the volume of hydrophobic non-polar molecules in water cause the waters to restructure around the non-polar molecules, decreasing the entropy of the water. When the non-polar molecules (B-blocks) aggregate, and the polar molecules (A-blocks) shield the water from non-polar molecules, favorable entropy is restored.[38]

Depending on the polymer composition, solvent, concentration, and temperature, the aggregation properties of A-B-A triblock copolymers can be altered in many ways. Besides spherical micelles, possible solution phases include worm-like micelles, bilayers, vesicles, inverse micelles, microemulsions, and various types of gel structures.[38, 39]

One A-B-A triblock copolymer, Pluronic F88, is composed of poly(ethylene oxide)$_{109}$ - poly(propylene oxide)$_{41}$ - poly(ethylene oxide)$_{109}$ abbreviated PEO_{109}-PPO_{41}-PEO_{109}. Solutions of 25 w/v% F88 polymer in water, will form micelles above 22.5 °C and forms a hydrogel at increased temperatures.[33, 40] The use of 7 coumarin dye molecules, mentioned previously makes it possible to probe multiple and selective environments in aqueous Pluronic F88 micellar phases.

1.3 Summary

The exploration of the topic of polarity and solubility is one that is not new, but has been undertaken for many years.[41] Defining the polarity and solubility of a specific molecule of interest, such as rilpivirine, is of importance for defining the best way to delivery this drug the most effectively and efficiently. Because rilpivirine is only one of many DAPY HIV inhibitors,[16] there is much work to be done on the delivery methods and mechanisms for any of these that may be of interest in the future.

Improved methods of characterizing the local environments of drug molecules in solution formulations is needed to improve the efficacy of the drug's ability to reach it's target in biological systems. Improved delivery systems are needed as well, and amphiphilic polymer design is a field open to new materials for drug molecules in need

of better bioavailability. Rilpivirine is one of these drugs.

HIV is a worldwide epidemic that affects over 33 million people and will continue to spread to approximately 3 million more people per year.[42] Approximatey two thirds of the people in the world living with HIV are in sub-Saharan Africa, where the inhibiting cost of healthcare prevents the population of HIV patients from receiving the help they need.[42] According to UNAIDS and World Health Organization, approximately 2.1 million people died from AIDS in 2007.[42] An increase in drug efficacy, a decrease in effective dosage, and improved delivery of HIV drugs would not only strive to reduce the cost of HIV treatments, but extend the availability of these treatments to people who really need them. This dissertation is a detailed molecular length scale description of local environments of small molecules in drug delivery solutions. While this work investigates HIV drug molecules on very small length scales, there is a hope to impact the development of needed treatments on a larger scale.

References

[1] C. A. Lipinski; Drug-like properties and the causes of poor solubility and poor permeability; *Journal of Pharmacological and Toxicological Methods* **2000**, *44*, 235–249.

[2] A. V. Kabanov, E. V. Batrakova, and V. Y. Alakhov; Pluronic block copolymers as novel polymer therapeutics for drug and gene delivery.; *Journal of Controlled Release* **2002**, *82*, 189–212.

[3] N. Y. Rapoport, J. N. Herron, W. G. Pitt, and L. Pitina; Micellar delivery of doxorubicin and its paramagnetic analog, ruboxyl, to hl-60 cells: effect of micelle structure and ultrasound on the intracellular drug uptake.; *J. Controlled Release* **1999**, *58*, 153–162.

[4] V. P. Torchilin; Targeted polymeric micelles for delivery of poorly soluble drugs.; *Cellular and Molecular Life Sciences* **2004**, *61*, 2549–2559.

[5] G. S. Kwon; Polymeric micelles for delivery of poorly water-soluble compounds.; *Critical Reviews in Therapeutic Drug Carrier Systems* **2003**, *20*, 357–403.

[6] G. S. Kwon; Block copolymer micelles as drug delivery systems.; *Advanced Drug Delivery Reviews* **2002**, *54*, 167.

[7] G. S. Kwon and M. L. Forrest; Amphiphilic block copolymer micelles for nanoscale drug delivery.; *Drug Development Research* **2006**, *67*, 15–22.

[8] R. Duncan; The dawning era of polymer therapeutics.; *Nature Reviews Drug Discovery* **2003**, *2*, 347–360.

[9] V. P. Torchilin; Micellar nanocarriers: Pharmaceutical perspectives.; *Pharmaceutical Research* **2007**, *24*, 1–16.

[10] L. Tian *et al.;* Amphiphilic scorpion-like macromolecules: Design, synthesis, and characterization.; *Macromolecules* **2004**, *37*, 538–543.

[11] H. Liu, A. Jiang, J. Guo, and K. E. Uhrich; Unimolecular micelles: synthesis and characterization of amphiphilic polymer systems.; *Journal of Polymer Science, Part A: Polymer Chemistry* **1999**, *37*, 703–711.

[12] K. E. Steege, J. Wang, K. E. Uhrich, and E. W. Castner Jr.; Local polarity and microviscosity in the hydrophobic cores of amphiphilic star-like and scorpion-like macromolecules; *Macromolecules* **2007**, *40*, 3739–3748.

[13] C. A. Lipinski, F. Lombardo, B. W. Dominy, and P. J. Feeny; Experimental and computational approaches to estimate solubility and permeability in drug discovery and evelopment settings; *Advanced Drug Delivery Reviews* **2001**, *46*, 3–26.

[14] J. Wang *et al.;* Development of reliable aqueous solubility models and their application in druglike analysis; *Journal of Chemical Information and Modeling* **2007**, *47*(4), 1395–1404.

[15] P. A. J. Janssen *et al.;* In search of a novel anti-hiv drug: Multidisciplinary coordination in the discovery of 4-[[4-[[4-[(1e)-2-cyanoethenyl]-2,6-dimethylphenyl]amino]-2- pyrimidinyl]amino]benzonitrile (r278474, rilpivirine).; *Journal of Medicinal Chemistry* **2005**, *48*, 1901–1909.

[16] Y. V. Frenkel *et al.;* Concentration and ph dependent aggregation of hydrophobic drug molecules and relevance to oral bioavailability.; *Journal of Medicinal Chemistry* **2005**, *48*, 1974–1983.

[17] K. Das, P. J. Lewi, S. H. Hughes, and E. Arnold; Crystallography and the design of anti-aids drugs: conformational flexibility and positional adaptability are important in the design of non-nucleoside hiv-1 reverse transcriptase inhibitors.; *Progress in Biophysics & Molecular Biology* **2005**, *88*, 209–231.

[18] B. L. De Corte; From 4,5,6,7-tetrahydro-5-methylimidazo[4,5,1-jk](1,4)benzodiazepin-2(1h)-one (tibo) to etravirine (tmc125): Fifteen years of research on non-nucleoside inhibitors of hiv-1 reverse transcriptase; *Journal of Medicinal Chemistry* **2005**, *48*, 1689–1696.

[19] Y. V. Frenkel, T. Emge, and E. Arnold unpublished, **2008**.

[20] R. J. Cave, K. Burke, and E. W. Castner Jr.; Theoretical investigation of the ground and excited states of coumarin 151 and coumarin 120.; *Journal of Physical Chemistry A* **2002**, *106*, 9294–9305.

[21] R. J. Cave and E. W. Castner Jr.; Time-dependent density functional theory investigation of the ground and excited states of coumarins 102, 152, 153, and 343.; *Journal of Physical Chemistry A* **2002**, *106*, 12117–12123.

[22] B. Valeur *Molecular Fluorescence: Principles and Applications;* Wiley-VCH, 2002.

[23] P. Krsko and M. Libera; Biointeractive hydrogels.; *Materials Today (Oxford, United Kingdom)* **2005**, *8*, 36–44.

[24] J. Khandare and T. Minko; Polymer-drug conjugates: Progress in polymeric prodrugs.; *Progress in Polymer Science* **2006**, *31*, 359–397.

[25] J. M. Harris and S. Zalipsky, Eds. *Poly (ethylene glycol): Chemistry and Biological Applications*, ACS Symposium Series 680; American Chemical Society, 1997.

[26] J. Miao *et al.;* Chain-folding and overall molecular conformation in a novel amphiphilic starlike macromolecule.; *Macromolecules* **2005**, *38*, 7074–7082.

[27] L. Xing and W. L. Mattice; Strong solubilization of small molecules by triblock-copolymer micelles in selective solvents.; *Macromolecules* **1997**, *30*, 1711–1717.

[28] M. L. Horng, J. A. Gardecki, A. Papazyan, and M. Maroncelli; Subpicosecond measurements of polar solvation dynamics: Coumarin 153 revisited.; *Journal of Physical Chemistry* **1995**, *99*, 17311–37.

[29] M.-L. Horng, J. A. Gardecki, and M. Maroncelli; Rotational dynamics of coumarin 153: Time-dependent friction, dielectric friction, and other nonhydrodynamic effects.; *Journal of Physical Chemistry A* **1997**, *101*, 1030–1047.

[30] F. Ingrosso and B. M. Ladanyi; Solvation dynamics of c153 in supercritical fluoroform: A simulation study based on two-site and five-site models of the solvent.; *Journal of Physical Chemistry B* **2006**, *110*, 10120–10129.

[31] F. Ingrosso, B. M. Ladanyi, B. Mennucci, and G. Scalmani; Solvation of coumarin 153 in supercritical fluoroform.; *Journal of Physical Chemistry B* **2006**, *110*, 4953–4962.

[32] clogp calculator www.daylight.com.

[33] C. D. Grant, K. E. Steege, M. R. Bunagan, and E. W. Castner Jr.; Microviscosity in multiple regions of complex aqueous solutions of poly(ethylene oxide)-poly(propylene oxide)-poly(ethylene oxide).; *Journal of Physical Chemistry B* **2005**, *109*, 22273–22284.

[34] L. Frauchiger, H. Shirota, K. E. Uhrich, and E. W. Castner Jr.; Dynamic fluorescence probing of the local environments within amphiphilic starlike macromolecules.; *Journal of Physical Chemistry B* **2002**, *106*, 7463–7468.

[35] V. Alakhov *et al.;* Block copolymer-based formulation of doxorubicin. from cell screen to clinical trials.; *Colloids and Surfaces, B: Biointerfaces* **1999**, *16*, 113–134.

[36] A. V. Kabanov *et al.;* Polymer genomics: shifting the gene and drug delivery paradigms.; *Journal of Controlled Release* **2005**, *101*, 259–271.

[37] D. Chandler; Interfaces and the driving force of hydrophobic assembly; *Nature* **2005**, *437*, 640–647.

[38] P. Alexandridis and T. Alan Hatton; Poly(ethylene oxide)-poly(propylene oxide)-poly(ethylene oxide) block copolymer surfactants in aqueous solutions and at interfaces: thermodynamics, structure, dynamics, and modeling.; *Colloids and Surfaces, A: Physicochemical and Engineering Aspects* **1995**, *96*, 1–46.

[39] G. Wanka, H. Hoffmann, and W. Ulbricht; Phase diagrams and aggregation behavior of poly (ox yethy1ene)-poly (oxypropylene) -poly(oxyet hylene) triblock copolymers in aqueous solutions; *Macromolecules* **1994**, *27*, 4145–4159.

[40] C. D. Grant *et al.;* Fluorescence probing of interior, interfacial, and exterior regions in solution aggregates of poly(ethylene oxide)- poly(propylene oxide)-poly(ethylene oxide) triblock copolymers.; *Langmuir* **2005**, *21*, 1745–1752.

[41] M. J. Kamlet, J. L. Abboud, and R. W. Taft; The solvatochromic comparison method. 6. the π^* scale of solvent polarities.; *Journal of the American Chemical Society* **1977**, *99*, 6027–6038.

[42] UNAIDS; Aids epidemic update; *UNAIDS and the World Health Organization* **2007**, *21*.

Chapter 2

Experimental Methods

2.1 Materials/ Sample Preparation

2.1.1 Rilpivirine Spectroscopy, Solvatochromism, and Structure

Solid rilpivirine (R278474, TMC-278) was obtained from Janssen Pharmaceutica in Belgium. A defined amount of solid rilpivirine was made into a stock solution of dichloromethane and appropriate aliquots of the stock solution were put into glass sample vials. The rilpivirine-dichloromethane solutions in the sample vials were then dried in a vacuum oven and heated to 37 °C and the pressure reduced to 1500 mPa for one hour to evaporate the solvent. 10 mL of new solvent was added to the remaining rilpivirine. The solvents used are as follows: dimethyl sulfoxide (DMSO), N,N-dimethylformamide (DMF), formamide, ethyl acetate, methanol, water, ethylene glycol (E.G.), dichloromethane (CH_2Cl_2), 1,2-dichlorobenzene (1,2-DCB), toluene, carbon tetrachloride (CCl_4), 2-methyltetrahydrofuran (2-MeTHF). All solutions were stirred for at least 24 hours for proper dissolution of the drug.

2.1.2 Rilpivirine in A-B-A Triblock Copolymer Solutions

Pluronic F88 was donated from BASF Company as solid and 2.5 g was dissolved in 10 mL Fluka Nanopure water (for luminescence, filtered by 0.2 μm pore size) to make aqueous 25 w/v% polymer solutions. Rilpivirine was obtained in solid powder form. A stock solution of rilpivirine was made in dichloromethane using a known amount of drug. The necessary aliquot of stock solution was put into a glass vial and this was then put into a vacuum oven to evaporate the solvent. Aqueous solution of 25 w/v% Pluronic was added to the vial containing rilpivirine. The most concentrated rilpivirine

solution was then diluted with more aqueous polymer solution to make a total of seven samples of different concentrations ranging from 1 to 80 μM rilpivirine. The absorbance spectrum of each rilpivirine sample was measured to calculate the exact concentration of rilpivirine in each solution.

2.1.3 Coumarin 153 in ASMs and AScMs

NC12P5 and NC6P5 amphiphilic star-like macromolecules (ASMs) and the M12P5 amphiphilic scorpion-like macromolecule (AScM) were synthesized and purified according to the previously published procedures by Lu Tian and Jinzhong Wang in the Uhrich group at Rutgers University.[1, 2, 3, 4] NC12P5 and NC6P5 are four diblock polymers, composed of a PEG (M_w 500) tail and an acylated (12 and 6 carbon alkyl chains, respectively) mucic acid core. The four diblock molecules are covalently bonded to one central carbon atom at the mucic acid core. This gives the macromolecule a 'star' configuration. M12P5, the AScM is a single diblock, consisting of the same PEG 500 tail and an acylated mucic acid (12 carbon alkyl chains) core. M12P5 aggregates to form micelles at critical micelle concentration and temperature.[5] For more details on ASM and AScM molecular structure, see Chapter 4.

Aqueous solutions of each of the three polymers were prepared using Fluka Nanopure water (for luminescence, filtered by 0.2 μm pore size) and stirred in the dark at room temperature for at least 48 hours. The polymer solutions were filtered through a 0.2 μm Whatman PTFE filter to remove impurities. Molar concentrations for these three solutions are 2x10^{-4} M for M12P5, 5x10^{-5} M for NC12P5 and 5x10^{-5} M for NC6P5, giving all solutions approximately the same weight-to-volume ratio of 1.2 to 1.3 g/L. The concentration of M12P5 solution is well above the cmc value of 1.25x10^{-7} M.[2] Solid coumarin 153 (C153) from Acros Organics was added to each polymer solution in a sealed vial and stirred for at least 24 hours until dissolved.

2.1.4 Seven Coumarins in F88 Solution

The A-B-A triblock copolymer poly(ethylene oxide)$_{109}$ - poly(propylene oxide)$_{41}$ - poly(ethylene oxide)$_{109}$, also called Pluronic F88, was generously donated from BASF

(Parsippany, NJ). For 25 w/v% solutions, 2.50 g F88 solid was dissolved in 10 mL Fluka Nanopure water (for luminescence, filtered by 0.2 μm pore size). For 5 w/v% F88 solutions, 0.50 g of F88 solid was dissolved in 10 mL Fluka Nanopure water. Solution vials were covered in aluminum foil to avoid exposure to outside light when possible and stirred for 24 hours by magnetic stir bar. Coumarin 314T, coumarin 153, coumarin 102, coumarin 152, coumarin 337, coumarin 151, and coumarin 343 were purchased from Kodak, sigma Aldrich chemicals. Coumarins 314T, 153, 102, 152, 337, and 151 were used as purchased from the company. Coumarin 343 was dissolved in a solution of 0.1 M sodium hydroxide, and this was dissolved in 10 mL of methanol. This solution was then evaporated to dissolve the solvent and leave $C343^{-}/Na^{+}$ salt. The $C343^{-}/Na^{+}$ anion was dissolved into the Pluronic F88 aqueous solution(s). A small amount (few granules) of each of the seven coumarins was dissolved into a separate solution of Pluronic F88 as described above. These seven solutions were also wrapped in aluminum foil and stirred magnetically for 24 hours to dissolve all of the coumarin. In the case of the more hydrophobic coumarins in 5 w/v% F88 solutions (C314T, C153, and C102) gentle heating of the solution was sometimes necessary to thoroughly dissolve the coumarin.

2.2 Methods

2.2.1 Electronic Structure

Coumarin 337 and Coumarin 314T

The Gaussian 03 computational chemistry program suite was used to calculate the AM1, ZINDO, and DFT electronic structures of coumarin 337 and coumarin 314T.[6] From these calculations, the ground state molecular conformation is predicted and the ground state (HOMO), lowest singlet excited state (LUMO) energies and ground state dipole moments are predicted.

Rilpivirine

Configuration interaction (CI) singles calculations were done using the INDO/S semi-empirical parameter set of Zerner and co-workers (ZINDO).[7, 8, 9] Solvent models were

incorporated using Born solvation models, where the molecule is placed in a spherical cavity and surrounded by a continuous medium having fixed dielectric constant and refractive index.[10] 12 solvents were modeled for the rilpivirine molecule using this self-consistent reaction field (SCRF) method.[10]

All ZINDO calculations were done using the Planaria software ArgusLab version 4.0.[11, 12, 13, 14, 15] Ground states, first and and second electronic excited state dipole moments, as well as transition energies between the ground state and first and second electronic excited states were calculated with this method. The ZINDO calculations were done for three structures of rilpivirine: the anhydrous crystal structure from X-ray diffraction (XRD), the structure from the crystal of anhydrous rilpivirine with 2 DMSO molecules from XRD, and the structure of rilpivirine from XRD of the drug in the binding pocket of the HIV-1 reverse transcriptase protein. The XRD structures were provided by Yulia Volovik Frenkel, Kalyan Das, and Eddy Arnold of the Center for Advanced Biotechnology and Medicine at the Robert W. Johnson University of Medicine and Dentistry of New Jersey and the Department of Chemistry and Chemical Biology at Rutgers University. The details of these structures are the topic of an upcoming publication.[16]

2.2.2 Differential Scanning Calorimetry

A Perkin-Elmer DSC 7 differential scanning calorimeter was used for the thermal analysis of 25 w/v% Pluronic F88 solution and 5 w/v% Pluronic F88 solution, as well as 25 2/v% F127 and F68 aqueous solutions. A one minute per degree ramping speed was used and the thermal scan repeated to ensure reproducability of peaks measured. Use of the DSC instrument was made possible by the laboratory of Dr. James Elliot and Professor Kenneth Bresslaur of Rutgers University Department of Chemistry and Chemical Biology.

2.2.3 Dynamic Light Scattering of ASMs and AScMs

A Nicomp 380 Submicron Particle Sizing System with drop-in sample loading and a 532 nm laser was used for particle size analysis of all polymer solutions. For DLS studies

at 37 C, polymer concentrations ranged from 1x10^{-9} M to 1x10^{-3} M. Temperature-dependent DLS measurements between 5 and 55 °Cwere done using polymer concentrations of 2x10^{-4} M for M12P5 and 5x10^{-5} M for both NC12P5 and NC6P5. Nicomp volume-weighted distributions are used for determination of polymer aggregate sizes. Before measurement, all solutions were centrifuged sand filtered through 0.2 μm syringe filters. All samples were allowed to equilibrate at the temperature set point for at least 10 minutes before measurement. Use of the DLS instrument was made possible by the laboratory of Professor Laurence Romsted of Rutgers University Department of Chemistry and Chemical Biology.

2.2.4 Calculated Molecular Volumes

Molecular volumes were calculated for rilipvirine, coumarin 153, M12P5, NC12P5, and NC6P5 according to the van der Waals incremental volume methods described by Bondi and Edward.[17, 18] This method makes use of van der Waals volumes and radii of atoms, compounds, and functional groups. By adding the appropriate van der Waals volumes of each atom or functional group in a molecular compound, it is possible to estimate the molecular volume of the entire compound.[17, 18]

2.2.5 Absorption Spectroscopy

Rilpivirine

Room temperature (typically 295-297 K) absorbance spectra for rilpivirine in most solvents were measured with a Cary-Varian 50 UV-visible spectrophotometer with 2 nm fixed bandpass using a cuvette of each solvent without fluorescence dye for a baseline correction of each sample. Spectra of rilpvirine in 2-methyltetrahydrofuran were provided by Goutham Kodali and Professor Robert J. Stanley of Temple University.[19] A quartz cuvette with 1-cm path length was used for all absorbance measurements.

Coumarin Dyes

The absorbance spectrum of all samples of coumarin dyes were measured before the measurement of fluorescence to check the optical density of the coumarin samples was below 0.2 and in the linear range of the fluorescence instrument. The coumarin concentration was in the range of $1x10^{-6}$ and $1x10^{-5}$ M.

2.2.6 Fluorescence Spectroscopy

The energy of fluorescence emission and the fluorescence lifetimes are dependent on the local solvent environment of the fluorophore.[20, 21] If a fluorophore is in a relatively non-polar environment, the peak fluorescence energy will be higher and the fluorescence time constant will be larger than in the case where the fluorophore is in a polar solvent environment.[20] The energy, wavelength, and polarization of the emitted light all change due to the solvent polarity, viscosity, and temperature.[21] Specifically, 7-aminocoumarin dye molecules such as the seven used in the studies presented on F88 micelles are all solvatochromic fluorophores, meaning that the emission wavelength is dependent upon solvent polarity.

The methodologies used in fluorescence spectroscopy have grown extensively in the past fifteen years. Time-correlated single photon counting (TCSPC) has brought the measurement of fluorescence lifetimes into the applications of biochemistry, materials science, and nanotechnology.[22, 20, 21] Fluorescence lifetimes relay information about the electronic transition for a population of molecules and how local solvent or surrounding dielectric environment affects this energy and rate from an excited state to the ground state.[20, 21] The decay of photons counted in the TCSPC method is extremely sensitive to changes such as these and the mathematical modeling of these decays, fit to Poissonian statistics makes TCSPC a robust method for tracking global parameters such as energy transfer, aggregation, solvent dielectric, binding, and changes in population distribution of a fluorophore. This holds true for both coumarin dyes and rilpivirine, the HIV inhibitor.

Solvatochromic Shifts and the π^* Empirical Polarity Scale

Solvatochromic shifts, such as in the fluorescence of coumarin dyes, are caused by interactions between the solute and solvent molecules.[23] These interactions can be specific, such as hydrogen bonding, or non-specific such as van der Waals interactions.[21, 23] Four types of non-specific interactions between solute and solvent molecules include dipole-dipole interactions, dipole-induced dipole interactions, Stark effect interactions, and dispersion interactions.[21, 23, 20] The interactions that are responsible for the solvatochromism of the coumarins used in this study are dipole-dipole interactions betweens solvent molecules and the solute in the excited state. Coumarins are positively solvatochromic, meaning that the fluorescence and absorbance spectra undergo a bathochromic shift (red shift) with increasing solvent polarity and an increased dipole moment in the Frank-Condon excited electronic transition state.[21, 23, 20, 24]

Empirical polarity scales are based on the dependence of fluorescence or absorbance of a molecular probed as a function of solvent polarity.[25, 26] There are many different empirical scales based on a number of fluorophores. Some of these scales take into account the various properties that affect the solvent interactions such as hydrogen accepting, hydrogen donating, and aromaticity. Because local polarity varies quite significantly from the bulk solution, empirical polarity scales are used to account for the difference in properties describing dielectric environments of a molecule. Two of the most widely used empirical polarity scales are the π^* scale[25] and the E_T^N scale.[24] I will use these two scales exclusively for the analysis of local solvent environments in this dissertation.

The π^* empirical polarity scale was first introduced in 1977 by Kamlet and Taft.[25, 27, 28] This scale has been widely used to quantify the effect of non-specific interactions by specific solvents.[29, 30, 5, 26] The π^* scale is based on the solvatochromic shift of molecular probes as measured by UV-visible absorption and/or fluorescence emission as a function of solvent polarity.[25, 26] Specifically, the probes used to build the π^* empirical polarity scale include over 40 chromophores used to evaluate and refine the scaling of π^* to correlate over 70 different solvents to the scale.[25] While dielectric

constants and dipole moments are responsible for much of a molecule's interaction with other molecules (solvent or solute), they do not take into account specific interactions such as hydrogen bonding or even some non-specific interactions. It is for this reason that the empirical scales such as π^* and $E_T(N)$ are useful in describing the polarity of a molecular environment in a known, comparable and measurable range.[25, 28, 24]

The $E_T(N)$ scale is the normalized $E_T(30)$ scale which was first developed by Dimroth, et. al in 1963.[31] The $E_T(30)$ empirical polarity scale is based on the negative solvatochromism of the dye pyridinium *N*-phenolate betaine.[24] The $E_T(30)$ is defined as the molar electronic transition energies of the dissolved betaine dye which was first published as formula number 30 and labeled as such.[24, 31] To get $E_T(N)$, the E_T values were normalized against two solvents of extreme ends of the polarity spectrum: TMS and water.[24]

The two polarity scales discussed above are empirical and are based on the solvatochromism of different dye molecules in a range of solvents. The term "polarity" to describe a specific solvent environment as reported by fluorescence or absorbance may be assigned a value on the range of these or numerous other empirically built scales based on the effects of specific and non-specific solvent-solute interactions. Polarity can be roughly described as being measured by the dielectric constant or the dipole moment of a molecule, but the dielectric constant of a solvent treats the solvent as a dielectric continuum.[32] The local interactions between solvent and solute are not accounted for in the use of dielectric constant as a definitive polarity scale.

Dipole Moments and the OLM Equation

The Ooshika-Lippert-Mataga (OLM) equation defines the correlation between the solvent-dependent absorption and emission frequencies at the maximum intensities and the solvent properties as shown in Equation 3.3.[33, 34, 35, 20, 21] The OLM plots were graphed for three categories of solvents: aromatic, aprotic, and hydrogen bond donating solvents . The intercepts of these plots are used to calculate the change in dipole moment using the Ooshika-Lippert-Mataga equation, Eq. 3.3, where $\tilde{\nu}_{abs}$ and $\tilde{\nu}_{fluor}$ are the reduced frequencies of the peak absorbance and fluorescence respectively, h is

Planck's constant, c is the velocity of light in a vacuum and a is the radius of the fluorophore estimated from the van der Waals volume, assuming spherical shape. The intercept, C, is obtained from the plot of $\tilde{\nu}_{abs}$ - $\tilde{\nu}_{fluor}$ versus the reaction field factor where F(ϵ,n) is the reaction field factor, calculated by Eq. 3.2.

$$\tilde{\nu}_{abs} - \tilde{\nu}_{fluor} = \frac{2F(\epsilon, n)}{hca^3}(\mu_e - \mu_g)^2 + C \tag{2.1}$$

$$F(\epsilon, n) = f(\epsilon_0) - f(n) = \frac{\epsilon_0 - 1}{2\epsilon_0 + 1} - \frac{n^2 - 1}{n^2 + 1} \tag{2.2}$$

Rilpivirine

Time-integrated emission and excitation spectra of rilpivirine in most solvents were measured using a Horiba Jobin Yvon FluoroMax-3 fluorometer with 0.1 second integration time and 2 nm bandpass used for both excitation and emission. The steady-state emission and excitation of rilpivirine in 1-butanol and in 2-methyltetrahydrofuran were measured with a SPEX FluoroMax-2 with 2 nm bandpass and 0.1 second integration. Samples were measured in a 1 cm pathlength quartz cuvette. Temperatures were regulated to ± 0.1°C by a Wavelength Electronics Peltier thermoelectric controller. Peak wavelength values were fit using Gaussian lineshape fitting to the top 10% of the emission curve and multiple gaussian lineshapes to the entire excitation curve for each sample.

The fluorescence decays of rilpivirine in 25 w/v% Pluronic F88 solutions were measured at 6 concentrations of rilpivirine between 1 and 80 μM and 20 temperatures between 2.5 and 90 °C for each concentration. The fluorescence lifetimes and polarization anisotropies were measured for solutions of 5.8 μM rilpivirine in PEG (M_w 400 Da) and 5.8 μM rilpivirine in PPO (M_w 2,000 Da) 6 temperatures between 5 and 80 °C for each solution. These solutions were measured as control solutions for comparison to the samples of rilpivirine in amphiphilic polymer micelles.

Coumarin 153 in ASMs and AScMs

The steady-state fluorescence emission and excitation spectra of C153 in each ASM and AScM solution were measured with a Horiba Jobin Yvon FluoroMax-3 fluorometer with 425 nm excitation and 510 nm and 530 nm emission wavelengths for ASMs and AScM samples, respectively. Slit widths were set to 2 nm and spectra were collected with 0.1 second integration times and 1 nm increments. Calcite polarizers were used for steady-state anisotropy measurements. The temperature of the sample was controlled using a Wavelength Electronics thermoelectric temperature controller to ±0.1 °C. Sample equilibration time at each temperature was 10 minutes. The peak wavelength for each spectrum was determined from the full-width of the intensity at 90% the peak maximum as fit to a Gaussian line shape.

Seven Coumarin Dyes in Pluronic F88

The time-integrated emission and excitation of seven coumarin dyes in 25 w/v% Pluroinc F88 in aqueous solution were measured using a Horiba Jobin Yvon FluoroMax-3 fluorometer. Slit widths were adjusted to 2 nm and spectra were measured using 0.1 sec integration times at 1 nm intervals for all samples. Both excitation and emission spectra were measured at 20 temperatures: {2.5, 5.0, 10.0, 15.0, 17.5, 20.0, 22.5, 25.0, 27.5, 30.0, 32.5, 35.0, 40.0, 45.0, 50.0, 55.0, 60.0, 70.0, 80.0, and 90.0 °C} A Wavelength Electronics thermoelectric controller regulated the sample temperature to ± 0.1 °C. Each solution was equilibrated for 10 minutes at each temperature prior to measurement of the spectrum. Excitation wavelengths were 430 nm for C314T, 430 nm for C153, 390 nm for C102, 400 nm for C152, 455 nm for C337, 375 nm for C151, and 420 nm for $C343^{-}/Na^{+}$ samples. Emission wavelengths were 490 nm for C314T, 530 nm for C153, 480 nm for C102, 500 nm for C152, 495 nm for C337, 485 nm for C151, and 480 nm for $C343^{-}/Na^{+}$ samples.

Emission and excitation measurements were repeated at 5, 20, 35, 50, 65, and 80 °C for each coumarin in six solvents to be used as control solutions for comparison of the spectral properties of coumarins in solutions of A-B-A triblock copolymers. These

solvents were poly(ethylene oxide) M_w 400 (PEO 400), poly(propylene oxide) M_w. 2,000 (PPO 2000), dimethyl sulfoxide, acetonitrile, carbon tetrachloride, and 1-pentane.

2.2.7 Time-Resolved Fluorescence Spectroscopy

Rilpivirine

Time-resolved fluorescence was measured using the method of time-correlated single photon counting. A Spectra-Physics Ti-sapphire Tsunami laser was tuned to 804 nm and the second and third-harmonic frequencies were generated using the appropriate doubling and tripling crystals. The third-harmonic generation (THG) of the fundamental laser frequency was used for excitation of the samples at a wavelength of 268 nm. The laser light was polarized using a calcite polarizer placed in front of the sample. Fluorescence decays were measured using an emission polarization angle of 0, 54.7, and 90° relative to the excitation polarizer. These measured angles are denoted VV for 0°, VM for 54.7° (magic angle), and VH for 90 ° relative to the polarization angle at excitation.

Decays at three polarization angles were fit simultaneously using a generalization of the methods developed by Cross and Fleming[36] to obtain fluorescence lifetimes and relative amplitudes, reorientation rates, and anisotropy values. The goodness of each fit was evaluated using a reduced χ_r^2 value. A good fit presented a χ_r^2 value close to unity and fitting residuals that are oriented randomly around zero.

Coumarin 153 in ASMs and AScMs

Fluorescence emission decays were measured over a 70 ns range using time-correlated single photon counting. The excitation source is a 5.0-Watt Tsunami Ti-Sapphire laser, tuned to a wavelength of 850 nm. The laser beam at 850 nm is passed through a pulse-selector, set for one pulse every 70 ns. Passing the fundamental beam through a doubling crystal and wave plate creates the second harmonic generation of the fundamental beam. The SHG beam at 425 nm and the fundamental beam are then passed through a prism and spatially separated. A calcite polarizer vertically polarizes the

SHG beam that is then passed through the sample, held in a quartz cuvette. The fundamental is focused onto a photodiode to provide a synchronization signal for the time-to-amplitude converter (TAC). The MCP-PMT detects the emitted photons from the sample and converts the voltage into photons over time between pulses. By building up a histogram of voltage over time, the emission decay is measured with 4096 data points. This procedure is performed by Becker and Hickl TCSPC detection, model SPC-630. The measured instrument temporal response was typically 80 ps at full width half maximum. The C153 emission decay transients were detected at 510 nm for NC12P5 and NC6P5 polymer samples and 530 nm for M12P5 polymer samples. Sample temperatures were controlled to ±0.1 °C using a Quantum Northwest TLC 50/100 thermoelectric temperature controller. Samples were given at least a 10 minute thermal equilibration time prior to the start of the TCSPC measurements.

$$K(t) = \sum_{i=1}^{n} \alpha_i \exp(\frac{-t}{\tau_i}) \tag{2.3}$$

$$I_{VM}(t) = K(t) \tag{2.4}$$

$$I_{VV} = \frac{1}{3} K(t) \left(1 + 2r(t)\right) \tag{2.5}$$

$$I_{VH} = \frac{1}{3} K(t) \left(1 - r(t)\right) \tag{2.6}$$

$$r(t) = \sum_{j=1}^{n} r_j exp(\frac{-t}{\theta_{j,rot}}) \tag{2.7}$$

Time-resolved emission decay transients at vertical (VV), magic (VM), and horizontal (VH) polarization angles of detection were simultaneously fit using Igor software[37] by a generalization of the simultaneous VV and VH transient fitting described by Cross and Fleming.[36] Equations 2.3 through 2.7 were used for simultaneous fitting of the three decays. Equations 2.3 and 2.4 for K(t) and I_{VM}(t) represent the fit to the emission decay transient measured at magic angle polarization, where the α_i are the normalized amplitudes that sum to unity, and the τ_i are the component time constants.

The emission decay transients measured at vertical and horizontal polarization angles are fit to Equations 2.5 and 2.6, respectively, and these are functions of K(t) and r(t), where r(t) is the time-resolved decay of polarization anisotropy, r_j are amplitudes that sum to the fundamental anisotropy, and $\theta_{j,rot}$ are the component reorientation time constants.[36, 20, 21]

Fits to a multi-exponential model for the VM fluorescence decay rates were combined with a multi-exponential anisotropy decay law, given in Equation 2.7.[38, 36] This fitting was done to calculate fluorescence decay rates and amplitudes, as well as reorientation rates and amplitudes. The emission transients, $I_{VV}(t)$, $I_{VM}(t)$, and $I_{VH}(t)$ are shown concatenated in Figure 2.1 with the reduced residuals from the simultaneous fit.

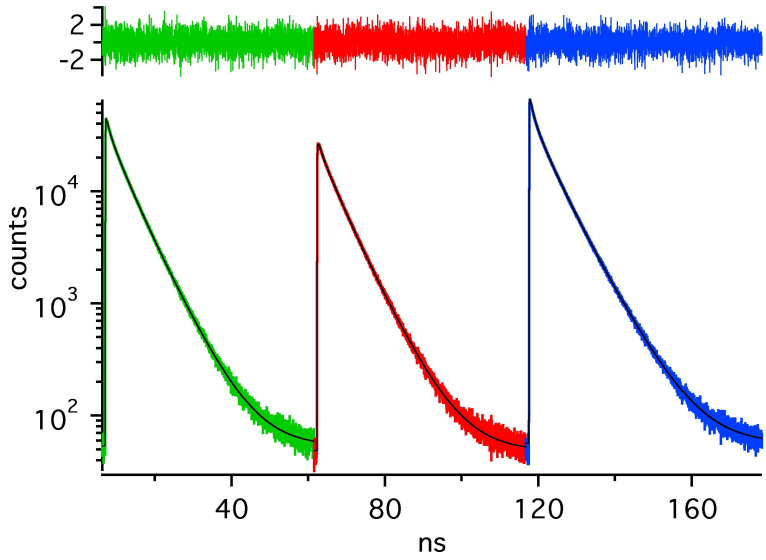

Figure 2.1: Time-resolved fluorescence transients of C153 emission at magic (green), horizontal (red) and vertical (blue) angles of polarization ($I_{VM}(t)$, $I_{VH}(t)$, and $I_{VV}(t)$). Reduced residuals are plotted at the top.

The value of χ_r^2 ranged between 1.02 to 1.14 for the non-linear least squares fits of the data to Equations 2.3-2.7. Simulations of time-resolved fluorescence data made using the experimental data parameters were fit to establish the robustness of the fitting method. For coumarin 153 in ASMs and AScMs, time-resolved emission decays were measured at five temperatures (5, 20, 37, 55, and 70°C) to obtain a range of

reorientation data in different conditions corresponding to refrigeration, room temperature, body temperature, and a heated environment. The range of temperatures also permits variation of the rigidity of the polymer cores due to thermal motion of both the polymer and water. While the window for the time-resolved fluorescence decays of C153 is 70 ns in this case, correct parameters were recovered from simulated data with given longer reorientation time constants beyond this window. Using simulated data sets, reorientation time constants as long as 250 ns can be retrieved accurately from simulated data using our simultaneous fitting method. While the error in accurately obtaining the longer reorientation time constants was greater than obtaining the faster rates within the window of measurement, the error was well within the range of the original calculations.

The limiting polarization anisotropy, r_0, is a measure of the fundamental anisotropy value of the fluorescence of a fluorophore in the absence of reorientational motion. The r_j values or component anisotropy values are a measure of how light emitted from a fluorophore is depolarized due to reorientational motions and thus are reduced from the value of r_0. If the fluorophore is reorienting at a faster rate, the light emitted is more depolarized and the anisotropy is reduced, while if the fluorophore is in a rigid environment, and moving more slowly, the light emitted is less depolarized and the r_j is closer to r_0 which has a theoretical maximum value of 0.4.[21, 20] The anisotropy, r, is measured by a ratio of intensities with regard to how the emission of the fluorophore is measured. Equation 2.8 shows the relationship between r_0 and r(t), the anisotropy decay. $r(t) = (I_{VV}(t) - I_{VH}(t))/(I_{VV}(t) + 2I_{VH}(t))$ relates r_0 to the intensity of emission (whether time-resolved or in the steady-state) measured at vertical polarization (0°) relative to vertical excitation and horizontal polarization (90°) relative to vertical excitation. These intensities are indicated as I_{VV} and I_{VH}.

$$r(0) = \sum_{j=1}^{n} r_j \tag{2.8}$$

Seven Coumarins in Pluronic F88 Solution

For experiments measuring seven different coumarins in 25 w/v% Pluronic F88 solution, fluorescence decays were measured at 20 temperatures between 2.5 and 90.0 °C. Each sample was equilibrated at each set temperature for at least 10 minutes prior to measurement. The TAC range for each coumarin sample was 70 ns. For C314T lifetime measurements, the excitation wavelength of the laser was 440 nm and the emission wavelength of detection was 485 nm. For C153 lifetime measurements, the excitation wavelength of the laser was 430 nm and the emission wavelength of detection was 520 nm for higher temperatures (above 22.5 °C) and 550 nm for lower temperatures (below 35.0 °C). For C102 lifetime measurements, the excitation wavelength of the laser was 400 nm and the emission wavelength of detection was 476 nm. For C152 lifetime measurements, the excitation wavelength of the laser was 400 nm and the emission wavelength of detection was 500 nm. For C337 lifetime measurements, the excitation wavelength of the laser was 450 nm and the emission wavelength of detection was 495 nm. For C151 lifetime measurements, the excitation wavelength of the laser was 390 nm and the emission wavelength of detection was 485 nm for lower temperatures (below 27.5 °C) and 480 nm for higher temperatures (above 25.0 °C). For $C343^{-}/Na^{+}$ lifetime measurements, the excitation wavelength of the laser was 430 nm excitation and the emission wavelength of detection was 480 nm.

Dielectric Friction versus Bulk Shear Viscosity

A Cambridge Applied Systems model ViscoLab 4100 automated viscometer was used for all shear viscosity measurements of polymers. A Lauda Brinkmann RMT-6 recirculating chiller provided temperature control of ±0.1 C. Each of the three polymer solutions was held at each temperature for at least 15 minutes for proper equilibration. A steel piston of 0.310-inch diameter was selected to measure viscosities in the range of 0.25 cP to 5 cP for all polymer solutions.

$$\theta_{rot} = \frac{V\eta}{k_B T} \tag{2.9}$$

When considering a solute molecule inside a solvent environment, the local friction experienced by that solute molecule depends greatly on the local dielectric field of the interacting solvent molecules.[39] The Stokes-Einstein-Debye (S-E-D) Equation 2.9 for small reorienting systems relates the reorientation time constant (θ_{rot}) of a fluorescence probe to the effective volume of reorientation (V), the bulk viscosity of the solution (η), and the temperature.[40, 21, 20, 18]

While S-E-D hydrodynamic theory holds true for some solvents, specific and non-specific interactions between the solute probe molecule and solvent molecules make the local friction of the solute stray from S-E-D hydrodynamics.[39, 29] Time-resolved fluorescence polarization anisotropy shows the difference between shear viscosity and local microviscosity by measuring the reorientation of a fluorophore on molecular length scales.[38, 5]

Some other factors to consider when examining local friction is the shape and size of the solute molecule in comparison to the shape and size of the solvent molecules.[39] The local friction will be quite different if the solvent molecules are much larger or much smaller than the solute molecules in question.[39] The shape of the solute molecule is also a factor, affecting the slip and stick hydrodynamics.[39] The local friction in each case, may correlate well with the viscosity of the bulk solution, but non-specific interactions between solvent and solute result in the local friction varying greatly from the shear viscosity by orders of magnitude.[39, 41, 5, 29] The local friction of small reorienting species in solution is of importance when speaking of amphiphilic polymers for the purpose of encapsulating such small molecules for applications such as hydrophobic drug delivery. High local friction of an encapsulated molecule in such a polymer could lead to changes in loading and release profiles.[5]

Time-resolved Emission Spectral Shift of Rilpivirine

Fluorescence decays of seven concentrations of rilpivirine in 25 w/v% were measured at isotropic polarization (magic angle 54.7° relative to 0° polarized excitation. Decays were measured at emission wavelengths from 20,750 to 34,500 cm^{-1} at 250 cm^{-1} intervals. The decay at each emission wavelength was fit to a sum of multiple exponential

equations as shown in Equation 2.3. The emission spectrum was then reconstructed at a series of logarithmically spaced time points from 1 ps to 100 ns based upon the lifetimes fit at each wavelength. The reconstructed emission spectra were then fit to the spectrum of rilpivirine in PEG400 using the NNLS method as described above. This fitting procedure was done for each concentration of rilpivirine in 25 w/v% F88 solution at 30 °C.

References

[1] H. Liu, A. Jiang, J. Guo, and K. E. Uhrich; Unimolecular micelles: synthesis and characterization of amphiphilic polymer systems.; *Journal of Polymer Science, Part A: Polymer Chemistry* **1999**, *37*, 703–711.

[2] L. Tian *et al.;* Core crosslinkable polymeric micelles from peg-lipid amphiphiles as drug carriers.; *Journal of Materials Chemistry* **2004**, *14*, 2317–2324.

[3] L. Tian *et al.;* Amphiphilic scorpion-like macromolecules: Design, synthesis, and characterization.; *Macromolecules* **2004**, *37*, 538–543.

[4] J. Wang, L. Tian, A. Argenti, and K. E. Uhrich; Nanoscale amphiphilic star-like macromolecules with carboxy-methoxy- and amine-terminated chain ends.; *J. Bioact. Compat. Polym.* **2006**, *21*, 297–313.

[5] K. E. Steege, J. Wang, K. E. Uhrich, and E. W. Castner Jr.; Local polarity and microviscosity in the hydrophobic cores of amphiphilic star-like and scorpion-like macromolecules; *Macromolecules* **2007**, *40*, 3739–3748.

[6] Gaussian 03, revision b.02. M. J. Frisch *et al.* Gaussian, Inc., Pittsburgh PA, 2003, **2003**.

[7] J. Ridley and M. Zerner; An intermediate neglect for differential overalap technique for spectroscopy: Pyrrole and the azines; *Theoretical Chemistry Accounts* **1973**, *32*, 111–134.

[8] M. C. Zerner, G. H. Loew, R. F. Kirchner, and U. T. Mueller-Westerhoff; An intermediate neglect of differential overlap technique for spectroscopy of transition-metal complexes. ferrocene.; *Journal of the American Chemical Society* **1980**, *102*, 589–99.

[9] M. C. Zerner *Semiempirical Molecular Orbital Methods in Reviews in Computational Chemistry*, Vol. 8; VCS Publishers Inc., 1991.

[10] M. M. Karelson and M. C. Zerner; Theoretical treatment of solvent effects on electronic spectroscopy.; *Journal of Physical Chemistry* **1992**, *96*, 6949–57.

[11] Arguslab version 4.0. M. A. Thompson Planaria Software LLC, Seattle, WA., **1996-2003**.

[12] M. A. Thompson and M. C. Zerner; A theoretical examination of the electronic structure and spectroscopy of the photosynthetic reaction center from rhodopseudomonas viridis.; *Journal of the American Chemical Society* **1991**, *113*, 8210–15.

[13] M. A. Thompson, E. D. Glendening, and D. Feller; The nature of k+/crown ether interactions: A hybrid quantum mechanical-molecular mechanical study.; *Journal of Physical Chemistry* **1994**, *98*, 10465–76.

[14] M. A. Thompson and G. K. Schenter; Excited states of the bacteriochlorophyll b dimer of rhodopseudomonas viridis: A qm/mm study of the photosynthetic reaction center that includes mm polarization.; *Journal of Physical Chemistry* **1995**, *99*, 6374–86.

[15] M. A. Thompson; Qm/mmpol: A consistent model for solute/solvent polarization. application to the aqueous solvation and spectroscopy of formaldehyde, acetaldehyde, and acetone.; *Journal of Physical Chemistry* **1996**, *100*, 14492–14507.

[16] Y. V. Frenkel, T. Emge, and E. Arnold unpublished, **2008**.

[17] A. Bondi; van der waals volumes and radii; *Journal of Physical Chemistry* **1964**, *68*, 441–51.

[18] J. T. Edward; Molecular volumes and the stokes-einstein equation; *Journal of Chemical Education* **1970**, *47*(4), 261–270.

[19] K. E. Steege *et al.;* Spectroscopy, solvatochromism, and structure of rilpivirine, a potent non-nucleoside reverse transcriptase inhibitor; **2008**, page to be published.

[20] J. R. Lakowicz *Principles of Fluorescence Spectroscopy;* Kluwer Academic/ Plenum Publishers, 2nd ed., 1999.

[21] B. Valeur *Molecular Fluorescence: Principles and Applications;* Wiley-VCH, 2002.

[22] W. Becker *Advanced time-correlated single photon counting techniques;* Springer: New York, 2005.

[23] P. Suppan; Invited review. solvatochromic shifts. the influence of the medium on the energy of electronic states.; *Journal of Photochemistry and Photobiology, A: Chemistry* **1990**, *50*, 293–330.

[24] C. Reichardt; Solvatochromic dyes as solvent polarity indicators.; *Chemical Reviews (Washington, DC, United States)* **1994**, *94*, 2319–2358.

[25] M. J. Kamlet, J. L. Abboud, and R. W. Taft; The solvatochromic comparison method. 6. the π^* scale of solvent polarities.; *Journal of the American Chemical Society* **1977**, *99*, 6027–6038.

[26] C. Laurence *et al.;* The empirical treatment of solvent-solute interactions: 15 years of π^*; *Journal of Physical Chemistry* **1994**, *98*, 5807–5816.

[27] M. J. Kamlet, T. N. Hall, J. Boykin, and R. W. Taft; Linear solvation energy relationships. 6. additions to and correlations with the p* scale of solvent polarities.; *Journal of Organic Chemistry* **1979**, *44*, 2599–604.

[28] M. J. Kamlet, J.-L. M. Abboud, M. H. Abraham, and R. W. Taft; Linear solvation energy relationships. 23. a comprehensive collection of the solvatochromic parameters, t*, a, and 0, and some methods for simplifying the generalized solvatochromic equation; *Journal of Organic Chemistry* **1983**, *48*, 2877–2887.

[29] M. L. Horng, J. A. Gardecki, A. Papazyan, and M. Maroncelli; Subpicosecond measurements of polar solvation dynamics: Coumarin 153 revisited.; *Journal of Physical Chemistry* **1995**, *99*, 17311–37.

[30] E. Buncel and S. Rajagopal; Solvatochromism and solvent polarity scales.; *Accounts of Chemical Research* **1990**, *23*, 226–31.

[31] K. Dimroth, C. Reichardt, T. Siepmann, and F. Bohlmann; Pyridiunium n-phenolbetaines and their use for the characterization of the polarity of solvents.; *Liebigs. Ann. Chem* **1963**, *661*, 1–37.

[32] L. Onsager; Electric moments of molecules in liquids; *Journal of the American Chemical Society* **1936**, *58*, 1486–1493.

[33] Y. Ooshika; Absorption spectra of dyes in solution; *Journal of the Physical Society of Japan* **1954**, *9*, 594.

[34] E. Lippert; *Z. Naturforsch* **1955**, *10a*, 541.

[35] N. Mataga, Y. Kaifu, and M. Koizumi; Sovent effects upon fluorescence spectra and the dipole moments of excited molecules; *Bulletins of the Chemical Society of Japan* **1956**, *29*, 465.

[36] A. J. Cross and G. R. Fleming; Analysis of time-resolved fluorescence anisotropy decays; *Biophysical journal* **1984**, *46*, 45–56.

[37] Wavemetrics Igor Pro 5.04b Edition. Wavemetrics, Inc. Lake Oswego, OR, **2005**.

[38] C. D. Grant *et al.;* Fluorescence probing of interior, interfacial, and exterior regions in solution aggregates of poly(ethylene oxide)- poly(propylene oxide)-poly(ethylene oxide) triblock copolymers.; *Langmuir* **2005**, *21*, 1745–1752.

[39] D. Ben-Amotz and J. M. Drake; The solute size effect in rotational diffusion experiments: A test of microscopic friction theories; *The Journal of Chemical Physics* **1988**, *89*(2), 1019–1029.

[40] M.-L. Horng, J. A. Gardecki, and M. Maroncelli; Rotational dynamics of coumarin 153: Time-dependent friction, dielectric friction, and other nonhydrodynamic effects.; *Journal of Physical Chemistry A* **1997**, *101*, 1030–1047.

[41] C. D. Grant, K. E. Steege, M. R. Bunagan, and E. W. Castner Jr.; Microviscosity in multiple regions of complex aqueous solutions of poly(ethylene oxide)-poly(propylene oxide)-poly(ethylene oxide).; *Journal of Physical Chemistry B* **2005**, *109*, 22273–22284.

Chapter 3

Fluorescence Spectroscopy of Rilpivirine: a Potent Non-Nucleoside Reverse Transcriptase Inhibitor

3.1 Summary

The fluorescence properties of rilpivirine, a potent non-nucleoside reverse transcriptase inhibitor, display strong solvatochromism from an electronic charge-transfer excited state. The fluorescence spectroscopy of rilpivirine is characterized in a set of 12 solvents with various dielectric constants, polarities, and viscosities. The electronic structure and dipole moment of rilpivirine are calculated in both the ground and electronic excited state by semi-empirical ZINDO calculations.[1] The electronic states of two conformations of anhydrous rilpivirine and one conformation of rilpivirine as found in the protein-bound form are compared by ZINDO calculations using self-consistent reaction field theory (SCRF) to predict the solvatochromic response of rilpivirine in absorption spectroscopy. The change in dipole moment between ground and excited states is determined by analysis of fluorescence spectroscopy in a range of commonly used solvents. A positive solvatochromic shift in the fluorescence peak between polar and non-polar solvent environments is used to scale the polarity and dielectric properties of the local solvent environment of rilpivirine. The rilpivirine molecule is an effective probe of its local environment by use of absorbance and fluorescence spectra.

Rilpivirine is dissolved in an aqueous solution of 25 w/v% A-B-A triblock copolymer, Pluronic F88 to study the local environment of rilpivirine unimers and aggregates encapsulated by polymer micelles. The fluorescence spectroscopy in both the steady-state and time-domain are measured as a function of drug concentration at a temperature where the A-B-A triblock copolymer is in a micellar phase. The spectra are also measured as a function of temperature at 5.8 μM rilpivirine where the drug is in both

monomer and aggregated form and the polymer is in aqueous unimer, micelle, and hydrogel phases. The fluorescence emission spectra, fluorescence time constants, and reorientation dynamics are found to have different characteristics for monomer and aggregated forms of rilpivirine and can be differentiated using fluorescence. The concentration dependence of rilpivirine in the solution of micelles is monitored and the critical aggregation concentration is found for the drug in the F88 micelle solution.

3.2 Overview

Rilpivirine (TMC 278, R278474) is a potent inhibitor of the HIV virus.[2, 3, 4, 5] The diarylpyrimidine (DAPY) structure of rilpivirine is shown in Figure 3.1. Rilpivirine not only has great possibility for the treatment of HIV, but is a challenge with regard to formulation and delivery of the the molecule. Because rilpivirine is so hydrophobic, the drug has been found to form aggregates in solutions of aqueous buffers, co-solvated with solvents such as DMSO, PEG 400, or the surfactant, tylaxopol.[2, 5] Extraordinarily, the particle size of these aggregates was found to be on the order of 58 nm in diameter; small enough to allow passage of rilpivirine into cells within the lymphatic system and the gastrointestinal tract.[2, 5] Although rilpivirine forms nanoparticle aggregates in some formulated solutions, the structure and the local environment of the drug in such solutions has yet to be determined. Fortunately, rilpivirine is a highly solvatochromic fluorophore. The ability of this HIV inhibitor to report on local environment, reorientational motions, and solvent dynamics through fluorescence spectroscopy is the premise of Chapter 3. In addition, four different conformations from both X-ray diffraction and electronic structure DFT calculations are shown in Figure 3.1 DFT geometry optimizations and calculations were performed by Benjamin Lee of Rutgers University, Department of Chemistry and Chemical Biology.[1] These conformational structures will be used in semi-empirical calculations to obtain physical properties such as electronic transition energies, molecular orbital configurations, and molecular dipole moments.

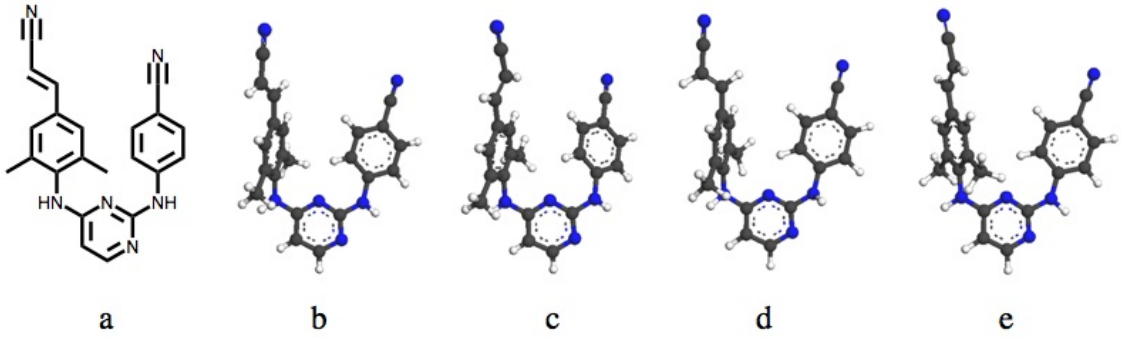

Figure 3.1: (a) Rilpivirine and conformations of the rilpivirine molecule from XRD measurements of (b) the anhydrous crystal, (c) the anhydrous crystal with ratio of 1 rilpivirine: 2 DMSO, (d) rilpivirine bound to HIV-1 RT-52A, and (e) TD-DFT optimized structure of rilpivirine from computational calculations.

3.2.1 A-B-A Triblock Copolymer Pluronic F88

The amphiphilic A-B-A triblock copolymer Pluronic F88 (BASF) has the molecular structure of poly(ethylene oxide)$_{109}$ - poly(propylene oxide)$_{41}$ - poly(ethylene oxide)$_{109}$ (PEO$_{109}$-PPO$_{41}$-PEO$_{109}$). The opposing solubility of the hydrophilic PEO A-groups and the hydrophobic PPO B-group cause this polymer to form micelles in aqueous solution.[6, 7, 8, 9, 10] At a concentration of 25 w/v% F88 in aqueous solution, the PPO cores aggregate together to form micelles with hydrophilic PEO coronas and hydrophobic PPO cores at a critical micellization temperature of 22.5 °C.[11, 10] F88 micelles have a diameter of approximately 17 nm and a PPO core diameter of approximately 9 nm at the aforementioned concentration and temperature.[7, 11, 10] Micelles such as these are commonly used as detergents, drug delivery polymers, and for other applications involving the uptake of small hydrophobic molecules for the purpose of improving the solubility of the hydrophobes.[12, 13, 14, 15, 1, 16, 8] Micellar nanocarriers are have shown successful results in increasing the bioavailability, improving the circulation time, and decreasing the toxicity of several drugs including doxorubicin, indomethacin, cisplatin, adriamycin, camptothecin, and many others.[12, 17, 14, 15, 13, 16, 18] Pluronic F88 is a triblock copolymer that forms such micelles. Rilpivirine is dissolved in micellar aqueous solution of 25 w/v% F88 and the fluorescence properties of rilpivirine are

applied to investigate rilpivirine spectroscopy in a complex solvent environment.

In this work, rilpivirine electronic spectroscopy is described using electronic structure calculations and optical spectroscopy methods. ZINDO calculations are performed on four conformations. These include the conformations of rilpivirine from:

1. X-ray diffraction of an anhydrous crystal
2. X-ray diffraction of an anhydrous crystal co-crystalized with DMSO in a 1 rilpivirine: 2 DMSO ratio
3. X-ray diffraction of the drug bound in the hydrophobic pocket of the 52A mutant of HIV-RT[19]
4. The geometry optimization from a ground-state density functional theory (DFT) calculation[1]

The predicted transition energies between the electronic ground state, S_0, and the first two electronic excited states, S' and S", by ZINDO methods are compared to experimental results from absorbance and fluorescence excitation spectra. The spectral properties of rilpivirine are compared in various solvents using properties such as dielectric, refractive index, and polarity to show how fluorescence spectroscopy characterizes the local environment of rilpivirine in solution.

We then look at rilpivirine spectroscopy in a more complex solvent environment. Rilpivirine is solubilized in aqueous solutions of 25 w/v% Pluronic F88 and the spectroscopy of rilpivirine molecules and aggregates are measured with variations in temperature (phase of the polymer), rilpivirine concentration (phase change of rilpivirine), and emission energy. The spectroscopy that is dependent on the aforementioned parameters is hypothesized to reveal information about the preferential form of rilpivirine in solutions where the molecule is confined by micelles or associated with polymeric unimers, the critical aggregation concentration of rilpivirine in such solutions, and the global changes in unimer fluorescence and aggregate fluorescence using a solution that contains both. For future work, this will serve as a basis for detecting the aggregation

state of rilpivirine in an unknown aqueous solution. Insight into the electronic transition pathway and transition states of both molecular and aggregated rilpivirine is found using fluorescence spectroscopy and changes over the temperature and concentration variables mentioned.

3.3 Results and Discussion: Spectroscopy, Solvatochromism, and Electronic Structure of Rilpivirine

The characterization of the molecular spectroscopy response to local environment of rilpivirine was accomplished by several methods. Fluorescence spectroscopy is the first method used to characterize the solvatochromic nature of rilpivirine. Both absorbance and excitation spectra show a transition energy in the form of peak wavelengths between the ground and the excited state. From the analysis of the emission spectra of rilpivirine measured in various solvents, a value for the difference between absorbance energy and emission energy is different in each solvent. The intercept of the plot of the difference between absorption and emission energy for rilpivirine in a range of solvents versus the solvent field factor parameter, F(ϵ_0,n), provides an estimate for the change in magnitude of the dipole moment between the ground state and the excited state using the Ooshika-Lippert-Mataga (OLM) equation.[20, 21, 22] The OLM equation and the equation for F(ϵ_0,n) are shown in Equations 3.3 and 3.2 where C is the intercept of $\tilde{\nu}_{abs}$-$\tilde{\nu}_{fluor}$ versus the field factor, F(ϵ_0,n), c is the speed of light, h is Planck's constant, and a is the hydrodynamic radius of the rilpivirine molecule.[20, 21, 22]

$$\tilde{\nu}_{abs} - \tilde{\nu}_{fluor} = \frac{2F(\epsilon, n)}{hca^3}(\mu_e - \mu_g)^2 + C \tag{3.1}$$

$$F(\epsilon, n) = f(\epsilon_0) - f(n) = \frac{\epsilon_0 - 1}{2\epsilon_0 + 1} - \frac{n^2 - 1}{n^2 + 1} \tag{3.2}$$

The emission wavelength of rilpivirine in various solvents can be correlated to the solvent polarity as shown by empirical scales such as the π^* and E_N^T.[23, 24] The second method of measuring the energies of the excited state transitions and dipole moments

of rilpivirine is ZINDO semi-empirical electronic structure calculation. Zerner's intermediate neglect of differential overlap method (ZINDO[25, 26, 27]) was used with self-consistent reaction field (SCRF) which applies a local dielectric field within a spherical cavity.[28] The solvent properties used in ZINDO-SCRF methods were matched to those used in fluorescence experiments. These two methods can be compared to measurements of electronic Stark spectroscopy, carried out by the Stanley group at Temple University. The Stark spectrum measures the electronic excited states with corresponding transition energies for the molecule in a glass such as low temperature 2-methyltetrahydrofuran (2-MeTHF). Stark spectroscopy also measures the dipole differences between the ground state and the excited state of rilpivirine, and the excited state polarizability of the molecule.[29]

Spectral properties of rilpivirine including molar extinction coefficient and quantum yield are reported. The ground to excited state transition energies and ground state and excited state dipole moments were used for comparison with experimental results. An understanding of the molecular spectroscopy of rilpivirine is helpful for the physical characterization of the drug in an unknown local environment by fluorescence methods.

3.3.1 Molar Extinction Coefficient and Quantum Yield

The Beer's law extinction coefficient for rilpivirine in dichloromethane was determined to be 50,036 $M^{-1}cm^{-1}$ at the absorption maximum of 308 nm. Absorbance spectra were used to determine the peak wavelength at the maximum optical density value for the optimum excitation wavelengths to utilize in each fluorescence emission measurement. Quantum yield measurements of rilpivirine in 1-pentane, 1,2-dichlorobenzene, dichloromethane, and DMSO were measured at room temperature using quinine sulfate in 0.1 M sulfuric acid (aq.) as a reference standard.[30] The quantum yield of rilpivirine in each of the four solvents was measured as 0.115, 0.366, 0.122, and 0.084 respectively. More information is provided in Appendix A.

3.3.2 S_0 →S' and S_0 →S" Transition Energies

When describing the electronic ground state of a molecule, S_0 is typically used to describe the electronic state of that molecule with zero energy. When energy is applied, electrons are excited to higher energy molecular orbitals and the molecule makes a transition to one or more excited states, described here as S', S", S"', etc.

The lowest energy transition from the ground to excited states S' and S" (S_0 →S' and S_0 →S") for the rilpivirine molecule were both measured by Stark[1] and fluorescence spectroscopy and calculated by ZINDO-SCRF using the four conformations displayed in Figure 3.1 and the properties of twelve solvents. These calculations of rilpivirine energies were also completed using the gas phase (no solvent or SCRF). The transitions between the ground state of the molecule and the first two electronic excited states are composed of many different orbital configurations from orbitals other than the HOMO and LUMO. The energies for the total S_0 →S' and S_0 →S" transitions found from ZINDO calculations are listed for the anhydrous crystal structure conformation of rilpivirine in Table 3.1. Energies for other conformations are listed in Appendix A.

Stark Spectroscopy

The absorption spectrum of rilpivirine in 2-methyltetrahydrofuran at room temperature and at 77 K was measured by Goutham Kodali and Prof. Robert Stanley of Temple University, Department of Chemistry.[1] The Stark spectrum of rilpivirine showed two predominant transitions corresponding to peaks at 31,500 cm^{-1} and a shoulder around 29,000 cm^{-1}.[1]

Electronic Structure Calculations

The ZINDO with SCRF was calculated for rilpivirine with twelve different solvent dielectrics . These solvents are listed in Table 3.1 with the energies of the transitions from the ground state (S_0) to the first three lowest electronic excited states (S', S", S"). The S_0 →S' energies from ZINDO were close to the transition energies found from electronic Stark and absorption spectra, as shown in Table 3.1. As expected, the peak absorbance energies are lower for rilpivirine in non-polar solvents (2-MeTHF) than

Table 3.1: Solvents, calculated reaction field factors F(ϵ,n), dielectric constants (ϵ_0) refractive indices (n) and polarities (π^* and E_T(N)) at 20 °C and transition energies (in 10^3 cm^{-1}) from fluorescence measurements ($\tilde{\nu}_{ex,n}$), and ZINDO calculations ($S_0 \rightarrow S'$ and S'').[31, 30, 23, 32]

Solvent	ϵ_0	n	π*	$\mathbf{E}_T$**(N)**	**F(**ϵ**,**n**)**	$\tilde{\nu}_{ex,1}$	$\tilde{\nu}_{ex,2}$	$\tilde{\nu}_{em}$	$\tilde{\nu}_{abs,RT}$	$\mathbf{S_0 \rightarrow S'}$	$\mathbf{S_0 \rightarrow S''}$
none										34.9	36.9
Polar Aprotic											
2-MeTHF	6.97	1.41		0.179	0.072	32.8	29.2	27.5	32.0	33.3	35.0
CCl_4	2.30	1.46	0.21	0.052	-0.135	35.5	33.0	26.9	32.9	32.6	32.8
ethyl acetate	6.03	1.37	0.45	0.228	0.079	32.3		25.3	38.0	33.2	33.3
CH_2Cl_2	9.02	1.42	0.80	0.309	0.082	36.0	31.8	25.2	32.5	29.3	31.5
DMF	37.06	1.43	0.88	0.386	0.137	31.9		22.3	35.3	31.7	34.0
DMSO	46.71	1.48	1.00	0.444	0.112	35.1	31.7	21.2	32.3	30.1	32.2
Aromatic Hydrocarbons											
1,2-DCB	10.36	1.55	0.43	0.225	0.018	32.3		25.9	32.2	28.9	31.0
toluene	2.43	1.49	0.49	0.099	-0.143	32.4		26.7	35.7	33.9	35.9
Polar H-bond Donors											
methanol	32.66	1.32	0.59	0.762	0.201	35.2	32.4	24.5	32.9	33.4	
ethylene glycol	37.70	1.43	0.92	0.713	0.135	30.8		24.8	32.4	30.1	322
formamide	111.00	1.45	0.97	0.775	0.139	36.4	29.6	24.0	32.2	29.6	31.7
water	80.00	1.33	1.09	1.000	0.211	35.7	28.9	23.9	34.0	31.3	33.4

more polar solvents (water) ranging from 32,000 to 35,700 cm^{-1}. From both Stark spectroscopy and ZINDO calculations, rilpivirine consistently shows two transitions, assigned as S_0 →S' and S_0 →S". The energies of these transitions are dependent on the solvent environment in which rilpivirine is surrounded.

From ZINDO calculations on the four conformations of rilpivirine, the S_0 →S' and S_0 →S" transitions are not simple electronic transitions from one highest occupied molecular orbital (HOMO) to a single lowest unoccupied molecular orbital (LUMO). Orbital #68 from the ZINDO Hamiltonian equation is assigned as the HOMO and orbital #69 from the ZINDO Hamiltonian is the LUMO, but the S_0 →S' transition is made up of multiple orbital-to-orbital transitions ranging from the orbitals HOMO-8 to LUMO+8 contributing to the electronic transition states. The true S_0 →S' transition, according to ZINDO calculations, can be described by at least ten different orbitals contributing to the transition. For example, Figure 3.2 shows the electronic surface plots of ten orbitals that contribute to 90% of the two lowest energy excited state transitions for the configuration of rilpivirine in the anhydrous crystal structure with 2-MeTHF solvent environment. Table 3.2 describes the contribution of each orbital-to-orbital transition using normalized coefficients ($c_{i,j}$) . These coefficients can be viewed as fractional percentages of the total contribution to the S_0 →S' or S" electronic transition. In the case of the anhydrous crystal structure conformation of rilpivirine in 2-MeTHF, the S_0 →S' has 13 orbital transitions contributing to the excited state, with orbital transition HOMO-3 to LUMO accounting for 29.5%. Similarly, in the corresponding S_0 →S" transition, the HOMO-1 to LUMO transition accounts for 23.4% of the total contribution. Also listed for the anhydrous crystal structure conformation of rilpivirine are the analogous results when DMSO and water solvent parameters were used in the SCRF. Orbital surface density plots and data tables for the other two conformations in 2-MeTHF, DMSO, and water can be found in Appendix A.

Fluorescence Spectroscopy

The emission and excitation spectra of rilpivirine are dependent on the polarity and dielectric constant of the solvent in which rilpivirine is dissolved. Non-polar solvents

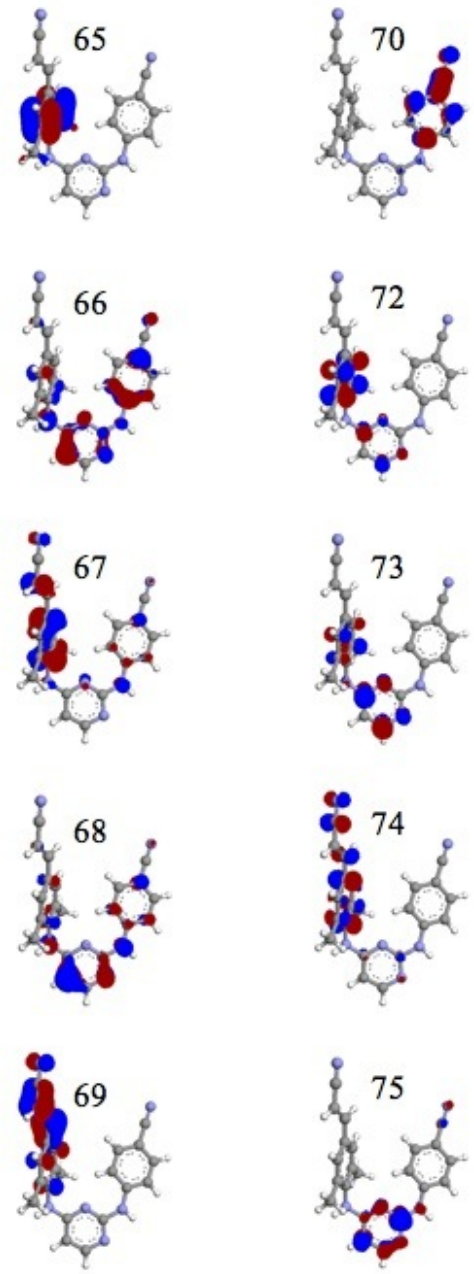

Figure 3.2: Molecular orbital surface plots of rilpivirine from ZINDO[33] calculations of the anhydrous crystal conformation in the electronic states of orbitals contributing to the $S_0 \rightarrow$S' and $S_0 \rightarrow$S" transitions, using 2-MeTHF solvent parameters in SCRF method. For the ZINDO Hamiltonian, the HOMO is designated as orbital 68 andthe LUMO is orbital 69.

Table 3.2: Orbitals that contribute to 90% of the S_0 →S' and the S_0 →S" transitions, with corresponding coefficients ($c_{i,j}$) from ZINDO-SCRF calculations of the anhydrous crystal structure conformation of rilpivirine in 2-MeTHF (ϵ = 6.97, n = 1.405, and r_{cavity} = 6.046 Å). Orbital 68 is the HOMO and orbital 69 is the LUMO for the ZINDO Hamiltonian.

Solvent	orbitals for S_0 →S'	$c_{i,j}$	orbitals for S_0 →S"	$c_{i,j}$
2-MeTHF	67→69	0.234	68→70	0.451
	68→69	0.190	67→ 69	0.139
	65→69	0.121	67→ 70	0.122
	68→73	0.105	68→ 69	0.066
	68→70	0.066	66→ 70	0.058
	68→70	0.066	68→ 75	0.048
	67→72	0.052	68→ 73	0.009
	67→73	0.039	68→ 72	0.009
	66→72	0.026	65→ 70	0.007
	67→70	0.019	66→ 75	0.007
	65→74	0.017	63→ 71	0.006
	66→70	0.009	68→ 74	0.005
	68→74	0.005	59→ 75	0.005
DMSO	67→69	0.452	68→70	0.541
	68→69	0.296	66→70	0.116
	68→70	0.066	67→70	0.091
	68→73	0.041	67→69	0.078
	68→75	0.024	68→77	0.055
	66→70	0.017	68→69	0.047
	66→69	0.013	68→75	0.008
	67→70	0.013	62→71	0.007
water	67→ 69	0.445	68→70	0.509
	68→ 69	0.279	66→70	0.105
	68→ 70	0.069	67→70	0.0989
	68→ 73	0.060	67→69	0.089
	66→ 70	0.017	68→77	0.055
	67→ 70	0.015	68→69	0.046
	65→ 69	0.014	68→ 71	0.008
	66→ 69	0.014	66→ 71	0.008
none	68→69	0.221	67→ 69	0.336
	68→71	0.201	68→ 69	0.177
	67→69	0.194	68→ 71	0.155
	65→71	0.121	68→ 70	0.087
	68→70	0.107	65→ 71	0.050
	67→70	0.046	65→ 74	0.0246
	63→71	0.015	67→ 70	0.024
	67→71	0.011	62→ 71	0.018
	65→74	0.009	68→ 74	0.015
	59→74	0.009	67→ 71	0.014

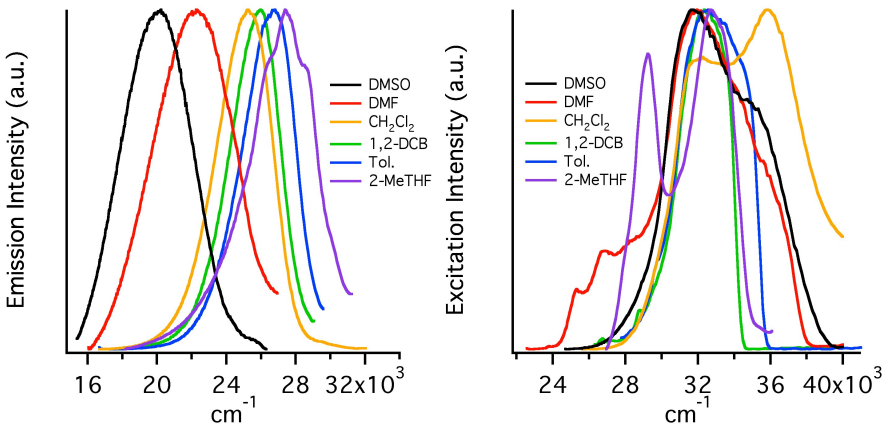

Figure 3.3: Emission (left) and excitation spectra (right) of rilpivirine in some selected solvents. (DMSO, DMF, CH_2Cl_2, 1,2-DCB, toluene, and 2-MeTHF)

such as 2-MeTHF and toluene cause rilpivirine to emit fluorescence at shorter wavelengths (higher energy) than polar solvents such as DMSO or water. Figure 6.2 displays some selected emission and excitation spectra of rilpivirine in a range of polarities from DMSO to 2-MeTHF. Figure 3.4 displays the peak frequency values for rilpivirine in twelve solvents measured as a function of the solvent polarity using the π^* empirical polarity scale. Some excitation spectra were fit to multiple peaks and all peak energies are presented in Figure 3.4. The peak values are listed in Table 3.1 along with the corresponding energies found from Stark measurements[1] and ZINDO calculations.

3.3.3 Molecular Dipole Moments

The difference in dipole moments were obtained in several ways. ZINDO electronic structure calculations can predict both ground and excited state dipole moments and dipole moment vectors. Electronic Stark spectroscopy measures the change in dipole moment associated with the excited state transition.[29] The spectral analysis of the electronic Stark spectrum of rilpivirine gave difference dipole moments for two electronic transitions: $S_0 \rightarrow$S' and $S_0 \rightarrow$S". Using local field correction factors of 1.1 to 1.4[34], the difference dioples are estimated to be 9.0±1.0 D and 11.8±1.3 D for the two transitions, respectively.[1] These electronic Stark measurements were performed by Goutham Kodali and Prof. Robert J. Stanley of Temple University Department of

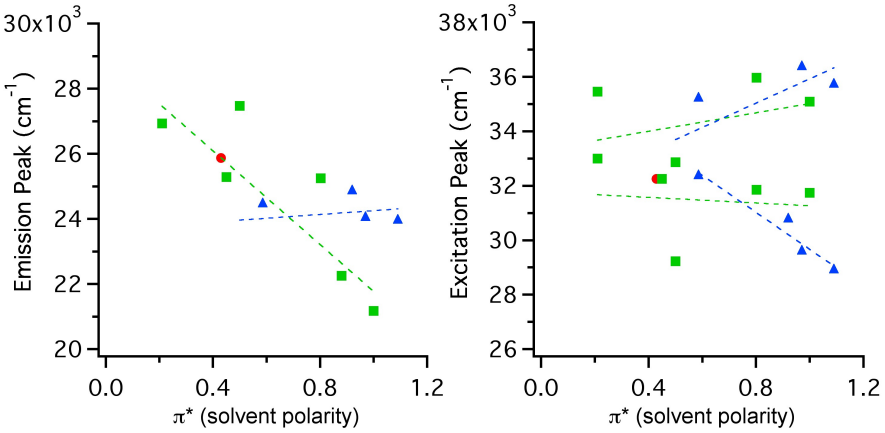

Figure 3.4: Emission (left) and excitation (right) peak reduced frequencies of rilpivirine in some selected solvents plotted versus solvent polarity in the π^* polarity scale for aromatic solvents ($\circ$), polar aprotic solvents ($\square$), and hydrogen-bond donating solvents ($\triangle$).

Chemistry.[1] When the absorbance and fluorescence spectra of a fluorophore are measured in a range of solvents that vary in dielectric and refractive index, the Ooshika-Lippert-Mataga (OLM) equation (Equation 3.3) can predict the change in dipole moment between the ground state and the emitting excited state.[20, 21, 22, 30, 31] All three of these methods are utilized for characterizing the difference dipole moments of the rilpivirine molecule.

Electronic Structure Calculations

Ground state (S_0) and excited state (S', S") dipole moments were calculated using the ZINDO-SCRF method and the difference dipole moment between the ground and excited states ware graphed for comparison with the difference dipole moments found from fluorescence and Stark spectroscopy. Table 3.3 shows the difference dipole moments found from each of these methods.

The difference dipole moment from the ground state to the first electronic excited state as predicted by ZINDO calculations of the rilpivirine conformation in the anhydrous crystal varies from 1.50 D using toluene properties in SCRF to 10.85 D using the properties of 1,2-dichlorobenzene. For the conformation of rilpivirine in the anhydrous

crystal with 2 DMSO molecules per one drug molecule, the change in dipole moment ranges from -2.17 D in 1,2-dichlorobenzene to 14.16 D in toluene. For the structure of rilpivirine as bound to HIV-1 RT, the change in dipole moment ranges from 1.55 D in 2-MeTHF to 18.9 D in dichloromethane, 1,2-dichlorobenzene, and formamide. The large differences in dipole moment between ground and excited states are a likely cause for the large solvatochromic shift observed in the fluorescence spectrum of rilpivirine.

Fluorescence Spectra and Solvatochromic Shift

$$\tilde{\nu}_{abs} - \tilde{\nu}_{fluor} = \frac{2F(\epsilon, n)}{hca^3}(\mu_e - \mu_g)^2 + C \tag{3.3}$$

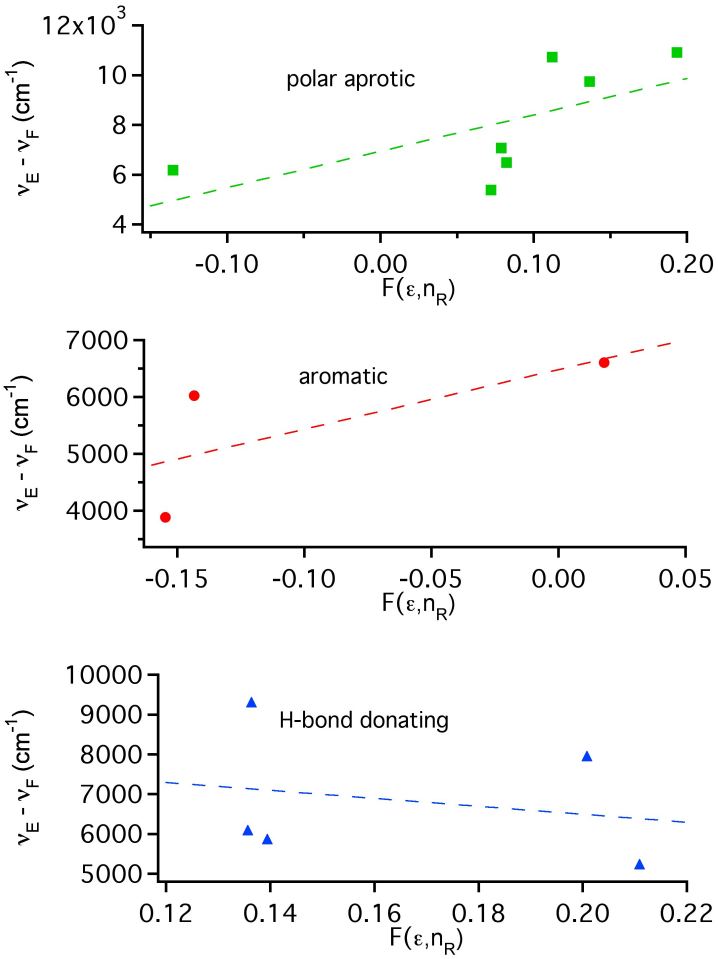

Figure 3.5: Ooshika-Lippert-Mataga plots of Stokes shift versus reaction field factor for polar aprotic solvents (top), aromatic solvents (center) and hydrogen-bond donating solvents (bottom).

The reaction field factor is dependent on ϵ_0 and n where ϵ_0 is the dielectric constant and n is the refractive index of the solvent.[31, 30] From the graph of $\tilde{\nu}_{abs}$ - $\tilde{\nu}_{fluor}$ versus the reaction field factor in Figure 3.5, the resulting values for the difference dipole moment between the ground and excited states of rilpivirine are presented in Table 3.3. These values of μ_e - μ_g range from 12.5 (in ethyl acetate) to 56.1 D (in DMSO). The large shift in dipole moment causes rilpivirine to have a large solvatochromic shift in the fluorescence emission spectrum between polar and non-polar solvents.[31, 30] In turn, this quality enables the fluorescence spectrum of rilpivirine to be related to the local solvent polarity in an unknown solvent environment. The difference dipole moments found from theoretical and experimental methods are listed in Table 3.3. These dipole moments are compared to the difference dipole moments of 9.0 ±1.0 and 11.8±1.3 D found from electronic Stark spectroscopy for S_0 →S' and S_0 →S", respectively.[1]

3.3.4 Aggregation of Rilpivirine

Stokes-Einstein-Debye hydrodynamics relates the reorientation time constant of the rilpivirine molecule to the solvent viscosity and the volume of the reorienting body.[30, 31] 1-Pentane, 1-hexane, acetonitrile, and benzene are outliers from the predicted reorientation time constants from using the S-E-D equation (see Equation 3.4). Deviations from predicted S-E-D hydrodynamics are shown by reorientation time constants with calculated hydrodynamic volumes that are larger than the molecular van der Waals volumes by factors of: 848 (1-pentane), 373 (acetonitrile), 181 (benzene) and 109 times (1-hexane) the molecular volume of rilpivirine. The large reorientational motions and associated hydrodynamic volumes indicate that rilpivirine forms aggregates in 1-pentane, acetonitrile, benzene, and 1-hexane.

Reorientation dynamics of rilpivirine are fit using single-exponential decays yielding one reorientation time constant for rilpivirine in each solvent. The reorientation time constants are dependent on the volume of the reorienting species, temperature and solvent viscosity and can be related by the S-E-D equation, shown in Equation 3.4 where θ_{rot} is reorientation time constant, V is volume of the reorienting species, η is solvent viscosity, k_B is Boltzmann's constant, and T is absolute temperature.[31, 30, 35, 36]

Table 3.3: The calculated change in magnitude of dipole moment $\triangle\mu_{fluor}$ (in units of D) of rilpivirine in aprotic, aromatic, and hydrogen-bonding solvents from fluorescence measurements at 20 °C and the OLM equation (3.3), the difference dipole moments from ZINDO-SCRF calculations for the first and second excited state transitions, S' and S" for the anhydrous crystal form (AN), the anhydrous / 2DMSO crystal form (AD), the RT-bound conformation (RT), and the geoemetry optimzied structure from DFT calculations(DFT).[31, 30, 23, 32]

Solvent	OLM	S' (AN)	S" (AN)	S' (AD)	S" (AD)	S' (RT)	S" (RT)	S' (DFT)	S" (DFT)
none		3.08	0.85	1.79	0.86	-3.79	0.53	2.6187	2.464
Polar Aprotics									
CCl_4	23.0	4.51	4.64	3.06	6.21	6.32	8.84		
ethyl acetate	12.5	3.79	5.13	6.28	1.88	6.15	8.78		
CH_2Cl_2	-	10.82	10.86	10.38	10.68	3.15	-2.85		
DMF	43.7	8.56	6.56	8.14	1.79	2.63	2.79		
DMSO	56.1	10.22	10.24	9.85	6.69	6.36	7.25		
2-MeTHF	-	5.28	6.97	6.29	0.79	6.07	8.77	7.38	7.28
Aromatic Hydrocarbons									
1,2-DCB	25.0	10.85	10.89	10.41	10.73	9.08	11.09		
toluene	17.3	4.73	4.72	4.91	2.85	3.23	3.50		
Polar H-bond Donators									
methanol	-	5.99	3.62	3.99	5.70	6.51	9.33		
ethylene glycol	-	10.27	3.41	10.71	4.03	6.56	7.13		
formamide	-	10.81	10.85	3.99	1.50	10.38	2.55		
water	-	9.31	9.20	8.96	3.16	17.90	8.38		

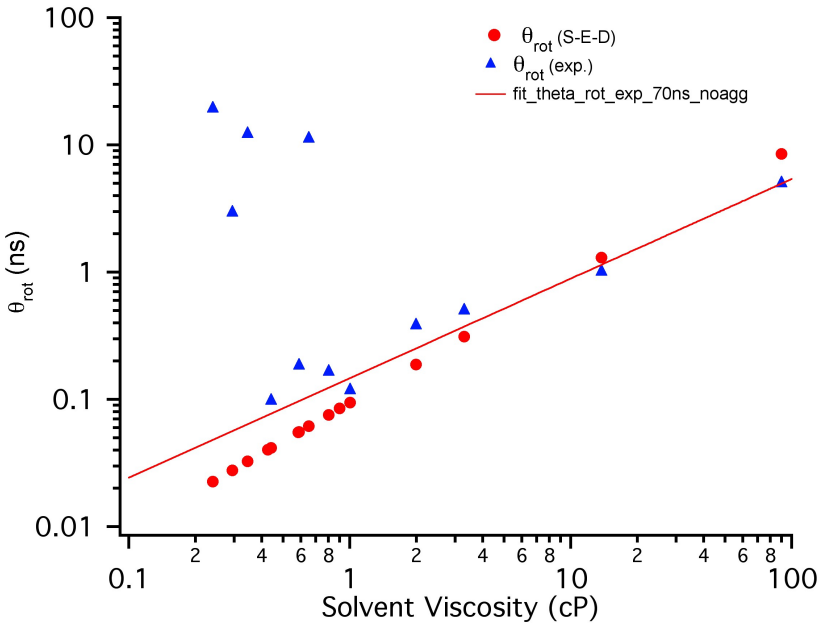

Figure 3.6: Predicted reorientation time constants of rilpivirine from S-E-D hydrodynamics (○) and measured reorientation time constants from TCSPC data (△) versus solvent viscosity for concentrations in the range of 0.3 to 76 μM rilpivirine.

$$\theta_{rot} = \frac{V\eta}{k_B T} \tag{3.4}$$

If the reorientation time constants of rilpivirine are graphed with solvent viscosity, the logarithmic fit results in the relationship between rilpivirine and the effective solvent viscosity: $\theta_{rot} = 0.147(\pm 0.02)\eta^{0.602\pm 0.04}$. This model deviates from predicted S-E-D hydrodynamic theory because of factors such as slip and stick hydrodynamics, solvent shape, and the change in fluorophore shape during excitation and emission.[37, 38, 39, 40] S-E-D assumes a spherical reorienting species, while rilpivirine has a butterfly conformation, as measured by crystal structures and predicted by electronic structure calculations.[4, 1]

Solvents such as 1-pentane, 1-hexane, acetonitrile, and benzene cause rilpivirine to aggregate in solution with hydrodynamic volumes from approximately 109 to 850 times the hydrodynamic volume of one rilpivirine molecule. The difference between the reorientation time constants of rilpivirine in these four solvents and expected reorientation

Table 3.4: Solvent viscosity (η in cP), reorientation time constants ($\theta_{rot,i}$), relative amplitudes ($r_{rot,i}$), limiting anistoropies (r_0), average time constants ($\theta_{rot,avg}$) and S-E-D (see Equation 3.4) predicted reorientation time constants of rilpivirine in various solvents. All θ_{rot}'s are in ns.

Solvent	η	$r_{rot,1}$	$r_{rot,2}$	$r_{rot,0}$	$\theta_{rot,1}$	$\theta_{rot,2}$	$\theta_{rot,avg}$	S-E-D θ_{rot}
1-pentane	0.24	0.39	0.00	0.39	19.25	0.00	19.25	0.023
1-hexane	0.29	0.26	0.245	0.55	5.86	0.25	2.93	0.028
acetonitrile	0.35	0.17	0.00	0.17	12.17	0.00	12.17	0.033
CH_2Cl_2	0.44	0.19	0.00	0.19	0.10	0.00	0.10	0.042
methanol	0.59	0.17	0.00	0.17	0.15	0.00	0.15	0.055
benzene	0.65	0.25	0.17	0.43	18.80	0.06	11.17	0.062
DMF	0.80	0.14	0.00	0.14	0.17	0.00	0.17	0.076
water	1.00	0.01	0.00	0.01	0.12	0.00	0.12	0.095
DMSO	2.00	0.17	0.00	0.17	0.38	0.00	0.38	0.189
formamide	3.30	0.16	0.00	0.16	0.50	0.00	0.50	0.312
ethylene glycol	13.80	0.14	0.09	0.22	1.60	0.11	1.01	1.306

time constants of single rilpivirine unimers is not two or three fold, but 100-fold or more. Rilpivirine is not forming dimers or trimers in these solvents, but aggregates of 109 to 850 rilpivirine molecules. If rilpivirine was forming dimers and trimers, the reorientation time constants would reflect an approximate two-fold increase from S-E-D hydrodynamic theory. Instead, the reorientational dynamics reflect single unimers and larger aggregate nanoparticles.

3.4 Results and Discussion: Rilpivirine Spectroscopy in Aqueous Solutions of A-B-A Triblock Copolymer F88

The spectroscopy of rilpivirine in aqueous solutions of A-B-A triblock copolymer Pluronic F88 is measured for four different objectives. The first goal is to detect the differences between the unimer form of rilpivirine and the aggregate form of rilpivirine in possible delivery formulations. This concentration dependence of rilpivirine in aqueous micellar F88 solution was measured with steady-state emission and excitation spectra, fluorescence time constants, and polarization anisotropies.

The second reason to measure rilpivirine fluorescence in aqueous F88 solutions is to investigate changes in aggregation state and local environment of rilpivirine in the different aqueous polymer phases of F88: unimers, micelles, and hydrogels. This study poses the questions of whether rilpivirine is encapsulated in polymer micelles, or forms

aggregates in the aqueous phase of F88 solutions. For these experiments, the temperature dependence of the spectroscopy of rilpivirine was measured in an aqueous solution of 25 w/v% F88 polymer at a single drug concentration where the drug is in both unimer and aggregate form.

Thirdly, the emission wavelength of rilpivirine is dependent on the unimer or aggregate state of the drug in solution. In aqueous solutions of F88 micelles, where the drug is present in both unimer and aggregate forms, the fluorescence dynamics and reorientational dynamics are investigated using time-resolved fluorescence spectroscopy. Depending on the single emission wavelength measured during these experiments, the fluorescence time constants change depending on the aggregation state emitting at that wavelength. In this way, it is hypothesized that the different aggregation states can be identified based on the detected wavelength.

The fourth set of experiments regarding rilpivirine in aqueous F88 solutions is the measurement of the time-resolved emission spectrum (TRES) of the drug. TRES measures the shift in emission spectrum over the fluorescence lifetime.[30] The shift in emission energy shifts as a result of solvent relaxation, hence the solvent relaxation time constants are measured as the rate of the emission shift. TRES is first measured for rilpivirine in a solvent in which rilpivirine is not forming aggregates: dichloromethane (CH_2Cl_2). TRES is also measured in a single solvent in which rilpivirine is forming aggregates: 1-pentane. These TRES results are then compared to the TRES of 5.8 μM rilpivirine in aqueous solution of 25 w/v% F88 at various temperatures (F88 phases). These investigations of rilpivirine spectroscopy are a foundation for measuring the spectroscopy of rilpivirine in unknown local solvent environments.

3.4.1 Concentration Dependence of Rilpivirine Spectra

Seven solutions of different concentrations of rilpivirine were made in aqueous solutions of 25 w/v% F88 at 30 °C. The drug concentrations range from 1 μM to 84 μM rilpivirine drug in aqueous F88 solution. The absorbance spectrum of rilpivirine in each solution was measured to obtain the exact concentrations of drug. The fluorescence excitation and emission spectra of these solutions were measured at 30 °C. The concentration

dependence of the average fluorescence time constants are reported.

Fluorescence Emission and Excitation

The concentration dependent emission and excitation spectra are shown in Figure 3.7 where it is clearly displayed that two emission and two excitation peak energies are shifting with increasing concentration of rilpivirine. The peaks energies, in cm^{-1}, are reported in Table 3.5 At 1.0 μM rilpivirine, the emission band is a single peak at 29,900 cm^{-1}. As the concentration of rilpivirine is increased, an emission band at 25,000 cm^{-1} appears and increases in amplitude while the emission at 29,900 cm^{-1} decreases in amplitude and then disappears. The fluorescence peak at 25,000 cm^{-1} results from the formation of rilpivirine aggregates in solution and appears at a concentration of 2.0 μM drug in solution. The emission peak at 25,000 cm^{-1} is not associated with excimers, but is a separate emission band associated with fluorescence from drug aggregates. The emission band associated with the unimer form of rilpivirine is decreasing in amplitude, indicating that this population is decreasing as the drug aggregates. The excitation spectrum of rilpivirine shows similar behavior with regard to drug concentration. At 1.0 μM drug concentration, an excitation fluorescence band is present at 37,000 cm^{-1}. At concentrations between 6 and 13 μM rilpivirine, a second band associated with aggregate formation appears at 32,000 $cm^{-1}$and shifts to 30,000 cm^{-1} at a concentration of 84 μM rilpivirine. Figure 3.9 displays the frequencies of the emission and excitation peaks of rilpivirine at various concentrations and three temperatures: 2.5, 30, and 90 °C, where the polymer solution is in aqueous unimer, micelle, and hydrogel phases, respectively. The change in two distinct peak energies and relative amplitudes in both emission and excitation spectra indicate that unimer and aggregate rilpivirine both absorb and fluoresce at different energies. The two forms of the drug in solution are easily distinguishable by fluorescence spectroscopy.

Table 3.5: Rilpivirine unimer (uni) and aggregate (agg) fluorescence emission and excitation spectral peak energies (λ in nm and $\tilde{\nu}$ in 10^3 cm^{-1}) for various concentrations (in μM) of rilpivirine in aqueous solution of 25 w/v% Pluronic F88 at 30 °C.

[Rilpivirine]	$\lambda_{em,uni}$	$\tilde{\nu}_{em,uni}$	$\lambda_{em,agg}$	$\tilde{\nu}_{em,agg}$	$\lambda_{ex,uni}$	$\tilde{\nu}_{ex,uni}$	$\lambda_{ex,agg}$	$\tilde{\nu}_{ex,agg}$
84			413	24.2	261	38.3	337	29.7
35	345	29.0	413	24.2	277	36.1	327	30.6
13	347	28.9	401	24.9	278	36.0	315	31.7
5.8	331	30.2	399	25.1	267	37.4		
2.4	337	29.7	392	25.5	268	37.3		
2.0	335	29.8			268	37.3		
1.0	334	29.9			268	37.3		

Fluorescence Dynamics

The time-resolved fluorescence transients for the same seven concentrations of rilpivirine in aqueous solutions of F88 micelles were measured at two different emission wavelengths. The concentration-dependent intensity-weighted average time constants[31] are presented in Figure 3.9. With regard to concentration dependence of rilpivirine, the average fluorescence time constant decreases with increasing concentration of rilpivirine. When the time constants of rilpivirine were measured at 345 nm emission associated with the unimer form of rilpivirine, the average fluorescence time constant decreased from 6.6 to 1.6 ns with increasing concentration. When the time-resolved transients were measured at 410 nm emission, the wavelength associated with aggregate rilpivirine, the average fluorescence time constant decreased from 5.9 to 1.6 ns with increasing concentration.

3.4.2 Temperature Dependence of Rilpivirine Spectra

The temperature dependence of rilpivirine fluorescence spectroscopy in aqueous solutions of Pluronic F88 depends on two variables. The first variable is the phase of the A-B-A triblock copolymer in solution. Rilpivirine will be localized in regions of different polarity and local friction and fluorescence spectroscopy will detect these differences. The second variable is the aggregation state of rilpivirine. It has already been shown that various fluorescence measurements can be used to detect the presence of aggregates and differentiate the presence of drug unimers in solution. In the following section, both

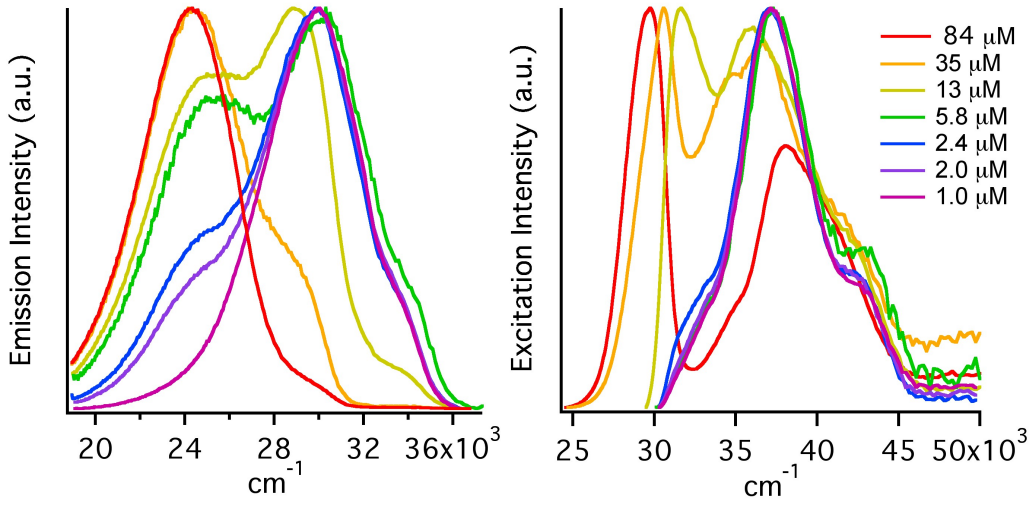

Figure 3.7: Fluorescence emission (left) and excitation (right) at seven concentrations of rilpivirine in aqueous solution of 25 w/v% F88 at 30 °C.

of these variables will be explored at different temperatures between 2.5 and 90 °C.

Fluorescence Emission and Excitation Spectra

The fluorescence emission spectrum of 5.8 μM rilpivirine in aqueous solution of 25 w/v% F88 shows a shift for both of the spectral peak energies discussed in the last section. The normalized spectra are shown in Figure 6.3. The first emission band at approximately 29,850 cm^{-1} at 2.5 °C shifts to higher energy of approximately 30,300 cm^{-1} with a direct correlation to the temperature at which the copolymer forms micelles in solution. This emission spectrum showing a 30,300 cm^{-1} frequency peak corresponds to a population of the rilpivirine drug that is in a polymeric unimer environment in aqueous solution. As the polymer aggregates, the rilpivirine drug is solubilized into the hydrophobic micelle core. The small solvatochromic shift of rilpivirine emission indicates that a population of the drug is moving to a more non-polar environment. At approximately 26,300 cm^{-1}, a second peak emerges in the emission spectrum, corresponding to an aggregated population of rilpivirine in aqueous polymer solution. The emission band at 26,300 cm^{-1} shifts to approximately 25,000 cm^{-1} upon polymer micellization. The intensity of the 26,300 cm^{-1} peak also increases upon micellization, indicating that

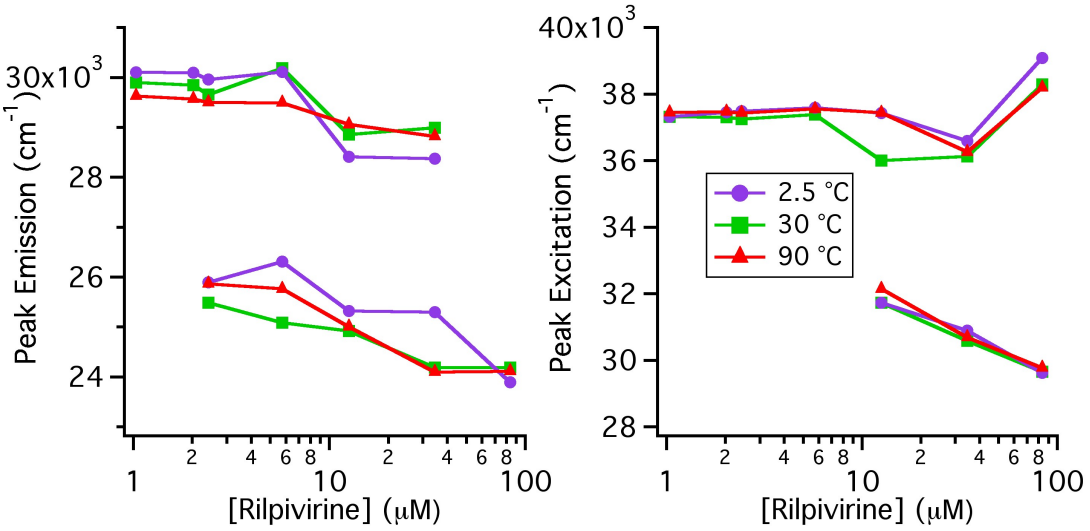

Figure 3.8: Frequencies of fluorescence emission (left) and excitation (right) peaks of rilpivirine at seven concentrations in aqueous solution of 25 w/v% Pluronic F88 at 2.5, 30, and 90 °C.

rilpivirine aggregates are present in the polymeric unimer solution at low temperatures, but the population of rilpivirine aggregates increases as the polymer forms micelles. The shift of the aggregate emission energy at higher temperatures is characteristic of the spectral behavior of aggregate formation.[30]

The other six concentrations of rilpivirine samples were also measured using temperature-dependent fluorescence spectroscopy. The peaks are displayed in Figure 3.11. There is an increase in emission peak energy at the micellization temperature (22.5 °C) of the aqueous Pluronic F88 solution, as shown by the 28,000 to 31,000 cm^{-1} peak for 35, 13, and 5.8 μM rilpivirine concentrations. The shift to higher energies indicates a change in local polarity of the unimer form of rilpivirine to more non-polar environments, consistent with the solubilization of rilpivirine in the the PPO core of triblock copolymer micelles.[10] It is known from the previous experimental results that the emission peak energy increases with decreasing polarity of rilpivirine's solvent environment. Rilpivirine unimers are encapsulated by F88 micelles in solution.

The rilpivirine aggregate emission energy from 23,000 to 26,000 cm^{-1} decreases in

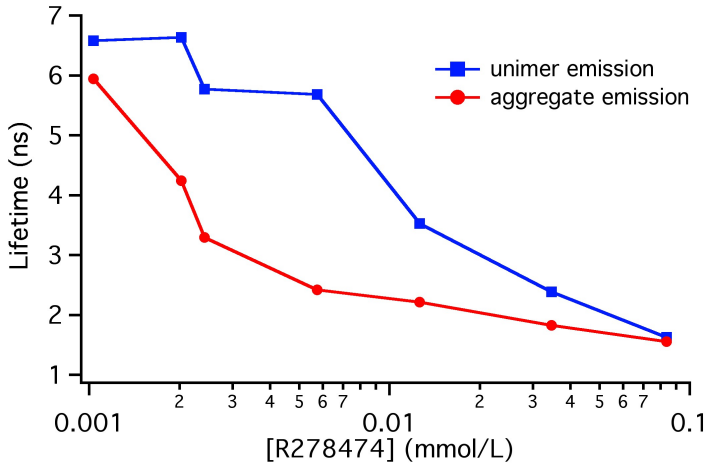

Figure 3.9: Average fluorescence time constants of rilpivirine at seven concentrations in aqueous solutions of 25 w/v% Pluronic F88 measured at 345 nm (unimers) and 410 nm (aggregates).

energy when the F88 polymer forms micelles in aqueous solution at rilpivirine concentrations of 35, 13, 5.8, and 2.4 μM. The local environment of the aggregates in these solutions is increasing in polarity. This shift to lower energies is consistent with aggregates forming in the bulk water of the aqueous F88 micelle solution and not in the PPO micellar cores. At the highest concentration of rilpivirine, the peak emission around 24,000 cm^{-1} shifts to higher energy at the micellization temperature of the A-B-A triblock copolymer. At this high concentration, the aggregate local environment is decreasing in polarity, but the local environment in the aqueous solution of F88 micelles is consistent with the local environment of aggregates at lower concentrations.

The temperature dependence of the rilpivirine excitation spectral peak energies is shown in Figure 3.11. The excitation spectra of the highest concentrations of rilpivirine (84, 35, 13) exhibit two bands, corresponding to both unimer and aggregate forms of the drug. A peak around 30,000 to 32,000 cm^{-1} is assigned to the aggregate form of rilpivirine and a band around 36,000 to 39,000 cm^{-1} is assigned to the unimer form of rilpivirine in solution. The lower concentrations of rilpivirine exhibit only the latter peak, which does not shift significantly as aqueous F88 forms micelles above 22.5 °C. The same excitation spectral peak for higher concentrations of rilpivirine decrease at

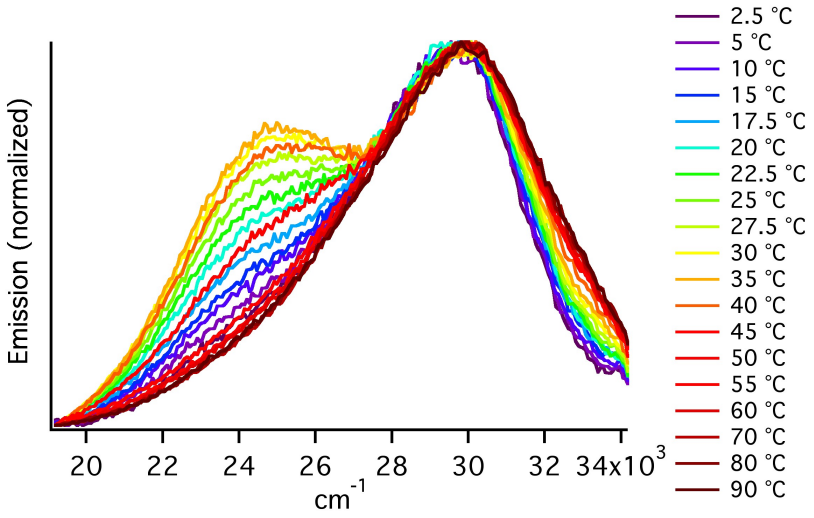

Figure 3.10: Normalized emission spectra of 5.8 μM rilpivirine in 25 w/v% Pluronic F88 in aqueous solution at different temperatures.

22.5 °C, consistent with a shift from rilpivirine unimers to aggregates.

Fluorescence Dynamics

The fluorescence time constants of 5.8 μM rilpivirine are measured at 6 temperatures from 5 to 80 °C in PEG 300 and PPO 3500 polymer solvents as control experiments. The fluorescence transients of rilpivirine in PEG 300 were fit to a sum of four exponential decay functions, revealing four individual fluorescence time constants. The individual time constants with corresponding amplitudes and the intensity-weighted average time constant are shown in Figures 3.12 and 3.13. The individual time constants of rilpivirine in PEG 300 shift from 0.21, 0.62, 1.37, and 3.71 ns at 5 °C to 0.05, 0.24, 0.80, and 7.05 ns at 80 °C. The average time constant of rilpivirine in PEG 300 shifts from 1.49 to 1.12 ns over the same temperature range.

The fluorescence transients of rilpivirine in PPO 3500 polymer solvent were also fit to a sum of four exponential decay functions. The four individual time constants of rilpivirine in PPO 3500 are 0.02, 0.71, 2.72, and 3.59 ns at 5 °C and shift to 0.09, 0.72, 1.50, and 3.55 ns at 80 °C. The average fluorescence time constant shifts from 3.06 to 1.71 over the same temperature range. These individual and average fluorescence time

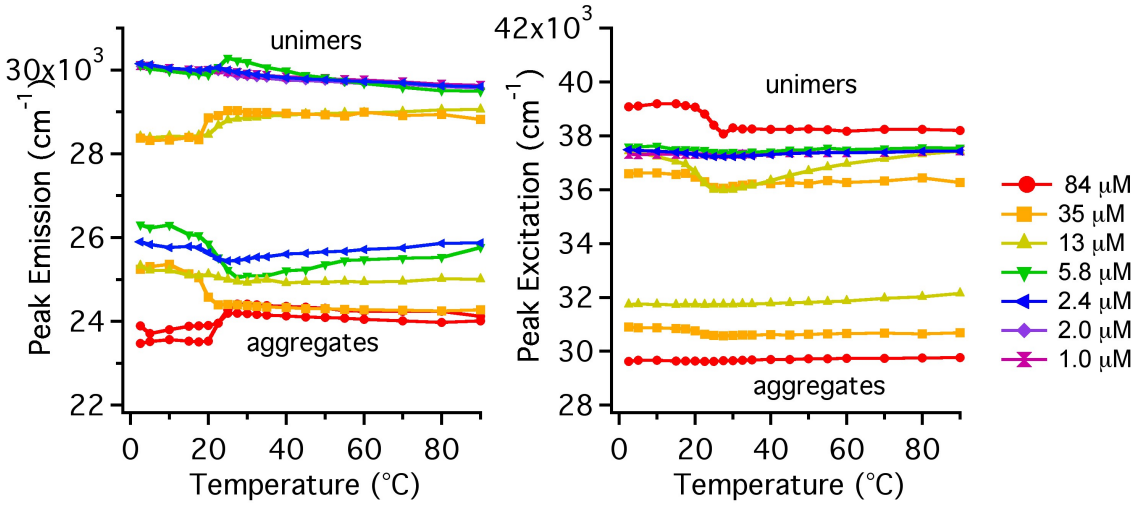

Figure 3.11: Temperature dependence of emission and excitation peak energies for 6 concentrations of rilpivirine in aqueous solution of 25 w/v% Pluronic F88. The separation between the spectral peaks of unimers and aggregates is clearly shown.

constants will be used for comparison of the time constants measured for rilpivirine in aqueous solutions of 25 w/v% F88.

The temperature-dependent fluorescence transients of rilpivirine in aqueous solution of 25 w/v% F88 were fit to a sum of six exponential decay functions, revealing six individual fluorescence time constants with corresponding normalized amplitudes. The fluorescence transients were measured at the 385 nm emission energy associated with rilpivirine aggregates. The values of the individual time constants with changing temperature of the aqueous F88 polymer solution are shown in Figure 3.14. The six time constants in unimer solution at 2.5 °C are 0.03, 0.13, 0.40, 1.40, 5.21, and 14.25 ns. In micelle solution at 25 °C, the time constants increase to 0.07, 0.26, 0.66, 2.24, 7.21, and 26.84 ns. The five smallest of the six individual time constants of rilpivirine in aqueous F88 solution can be assigned to rilpivirine in a PEG environment, as the time constants of rilpivirine in PEG 300 are very similar. The time constants of rilpivirine in PPO 3500 are somewhat similar to the 1.4 and 5 ns time constants measured in aqueous F88 solution, but these time constants are also consistent with rilpivirine in PEG 300. The smallest of the time constants at approximately 30 to 90 ps may be

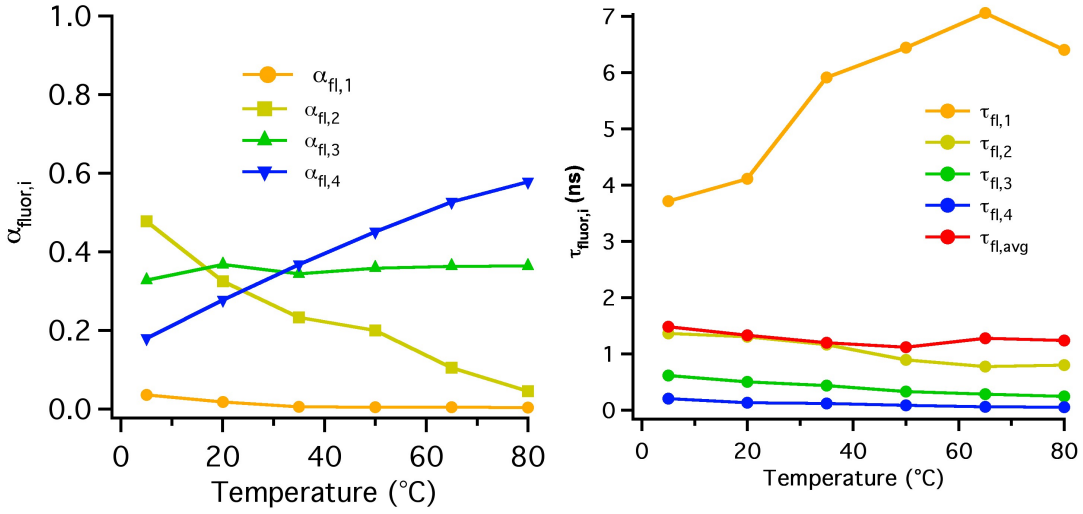

Figure 3.12: Fluorescence time constants of 5.8 μM rilpivirine in poly(ethylene glycol) (M_w 300) at various temperatures.

associated with rilpivirine in a PPO environment within F88 unimers in solution. The largest time constant (14 to 26 ns) is not comparable to any time constant measured in either PEG or PPO solution and so may be assigned to rilpivirine unimers in an aqueous polymer environment.

The six individual fluorescence time constants actually shift very little as the A-B-A triblock copolymer changes from unimer to micelles to hydrogels in solution. There is a small but sharp shift in all of the individual time constants at the 22.5 °C consistent with the temperature at which F88 micelles form.[10] The more noticeable shift in fluorescence time constant is that of the average of the six individuals. Because the two highest normalized amplitudes (which are associated with the two smallest time constants) diverge and are predominant in the intensity-weighed average, the average fluorescence time constant decreases from 6.8 to 3.6 ns over the F88 transition from unimers to micelles. Above 30 °C, the average time constant increases back up to 6.6 ns as F88 forms a hydrogel. Because the rilpivirine aggregates are not likely inside the F88 micelle cores, the shift in fluorescence time constant indicates that the aggregates are associating with unimers at low temperatures, change local environments in the bulk water of micelle solutions, and are again associated with F88 polymer in the hydrogel

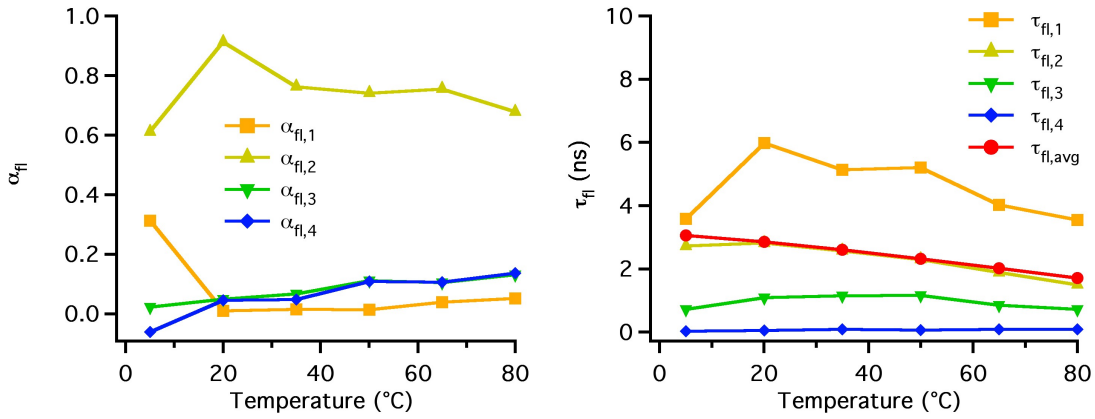

Figure 3.13: Fluorescence time constants of rilpivirine (5.8 μM) in poly(propylene oxide) (M_w 3500) at various temperatures.

at higher temperatures.

Reorientational Dynamics from Polarization Anisotropy

The temperature dependence of the reorientational dynamics of rilpivirine in 25 w/v% F88, in PEG 400, and in PPO 2000 are measured and compared. Because A-B-A triblock copolymer F88 is composed of PEG A-blocks and PPO B-blocks, these solvents were used as a control for measuring the reorientation time constants in aqueous unimer, micelle and hydrogel solutions of F88. The time-resolved fluorescence of rilpivirine in 25 w/v% F88 in aqueous solution was measured at 25,640 cm^{-1} emission, the emission peak of the rilpivirine aggregates.

Figure 3.15 shows the polarization anisotropy ($r_{rot,j}$) and the reorientational time constants ($\theta_{rot,j}$) over six temperatures for rilpivirine in PEG 400 and PPO 2000. The r_0 value, or the limiting anisotropy is a measure of the reorientational motion of the rilpivirine fluorophore. For rilpivirine in PEG 400, the r_0 value increases slightly, but is fairly constant over the measured temperature range, displaying that rilpivirine is not experiencing any large changes in reorientational motion. Rilpivirine in PEG 400 was found to have a single exponential anisotropy decay, r(t) (See Chapter 2) having one reorientation time constant that decreased with increasing temperature of the polymer. The reorientation time constant decreases because rilpivirine is reorienting at faster

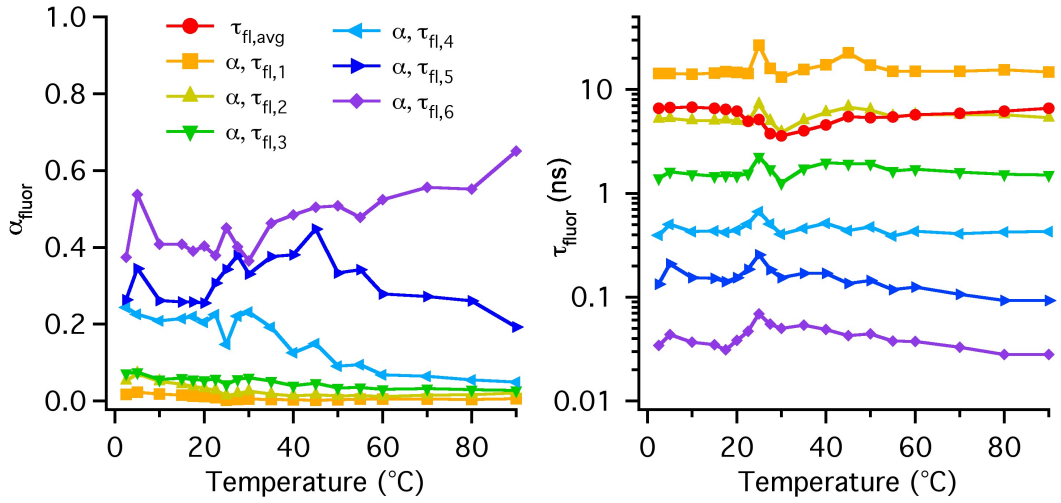

Figure 3.14: Relative amplitudes (left) and Individual fluorescence time constants (right) of 5.8 μM rilpivirine in aqueous solution of 25 w/v% Pluronic F88 at different temperatures.

rates as the viscosity of PEG 400 decreases with increasing temperature. The value of θ_{rot} for rilpivirine in PEG 400 decreases from 10.17 to 1.05 ns from 5 to 80 °C. These time constants are consistent with the reorientation of a single rilpivirine molecule in PEG 400 as predicted by S-E-D hydrodynamics. The S-E-D equation (Equation 3.4) relates the volume of a reorienting species in a solvent to the viscosity of the solvent. The volume of one rilpivirine molecule is approximately 381 Å^{3}and the viscosity of PEG 400 changes with temperature. At 20 °C, the viscosity of PEG 400 is 84 cP.

The plot of $\theta_{rot,j}$ and $\theta_{rot,avg}$ versus temperature for rilpivirine in PPO 2000 is shown in Figure 3.16. The r(t) anisotropy decay was fit to a sum of two exponential decay functions, yielding two reorientational time constants and two anisotropy values as amplitudes of these time constants. The anisotropy values both increased with increasing temperature of PPO, and the limiting anisotropy, r_0 increased form 0.3 to 0.5 over the measured temperature range. The reorientation time constants decrease and then $\theta_{rot,1}$ increases with increasing temperature of the PPO. $\theta_{rot,2}$ decreases with increasing temperature, but the The amplitude-weighted average[31] reorientation time constant of rilpivirine increases from 17.3 to 51.3 ns from 5 to 80 °C in PPO 2000. The

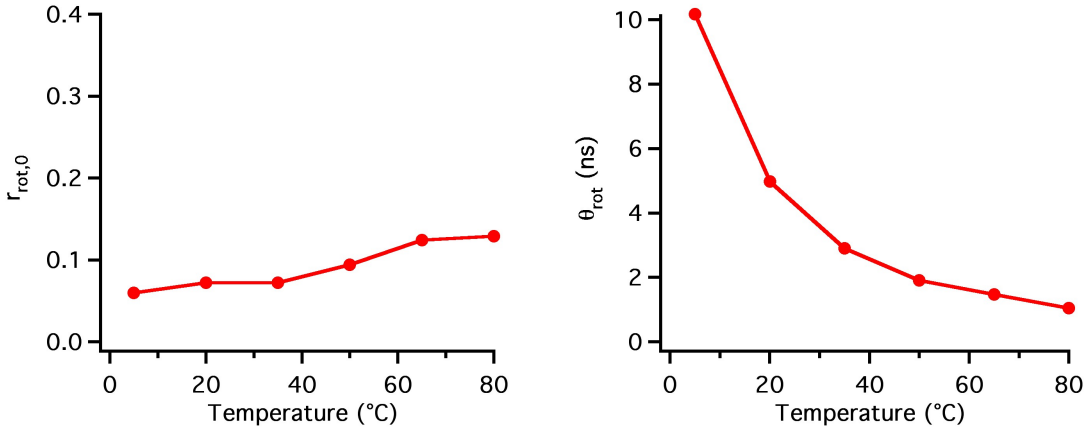

Figure 3.15: Limiting anisotropy, r_0 values and reorientation time constants $\theta_{rot,j}$ (red) of 5.8 μM rilpivirine in poly(ethylene glycol) (400 average molecular weight) over six temperatures from 5 to 80 °C.

predicted reorientation time constant for a single molecule of rilpivirine in PPO 2000 is 25.7 ns, in PEG 400 is 7.6 ns, and in water is 67 ps.

As the temperature increases, the polymer solution forms a hydrogel. The rilpivirine aggregates reorient at faster rates caused by thermal motion, but are not inhibited by the higher viscosity of the polymer gel phase. The time-resolved anisotropy decay of rilpivirine in F88 was fit to a 2-exponential decay function. The anisotropy values in the steady-state were also measured as a function of temperature and are included in Figure 3.17. The steady-state polarization anisotropy values follow the same trend as $r_{rot,1}$ individual anisotropy from time-resolved measurements, showing a slower reorientation in aqueous solution of F88 micelles than in aqueous F88 unimer solution. The $r_{rot,2}$ value diverges from the value of $r_{rot,1}$, decreasing with the formation of F88 micelles. This is indicative of two populations of rilpivirine in solution, and this has already been confirmed in the steady-state spectra. The r_0 of rilpivirine increases from 0.18 to 0.30 with increasing temperature and the formation of micelles in solution. The shift in reorientational dynamics with temperature is clearly shown by the individual anisotropies, $r_{rot,1}$ and $r_{rot,2}$.

The reorientational time constants of rilpivirine in aqueous F88 unimers, micelles

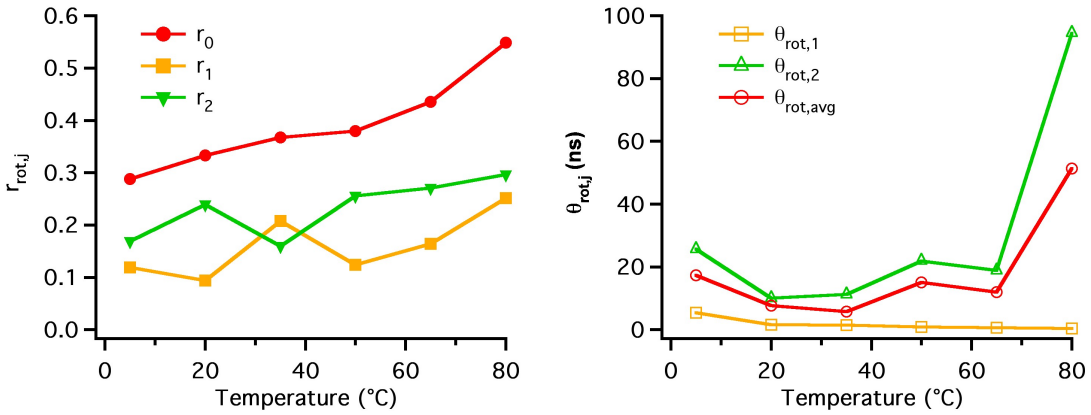

Figure 3.16: Anisotropies, r_0 values, individual and average reorientation time constants $\theta_{rot,j}$ (red) of 5.8 μM rilpivirine in poly(propylene oxide) (2,000 average molecular weight) over six temperatures from 5 to 80 °C.

and gels are changing in agreement with the nanoscale phase change of the F88 polymer solution. As the A-B-A triblock copolymer forms micelles, the individual and average reorientation time constants increase, showing an increase in the local solvent friction in the environments of both drug aggregates and unimers. The amplitude-weighed average[31] value of θ_{rot} for rilpivirine in 25 w/v% F88 solution shifts from approximately 1 ns to 5 ns over the micellization of the polymer. The reorientation time constant then decreases with the heating of the polymer as rilpivirine aggregates localize outside the F88 micelles in a less viscous local environment. S-E-D reorientation time constants were predicted from the molecular volume of one rilpivirine molecule and the measured shear viscosity of aqueous solution of 25 w/v% F88 up to 40 °C.[11] The predicted reorientation time constant of single rilpivirine molecules in solution is in very good agreement with the measured values displayed in Figure 3.17.

3.4.3 Fluorescence Wavelength Dependence

Fluorescence Dynamics

The fluorescence time constants were measured for the sample of 5.8 μM rilpivirine in aqueous micelle solution of 25 w/v% F88 at 30 °C where the aggregate and unimer form of rilpivirine is present in solution. The time-resolved transients were measured for 31

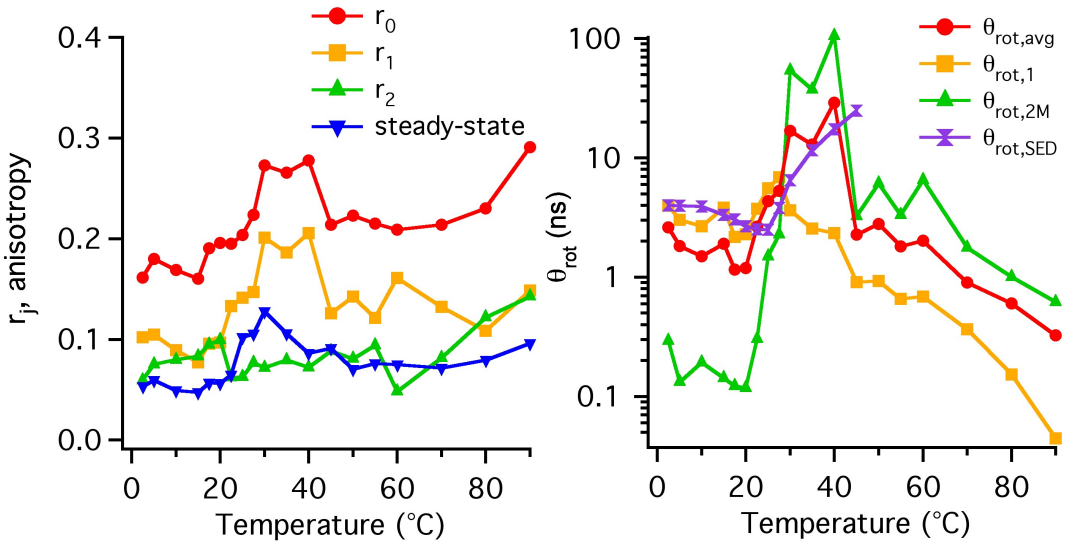

Figure 3.17: Left: individual anisotropies, r_j, and steady-state anisotropies. Right: Predicted reorientation time constants from S-E-D (Equation 3.4), measured individual reorientation time constants $\theta_{rot,j}$, and average time constants, $\theta_{rot,avg}$ of 5.8 μM rilpivirine in 25 w/v% Pluronic F88 in aqueous solution with changing temperature.

different emission wavelengths ranging from 20,000 to 35,000 cm^{-1} in 500 cm^{-1} increments. The transients were fit to a sum of six exponential decay functions, yielding six individual time constants and corresponding $\alpha_{fl,i}$ values (See Equation . These values are plotted in Figure 3.18 versus the emission wavelength at which fluorescence was measured. Like the temperature-dependent fluorescence time constants, the smallest time constant has the highest normalized amplitude. In this case, the time constant in aggregates is 2.2 ns at the aggregate emission peak. At the emission peak corresponding to rilpivirine in unimer form, the average fluorescence time constant is 5.8 ns. The decrease of the average time constant is caused by the fluctuation in the amplitudes of the individual time constants associated with unimer or aggregate rilpivirine. As the emission wavelength is shifted to an energy where more unimers emit, the normalized amplitude of that particular time constant increases, as does the average time constant value.

The previous statement is held true when the wavelength dependence of the fluorescence time constant is measured at different concentrations of rilipivirine, as shown

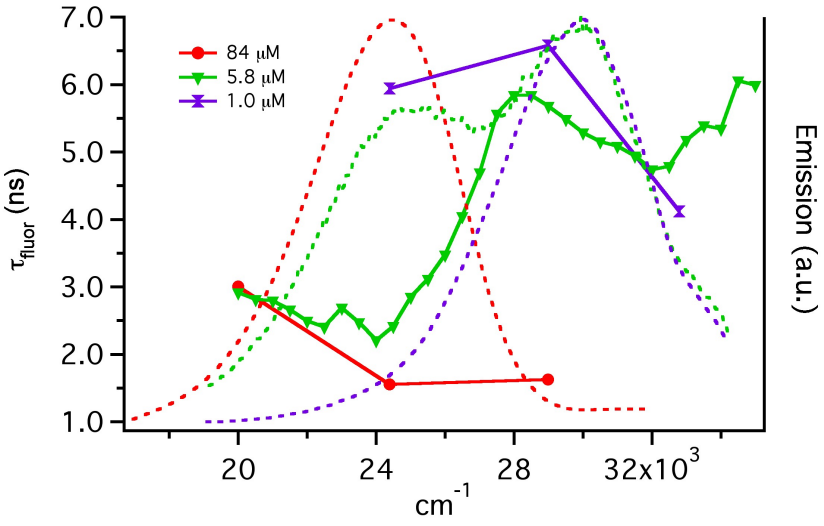

Figure 3.18: Emission wavelength dependence of fluorescence time constants for three concentrations of rilpivirine in 25 w/v% F88 solution: 84 (red), 5.8 (green), and 1.0 (purple) μM rilpivirine. Overlaid are the steady-state emission spectra of the same three solutions.

in Figure 3.18. Here, the emission spectra of 84, 5.8, and 1.0 μM rilpivirine solutions in 25 w/v% F88 micelles are overlaid with the average time constants measured at several different wavelengths. When only rilpivirine aggregates are present in solution, such as at 84 μM concentration, the average time constant is on the order of 2 to 3 ns. When only rilpivirine unimers are present in solution, such as at 1.0 μM concentrations, the average time constant is higher and on the order of 4 to 6 ns. When both unimer and aggregate forms of rilpivirine are present in solution, the time constant is dependent on the emission wavelength at which the fluorescence is measured, as shown by the 5.8 μM concentration of rilpivirine in F88 solution.

Reorientational Dynamics

The sample of 5.8 μM rilpivirine in A-B-A triblock copolymer solution at 30 °C was chosen to study the dependence of the emission wavelength detected for fluorescence time constants and polarization anisotropies because of two conditions: rilpivirine is in both aggregated and non-aggregated form and the polymer solution is in the form of aqueous micelles.

Figure 3.19 shows the fluorescence emission spectrum of the aforementioned sample with the described conditions, overlaid with the individual and limiting anisotropies, $r_{rot,j}$ and r_0 on the left and the individual and average reorientation time constants, $\theta_{rot,j}$ on the right, measured at different wavelength values across the entire emission spectrum. Because it has been stated that the peak at approximately 25,000 cm^{-1} results from the aggregate form of rilpivirine, it is consistent that the measured reorientation time constant at this wavelength would be significantly higher than the time constant measured at the peak attributed to monomeric drug at 28,600 cm^{-1}. These values show that the smaller species reorients faster in solution than an aggregate with both multiple times the volume of a single rilpivirine and in a microviscosity that is lower than the local environment of the rilpivirine unimer encapsulated in a micelle core. If the molecular volume of the aggregate scales to a single molecule of rilpivirine, the aggregate may be composed of approximately 100 rilpivirine molecules according to time-resolved fluorescence polarization anisotropy meaurements.

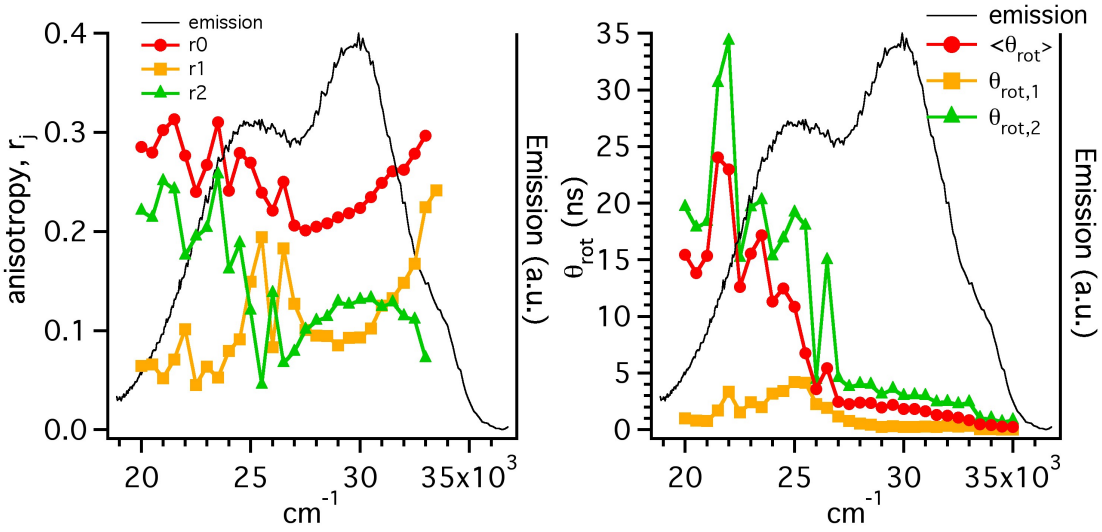

Figure 3.19: Left: Emission wavelength dependence of time-resolved anisotropy values. Right: Wavelength dependence of individual and average reorientation time constants $\theta_{rot,j}$ (red) of 5.8 μM rilpivirine in 25 w/v% Pluronic F88 in aqueous solution.

S-E-D hydrodynamics relates the diffusive reorientational motion of a fluorophore to

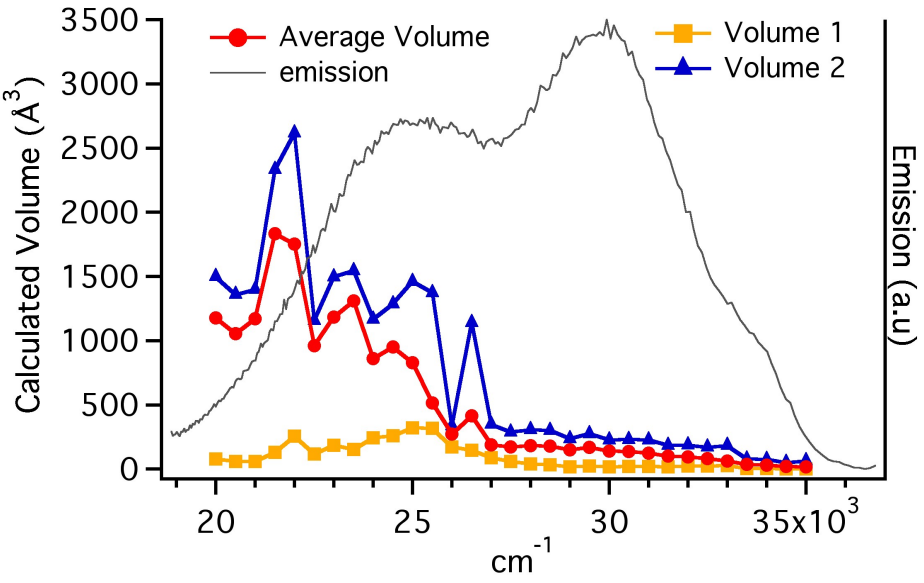

Figure 3.20: Calculated S-E-D hydrodynamic volumes from individual and average reorientation time constants $\theta_{rot,j}$ (red)of 5.8 μM rilpivirine in 25 w/v% Pluronic F88 at 30 °C in aqueous solution with various emission wavelengths. Also plotted for reference is the hydrodynamic volume of one rilpivirine molecule from molecular volume calculations.[35, 36]

the volume of the reorienting species and the viscosity of the solvent in which the fluorophore is localized.[30, 31] The reorientational time constants for rilpivirine were input into Equation 3.4 and the viscosity of aqueous 25 w/v% Pluronic F88 solution at 30 °C (45.9 cP) was used to calculate the hydrodynamic volume of rilpivirine or rilpivirine aggregates as measured by fluorescence methods.[11] The volumes were graphed against the emission wavelength at which fluorescence was measured. This data is shown in Figure 3.20 which plots the hydrodynamic volumes calculated from $\theta_{rot,1}$, $\theta_{rot,2}$, and $\theta_{rot,avg}$ as well as a reference line for the volume of a single rilpivirine molecule (0.381 nm^3). As a reference to the molecular volumes of the F88 polymer nanophases, the average volume of an F88 micelle at this concentration and temperature is about 2,145 nm^3 and the average volume of the PPO core of an F88 micelle is approximately 195 nm^3.[7] The aggregates measured by TCSPC fluorescence methods have average hydrodynamic volumes from average reorientation time constants up to 105 times larger than

the effective reorientational volume of a single molecule of rilpivirine. The hydrodynamic volumes from the average reorientation time constants of rilpivirine were divided by the effective volume of one rilpivirine molecule to get approximate aggregation numbers. These values are plotted in Figure 3.21 and rilpivirine aggregates range from 10 to 105 times the volume of one drug molecule. These values are based on spherical reorienting species and a constant local viscosity. It is known that the local viscosity inside the hydrophobic core of F88 micelles is significantly greater than the local viscosity in the water outside the polymeric micelles.[11] By approximation, it is possible to detect unimer or aggregate forms of rilpivirine using fluorescence spectroscopy techniques.

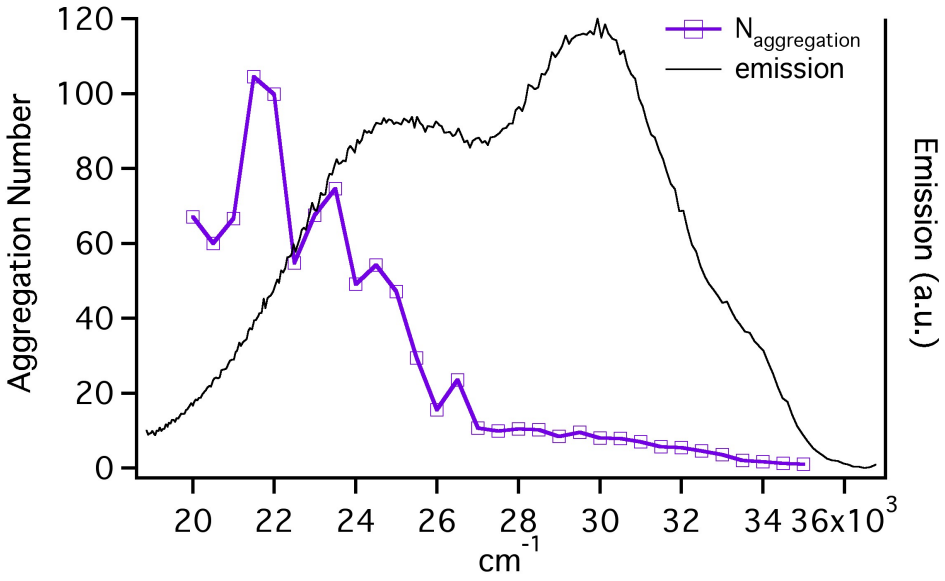

Figure 3.21: Predicted aggregation numbers of rilpivirine in solution calculated from reorientation time constants measured at different emission wavelengths from 20,000 to 35,000 cm^{-1}. The emission spectrum of rilpivirine from the same solution is overlaid on the graph.

3.4.4 Solvent Relaxation Dynamics of Unimers and Aggregates

Time-Resolved Emission in Three Organic Solvents

Time-resolved emission spectra (TRES) are plotted in Figures 3.22 and 3.23 for rilpivirine in CH_2Cl_2 and pentane. The peak emission energy in units of cm^{-1} is plotted versus time in ns. Rilpivirine is shown to form aggregates in 1-pentane. The drug is

in unimer form when dissolved in CH_2Cl_2 as found from reorientational time constant measurements in these solutions.

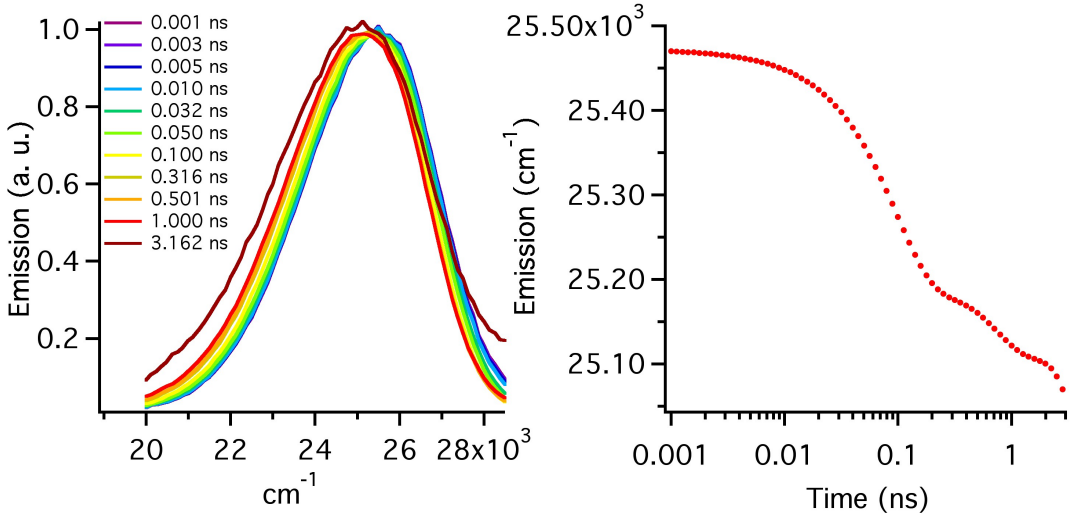

Figure 3.22: Left: Time-resolved emission spectra of rilpivirine unimers in CH_2Cl_2 at 20.0 °C from 1 ps to 10 ns. Right: Emission energy versus time, showing solvent relaxation rates for rilpivirine unimers in CH_2Cl_2.

The time resolved emission of rilpivirine in CH_2Cl_2 shifts from approximately 25,460 to 25,050 cm^{-1} over a 3 ns time scale. The emission spectra at delays after photoexcitation from 1 ps to 3.2 ns are shown in Figure 3.22 with the emission frequency plotted versus time delay. The clear change in solvent relaxation rate at approximately 0.1 ns indicates that multiple species of rilpivirine, yielding multiple solvent relaxation rates. These rates were found to be 7.8 ns, 3.7 ns, 72 ps, and 27 ps from a fit to a sum of four exponential equations. From reorientational time constants discussed previously, it is known that rilpivirine is in the unimer form in CH_2Cl_2 and this is the control experiment for measuring the solvent relaxation by TRES for unimer rilpivirine in solution.

The time resolved emission of rilpivirine in 1-pentane has multiple bands that shift over the lifetime of rilpivirine in solution.The emission band at approximately 28,000 cm^{-1} associated with aggregate rilpivirine increases from approximately 28,000 to 31,100 cm^{-1} over a 10 ns time scale. This peak is labeled Peak 1. The second peak at approximately 31,500 cm^{-1} shifts to 30,300 cm^{-1} over a 10 ns time scale. A sharp

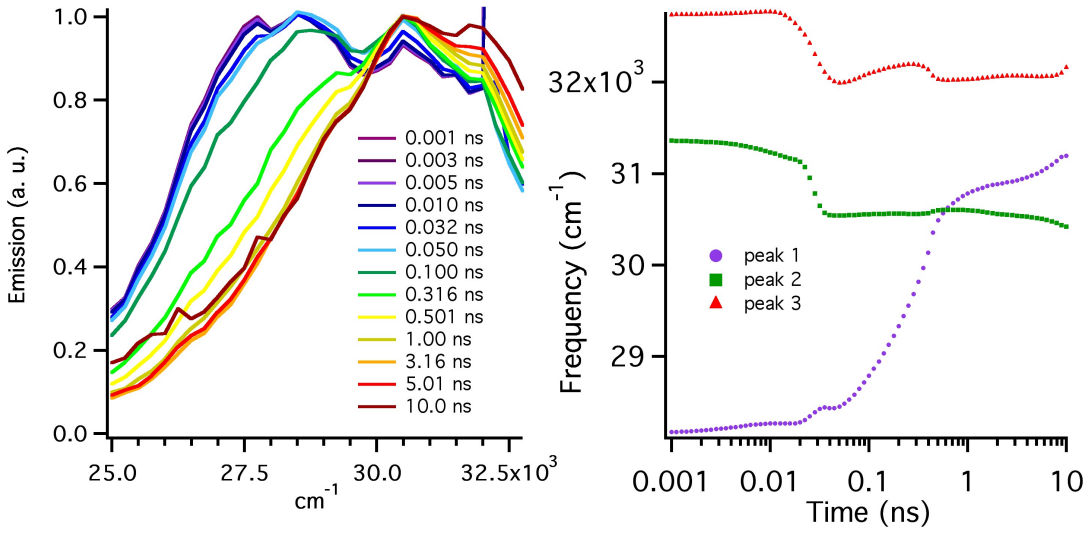

Figure 3.23: Left: Time-resolved emission spectra of rilpivirine in 1-pentane (aggregates) at 20.0 °C from 1 ps to 10 ns. Right: Emission energy versus time, showing solvent relaxation rates for rilpivirine aggregates in 1-pentane.

decrease in energy at approximately 0.02 ns indicates multiple forms of rilpivirine which yield multiple solvent relaxation rates.[30] The third emission peak (Peak 3) shifts from about 32,800 to 32,000 cm^{-1} and also has a sharp drop in emission energy at around 0.02 ns. The multiple peaks and complex solvent relaxation rates are indicative of the aggregate form of rilpivirine present in 1-pentane. This is a control experiment for measuring the solvent relaxation for aggregate rilpivirine in solution.

The TRES of rilpivirine in PEG 400 is a control measurement for rilpivirine in polymer environments similar to aqueous solutions of A-B-A triblock copolymer F88 micelles and hydrogels. The time-resolved emission spectra for rilpivirine in PEG 400 are plotted in Figure 3.24 with the peak emission energy plotted versus time delay. The single emission band shifts from approximately 29,600 to 27,700 cm^{-1} over a 6 ns time scale. Multiple relaxation times are present in this decay, but not do not have dramatic changes such as in the TRES measurement of rilpivirine aggregates. The relaxation rates found from a fit of the peak frequency versus time to a sum of three exponential decays is: 73 ps, 471 ps, and 2.77 ns.

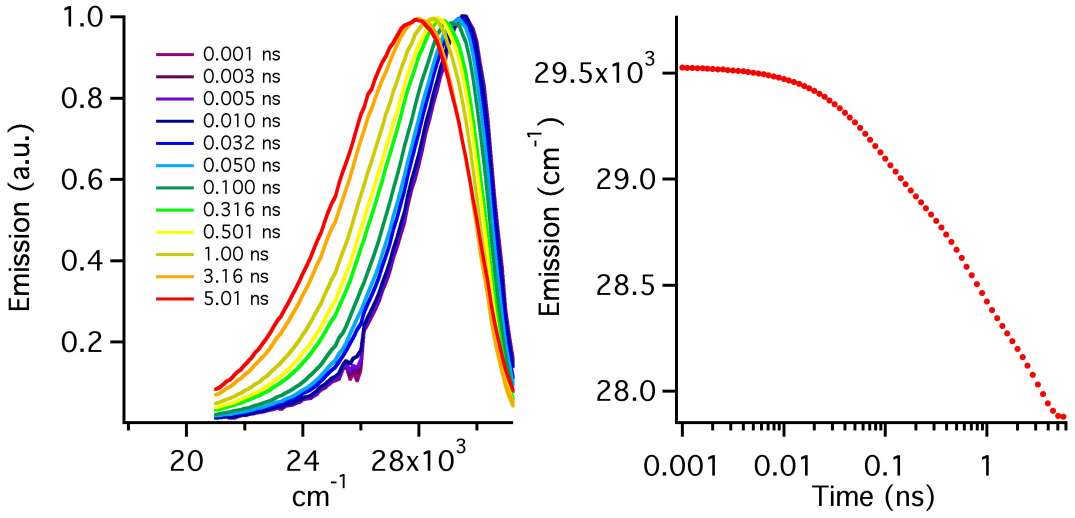

Figure 3.24: Time-resolved emission spectra of rilpivirine in PEG (Mw 400 g/mol) at 20.0 °C.

Time-Resolved Emission in Aqueous F88

Time-resolved emission spectra show a shift in peak emission energy at time delays after photoexcitation. Here, we look at the TRES shift for rilpivirine measured at various temperatures and times in 25 w/v% Pluronic F88. At low temperatures, below 20 °C, the emission peak is resulting from the fluorescence of unimer drugs in solution at emission wavelengths of around 325 nm (30,769 cm^{-1}). From 20 to 30 °C, the solvent dynamics reflect the enivronments of rilpivirine unimers and aggregates, and at higher temperatures, those above 30 °C, the rilpivirine drug is in the form of mostly drug aggregates in solution. The peak for the aggregate species of rilpivirine increases in intensity, appearing at approximately 390 nm (25,641 cm^{-1}).

Temperature dependence and time dependence of the emission spectrum of rilpivirine differ between unimer drug and aggregate drug solutions. Aggregates clearly emit at longer wavelengths (lower energies), at longer times during solvent relaxation, and aggregates predominate at higher temperatures and emit on faster time scales in solutions of rilpivirine micelles and gels. Figure 3.25 shows the time slices of rilpivirine at 1, 10, 100 ps, and 1, 10, and 100 ns delays after photoexcitation for 10 temperatures

between the unimer and micelle phases of Pluronic F88 in aqueous solutions. At 1 ps after the excitation of rilpivirine, both unimer and aggregate forms of the drug are emitting and the fluorescence of the drug that is most intense in the spectrum is entirely dependent on temperature and polymer phase. In F88 unimer solutions, the unimer form of rilpivirine emits at 31,000 cm^{-1} with a small peak around 25,000 cm^{-1}. At higher temperatures, as F88 forms aqueous micelles, the fluorescence of the aggregate form of rilpivirine is the most intense emission peak at 25,000 cm^{-1} with a small unimer emission band at 31,000 cm^{-1}. At short time scales within the lifetime of rilpivirine fluorescence, the unimer form of rilpivirine emits strongly from aqueous solutions of Pluronic F88 unimers.

At 10 ps after excitation, the trend in emission energies is the same as at 1 ps delays, but the peak at 25,000 cm^{-1} is decreased in intensity at lower temperatures (below 25 °C) and still predominant at higher temperatures of the polymer solution.

At 100 ps and at lower temperatures (below 25 °C), the peak at 25,000 cm^{-1} is diminished in intensity, and continues to decrease in relative intensity at 1 ns. By 10 ns, the emission peak at 25,000 cm^{-1} associated with rilpivirine aggregates is almost completely diminished in relative intensity at all temperatures. At 50 ns, one peak at approximately 27,500 cm^{-1} is present at all temperatures and all phases of F88 in 25 w/v% polymer in aqueous solution.

The time-resolved emission of rilpivirine reveals that solvent relaxation rates are faster around rilpivirine aggregates than rilpivirine unimers. The shift in emission energy for the aggregate is small, while the emission energy of rilpivirine unimers shifts from 31,000 to 27,500 cm^{-1} over a 50 ns time scale.

3.5 Conclusions

3.5.1 Spectroscopy, Solvatochromism, and Structure of Rilpivirine Solutions

Rilpivirine has a solvatochromic shift resulting from a large change in dipole moment between the ground and excited states. Dipole moments, absorption, and emission energy vary with solvent dielectric, refractive index, and polarity of the solvent. In

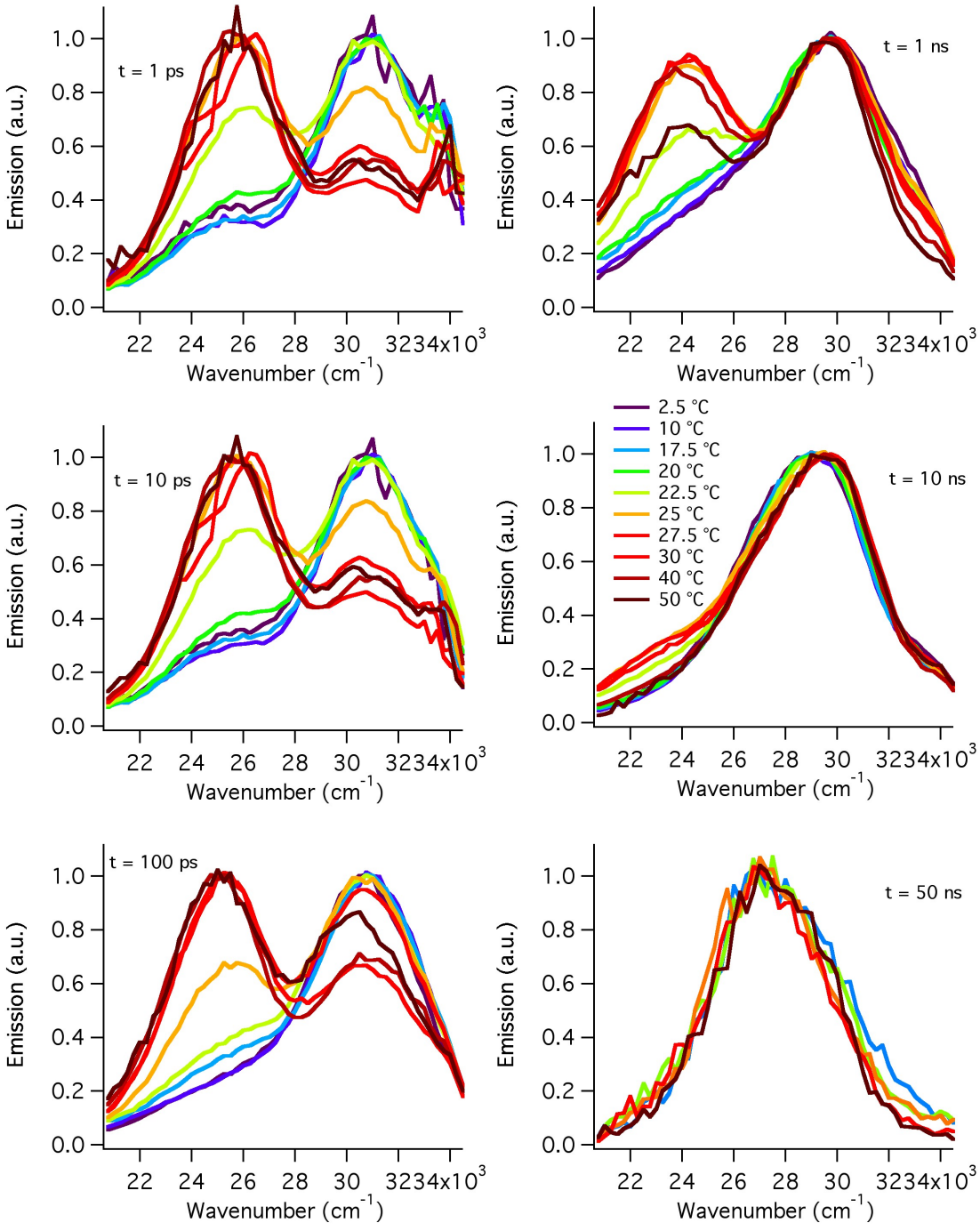

Figure 3.25: Emission spectra for 5.8 μM rilpivirine in 25 w/v% Pluronic F88 at 1 ps, 10 ps, 100 ps, 1 ns, 10 ns, and 50 ns delays (after photoexcitaton) at temperatures of 2.5, 10, 17.5, and 20, (F88 unimers), 22.5, 25, 27.5, and 30.0, (F88 micelles), and 40.0, and 50.0 °C (F88 hydrogels).

strongly polar solvents, such as DMSO, rilpivirine has an emission energy close to 24,400 cm^{-1} while in more non-polar solvents such as 2-MeTHF, the emission peak energy is approximately 27.500 cm^{-1}. The relationship between solvent polarity and emission wavelength is not a simple one, for specific interactions such as hydrogen bonding, and non-specific interactions such as dipole-dipole interactions between the rilpivirine molecule and surrounding solvent molecules cause the relationship between solvent dielectric and emission energy to not be a linear relationship for all solvents. Both the absorbance peaks and the emission peaks for rilpivirine in twelve solvents are outlined for future use of the drug as a fluorescent probe molecule.

Rilpivirine is strongly polar, making it insoluble in many solvents and causing aggregation of the drug in some (mostly non-polar) solvents. These aggregation-causing solvents include 1-pentane, 1-hexane, acetonitrile, and benzene. While rilpivirine has a large solvatochromic shift, the aggregation of the rilpivirine molecule in such solvents causes the spectroscopy to be different than the expected trend for rilpivirine in solvents that do not stimulate aggregation.

The absorbance spectrum of rilpivirine consistently has two peak energy bands resulting from the strong mixing of orbital configurations in excited state transitions. Because $S_0 \rightarrow$S' and the $S_0 \rightarrow$S" transitions both have relatively high oscillator strengths, the transitions are both favorable in the absorption phenomenon.

Many fluorophores have n$\rightarrow \pi^*$ and $\pi \rightarrow \pi^*$ transitions that are directly responsible for the HOMO→LUMO electronic transition, also most often assigned as the transition to the first electronic excited state ($S_0 \rightarrow$S').[41] This is often measured by absorbance spectroscopy. The HOMO→LUMO transition occurs for rilpivirine, as in all molecules, but the $S_0 \rightarrow$S' transition has many orbital configuration states associated with the transition. The mixing of orbitals within the electronic transition causes the absorption and fluorescence spectroscopy of rilpivirine to be complex.

3.5.2 Spectroscopy of Rilpivirine in Aqueous Solutions of Triblock Copolymer F88

We have found that rilpivirine is a fluorescent molecule and a self-reporter of local environment in solution. Fluorescence spectroscopy is an informative method to characterize the aggregation properties of rilpivirine which are important to the formulation and delivery of this hydrophobic drug. In aqueous solutions of 25 w/v% PEO-PPO-PEO triblock copolymer F88, at a concentration of 5.8 μM drug, rilpivirine is present in the form of both monomeric drug and drug aggregates as shown by the multiple peak formation in the fluorescence emission spectrum. The monomeric drug and the aggregate form of the drug emit at different wavelengths as different fluorescing species.

The drug concentration dependence of the steady-state fluorescence spectrum of rilpivirine shows that in 25 w/v% PEO-PPO-PEO solution at 30 °C, the critical aggregation concentration is approximately 2.0 μM drug in micellar solution. The emission wavelength of the unimer drug in this solution was approximately 345 nm (28,986 cm^{-1}) and the emission wavelength of the aggregate drug species is approximately 400 nm (25,000 cm^{-1}).

For temperature-dependent measurements, a concentration of 5.8 μM rilpivirine in polymer solution was used to measure both monomeric drug and aggregate drug species in the same sample. The distribution of species in the steady-state emission spectrum and the distribution of fluorescence time constants with changing temperature show a shift corresponding to the micellization of the A-B-A triblock copolymer at 22.5 °C.

The temperature dependence of the emission spectrum of rilpivirine shows a shift at the temperature where F88 forms micelles in aqueous solution. The time constants of rilpivirine in the same solution showed trends corresponding to a local environment similar to that of our two control solutions of rilpivirine in poly(ethylene glycol) and poly(propylene oxide) polymers. While the individual fluorescence time constants shown small shifts corresponding to the polymer micellization temperature, the average of the locally fit individual time constants show a sharp transition from approximately 6 ns to 4 ns. The temperature dependent reorientation time constants and anisotropy values show a transition to slower reorientational dynamics upon micellization of the

polymer. The average reorientation time constant measured at 390 nm emission shifts from 1 ns to 5 ns within the micellization temperature range. This shows that the rilpivirine species present and emitting at 390 nm has a solvent environment that is increasing in local friction. This is consistent with the encapsulation of rilpivirine as F88 forms micelles in solution.

The wavelength dependence of the time-resolved fluorescence spectroscopy was measured and fit to see what differences are present between the two clear peaks in the fluorescence emission spectrum. The peak at lower energy, assigned to the aggregated form of rilpivirine in solution shows reorientational dynamics over 100 times slower than measured at higher energies assigned to monomeric drug. At 5.8 μM rilpivirine in 25 w/v% F88 solution of polymer micelles at 30 °C, the aggregates diameters range somewhere between 65 and 150 times the size of a single rilpivirine molecule because the reorientation time constant is directly proportional to the volume of the reorienting species using S-E-D hydrodynamics.

Time-resolved emission shows the shifting of two characteristic emission peaks over a time period of 1 ps to 50 ns. The temperature-dependence of these two peaks indicates that at low temperatures where the polymer is in unimer form, the monomeric form of the drug is predominantly fluorescing. At polymer micellization (22.5 °C, both monomeric drug and aggregated drug are emitting fluorescence with the solvent relaxation occuring faster around the aggregated drug. At temperatures above 22.5 °C, when the polymers are aggregated to form micelles, the aggregated species of rilpivirine is predominant with solvent relaxation occuring on the 1 ps to 1 ns time scales. The monomeric rilpivirine emission peak shows slower solvent relaxation dyanmics occuring over the entire 1ps to 50 ns range.

The study of rilpivirine aggregates using fluorescence spectroscopy is meant to characterize the various forms of this hydrophobic drug that may occur in formulated solutions. The bioavailability of rilpivirine is dependent on the local solvent environment and the form in which the rilpivirine molecule is delivered. Aggregate sizes and volumes, as well as formulations for rilpivirine unimers and aggregates are characteristics

of the drug that help in more efficient delivery solutions. The hydrophobicity of rilpivirine should not be a barrier for efficient delivery if the drug is effective and safe for helping HIV patients. Fluorescence spectroscopy methods are an important solution for characterizing future formulations of what could be a very effective and important drug.

References

[1] K. E. Steege *et al.;* Spectroscopy, solvatochromism, and structure of rilpivirine, a potent non-nucleoside reverse transcriptase inhibitor; **2008**, page to be published.

[2] P. A. J. Janssen *et al.;* In search of a novel anti-hiv drug: Multidisciplinary coordination in the discovery of 4-[[4-[[4-[(1e)-2-cyanoethenyl]-2,6-dimethylphenyl]amino]-2- pyrimidinyl]amino]benzonitrile (r278474, rilpivirine).; *Journal of Medicinal Chemistry* **2005**, *48*, 1901–1909.

[3] B. L. De Corte; From 4,5,6,7-tetrahydro-5-methylimidazo[4,5,1-jk](1,4)benzodiazepin-2(1h)-one (tibo) to etravirine (tmc125): Fifteen years of research on non-nucleoside inhibitors of hiv-1 reverse transcriptase; *Journal of Medicinal Chemistry* **2005**, *48*, 1689–1696.

[4] K. Das, P. J. Lewi, S. H. Hughes, and E. Arnold; Crystallography and the design of anti-aids drugs: conformational flexibility and positional adaptability are important in the design of non-nucleoside hiv-1 reverse transcriptase inhibitors.; *Progress in Biophysics & Molecular Biology* **2005**, *88*, 209–231.

[5] Y. V. Frenkel *et al.;* Concentration and ph dependent aggregation of hydrophobic drug molecules and relevance to oral bioavailability.; *Journal of Medicinal Chemistry* **2005**, *48*, 1974–1983.

[6] R. K. Prud'homme, G. Wu, and D. K. Schneider; Structure and rheology studies of poly(oxyethylene-oxypropylene-oxyethylene) aqueous solution; *Langmuir* **1996**, *12*, 4651–4659.

[7] N. J. Jain, V. K. Aswal, P. S. Goyal, and P. Bahadur; Micellar structure of an ethylene oxide-propylene oxide block copolymer: a small-angle neutron scattering study.; *Journal of Physical Chemistry B* **1998**, *102*, 8452–8458.

[8] P. Alexandridis; Polymers and nanomaterials.; *Current Opinion in Colloid & Interface Science* **2003**, *8*, 62–63.

[9] P. Alexandridis and T. Alan Hatton; Poly(ethylene oxide)-poly(propylene oxide)-poly(ethylene oxide) block copolymer surfactants in aqueous solutions and at interfaces: thermodynamics, structure, dynamics, and modeling.; *Colloids and Surfaces, A: Physicochemical and Engineering Aspects* **1995**, *96*, 1–46.

[10] C. D. Grant *et al.;* Fluorescence probing of interior, interfacial, and exterior regions in solution aggregates of poly(ethylene oxide)- poly(propylene oxide)-poly(ethylene oxide) triblock copolymers.; *Langmuir* **2005**, *21*, 1745–1752.

[11] C. D. Grant, K. E. Steege, M. R. Bunagan, and E. W. Castner Jr.; Microviscosity in multiple regions of complex aqueous solutions of poly(ethylene oxide)-poly(propylene oxide)-poly(ethylene oxide).; *Journal of Physical Chemistry B* **2005**, *109*, 22273–22284.

[12] V. P. Torchilin; Micellar nanocarriers: Pharmaceutical perspectives.; *Pharmaceutical Research* **2007**, *24*, 1–16.

[13] G. S. Kwon and M. L. Forrest; Amphiphilic block copolymer micelles for nanoscale drug delivery.; *Drug Development Research* **2006**, *67*, 15–22.

[14] R. Duncan; The dawning era of polymer therapeutics.; *Nature Reviews Drug Discovery* **2003**, *2*, 347–360.

[15] G. S. Kwon; Polymeric micelles for delivery of poorly water-soluble compounds.; *Critical Reviews in Therapeutic Drug Carrier Systems* **2003**, *20*, 357–403.

[16] A. V. Kabanov, E. V. Batrakova, and V. Y. Alakhov; Pluronic block copolymers as novel polymer therapeutics for drug and gene delivery.; *Journal of Controlled Release* **2002**, *82*, 189–212.

[17] V. P. Torchilin; Targeted polymeric micelles for delivery of poorly soluble drugs.; *Cellular and Molecular Life Sciences* **2004**, *61*, 2549–2559.

[18] N. Y. Rapoport, J. N. Herron, W. G. Pitt, and L. Pitina; Micellar delivery of doxorubicin and its paramagnetic analog, ruboxyl, to hl-60 cells: effect of micelle structure and ultrasound on the intracellular drug uptake.; *J. Controlled Release* **1999**, *58*, 153–162.

[19] Y. V. Frenkel, T. Emge, and E. Arnold unpublished, **2008**.

[20] Y. Ooshika; Absorption spectra of dyes in solution; *Journal of the Physical Society of Japan* **1954**, *9*, 594.

[21] E. Lippert; *Z. Naturforsch* **1955**, *10a*, 541.

[22] N. Mataga, Y. Kaifu, and M. Koizumi; Sovent effects upon fluorescence spectra and the dipole moments of excited molecules; *Bulletins of the Chemical Society of Japan* **1956**, *29*, 465.

[23] M. J. Kamlet, J. L. Abboud, and R. W. Taft; The solvatochromic comparison method. 6. the π^* scale of solvent polarities.; *Journal of the American Chemical Society* **1977**, *99*, 6027–6038.

[24] C. Reichardt; Solvatochromic dyes as solvent polarity indicators.; *Chemical Reviews (Washington, DC, United States)* **1994**, *94*, 2319–2358.

[25] J. Ridley and M. Zerner; An intermediate neglect for differential overalap technique for spectroscopy: Pyrrole and the azines; *Theoretical Chemistry Accounts* **1973**, *32*, 111–134.

[26] M. C. Zerner, G. H. Loew, R. F. Kirchner, and U. T. Mueller-Westerhoff; An intermediate neglect of differential overlap technique for spectroscopy of transition-metal complexes. ferrocene.; *Journal of the American Chemical Society* **1980**, *102*, 589–99.

[27] M. C. Zerner *Semiempirical Molecular Orbital Methods in Reviews in Computational Chemistry*, Vol. 8; VCS Publishers Inc., 1991.

[28] M. M. Karelson and M. C. Zerner; Theoretical treatment of solvent effects on electronic spectroscopy.; *Journal of Physical Chemistry* **1992**, *96*, 6949–57.

[29] G. U. Bublitz and S. G. Boxer; Stark spectroscopy: applications in chemistry, biology, and materials science.; *Annual Review of Physical Chemistry* **1997**, *48*, 213–242.

[30] J. R. Lakowicz *Principles of Fluorescence Spectroscopy;* Kluwer Academic/ Plenum Publishers, 2nd ed., 1999.

[31] B. Valeur *Molecular Fluorescence: Principles and Applications;* Wiley-VCH, 2002.

[32] C. Laurence *et al.;* The empirical treatment of solvent-solute interactions: 15 years of π^*; *Journal of Physical Chemistry* **1994**, *98*, 5807–5816.

[33] Arguslab version 4.0. M. A. Thompson Planaria Software LLC, Seattle, WA., **1996-2003**.

[34] G. Kodali, K. A. Kistler, S. Matsika, and R. J. Stanley; 2-aminopurine excited state electronic structure measured by stark spectroscopy; *Journal of Physical Chemistry B* **2008**, *in press*.

[35] A. Bondi; van der waals volumes and radii; *Journal of Physical Chemistry* **1964**, *68*, 441–51.

[36] J. T. Edward; Molecular volumes and the stokes-einstein equation; *Journal of Chemical Education* **1970**, *47*(4), 261–270.

[37] C.-M. Hu and R. Zwanzig; Rotational friction coefficients for spheroids with the slipping boundary condition.; *Journal of Chemical Physics* **1974**, *60*, 4354–7.

[38] G. K. Youngren and A. Acrivos; Rotational friction coefficients for ellipsoids and chemical molecules with the slip boundary condition.; *Journal of Chemical Physics* **1975**, *63*, 3846–8.

[39] G. B. Dutt and A. Sachdeva; Temperature-dependent rotational relaxation in a viscous alkane: Interplay of shape factor and boundary condition on molecular rotation; *Journal of Chemical Physics* **2003**, *118*(18), 8307–8314.

[40] G. B. Dutt and T. K. Ghanty; Is molecular rotation really influenced by subtle changes in molecular shape?; *Journal of Chemical Physics* **2004**, *121*(8), 3625–3631.

[41] N. J. Turro *Modern Molecular Photochemistry v. 2;* University Science Books, 1991.

Chapter 4

Local Polarity and Microviscosity in the Hydrophobic Cores of Amphiphilic Star-like and Scorpion-like Macromolecules

4.1 Summary

Fluorescence spectroscopy is used to probe the polarity and local friction in aqueous solutions of three amphiphilic polymers. Aggregate core polarity and local friction on the nanoscale are observed by measuring the steady-state and time-resolved fluorescence spectroscopy of coumarin 153 (C153) in three amphiphilic polymers as a model for hydrophobic drug encapsulation. Three solutions of polymers are studied: one amphiphilic scorpion-like macromolecule (AScM), M12P5, and two amphiphilic star-like macromolecules (ASMs), NC12P5 and NC6P5. Both ASMs and AScMs consist of hydrophobic segments of acylated mucic acid and hydrophilic poly (ethylene glycol) chains. In aqueous solution, the scorpion-like M12P5 forms micellar aggregates through hydrophobic interactions, while the star-like polymers are covalently bonded macromolecules. Micelle and aggregate sizes are compared using dynamic light scattering measurements. A shift in the steady-state emission wavelength of C153 indicates distinct differences in polarity between the core environments of the scorpion-like polymer micelles and those of the two star-like polymers. The two reorientation time constants from C153 fluorescence anisotropies show that the hydrophobic cores of M12P5 micelles are relatively flexible. The covalently linked, rigid cores of the two star-like macromolecule nanocarriers, NC6P5 and NC12P5, show a third reorientation time constant for which the local friction of the dye is remarkably higher.

4.2 Overview

In the following, C153 is solubilized by three different amphiphilic polymers designed for encapsulation of hydrophobic drugs. The first of the three polymers is an amphiphilic scorpion-like macromolecule (AScM) composed of a hydrophilic, hydroxy-terminated PEG tail of molecular weight 5,000 g/mol and a hydrophobic constituent consisting of acylated mucic acid with twelve aliphatic carbons on each of four ester groups.[1] This polymer is called M12P5 and is shown in Figure 4.1.[2] M12P5 forms micelles in aqueous solution with a cmc of $1.25\text{x}10^{-7}$ mol/L at room temperature.[1]

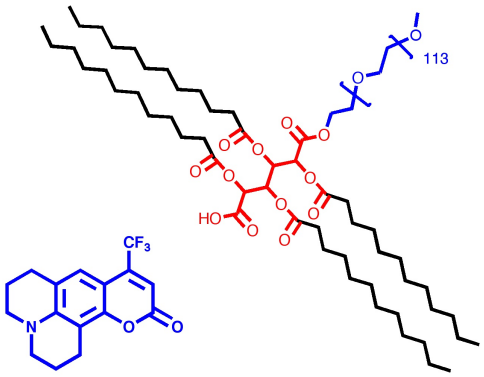

Figure 4.1: Structure of fluorescence dye **C153** (left) and amphiphilic scorpion-like macromolecule, **M12P5** (right).

The second drug-delivery polymer shown in Figure 4.2 is called NC12P5 and is one of two amphiphilic star-like macromolecules (ASMs).[3, 4] Like M12P5, NC12P5 has a hydrophilic PEG (M_w 5,000 g/mol) tail attached to the acylated mucic acid core.[3] Unlike an AScM, NC12P5 has four amphiphilic branches covalently joined in the center to form a single star-like macromolecule that behaves like a 'unimolecular micelle.' [3, 4] The third polymer is another ASM called NC6P5, and differs from NC12P5 by having only six carbon chains on each of the four mucic acid acylation sites.[4] The structure of NC6P5 is shown in Figure 4.3.[4] The two ASM molecules under study here have methoxy-terminated PEG chains as opposed to the hydroxy-terminated PEG in M12P5.[4, 1]

The difference in hydrophobic cores between the star-like macromolecules and the

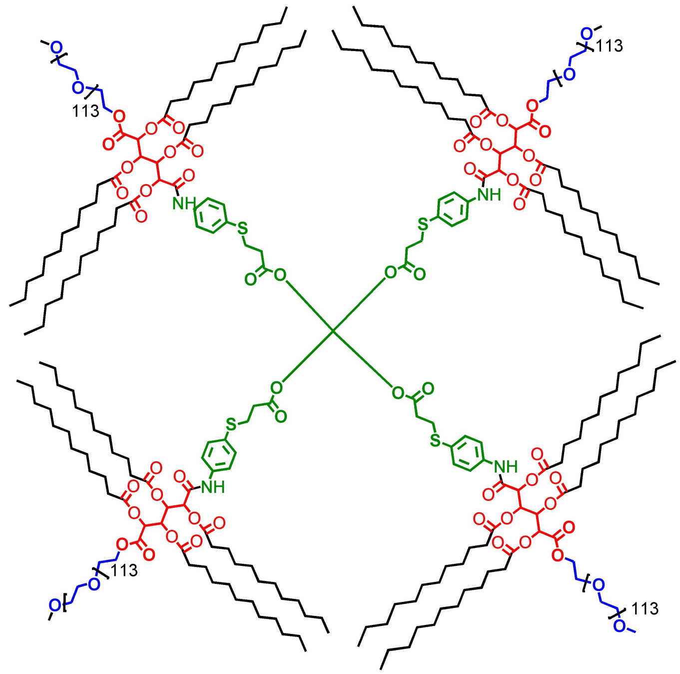

Figure 4.2: Structure of amphiphilic star-like macromolecule, **NC12P5**.

scorpion-like macromolecules leads to questions about the resulting structures, the size scales, and the aggregation properties of each of the polymers in aqueous solution. M12P5 scorpion-like macromolecules aggregate in water to form spherical micelles, as seen by transmission electron microscopy (TEM) in a previous study.[5, 4] In the case of the TEM study, the images taken were done in vacuum, with samples prepared by freeze-fracture methods.[5, 4] In this study, we use dynamic light scattering to measure particle size distributions of each of the three polymers in solution.

The volume for each polymeric unimer is estimated from incremental van der Waals volume calculations.[6, 7] The volume of each aggregate obtained from analysis of the DLS data can then be compared to the volume of a single unimer and to the effective volume of coumarin 153 reorientation found from time-resolved fluorescence anisotropy measurements. This last effective volume provides insight into the local friction felt by an encapsulated hydrophobic molecule in each of the three nanocarriers in question. This local friction is relevant to the capacity for each polymeric nanocarrier to encapsulate and release hydrophobic molecules in solution.

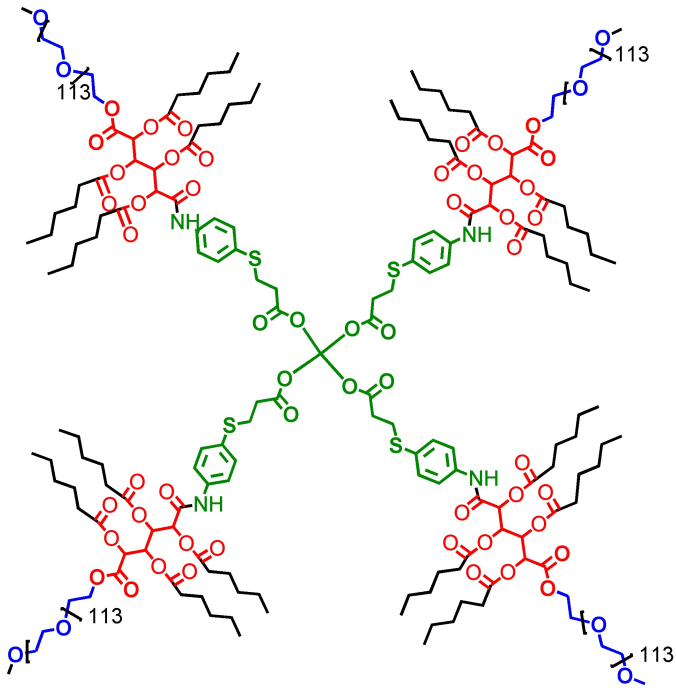

Figure 4.3: Structure of amphiphilic star-like macromolecule, **NC6P5**.

The local friction experienced by C153 solvated in each nanocarrier differs from the bulk viscosity of these dilute solutions. As shown by Horng, et.al, the reorientation of a polar molecule such as C153 is governed by dielectric friction with its surrounding solvent environments of various polarities.[8] This friction strays from typical hydrodynamic theory in many cases, thus causing a difference in macroscopic and nanoscale viscosities.[8, 9]

The purpose of the following study is to use C153 fluorescence to characterize the local environment in the core of each drug-delivery polymer. Properties of the C153 local environment such as solvent polarity, microviscosity, and effective size serve as a model for probing the core environment of an encapsulated drug molecule.[10, 11, 12] By revealing the nature of the local environment inside each nanocarrier, the polarity and flexibility of each drug delivery vehicle may be compared relative to each other for the purpose of encapsulating a hydrophobic molecule. The aggregation properties and size scales are explored by dynamic light scattering, by van der Waals molecular volume calculations, and by investigating the fluorescence and reorientation of C153

inside each polymer solution.

4.3 Measuring Size Scales and Micelle Transition

4.3.1 Dynamic Light Scattering

Particle size dependence on polymer concentration and temperature was characterized by DLS. Hydrodynamic radii were obtained from the DLS diffusion coefficients assuming Stokes-Einstein hydrodynamics.[7, 13] The Stokes-Einstein equation (Eq. 4.1) relates the translational diffusion coefficients (D_0) to the hydrodynamic radii (R_H), where T is the absolute temperature, k_B is the Boltzmann constant, and η is the solvent viscosity.[7, 13]

$$D_0 = \frac{k_B T}{6\pi\eta R_H} \tag{4.1}$$

Particle diameters were measured for aqueous solutions ranging in polymer concentration from 1x10^{-9} mol/L to 1x10^{-3} mol/L. Figure 4.4 shows the volume-weighted distribution of particle diameters found for all three polymer solutions at 37 °C at the same concentrations used for fluorescence experiments. The polymer aggregate diameters obtained from DLS data at 37 °C are plotted versus concentration in the top graph of Figure 4.5. These data indicate that aggregates begin to form in each of the three aggregate polymer solutions, as the concentration approaches 1x10^{-6} mol/L, and that the polymers exist as unimers in solution below 100 nM concentration. For concentrations in the range from 1x10^{-7} to 1x10^{-6} mol/L, micellar aggregates are formed. On increasing polymer concentration, the M12P5 aggregates increase and then decrease in size, ranging from 10 nm to 28 nm in diameter.

The NC12P5 and NC6P5 ASM polymers form larger aggregates at approximately the same polymer concentration. The star-like NC12P5 forms aggregates ranging in diameter of 23 nm to 45 nm. The other star-like macromolecule NC6P5 forms aggregates ranging in diameter from 14 nm to 47 nm over the same concentration range. NC6P5 aggregates are smaller compared to the NC12P5 aggregates due to the smaller number of aliphatic carbons present in the NC6P5 molecule. The lower bound for hydrodynamic

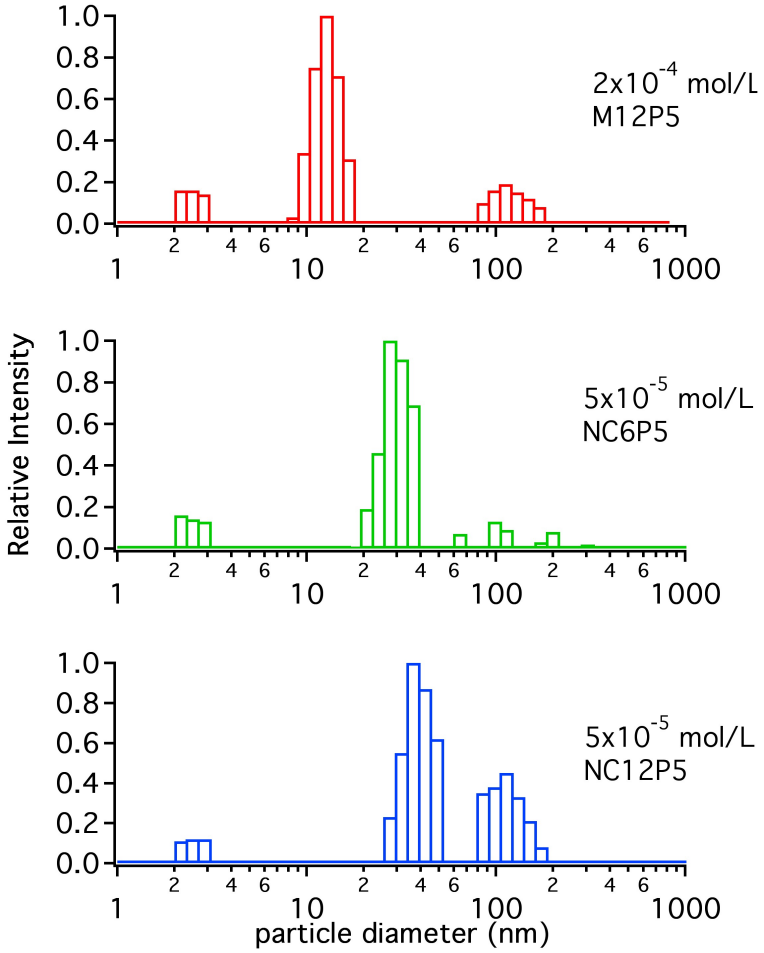

Figure 4.4: Volume-weighted particle size distributions of M12P5, NC12P5, and NC6P5 polymer solutions at 37 °C, obtained from DLS data.

radii obtained from the analysis of DLS data is approximately 1 nm for both ASMs and AScMs. This radius is consistent with the size estimated for ASM and AScM unimers.

For comparison with fluorescence experiments, the temperature dependence of particle size for all three polymer solutions was measured at the same concentrations used for fluorescence samples. In the range of 5 to 55 °C, M12P5 aggregates are tri-modal, with unimers, micelles, and larger aggregates present at approximately 100 nm diameters. The micellar aggregates, which are dominant in solution, have a diameter of 9 nm at 5 °C. The diameters increase to 21 nm at 55 °C. NC12P5 and NC6P5 also display tri-modal particle size distributions. The dominant diameter of NC12P5 aggregates

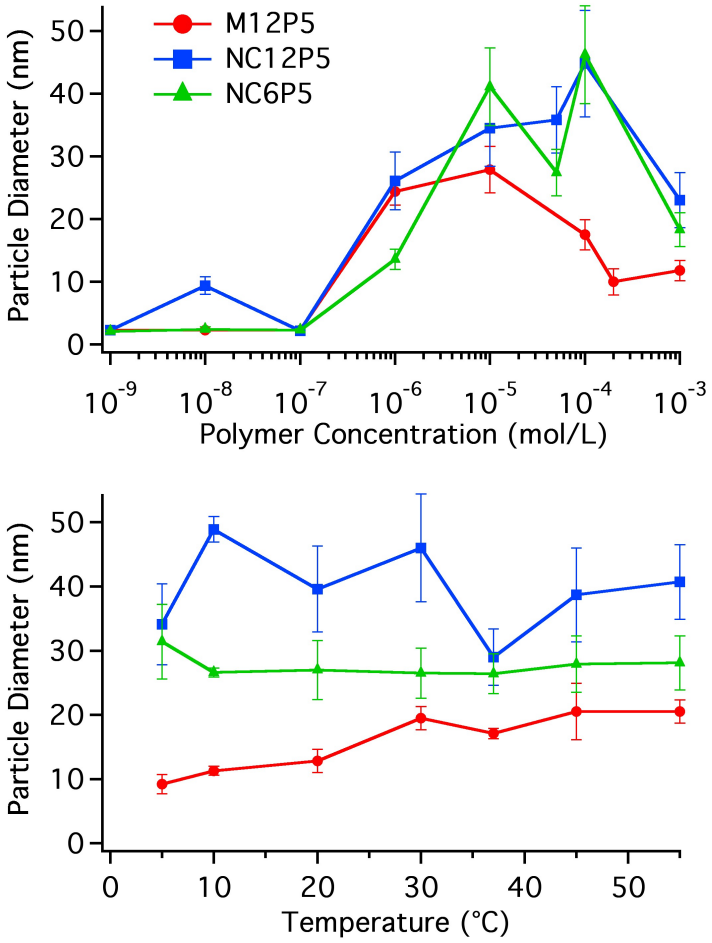

Figure 4.5: Particle diameters from DLS data versus concentration (top) at 37 °C and versus temperature (bottom) at 2x10^{-4} mol/L of M12P5, and 5x10^{-5} mol/L of both NC12P5, and NC6P5 polymer solutions.

is 40 nm. NC6P5 aggregates have an average diameter of 28 nm over the same temperature range. The diameter of NC12P5 aggregates is larger than the aggregates of NC6P5 polymer due to the greater number of hydrocarbons in the hydrophobic core of the NC12P5 ASM. Again, a small population of larger aggregates are also present around 100 nm particle sizes. The temperature dependence of the dominant aggregate diameters are shown in Figure 4.5 for all three polymer aggregates. The particle size distribution of each polymer solution at the concentrations of 2x10^{-4} mol/L M12P5, 5x10^{-5} mol/L NC12P5 and 5x10^{-5} mol/L NC6P5 showed relatively little change with increasing temperature. Further details of the polymer particle size distributions are

provided in Appendix B.

4.3.2 Viscosity of Solution Versus Microviscosity in ASM and AScM Cores

The shear viscosity of each of the three polymer solutions at high concentration (1x10^{-3} mol/L) and the concentrations used in fluorescence measurements (2x10^{-4} mol/L M12P5 and 5x10^{-5} mol/L NC12P5 and NC6P5) were used to calculate the effective volume of each polymer aggregate from reorientation time constants found from fluorescence anisotropy measurements. At high polymer concentrations of 0.001 mol/L, the viscosity of each of the three solutions was increased to 1.7 cP for M12P5, 2.8 cP for NC12P5, and 2.5 cP for NC6P5 at 5 °C (See Appendix B). At the dilute polymer concentrations used in fluorescence measurements, the viscosities of all three polymer solutions were the same as the viscosity of pure water within experimental error.

4.3.3 Steady-state Fluorescence Spectroscopy of Coumarin 153

Steady-state fluorescence emission spectra were measured for C153 in each of the three polymer solutions and are shown in Figure4.6. The emission wavelength of C153 is a sensitive reminder of the polarity of its local environment.[14, 15] From a previous study done with coumarins in amphiphilic tri-block copolymers, the broadened lineshape results from the coumarin dye experiencing more than one environment and therefore, experiencing a distribution of local polarities.[11] The C153 emission maximum is 535 nm for the M12P5 aqueous solution. This peak wavelength indicates that C153 is localized in a polar, water-like environment in the core of the M12P5 micelle.[11, 14, 15] Although the core is composed of hydrophobic, aliphatic carbons, water is likely present in or near the interior of the micelle. When C153 is solubilized in the cores of each of the two star-like macromolecules, the emission maximum is 510 nm. This peak wavelength value corresponds to a less polar environment around C153.[11, 14, 15] The cores of NC12P5 and NC6P5 macromolecules are more hydrophobic and do not contain polar water molecules to the extent that the core of M12P5 does, according to the fluorescence emission of C153. The peak emission of C153 in both ASM solutions corresponds to a dry core, much like the cores of Pluronic F88 amphiphilic triblock copolymer micelles,

as seen in a previous study.[12]

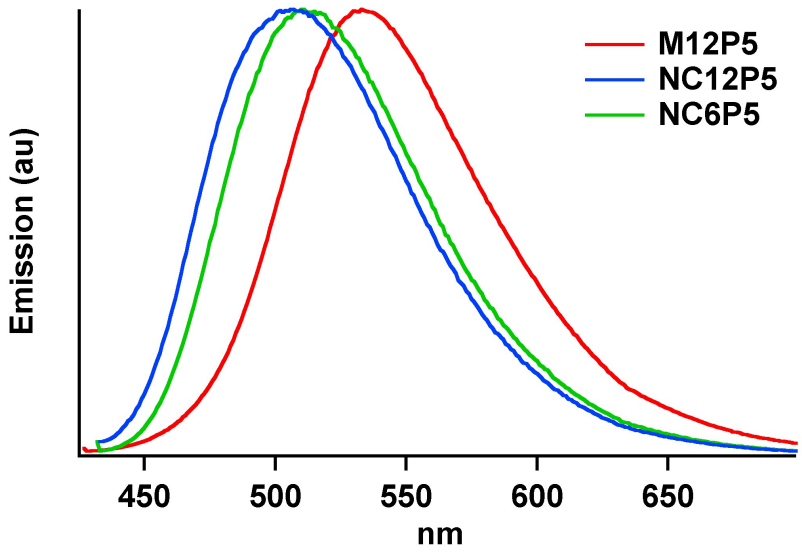

Figure 4.6: Steady-state emission spectra of coumarin 153 in aqueous solutions of M12P5, NC12P5, and NC6P5 solutions.

The peak wavelengths of the C153 emission spectra at 37 °C are shown in Figure 4.7. The π^* scale is a well known empirical solvent polarity scale used for a wide variety of common solvents.[16] Values of π^* correlate linearly to the maximum absorption and emission frequencies of C153.[15] As examples of two extremes of the π^* polarity scale, cyclohexane has a π^* of 0.0 and dimethyl sulfoxide has a π^* of 1.00.[15, 16] We can compare the local polarity of the C153 probe molecule while encapsulated in the polymeric aggregate using the effective π^* empirical polarity scale discussed by Horng, et. al.[15] In this way, we can compare the polarity of the molecular probe environment with the values for common organic solvents using the relation: $\widetilde{\nu}_{em}[10^{-3}$ $cm^{-1}] = 21.217 - 3.505\ \pi^*$. By means of this relationship, the π^* values of the local environment of C153 in M12P5 micelles ranges from 0.72 to 0.74 from 5 to 70 °C. This effective π^* value is similar to the polarity of dichloromethane, which has a value of $\pi^* = 0.73$.[15, 16] In NC6P5 and NC12P5, the local environment of C153 has π^* values ranging from 0.43 to 0.55 over the same temperature range. The more polar end of this range with $\pi^* = 0.55$ reflects a local polarity similar to THF or benzene.[15, 16]

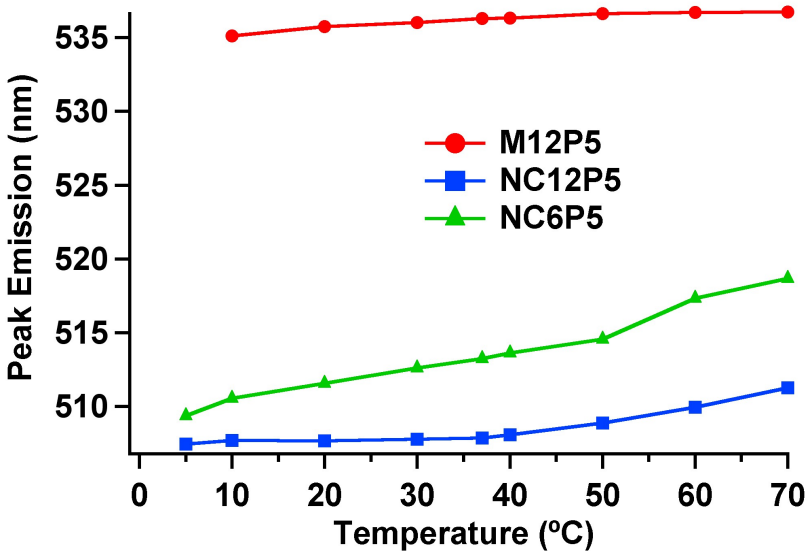

Figure 4.7: Temperature dependence of steady-state emission peak wavelength of coumarin 153 in M12P5, NC12P5, and NC6P5 aqueous solutions.

The lower end of this range is similar to the polarity of *p*-xylene and ethyl acetate, which both have π^*= 0.45.[15, 16] A plot of the effective π^* versus temperature is given in Appendix B. The difference in local polarity between C153 in the ASMs and C153 in the AScM nanocarriers is reminiscent of the shift observed for the $\widetilde{\nu}_{em}$ of C153 during aggregation of poly(ethylene oxide)-poly(propylene oxide)-poly(ethylene oxide) triblock copolymers undergoing the unimer-to-micelle nanoscale phase transition.[11] In this case, the local solvation environment of C153 in M12P5 is more polar than the triblock copolymer micelle cores previously studied, and the local environment of C153 in both ASM polymers is less polar than the presumably 'dry' micelle cores.[11]

The temperature dependence of the local polarity of C153 shows that π^* increases slightly with increasing temperature. This rise in polarity is consistent with the rearrangement of ordered water molecules closest to the core of each nanocarrier, causing increased penetration of polar waters towards the hydrophobic core.[17] The emission spectrum of C153 is sensitive to the proximity as well as the electric field of polar water molecules that affects the local solvation polarity around the coumarin dye.[18, 19]

4.4 Reorientational Dynamics and Length Scales

4.4.1 C153 Fluorescence Polarization Anisotropies

The fluorescence anisotropy is a ratio of the emission intensities detected at vertical and horizontal orientation, and is a measure of the amount of depolarization of emitted light due to reorientational motion of the fluorophore.[13] The limiting, or fundamental anisotropy, r(0), value ranges from 0.373 to 0.378 for C153 in a rigid, glassy solvation environment.[20, 11] Steady-state anisotropy values were measured with 425 nm excitation and 510 nm emission for the star-like NC12P5 and NC6P5 polymers, and at 530 nm for the M12P5 polymer. These values are plotted in Figure 4.8 (top). The limiting value of the time-dependent anisotropy (Equation 4.2), measured from the TCSPC data, is plotted in Figure 4.8 (bottom).

$$r(0) = \sum_{j=1}^{n} r_j \tag{4.2}$$

Both the steady-state and time-resolved limiting anisotropies for C153 in M12P5 are lower than those for C153 in the two star-like macromolecules. The plot of the limiting anisotropy from TCSPC methods versus temperature has the same trend as those values found from steady-state anisotropies. This phenomenon can be attributed to the two star-like macromolecules having a more rigid and hydrophobic core than the scorpion-like polymer micelles. We presume that the AScM micelles are flexible and undergo frequent reorganization and exchange among the monomer constituents, as has been shown to be the case for a number of other micelle systems.[21, 22, 23, 24] Because the cores of ASMs are more rigid, the fluorescence of C153 is not as depolarized as the emission of C153 in the more flexible M12P5 micelle core. The degree of depolarization, and therefore, the fundamental anisotropy, r(0), is dependent on the rotational motion of the fluorophore.[25, 13] If the C153 molecule is reorienting relatively rapidly in a water-like environment such as the core of the M12P5 micelle, the emission is more depolarized and r(0) is lower.[13] If C153 is reorienting slowly in a rigid environment, such as the core of a star-like macromolecule, the degree of depolarization is reduced and r(0) is closer to the maximum of 0.4.[25, 13]

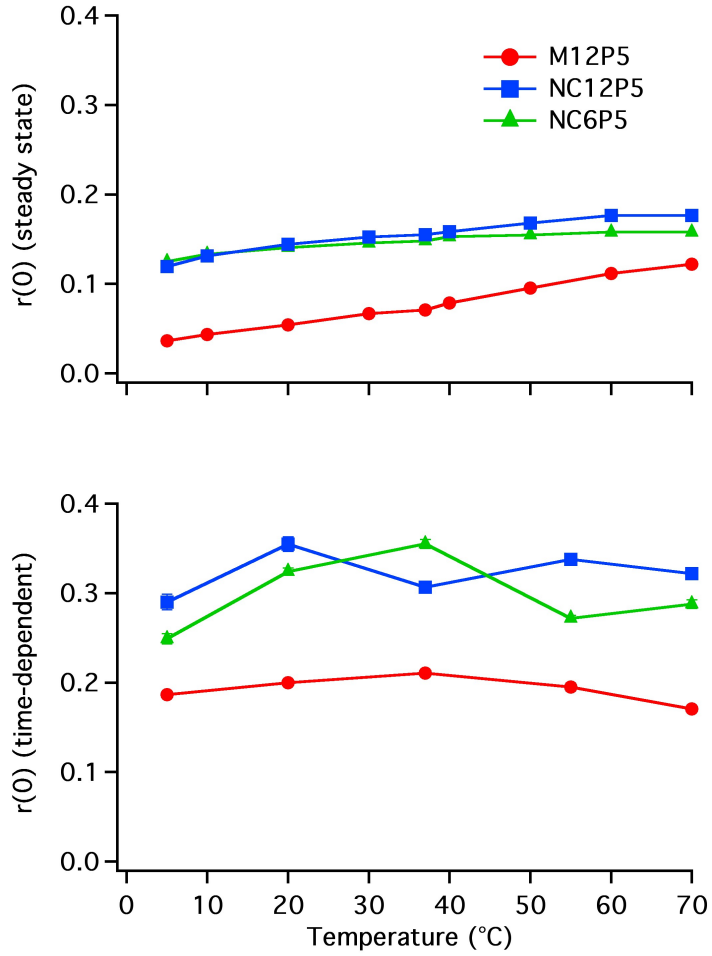

Figure 4.8: Temperature dependence of the limiting anisotropy from steady-state (top) and time-dependent (bottom) fluorescence depolarization of coumarin 153 in M12P5, NC12P5, and NC6P5 solutions.

4.4.2 C153 Reorientational Dynamics

Drug delivery systems require sequestration and solubilization of hydrophobic drugs, as well as the ability to ultimately release the drug. Thus, in successful drug delivery systems, the drug cannot be tightly or chemically bound so as to prevent drug release from the delivery system. We expect that the association characteristics of a drug (or C153 drug model) in ASMs and AScMs will display a complex range of orientational dynamics, consistent with the existence of weak association of the drug to multiple sites in the carrier. To investigate the nature of the model drug association with the hydrophobic

macromolecular core, we measured the fluorescence depolarization anisotropies of C153.

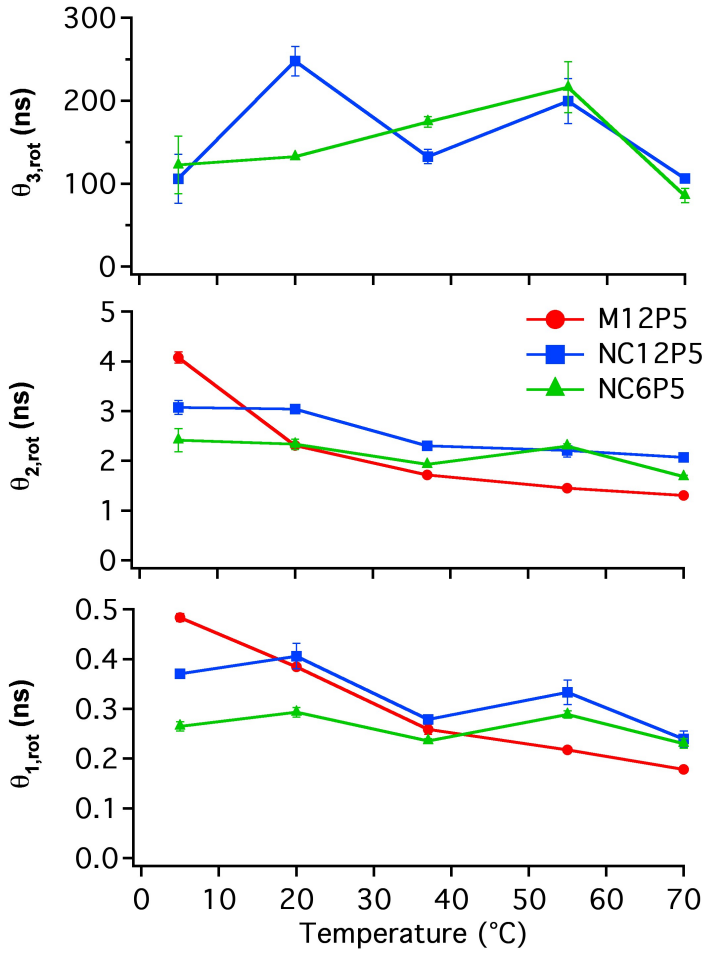

Figure 4.9: Temperature dependence of reorientation time constants, $\theta_{j,rot}$'s, for coumarin 153 in aqueous solutions of M12P5, NC12P5, and NC6P5.

$$\theta_{rot} = \frac{V\eta}{k_B T} \tag{4.3}$$

The Stokes-Einstein-Debye (S-E-D) equation (9) for small reorienting systems relates the reorientation time constant ($\theta_{i,rot}$) of a fluorescence probe to the effective volume of reorientation (V), the bulk viscosity of the solution (η), and the temperature.[8, 13, 26, 7] The viscosities measured for all polymer solutions were close to that of pure water because the solutions are dilute. Thus, the reorientation time constants give information about the local friction of the fluorophore environment. Reorientational

Table 4.1: C153 reorientation time constants, associated fractional amplitudes, and anisotropies in solutions of M12P5, NC12P5, and NC6P5 ranging from 5 °C to 70 °C. (Note: For r(0) See Eq. 7.)

Polymer	$\theta_{1,rot}$ (ns)	$\theta_{2,rot}$ (ns)	$\theta_{3,rot}$ (ns)	r_1	r_2	r_3
M12P5	0.18-0.48	1.30-4.07		0.08-0.12	0.05-0.11	
NC12P5	0.24-0.41	2.07-3.07	106-248	0.08-0.12	0.09-0.11	0.10-0.15
NC6P5	0.23-0.29	1.68-2.42	85.6-216	0.07-0.11	0.06-0.08	0.09-0.18

dynamics studied by fluorescence depolarization are relatively uncomplicated for the case of a fluorophore that is rigidly attached to a spherical macromolecule (or nanoparticle). For this case, S-E-D hydrodynamics predictions are often quite accurate. The case of a fluorescence probe that is labile is rather more complex.

The C153 emission decay transients detected at three angles of polarization were concatenated and simultaneously fit to the multiple exponential equations given in Equations 1 through 5. Best fits yielded three fluorescence time constants and two reorientation time constants for C153 in aqueous M12P5 solution. For C153 in NC12P5 and NC6P5 solutions, best fits yielded four fluorescence time constants and three reorientation time constants. Because the fluorescence anisotropy decay of C153 in each solution has multiple fluorescence and reorientation time constants, we deduce that C153 is in multiple solvation environments within each polymeric nanocarrier.[25, 8]

The most significant difference between the two classes of polymers is in the reorientation time constants of C153 between the AScM solution in contrast to ASM solutions. C153 shows a third, longer reorientation time constant in both ASMs, indicating that C153 is moving more slowly, likely experiencing motion with higher local friction in the two ASM solutions than in the more flexible core of the M12P5 AScM micelles. In many cases, it is useful to report the amplitude weighted average of multiple reorientation time constants.[26, 13] In this study, we report all $\theta_{j,rot}$'s separately, since the long reorientation time constants of C153 in the two ASM solutions greatly dominate such an average and the full range of C153 reorientation time scales will be distorted. Figure 4.9 shows the individual reorientation time constants of C153 in all three polymers: three in each ASM and two in the AScM solution. Figure 4.10 shows the percent amplitudes

for each reorientation time constant. These data illustrate that each reorientation time constant has a similar contribution to the total reorientation of the fluorophore.

The values of $\theta_{j,rot}$ and individual anisotropy contributions are listed in Table I. The two fastest reorientation time constants for C153 in all three polymer solutions are on similar time scales, meaning that the faster motions of the C153 dye are similar in all three nanocarriers. The fastest reorientation time constant ranges from about 0.2 to 0.5 ns over the 5 to 70 °C temperature range and the second reorientation time constant ranges from about 1.3 to 4.1 ns. The slowest reorientation time constant, which is only present for C153 in the two ASM solutions, ranges from approximately 86 to 248 ns.

DLS measurements indicate tri-modal particle size distributions for all three polymer solutions, however, the distributions of unimers and large aggregates (>100 nm) are minimal in each case. While the tri-modal distribution may affect the distribution of local environments measured, we believe that this is a minimal effect since the hydrophobic C153 will preferentially localize within the more non-polar micelle or aggregate core that dominates the particle size distribution in all three polymers. We maintain that the C153 and polymer dynamics will remain similar in both aggregate and macro-aggregate environments. With this said, we keep in mind that the hydrodynamic volumes of ASM and AScM unimers and aggregates found from DLS are a result of measuring the translational diffusion of these solutions while the hydrodynamic dimensions estimated from the analysis of the TCSPC data is a result of measuring orientational diffusion of the coumarin dye. The similarities and differences that arise in these two methods are displayed in Table 4.2.

Several possibilities may occur that lead to reorientation time constants that are faster than are predicted by the S-E-D equation (Equation 9). The probe may be localized within a region of lower viscosity, such as the water pool in a reverse micelle[27, 28, 29] or within a fluid-like micellar core.[11] Another possibility is that the probe is weakly associated with the macromolecule such that there is a more rapid 'wobble-in-cone' torsional motion that is sampled by the probe depolarization.[26, 13] This effect may be combined with a slower time constant correlated with the overall motion of the macromolecule.

Other possibilities include weak association of the C153 to the polymer. The reorientational dynamics of a probe may show the probe to be rigidly coordinated to the macromolecule, and its motion punctuated by bursts of rapid 'free' reorientation during brief moments when the probe is unassociated.[13] A case such as this could arise from a probe undergoing sequential release and geminate recombination to the same association site of a macromolecule. Alternatively, a weakly associated fluorescence probe may be sampling a multiplicity of association conformations and/or multiple sites. For any of these cases of weak association to be experimentally observable, association and release must be occurring during the temporal window for fluorescence, which is about ten times the average fluorescence time constant. The S-E-D hydrodynamics law for molecular reorientation dynamics does not provide information exclusively about the molecular volume of the reorientation species nor about the effective local viscosity: rather, S-E-D indicates that time constants obtained by measurement of reorientational dynamics should scale as the product of effective volumes and local viscosities.

Considering the case of a single, rigid unimer of each macromolecule, θ_{rot} values can be predicted by S-E-D using the estimated incremental van der Waals volume of a one unimer and the measured viscosity of each polymer solution.[6, 7] These predictions range from 0.5 to 2.2 ns for an M12P5 unimer, 2.5 to 11.6 ns for an NC12P5 unimer, and from 1.8 to 8.4 ns for an NC6P5 unimer over the temperature range from 5 to 70 °C. The predicted values for the observed reorientation time constant of single unimers are between the second and third time constants of C153 found by TCSPC methods. (See Appendix B)

The dimensions obtained from this analysis of the C153 fluorescence anisotropy data, assuming S-E-D hydrodynamic behavior, can be compared to the hydrodynamic radii obtained from the DLS data. For the DLS particle size distributions, the smaller diameters obtained are much larger than the diameters inferred from the C153 $\theta_{j,rot}$ values. Applying the methods of Bondi[6] and Edward,[7] the van der Waals volumes for AScM and ASM unimers were estimated to be 5.6 nm^3 for an M12P5 unimer, 29.3 nm^3 for an NC12P5 unimer, and 21.3 nm^3 for an NC6P5 unimer. Assuming that the random-coil polymers are spherical, the corresponding diameters for an M12P5 unimer,

an NC12P5 unimer and an NC6P5 unimer, respectively, are 2.2, 3.8, and 3.4 nm.

Because the polymers exhibit flexible random coil behavior in solution, the fastest reorientation time constants, $\theta_{1,rot}$ from C153 fluorescence represent a smaller volume and a faster motion than the reorientation of an entire unimer for each of the three polymers. These time constants range from 0.2 to 0.5 ns, and are assigned to hindered orientational diffusion of C153 molecules loosely associated with the ASM or AScM polymers. The corresponding diameters are therefore in the range of 0.2 to 0.5 nm, approximately the diameter of the coumarin molecule itself.

Assuming that the bulk viscosity also is an accurate measure of the local friction, t he second reorientation time constants, $\theta_{2,rot}$ correlate to slightly larger effective volumes in all three polymer solutions. $\theta_{2,rot}$ for C153 in M12P5 solution correlates well with the volume of a unimer having a diameter of 2.2 nm. The effective diameters obtained from C153 reorientation in the second mode are on the order of 1.5 to 3.9 nm; approximately the same dimensions of each polymeric unimer according to incremental van der Waals molecular volumes.[6]

The third reorientation time constant, $\theta_{3,rot}$, for C153 in the three polymer solutions, corresponds to effective diameters larger than a single ASM unimer, and approximately the same or slightly larger than the dominant aggregate sizes indicated by DLS. For NC12P5, the range of diameters predicted from C153 reorientational dynamics are 43 to 285 nm. Likewise, the range of diameters deduced from C153 fluorescence anisotropy in NC6P5 solution range from 49 to 309 nm. The existance of the third, longer reorientation time constant, $\theta_{3,rot}$, in the two ASM polymer solutions further indicates that aggregation is occuring and that C153 is experiencing local reorientation on a size scale close to that of an aggregate. A comparison of the predicted diameters for each of the polymers in solution is presented in Table II.

The Stokes-Einstein-Debye (S-E-D) equation has shown to be quite useful for correlating the viscosity, temperature, and molecular volume of the reorienting species with the orientational correlation time constant for aqueous and organic solvent solutions.[8, 13, 26] The local friction actually experienced by a molecular probe is often poorly correlated to the bulk solution viscosity. In polymer solutions, the S-E-D equation is

Table 4.2: Calculated effective diameters from C153 reorientation (Method = C153), diameters of polymer aggregates from DLS (Method = DLS), and diameters (in nm) of unimers from van der Waals incremental volumes (Method = vdW).[6, 7]

Polymer	Method	d_1 (nm)	d_2 (nm)	d_3 (nm)	d_{unimer} (nm)
M12P5	C153	0.19 - 0.33 (±0.01)	1.5 - 2.4 (±0.05)		
	DLS	5.8 - 6.7 (±0.8)	9.2 - 21 (±1.8)	50 - 340 (±24)	
	vdW				2.11
NC12P5	C153	0.15 - 0.48 (±0.04)	1.2 - 3.9 (±0.2)	43 - 285 (±39)	
	DLS	5.7 - 5.8(±0.8)	29 - 49 (±8)	83 - 164 (±17)	
	vdW				3.82
NC6P5	C153	0.11 - 0.43 (±0.02)	0.97 - 3.3 (±0.09)	49 - 309 (±44)	
	DLS	2.3 - 11.1(±0.2)	26 - 31 (±5)	53 - 95(±14)	
	vdW				3.44

applied in a different way than for the simpler case of organic solvents. Horng, et al. have derived an empirical equation for obtaining the effective solvent viscosity from the measured reorientational time constants obtained from C153 fluorescence anisotropy experiments.[8] Their equation $\langle\theta_{rot}\rangle_{polar} = (58.1 \pm 1.6)\,\eta^{(0.96\pm0.03)}$ holds for a wide range of polar organic solvent environments.[8] We have shown above that the effective polarity of the environments ranges from about 0.4 to 0.7 on the π^* empirical solvent polarity scale, which shows that our C153 probe is always experiencing a polar environment.

One interpretation of the multiple exponential orientational time constants that we observe for C153 in the ASM and AScM solutions is that the C153 is distributed heterogeneously among sites with different microviscosities. Making this assumption we can predict the effective microviscosity experienced by the C153 using the equation of Horng, et.al, above.[8] The results from applying this equation are presented in Table III. The fastest reorientation time constants lead to microviscosity values η_1 in the 3.2 to 9.1 cP range, consistent with weak entanglement in a hydrophilic polymer solution. The second time constants lead to predicted microviscosities η_2 in the range from 25.6 to 84 cP. Only in the ASMs NC6P5 and NC12P5 are the higher friction values observed. For these solutions, the third reorientational time constant can be used to predict a microviscosity ranging from 2500 to 6050 cP. These values are larger than we observed in the micellar cores of PEO-PPO-PEO triblock copolymer model systems, for which the maximum microviscosity of 890 cP was found for a *bcc* hydrogel solution of micelles.[11] The measured bulk viscosities of the aqueous polymer solutions are available in Appendix B and range from 0.4 to 1.6 cP. The local friction of C153 experienced in these polymer solutions is much larger than the bulk solution viscosity for all solutions and temperatures measured. The difference in local friction of C153 between the three polymers is a further indication that C153 is more rigidly encapsulated inside the two amphiphilic star-like macromolecules than in the scorpion-like M12P5 micelle.

Table 4.3: Calculated local frictions of C153 in each aqueous polymer solution from individual reorientation time constants.[8]

Polymer	η_{local} 1(cP)	η_{local}2 (cP)	η_{local}3 (cP)
M12P5	3.2-9.1	26-84	
NC12P5	4.4-7.6	41-63	2500- 6050
NC6P5	4.2-5.4	33-49	2000 - 5250

4.5 Conclusions

The fluorescent coumarin 153 dye was solubilized in three amphiphilic polymers that were designed and synthesized for the purpose of hydrophobic drug encapsulation. Steady-state and time-resolved fluorescence studies of C153 in each solution were performed over a range of temperatures from 5 to 70 °C to reflect encapsulation behavior at several temperatures. Analysis of the steady-state emission shows that C153 is in a polar environment in the AScM polymer solution and in a less polar environment in the two ASM polymers. Dynamic light scattering measurements provide insight into the aggregation of both ASM and AScM polymers. DLS results show aggregates in solution with a distribution of sizes from 10 nm to 40 nm, which is well under the 100 nm limit for good bioavailability.[30, 31] Hydrodynamic radii obtained from analysis of DLS data were compared to those deduced from C153 polarization anisotropy as well as estimated unimer diameters found from incremental van der Waals volumes.[6, 7] From shear viscosity measurements, the bulk viscosity of these solutions is close to that of bulk water,[32] while the local friction as reported by C153 is substantially higher for each of three orientational motions of C153 detected.

Analysis of time-resolved fluorescence anisotropy measurements yielded multiple rates of fluorescence and multiple reorientation time constants for C153 in each of the polymer local environments. The fluorescence lifetimes do not reflect any nanoscale phase changes such as micellization or de-micellization at the polymer concentrations studied, but indicate that the C153 probe is in a more polar core environment in the M12P5 micelle than in the NC12P5 scorpion-like macromolecule. The lifetimes also show that the core of NC6P5 has an intermediate polarity in comparison to the other two nanocarriers.

It is likely is that C153 is experiencing multiple solvation sites within polymer aggregates. Though unimers are likely to be diffusing in and out of different aggregates, C153 seems to localize in the covalently bonded core of each polymer, near the hydrocarbon chains at each acylated mucic acid region, or at the interface between the hydrocarbon core and the PEG corona of each nanocarrier.

In comparing the ASMs and AScMs, the individual reorientation time constants found from polarization anisotropy measurements show that C153 is more rigidly associated with the non-polar core of each ASM polymer and in a more polar environment in the flexible core of the AScM micelle. The effective diameters from C153 reorientation applying S-E-D hydrodynamics correlate to multiple reorientational motions of C153 in both ASMs and AScM solutions. These data support the conclusion that C153 is solvated in multiple regions inside the core of each polymeric nanocarrier. The longer reorientation time constants of C153 in NC12P5 and NC6P5 polymers are evidence that C153 is rigidly solvated in the core of the star-like nanocarriers, while the dye is loosely solvated in the polar core of the AScM micelles.

These C153 fluorescence studies provide sensitivity to the details of the local environment within the encapsulated sites of the ASM and AScM polymers. Specifically, the C153 probe senses the local polarity and microviscosity. If an encapsulated drug requires increased solubility, but a longer retention profile, the more hydrophobic, rigid core of the two ASM polymers may be more useful than the flexible core of AScM micelles. The local drug solvation properties of future derivatives of these three polymeric macromolecules and others can be methodically characterized using the methods described in this study.

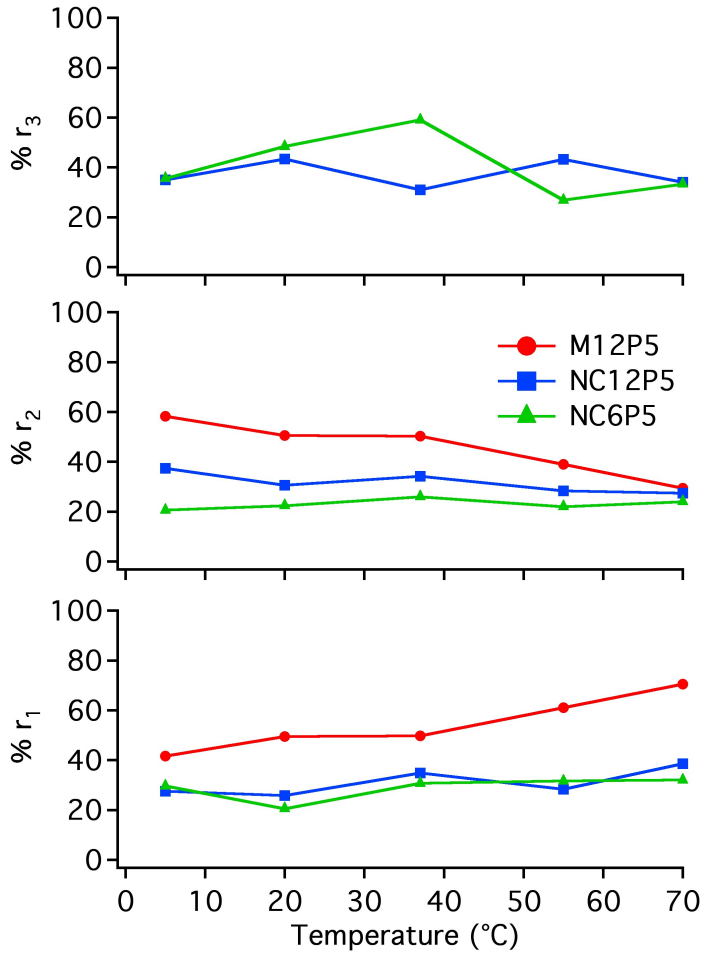

Figure 4.10: Temperature dependence of percent amplitudes ($\%r_j$ of r(0)) for C153 time constants in aqueous solutions of M12P5, NC12P5, and NC6P5.

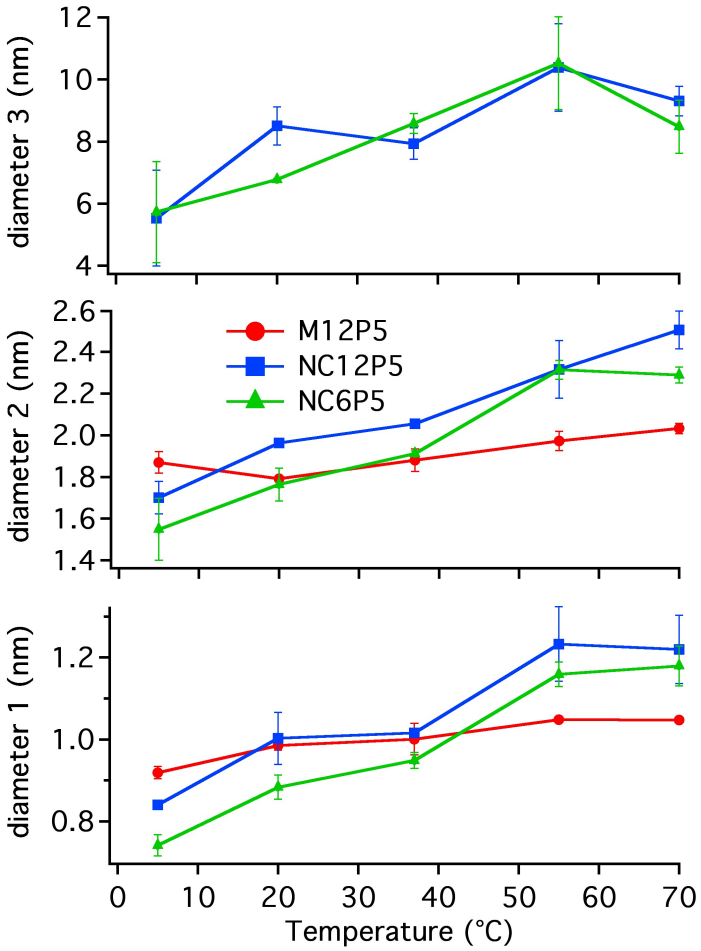

Figure 4.11: Temperature dependence of effective diameters of coumarin 153 reorientation in M12P5, NC12P5 and NC6P5 polymer solutions.

References

[1] L. Tian *et al.;* Amphiphilic scorpion-like macromolecules: Design, synthesis, and characterization.; *Macromolecules* **2004**, *37*, 538–543.

[2] L. Tian *et al.;* Core crosslinkable polymeric micelles from peg-lipid amphiphiles as drug carriers.; *Journal of Materials Chemistry* **2004**, *14*, 2317–2324.

[3] H. Liu, A. Jiang, J. Guo, and K. E. Uhrich; Unimolecular micelles: synthesis and characterization of amphiphilic polymer systems.; *Journal of Polymer Science, Part A: Polymer Chemistry* **1999**, *37*, 703–711.

[4] L. Tao and K. E. Uhrich; Novel amphiphilic macromolecules and their in vitro characterization as stabilized micellar drug delivery systems.; *Journal of Colloid and Interface Science* **2006**, *298*, 102–110.

[5] J. Djordjevic, M. Barch, and K. E. Uhrich; Polymeric micelles based on amphiphilic scorpion-like macromolecules: Novel carriers for water-insoluble drugs.; *Pharmaceutical Research* **2005**, *22*, 24–32.

[6] A. Bondi; van der waals volumes and radii; *Journal of Physical Chemistry* **1964**, *68*, 441–51.

[7] J. T. Edward; Molecular volumes and the stokes-einstein equation; *Journal of Chemical Education* **1970**, *47*(4), 261–270.

[8] M.-L. Horng, J. A. Gardecki, and M. Maroncelli; Rotational dynamics of coumarin 153: Time-dependent friction, dielectric friction, and other nonhydrodynamic effects.; *Journal of Physical Chemistry A* **1997**, *101*, 1030–1047.

[9] D. Ben-Amotz and J. M. Drake; The solute size effect in rotational diffusion experiments: A test of microscopic friction theories; *The Journal of Chemical Physics* **1988**, *89*(2), 1019–1029.

[10] L. Frauchiger, H. Shirota, K. E. Uhrich, and E. W. Castner Jr.; Dynamic fluorescence probing of the local environments within amphiphilic starlike macromolecules.; *Journal of Physical Chemistry B* **2002**, *106*, 7463–7468.

[11] C. D. Grant, K. E. Steege, M. R. Bunagan, and E. W. Castner Jr.; Microviscosity in multiple regions of complex aqueous solutions of poly(ethylene oxide)-poly(propylene oxide)-poly(ethylene oxide).; *Journal of Physical Chemistry B* **2005**, *109*, 22273–22284.

[12] C. D. Grant *et al.;* Fluorescence probing of interior, interfacial, and exterior regions in solution aggregates of poly(ethylene oxide)- poly(propylene oxide)-poly(ethylene oxide) triblock copolymers.; *Langmuir* **2005**, *21*, 1745–1752.

[13] B. Valeur *Molecular Fluorescence: Principles and Applications;* Wiley-VCH, 2002.

[14] M. Maroncelli and G. R. Fleming; Picosecond solvation dynamics of coumarin 153: the importance of molecular aspects of solvation.; *Journal of Chemical Physics* **1987**, *86*, 6221–39.

[15] M. L. Horng, J. A. Gardecki, A. Papazyan, and M. Maroncelli; Subpicosecond measurements of polar solvation dynamics: Coumarin 153 revisited.; *Journal of Physical Chemistry* **1995**, *99*, 17311–37.

[16] M. J. Kamlet, J. L. Abboud, and R. W. Taft; The solvatochromic comparison method. 6. the π^* scale of solvent polarities.; *Journal of the American Chemical Society* **1977**, *99*, 6027–6038.

[17] K. Bhattacharyya and B. Bagchi; Slow dynamics of constrained water in complex geometries.; *Journal of Physical Chemistry A* **2000**, *104*, 10603–10613.

[18] L. Reynolds *et al.;* Dipole solvation in nondipolar solvents: Experimental studies of reorganization energies and solvation dynamics.; *Journal of Physical Chemistry* **1996**, *100*, 10337–10354.

[19] G. Jones II, W. R. Jackson, C. Y. Choi, and W. R. Bergmark; Solvent effects on emission yield and lifetime for coumarin laser dyes. requirements for a rotatory decay mechanism.; *Journal of Physical Chemistry* **1985**, *89*, 294–300.

[20] J. A. Gardecki and M. Maroncelli; Solvation and rotational dynamics in acetonitrile/propylene carbonate mixtures: a binary system for use in dynamical solvent effect studies.; *Chemical Physics Letters* **1999**, *301*, 571–578.

[21] A. Halperin and S. Alexander; Polymeric micelles: their relaxation kinetics.; *Macromolecules* **1989**, *22*, 2403–12.

[22] B. Michels, G. Waton, and R. Zana; Dynamics of micelles of poly(ethylene oxide)-poly(propylene oxide)-poly(ethylene oxide) block copolymers in aqueous solutions.; *Langmuir* **1997**, *13*, 3111–3118.

[23] H. Mays and M. Almgren; Temperature-dependent properties of water-in-oil microemulsions with amphiphilic triblock-copolymer. part i: Dynamics, particle interactions, and network formation.; *Journal of Physical Chemistry B* **1999**, *103*, 9432–9441.

[24] R. Lund *et al.;* Logarithmic chain-exchange kinetics of diblock copolymer micelles.; *Physical Review Letters* **2006**, *96*, 068302/1–068302/4.

[25] C. N. Bialik *et al.;* Dynamics of biomolecules: assignment of local motions by fluorescence anisotropy decay.; *Biophysical Journal* **1998**, *75*, 2564–2573.

[26] J. R. Lakowicz *Principles of Fluorescence Spectroscopy;* Kluwer Academic/ Plenum Publishers, 2nd ed., 1999.

[27] N. E. Levinger; Ultrafast dynamics in reverse micelles, microemulsions, and vesicles.; *Current Opinion in Colloid & Interface Science* **2000**, *5*, 118–124.

[28] D. Pant and N. E. Levinger; Polar solvation dynamics in nonionic reverse micelles and model polymer solutions.; *Langmuir* **2000**, *16*, 10123–10130.

[29] M. R. Harpham, B. M. Ladanyi, N. E. Levinger, and K. W. Herwig; Water motion in reverse micelles studied by quasielastic neutron scattering and molecular dynamics simulations.; *Journal of Chemical Physics* **2004**, *121*, 7855–7868.

[30] R. Duncan; The dawning era of polymer therapeutics.; *Nature Reviews Drug Discovery* **2003**, *2*, 347–360.

[31] G. S. Kwon; Polymeric micelles for delivery of poorly water-soluble compounds.; *Critical Reviews in Therapeutic Drug Carrier Systems* **2003**, *20*, 357–403.

[32] R. C. Weast and M. J. Astle, Eds. *CRC Handbook of Chemistry and Physics;* CRC Press, Inc., 61 ed., 1980.

Chapter 5

Fluorescence Probing of Aqueous Triblock Copolymer Pluronic F88

5.1 Overview

Seven coumarin fluorescence probe molecules of varying solubilities are used to probe the hydrophilic, hydrophobic, and interfacial regions of A-B-A triblock copolymer poly(ethylene oxide)$_{109}$ - poly(propylene oxide)$_{41}$ - poly(ethylene oxide)$_{109}$ spherical micelles in aqueous solution. Bulk polymer solution characterization is carried out by differential scanning calorimetry, dynamic light scattering, and shear viscosity measurements. Steady-state and time-resolved fluorescence measurements are used to measure the local environment polarity, viscosity, and reorientational motions on molecular and nanometer length scales for each of the seven coumarin molecules. These parameters correspond directly to the solubility of the coumarin molecule and the nanophase transition of the polymer solution from unimers to micelles. The local environment of each coumarin fluorophore is investigated with respect to local polarity and viscosity, enabling the various local environments of the polymer solution to be examined.

5.1.1 Pluronic F88: An A-B-A Triblock Copolymer

Pluronic F88, an A-B-A triblock copolymer, is composed of poly(ethylene oxide)$_{109}$ - poly(propylene oxide)$_{41}$ - poly(ethylene oxide)$_{109}$ abbreviated PEO$_{109}$-PPO$_{41}$-PEO$_{109}$. The structure of Pluronic F88 is shown in Figure 5.1 with poly(ethylene oxide) blocks colored in blue and the poly(propylene oxide) block in red. F88 in solution is known to form spherical micelles at a critical micellization concentration and temperature. The hydrophobic PPO blocks of the copolymer aggregate in water because of the hydrophobic effect, forming a water-soluble corona around the PPO core of the micelle.[1, 2]

Pluronics are of interest because these triblock copolymers have been used in various works for drug encapsulation and delivery.[3, 4, 5, 6, 7] From SANS studies, F88 forms spherical micelles of approximately 17 nm in diameter in aqueous solutions with PPO cores ranging from 7 to 10 nm in diameter.[8]

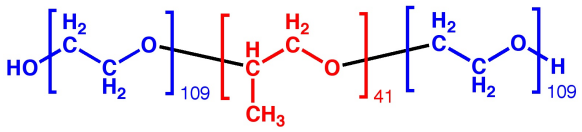

Figure 5.1: Structure of A-B-A Triblock Copolymer Pluronic F88

5.1.2 Coumarin Solvatochromic Fluorescence Probes

7-aminocoumarins are a class of well-characterized and widely used solvatochromic fluorescent molecules. Solvatochromism means that the fluorescence emission wavelength of a molecule is dependent upon the polarity of the solvent environment of the fluorophore.[9, 10] The seven coumarin fluorescent probes used in this study include, in order of increasing solubility coumarin 314T (C314T), coumarin 153 (C153), coumarin 102 (C102), coumarin 152 (C152), coumarin 337 (C337), coumarin 151 (C151), and coumarin $343^{-}/Na^{+}$ ($C343^{-}/Na^{+}$). These seven molecules are similar in structure, but vary in solubility from the most hydrophobic C314T to the most water-soluble $C343^{-}$ anion. To show the difference in solubility, we use the calculated octanol-water partition coefficient or clogP value of each coumarin. The octanol-water partition coefficient (clogP) is an empirically calculated value that reflects the differential solubility of a molecule in octanol and water as solvents. This scaling of hydrophobicity and hydrophilicity is widely used for describing pharmaceutical bioavailability where a clogP value of 0 indicates that a molecule is 100% soluble in octanol and 0% soluble in water, while a clogP value of 10 indicates the opposite.[11] The structure, molecular volume (in $Å^3$), and clogP value of each coumarin molecule is shown in Figure 5.2.

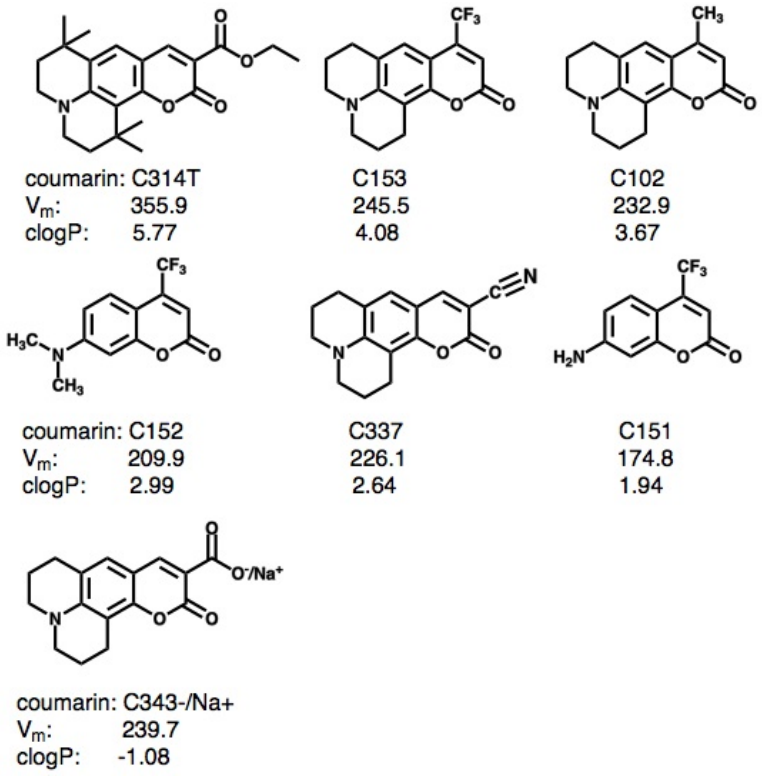

Figure 5.2: Structure, molecular volume (Å^3) and clogP values of coumarin fluorescence probes coumarin 314T (C314T), coumarin 153 (C153), coumarin 102 (C102), coumarin 152 (C152), coumarin 337 (C337), coumarin 151 (C151), and coumarin 343$^-$/Na$^+$ (C343$^-$/Na$^+$)

5.2 Results and Discussion

5.2.1 Polymer Length Scales and Aggregate Phases

The size scales of interest for solutions of F88 range from molecular length scales of several angstroms (diameter of an encapsulated coumarin), to F88 unimers of several nanometers, to micelle aggregates up to approximately 20 nm. Dynamic light scattering (DLS) is used to measure particle sizes in aqueous solutions of F88 from 2 nm unimers to 20 nm micelles.[12] Thermal analysis of the polymer solutions by differential scanning calorimetry (DSC) allows the micellization phase transition temperature to be identified. Steady-state and time-resolved fluorescence spectroscopy measure the solution dynamics on molecular length scales.

Differential Scanning Calorimetry of Polymer Solutions

Differential scanning calorimetry (DSC) was used for thermal analysis of the microphase transition from unimers to micelles. Figure 4 shows endothermic peaks for Pluronic F88 in 5 w/v% and 25 w/v% polymer solutions. The onset of each of these peaks is the micellization temperature for each of these polymers at the measured concentrations in aqueous solution. This shows the decrease in micellization temperature with the increase of the length of the hydrophobic block in the A-B-A triblock copolymers. For 25 w/v%F88, the micellization temperature is 22.5 °Cwhile at 5 w/v% F88 solution, the micellization temperature is 34.8 °C.

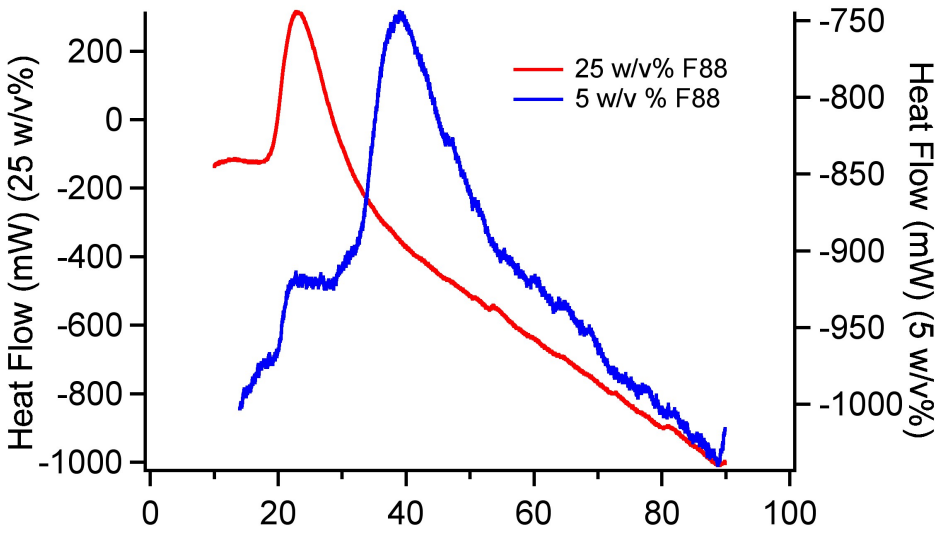

Figure 5.3: Differential scanning calorimetry of Pluronic F88 in 5 w/v% (blue) and 25 w/v% polymer in aqueous solution illustrates the micellization temperature at the onset of the thermal peak.

5.2.2 Electronic Structures of Coumarin Solvatochromic Probe Molecules

The difference in dipole moments between the electronic ground state and the electronic excited state in a coumarin molecule is the reason that a coumarin molecule is solvatochromic with respect to its fluorescence spectrum.[13, 14, 9, 15] Empirical electronic

structure calculations such ZINDO give some insight into the magnitude of the solvatochromism. A ground state electronic structure and potential energy surface is very different from the excited stat electronic structure and potential energy surface when the solvatochromic shift is large in response to local solvent polarity. In Figures 5.4 and 5.5, the electronic surface of two coumarin molecules is shown in both the ground state or highest occupied molecular orbital HOMO) and the electronic excited state or lowest unoccupied molecular orbital (LUMO). Coumarin 337 and coumarin 314T show differences between ground and excited states, giving rise to their solvatochromic nature. The electronic structure of the other five coumarin molecules studied in this work has been published by Cave and coworkers.[13, 14]

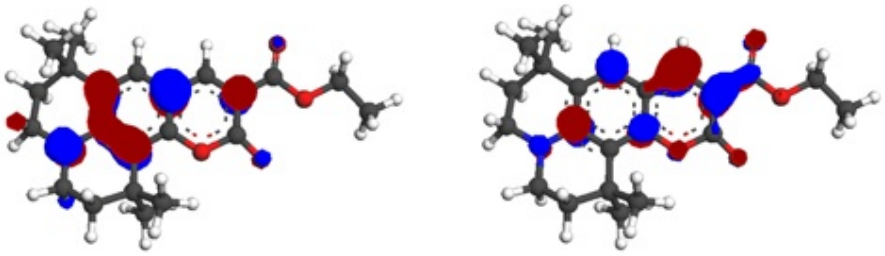

Figure 5.4: HOMO (left) and LUMO (right) of C314T obtained from a ZINDO[16, 17, 18, 19, 20] calculation using a configuration interaction window of [HOMO-20, LUMO+20].

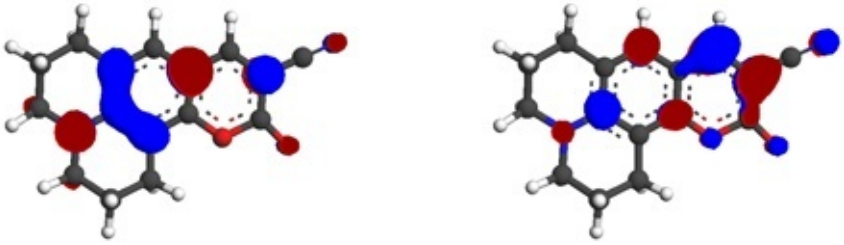

Figure 5.5: HOMO (left) and LUMO (right) of C337 obtained from a ZINDO[16, 17, 18, 19, 20] calculation using a configuration interaction window of [HOMO-20, LUMO+20].

Table 5.1: Ground state dipole moments, μ_{S_0} (D), energies (in eV) from the ground state to the first electronic excited state ($\triangle E_{S_0 \rightarrow S_1}$) and excited state dipole moments, μ_{S_1} (D) from ZINDO[16, 17, 18] electronic structure calculations of 7 coumarin molecules using ArgusLab.[19, 20]

Coumarin	μ_{S_0} (D)	$\triangle E_{S_0 \rightarrow S_1}$(eV)	μ_{S_1} (D)
C314T	8.77	3.31	15.40
C153	7.31	3.90	14.14
C102	8.59	3.65	12.47
C152	7.02	3.62	13.84
C337	12.33	3.35	18.56
C151	6.79	3.69	12.44
C343	8.02	3.44	9.82

5.2.3 Local Polarity in Aqueous Solutions of Unimers, Micelles, and Hydrogels

The solvent environment of a coumarin molecule affects the fluorescence emission and excitation spectra of the coumarin because of the interactions between solvent and solute (coumarin) in both the ground state and the excited state.[21, 9] Non-specific interactions, such as those between solvent and solute dipole moments, dipole and induced dipole moments, the solvent Stark effect, and dispersion interactions all affect solvatochromic shifts.[9, 22, 10] Other interactions between solvent and solute include specific interactions, such as hydrogen bonding.[9] The most significant interactions that affect the solvatochromism of coumarin molecules are dipole-dipole interactions.[23, 24, 13] In the case of the seven coumarin molecules used here, the excited state sees a relatively drastic increase in dipole moment compared to the ground state according to electronic structure calculations such as ZINDO and DFT.[13, 14] The interactions between the coumarin solute and solvent therefore affect the change in dipole moment between the ground and excited electronic states. Because of the change in coumarin dipole moment, the polarity of the solvent scales with the shift in energy absorbed upon excitation and emitted during fluorescence.[9, 10, 24] While roughly all the same structure, the sizes of the coumarin molecules do vary slightly. This size variation will most likely cause small differences in the ability for each coumarin molecule to diffuse within a polymeric micelle solution. Also, some coumarins have ligands which may either accept or donate

a hydrogen bond. Specific interactions between the coumarin and solvent molecules will have an effect on the region of the coumarin solvent environment and consequently the spectroscopy of the coumarin molecule.[9, 25]

In the case of A-B-A triblock copolymer PEO_{109}-PPO_{41}-PEO_{109}, at a concentration of 25 w/v% polymer in water, the structure of the solution is directly dependent on the temperature of the solution.[12] At low temperature, below 22.5 °C, the polymer is in polymeric unimer form in solution. At 22.5 °C, the PPO blocks of F88 aggregate to form spherical micelles approximately 17 Å in diameter.[26, 12] At approximately 42 °Cand above, the micelles associate to cubically packed hydrogels.[12] As temperature increases beyond 42 °C, the gel begins to gradually melt again.[12] Throughout this temperature-dependent nanophase transition, the phase and local structure of the polymer solution changes accordingly. To detect these local changes on molecular length scales, coumarin fluorescence probes are solubilized and the time-integrated and time-resolved fluorescence is measured at temperatures throughout the transition.

Steady-State Solvatochromic Spectral Shifts

The following sections describe the excitation and emission spectra of each of the seven coumarin probes in 25 w/v% F88 solution and in six solvent of various polarities. For each coumarin, the normalized amplitudes, energies at peak amplitude, and fwhm of both emission and excitation spectra are graphed at approximately 20 different temperatures between 2.5 and 90 °C. The position of the emission and excitation bands for each coumarin may be compared to the position of the coumarin emission and excitation peaks in various solvents.

Coumarin 314T

By comparison of the fluorescence spectra of C314T in some control solvents (Figure 5.6)and the spectra in solution of F88 (Figure 5.7), the C314T spectral peaks in F88 unimer solution are comparative to those of C314T in PEG 300. The C314T spectral peaks in F88 micelles and hydrogel solutions at T> 22.5 °Care comparative to the spectrum of C314T in PPO 2000.

In the case of the most hydrophobic coumarin molecule, C314T, the hypothesis

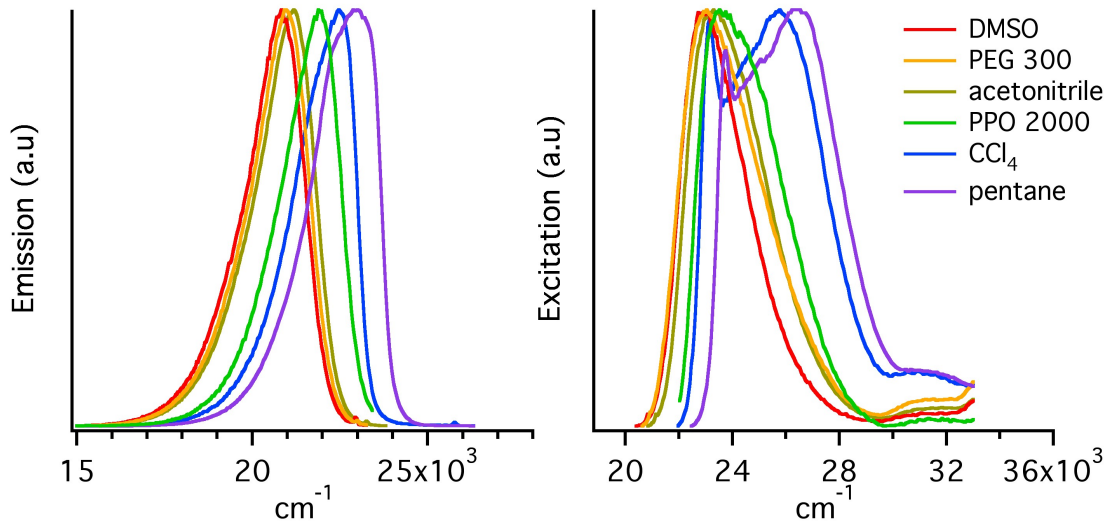

Figure 5.6: Emission and excitation spectra of C314T in 6 solvents ranging in polarity: DMSO (red), PEG 300 (orange), acetonitrile (yellow), PPO 2000 (green), CCl_4 (blue), and 1-pentane (purple).

is that the fluorophore will localize in the hydrophobic PPO core of the F88 micelles in solution. The temperature-dependent steady-state emission and excitation spectra of C314T in F88 solution are shown in Figure 5.7. The temperature-dependent peak energies (in cm^{-1}) and normalized amplitudes are shown in Figure 5.8. The peak of the emission spectrum shifts approximately 8 nm to lower wavelengths (higher energies) at 22.5 °C, the micellization temperature of the F88 polymer solution. The shift in fluorescence spectrum reflects the change in solvent environment of C314T from a polar, water-rich unimer solution to the non-polar, hydrophobic PPO core of F88 micelles. The shift in C314T emission is small relative to the shift observed for some of the other coumarin fluorophores. C314T is dissolved in polymer, even in unimer solutions at low temperatures because it is so insoluble in pure water. Therefore, the change in local environment polarity is not as extreme as the change in local environment of a slightly more water-soluble coumarin. The fwhm also changes at exactly the temperature of polymer micellization meaning that C314T is solubilized in micelles and the coumarin is experiencing a wider distribution of local environments. In comparison to other coumarins, the shift is small and the distribution of environments is changing only

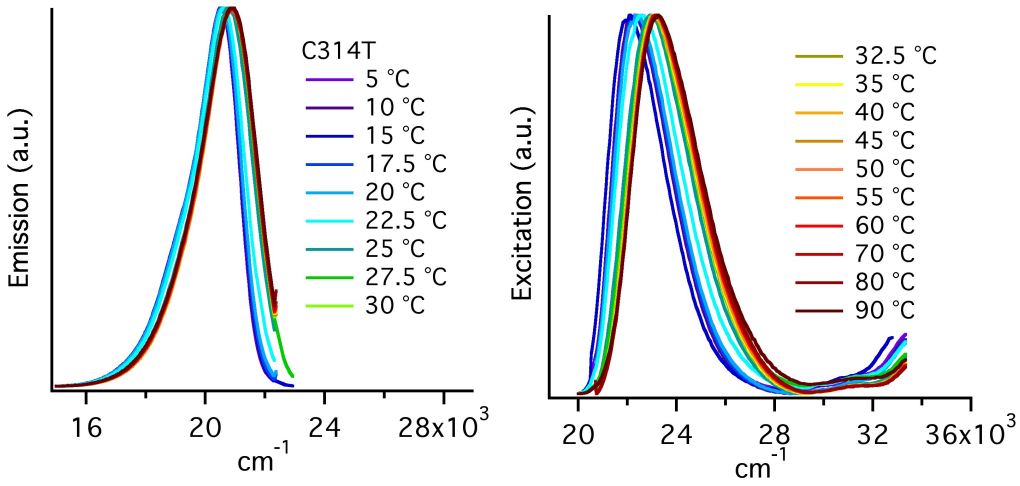

Figure 5.7: Temperature dependence of normalized emission and excitation spectra of C314T in 25 w/v% Pluronic F88. Temperatures range from 2.5 to 90 °C.

slightly.

Coumarin 153

By comparison of the fluorescence spectra of C153 in some control solvents (Figure 5.9)and the spectra in solution of F88 (Figure 5.10), the C153 spectral peaks in F88 unimer solution are comparative to those of C153 in PEG 300. The C153 spectral peaks in F88 micelles and hydrogel solutions at T> 22.5 °Care comparative to the spectrum of C153 in PPO 2000.

Coumarin 153 has been well characterized previously using fluorescence spec troscopy.[27, 28, 24, 23, 29, 30, 31, 32, 12, 33, 34, 35] The steady-state emission peak frequency, ν_{em}, can be assigned to a local polarity on the π^* empirical polarity scale using the equation: $\nu_{em}[10^3\ \mathrm{cm}^{-1}] = 21.217 - 3.505\pi^*$ defined by Horng, et.al.[24, 35] Similarly, using the equation: $\nu_{abs}[10^3\ \mathrm{cm}^{-1}] = 25.774 - 2.066\pi^*$, the peak excitation can also be assigned to a value on the π^* polarity scale.[24, 35] As a reference, the π^* value of cyclohexane, a non-polar solvent, is 0.00 and the value for dimethyl sulfoxide, a polar solvent, is 1.00 on the π^* empirical polarity scale.[36] The π^* local solvent polarity of C153 in F88 with increasing temperature is plotted in Figure 5.12. The values of π^* can be found in Appendix C. Using the emission peak, C153 in a unimer solution has local solvation

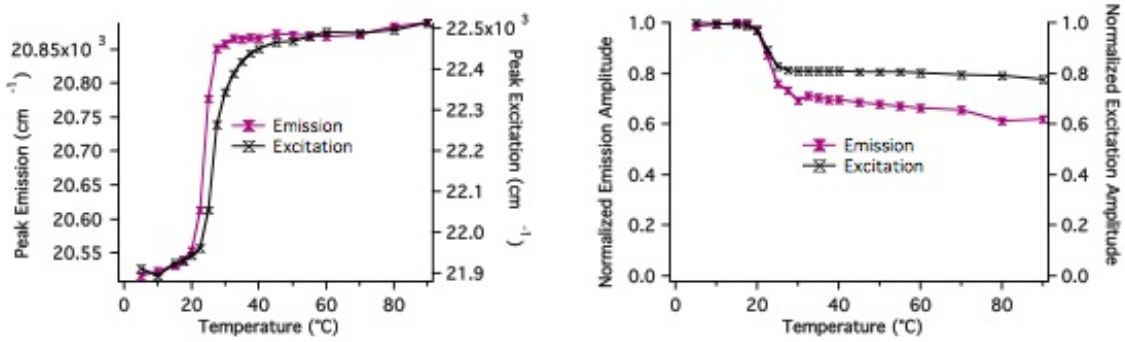

Figure 5.8: Temperature dependence of C314T emission and excitation peak frequency and normalized peak amplitude demonstrating the ability for C314T to detect the unimer-to-micelle phase transition of F88.

with a polarity similar to dichloromethane with π^* values at approximately 0.81. Upon micellization, C153 is encapsulated in the presumably dry PPO core. According to the emission peak frequency and the equations derived by Horng, et.al., in F88 micelles, C153 is seeing solvation with a polarity similar to THF and benzene ($\pi^* = 0.58$); a slightly more non-polar solvent environment. Using the excitation peak frequencies of C153 in F88 and the equation from Horng, et.al., C153 shows a similar trend in local solvent environment polarity. These results are plotted in Figure 5.12 with increasing temperature of F88 solution. According to the shift in excitation peak frequency, C153 in unimer solution has a solvation with polarity more polar than dimethyl sulfoxide or formamide, polar solvents. Upon the micellization of F88, C153 changes local environment to have a polarity similar to pyridine or benzonitrile. This trend is similar to that of the π^* values found from the emission spectrum over changing temperature. The observable change in local solvent polarity corresponds with C153 being in a unimer solution and then being encapsulated in the micellar core of A-B-A triblock copolymer F88.[32] C153 is sensitive to the presence of water molecules, so the change in solvation is a very good indicator that C153 is in the hydrophobic core in micellar solution.[27, 32, 12] C153 is used in Chapter 4 to probe the hydrophobic cores of three amphiphilic polymeric nanocarriers in a similar way.[35]

Coumarin 102

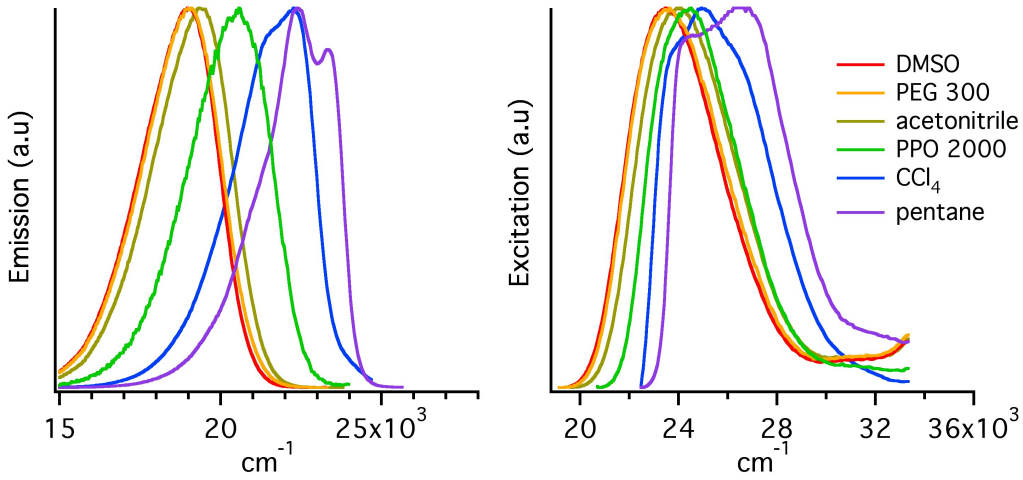

Figure 5.9: Emission and excitation spectra of C153 in 6 solvents ranging in polarity: DMSO (red), PEG 300 (orange), acetonitrile (yellow), PPO 2000 (green), CCl_4 (blue), and 1-pentane (purple).

By comparison of the fluorescence spectra of C102 in some control solvents (Figure 5.13)and the spectra in solution of F88 (Figure 5.14), the C102 spectral peaks in F88 unimer solution are comparative to those of C102 in PEG 300. The C102 spectral peaks in F88 micelles and hydrogel solutions at T> 22.5 °Care comparative to the spectrum of C102 in PPO 2000.

Coumarin 102 is a hydrophobic molecule, with similar structure to C153 and has a methyl group in place of the trifluoromethyl group present in C153. This gives C102 a slightly lower clogP value of 3.67.[37, 12] While C153 is localized primarily in the PPO core of F88 micelles, C102, being slightly water-soluble, localizes in multiple regions: the PPO core, in the PEO corona, and at the interface between the two regions of the aggregate.[32, 12] Because C102 is slightly less hydrophobic than C153, the shift in emission peak wavelength is only 13 nm and the shift in excitation is 18 nm. The shift in both excitation and emission are caused by the minimal solubility of C102 in water and upon micellization, C102 is solubilized in both the PPO core and in the PEO-water corona of the F88 micelles. The distribution of local environments sampled by C102 does not change as much during F88 micellization compared to that of C153, which

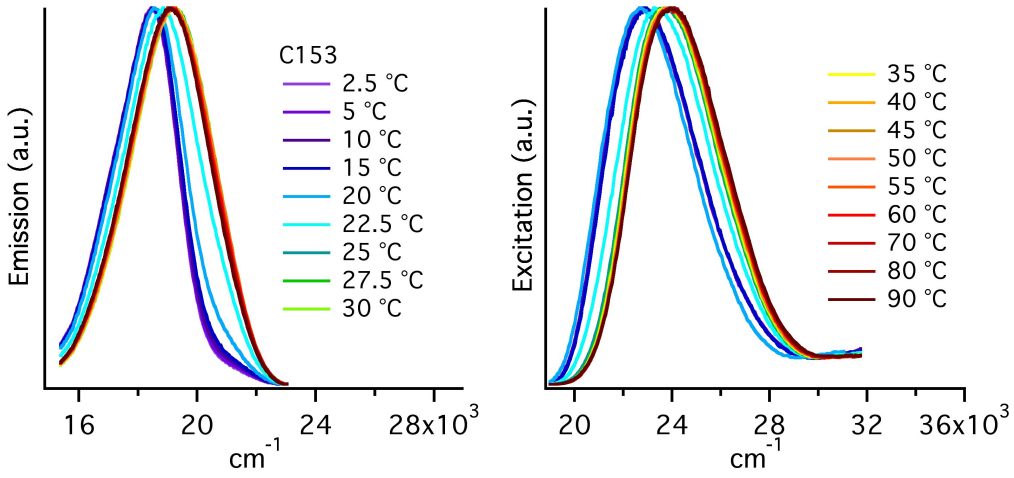

Figure 5.10: Temperature dependence of normalized emission and excitation spectra of C153 in 25 w/v% Pluronic F88. Temperatures range from 2.5 to 90 °C.

localizes primarily in the micelle core.

The broader distribution of local environments sampled by C102 can be deduced from the emission and excitation spectral fwhm values, which are broader than either C314T or C153. This inhomogeneous broadening of the electronic spectra is a consequence of the change in the distribution of local environments between core, corona, and interfacial regions of the polymer aggregates.[32, 12] The fwhm does undergo a change at the micellization temperature. Like C153, the emission spectrum of C102 becomes broader upon F88 micellization, indicating that the spectrum of C102 is shifting because of a larger distribution of local environments. More information on the spectral fwhm values can be found in Appendix C.

Coumarin 152

By comparison of the fluorescence spectra of C153 in some control solvents (Figure 5.16)and the spectra in solution of F88 (Figure 5.17), the C152 spectral peaks in F88 unimer solution are comparative to those of C152 in PEG 300. The C152 spectral peaks in F88 micelles and hydrogel solutions at T> 22.5 °Care comparative to the spectrum of C152 in PPO 2000. The excitation spectra of C152 are much broader than the spectra in single solvents, indicating that C152 is localized in multiple solvent environments.

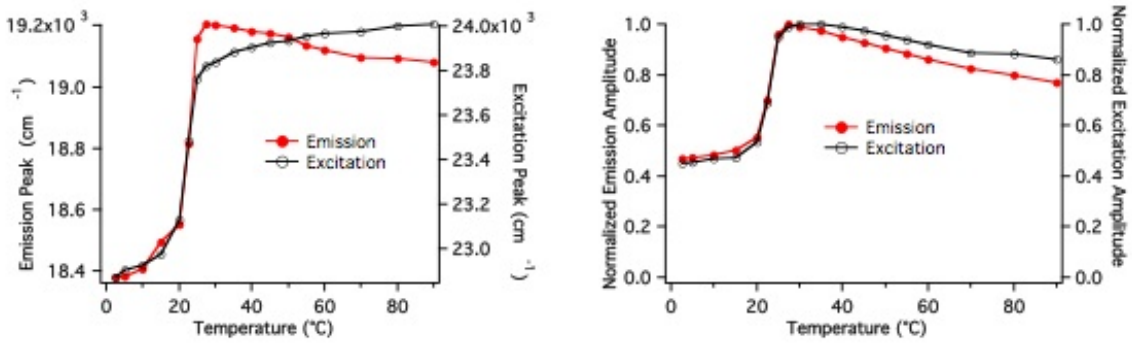

Figure 5.11: Temperature dependence of C153 emission and excitation peak frequency and normalized peak amplitude demonstrating the ability for C153 to detect the unimer-to-micelle phase transition of F88.

The C152 emission spectrum shifts the most of all 7 coumarins over the unimer-to-micelle phase transition of F88. C102 has intermediate solubility and comparatively small molecular volume. The emission peak of C152 shifts 38 nm to lower wavelengths (higher energies). C152 has a clogP value of 2.99 and a molecular volume of 209.9 $Å^3$.

The spectral fwhm of C152 emission is the broadest of all seven of the coumarin fluorophores and this broad distribution of local environments of C152 increases upon micellization. This trend is also shown very clearly in the excitation spectrum of C152. The peak shifts approximately 29 nm to lower wavelengths and the spectral width narrows, showing a clear transition at 22.5 °C as well. Like the spectrum of C102, the spectral shape of the C152 excitation spectrum shifts to show a more distinct separation of local environments. The excitation peak lineshape analysis is described in detail in Appendix D but the overall analysis concludes that when C152 is in an F88 micelle solution, because of its intermediate solubility, it is soluble in both the F88 micelle core and in the PEO corona, as well as in the bulk water.

C152 samples a broad range of local environments: bulk water, PEO corona, PPO core, and interfacial regions. As the polymer solution changes from unimers to aggregates with more distinct local environments, the distribution of C152 local environments narrows, as shown by the temperature-dependent fwhm. The values for the spectral linewidths can be found in Appendix C.

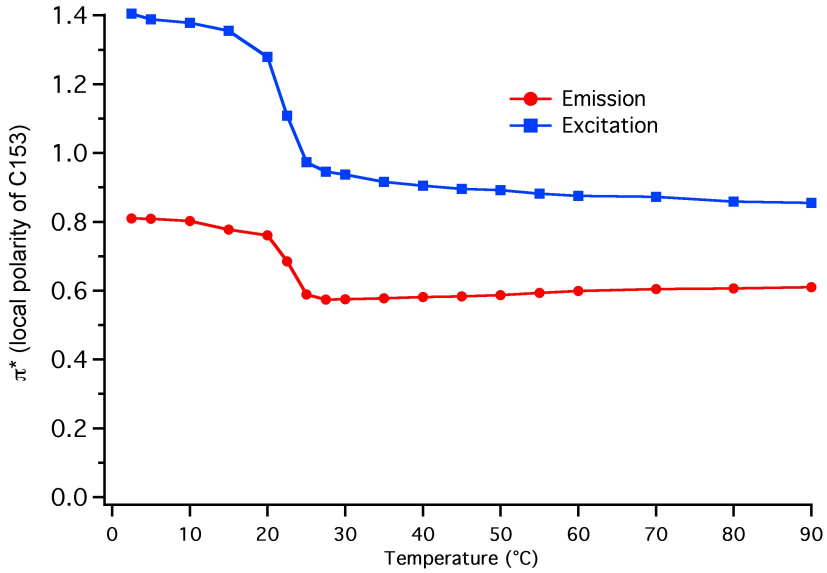

Figure 5.12: Temperature dependence of local polarity (π^*) from excitation and emission spectra of C153 in 25 w/v%Pluronic F88 solution.

It is also characteristic of fluorophores to show vibrational structure when solubilized in less polar solvents, as shown in Figure 5.16.[9, 21, 10] If C152 is fluorescing from the interior of an F88 micelle, this is the case in the very blue wavelengths of the excitation spectrum.

Coumarin 337

By comparison of the fluorescence spectra of C337 in some control solvents (Figure 5.19)and the spectra in solution of F88 (Figure 5.20), the C337 spectral peaks in F88 unimer solution are comparative to those of C337 in PEG 300. The C337 spectral peaks in F88 micelles and hydrogel solutions at T> 22.5 °Care also comparative to the spectrum of C337 in PEG 300.

C337 is also a coumarin with intermediate solubility and has a clogP value of 2.64.[37] C337 is also of intermediate size in comparison with the other coumarins used in this study. When solubilized in 25 w/v%Pluronic F88 aqueous solution, the emission peak wavelength shifts to lower wavelengths at 22.5 °Cby 5 nm. 5 nm is not a large shift in comparison to the shifts in the spectra of other coumarins, but the higher solubility in water of C337 in comparison to the other coumarin molecules causes

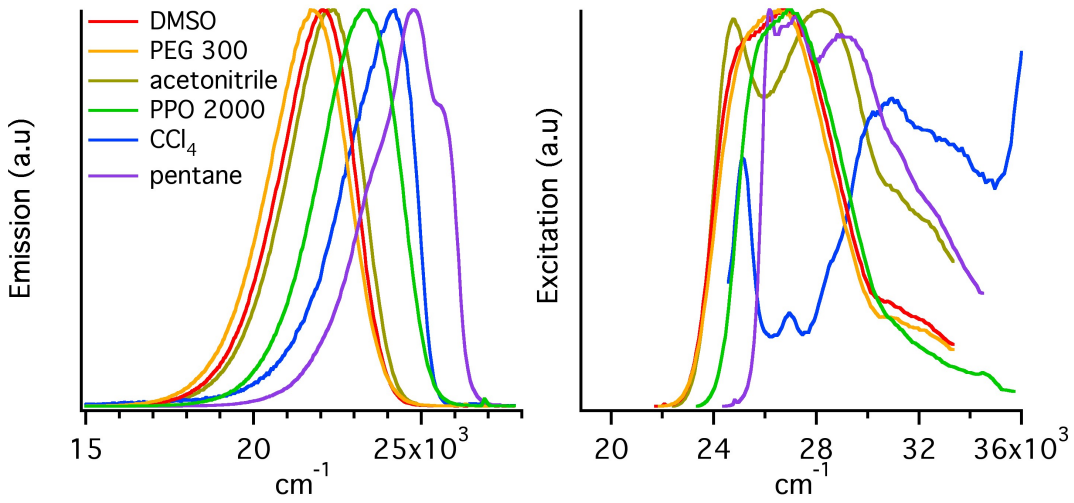

Figure 5.13: Emission and excitation spectra of C102 in 6 solvents ranging in polarity: DMSO (red), PEG 300 (orange), acetonitrile (yellow), PPO 2000 (green), CCl_4 (blue), and 1-pentane (purple).

the likelihood of C337 localizing minimally in the core of the F88 micelles. The C337 molecule, much like C152, may be localized in multiple environments: the PPO micelle core, the PEO corona, the bulk water, or at any of these interfaces. The fwhm of the emission spectrum for C337 shifts corresponding to the micellization of the molecule, becoming broader when C337 is in micelle solution. The overall fwhm of the emission spectrum is relatively narrow in comparison to C152 or C153. This may be caused by the coumarin primarily localizing in one environment, perhaps the PEO corona or the bulk water. When the F88 polymer forms micelles, the distribution of local C337 environment, as shown by the fwhm of the emission, does shift, but not dramatically relative to the other more hydrophobic coumarin probe molecules.

The excitation peak wavelength of C337 in aqueous F88 solution shifts to lower wavelengths by approximately 13 nm when the polymer forms micelles. Again, a shift is detected, but it is not as dramatic as that seen by C152 or C153. The excitation spectrum is also narrow in comparison to the other coumarin moelcules. The fwhm of the excitation spectrum is similar to that of C314T, being around 55-60 nm and showing a very slight broadening at the micellization temperature, only within a few

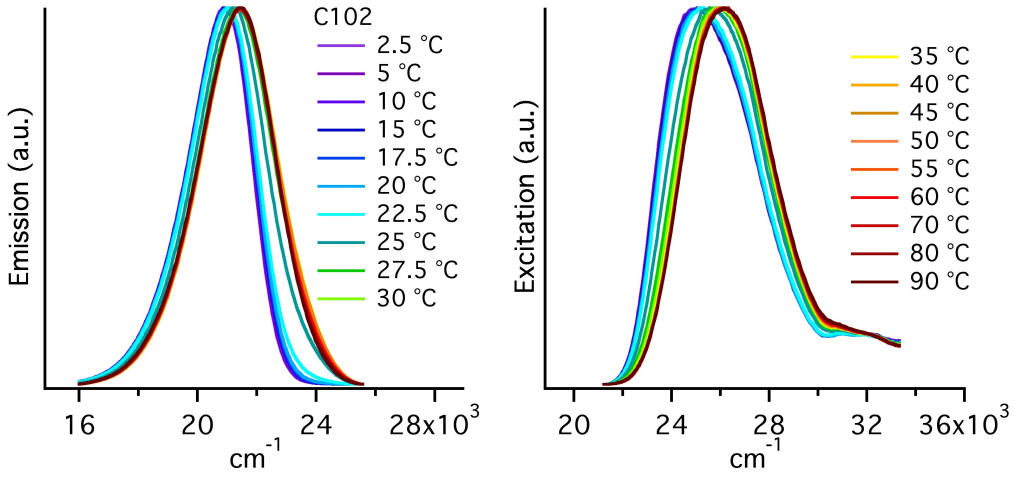

Figure 5.14: Temperature dependence of normalized emission and excitation spectra of C102 in 25 w/v% Pluronic F88. Temperatures range from 2.5 to 90 °C.

nanometers. This indicates that C337 is not seeing a very significant change in local polarity or distribution of environments between F88 unimer solution and aggregated micelles.

Coumarin 151

By comparison of the fluorescence spectra of C151 in some control solvents (Figure 5.22)and the spectra in solution of F88 (Figure 5.23), the C151 spectral peaks in F88 unimer solution are comparative to those of C151 in PEG 300. The C151 spectral peaks in F88 micelles and hydrogel solutions at T> 22.5 °Care also comparative to the spectrum of C151 in PEG 300.

C151 has the second lowest clogP value of 1.94 of the seven coumarins, meaning that the molecule is relatively water-soluble.[37] In both unimer and micelle solutions of F88, the distribution of local environments as reported by fluorescence emission are larger and the change in local polarity from unimer to micelle solution is much smaller in comparison to more hydrophobic coumarins. There is only a 3 nm shift in emission peak wavelength at 22.5 °Cand the broad fwhm of the emission spectrum spans approximately 75 nm. The temperature-dependence of the emission peak wavelength and fwhm are shown in Figures 5.24 and more information can be found in Appendix

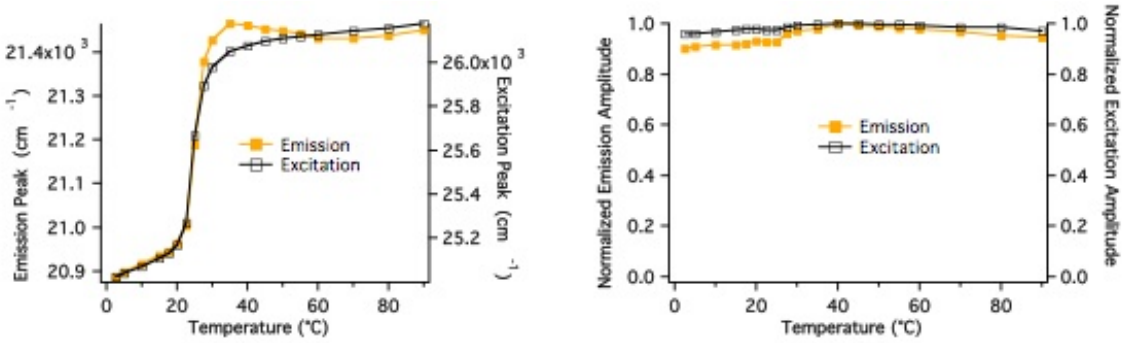

Figure 5.15: Temperature dependence of C102 emission and excitation peak frequency and normalized peak amplitude demonstrating the ability for C102 to detect the unimer-to-micelle phase transition of F88.

C.

Similarly, the excitation of C151 shifts as F88 transitions from unimers to micelles in solution. The excitation peak shifts to higher wavelengths, meaning that the C151 is sampling more polar environment in the micelle solution. C151 is sampling local environments outside the micelle aggregates once they are formed. The local environment of C151 in the bulk water is indeed more polar than a homogeneous solution of polymeric unimers at low temperatures.

Coumarin $343^{-}/Na^{+}$

By comparison of the fluorescence spectra of $C343^{-}/Na^{+}$ in some control solvents (Figure 5.25)and the spectra in solution of F88 (Figure 5.26), the $C343^{-}/Na^{+}$ spectral peaks in F88 unimer solution are comparative to those of $C343^{-}/Na^{+}$ in PEG 300. The $C343^{-}/Na^{+}$ spectral peaks in F88 micelles and hydrogel solutions at T> 22.5 °Care also comparative to the spectrum of $C343^{-}/Na^{+}$ in PEG 300.

On the solubility scale, $C343^{-}$ anion is the most hydrophilic of the coumarin fluorophores used. It has a clogP of -1.08, meaning that $C343^{-}$ is water soluble. This anion localizes in the bulk water of F88 polymer solution, whether the polymer is in unimer or micelle form. In the emission spectrum of $C343^{-}$, no observable shift is present upon the micellization of F88 as shown in Figures 5.26 and 5.27. With regard to spectral peak energies shown in Figure 5.27, this is an indication that $C343^{-}$ is not seeing a

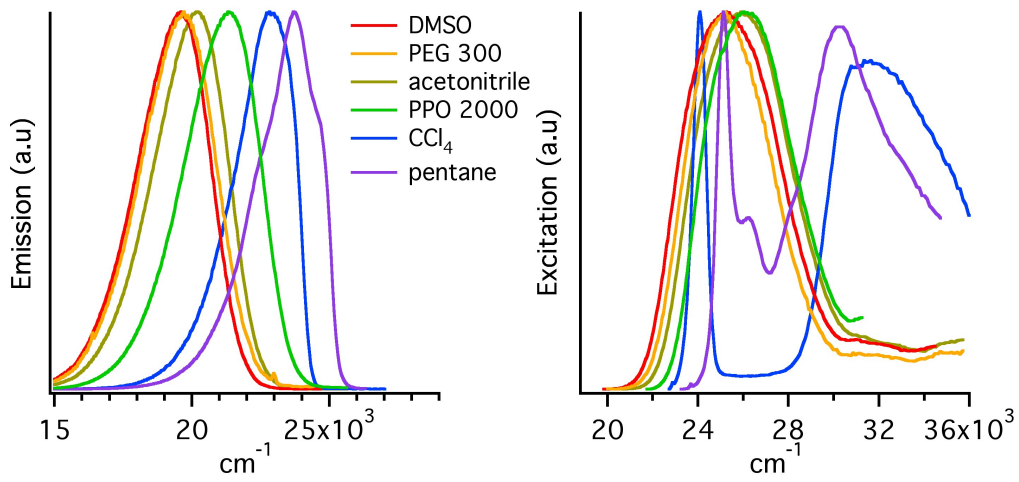

Figure 5.16: Emission and excitation spectra of C152 in 6 solvents ranging in polarity: DMSO (red), PEG 300 (orange), acetonitrile (yellow), PPO 2000 (green), CCl_4 (blue), and 1-pentane (purple).

change in local environment and is not encapsulated by F88 micelles as polymer aggregation occurs[32, 12] The emission spectrum of $C343^-$ does not change in spectral width, indicating that its distribution of local environments is not changing either.

The excitation spectrum of $C343^-$ shifts gradually to higher energies as shown in Figure 5.27, but does not show a sharp transition as do the other more hydrophobic coumarins. However, the excitation spectrum of $C343^-$ broadens with the temperature-dependent micellization of F88. This behavior is also seen in the spectra of C314T and C337, but not in C153, C102, C151, or C152. The increasing fwhm of the $C343^-$ excitation spectrum corresponds to a shift of the coumarin to a wider distribution of solvation environments and can be clearly observed in Figures 5.26. $C343^-$ is reporting fluorescence from a local environment of the water/ unimer polymer solution (where it is both in bulk water and partially localized in F88 unimers) and as the F88 micellizes, the local environment changes to bulk water and various interfacial environments on the outside the F88 micelle aggregate.

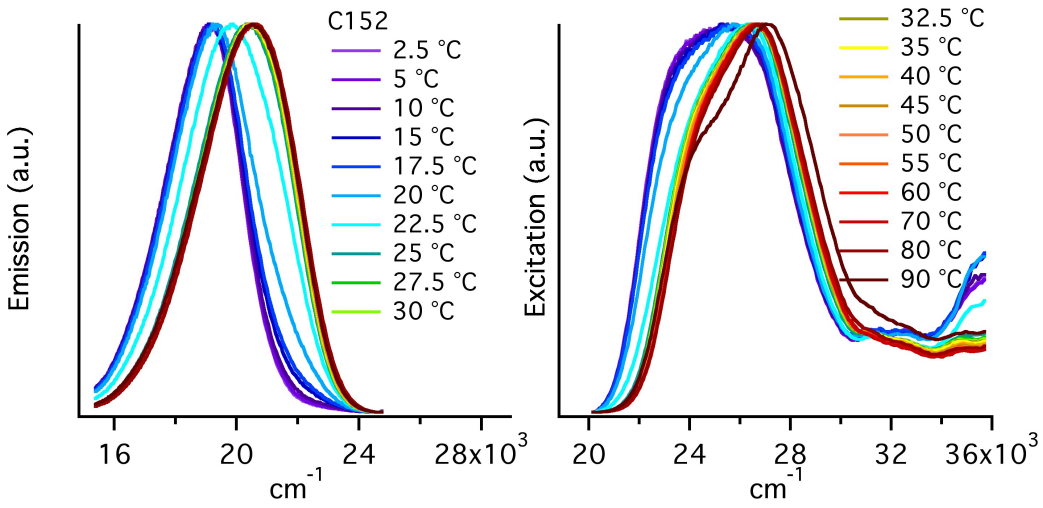

Figure 5.17: Temperature dependence of normalized emission and excitation spectra of C152 in 25 w/v% Pluronic F88. Temperatures range from 2.5 to 90 °C.

Comparison of Coumarin Spectral Shifts

Figure 6.3 indicates that there is clearly a shift in local polarity for most of the coumarins at 22.5 °C, the micellization temperature of the F88 polymer in solution. The emission spectra of the six most hydrophobic coumarins shifts to higher energies. This shift reveals that the more hydrophobic and intermediately soluble coumarins are reporting from more hydrophobic local environments as F88 aggregates. The water-soluble coumarin, $C343^{-}/NA^{+}$ is not encapsulated by the polymer upon micellization, therefore the emission and excitation spectra of $C343^{-}/NA^{+}$ do not shift to higher energies at 22.5 °C.[12]

Fluorescence Time Constants of Coumarins in F88 Solutions

The fluorescence time constants of coumarin solvatochromic probes are another indicator of local polarity. If a coumarin molecule is in a more polar, water-rich solvent environment, the fluorescence time constant will be smaller than if the fluorophore is in a hydrophobic, non-polar environment.[10, 12] Coumarins in the bulk water, or PEG-water interface will fluorescence time constants smaller than the same coumarin in the non-polar PPO core of an F88 micelle aggregate. Because each of the coumarins has

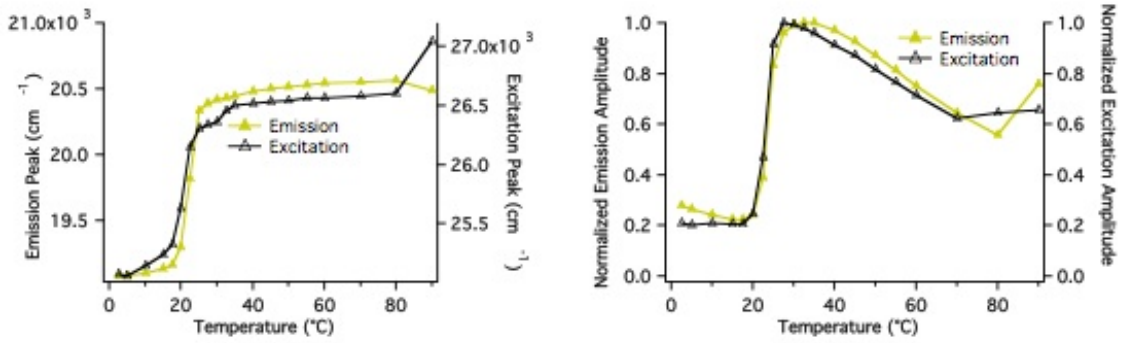

Figure 5.18: Temperature dependence of C152 emission and excitation peak frequency and normalized peak amplitude demonstrating the ability for C152 to detect the unimer-to-micelle phase transition of F88.

populations in multiple regions of F88 unimer, micelle and hydrogel solutions, multiple fluorescence time constants are measured at each temperature. Figure 5.29 displays the relative normalized amplitudes ($\alpha_{i,fl}$) and corresponding time constants ($\tau_{i,fl}$) measured over the same temperature range as used for steady-state measurements. The individual time constants of the seven coumarins do not show the sharp transition at 22.5 °Cas was present in the fluorescence shifts. Instead, the fractional amplitudes of the individual time constants are changing, indicating that the population of coumarin molecules in a particular local environment is changing to a different local environment.

Most of the coumarin fluorescence transients were fit to a 3-exponential decay function, loosely assigning each of the three individual time constants to a population of coumarins in a particular local environment. The fluorescence time constants of each of the seven coumarins measured are discussed in detail below.

Coumarin 314T Fluorescence Dynamics

Coumarin 314T has two fluorescence time constant distributions and both of these change with the micellization of the polymer at 22.5°C. As shown in Figure 5.30, the smallest fluorescence time constant of C314T is about 400 ps in the F88 unimer solution and this increases to 1 ns as the polymer forms micelles and C314T is solubilized inside the hydrophobic core. The second, larger time constant is consistently around 4 ns. This time constant increases and then decreases as micelles form in solution, but remains

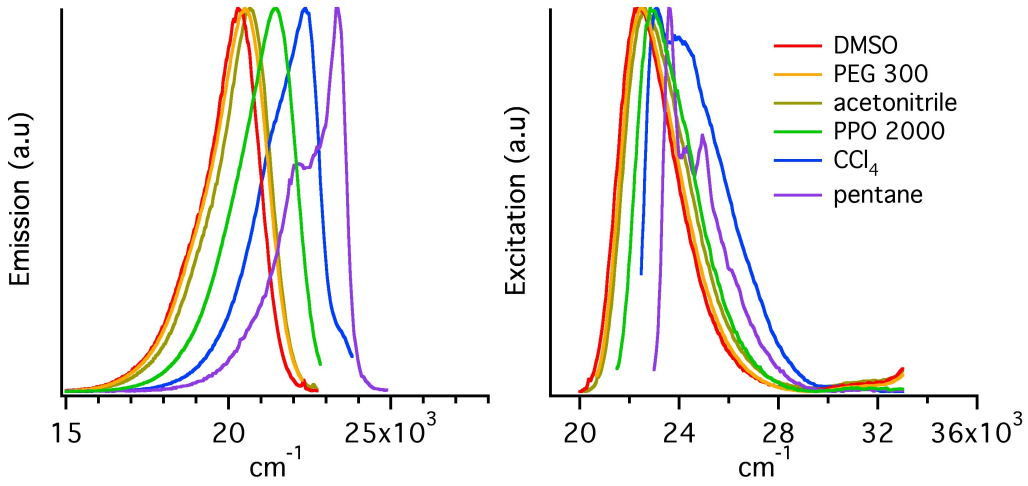

Figure 5.19: Emission and excitation spectra of C337 in 6 solvents ranging in polarity: DMSO (red), PEG 300 (orange), acetonitrile (yellow), PPO 2000 (green), CCl_4 (blue), and 1-pentane (purple).

centered at 4 ns. The smaller time constants in unimer solution indicate that C314T is solubilized by individual polymer unimers at low concentrations. While some polymeric unimers completely encapsulate the coumarin molecules, some may be exposing C314T partially to the PEG-water interface of the micelle corona.

Coumarin 153 Fluorescence Dynamics

Coumarin 153 also has two fluorescence time constants that change with the micellization of the polymer as shown in Figure 5.31. At low temperatures below 25°C, the first time constant at approximately 600 ps has small fractional amplitude. This time constant increases and decreases to approximately 300 ps after the polymer forms micelles at higher temperatures. The second, larger time constant with large fractional amplitude is 2.8 ns in unimer solution and increases to 5 ns at the micellization temperature. The fractional amplitude of the C153 population with this time constant decreases from 0.8 to less than 0.1 as C153 is solubilized by F88 micelles . The largest fluorescence time constant of C153 in F88 solution is approximately 3.8 ns in unimer solution and increases to 4.7 ns in F88 micelles and the population associated with this fluorescence time constant is increasing as F88 forms micelles and the majority of C153

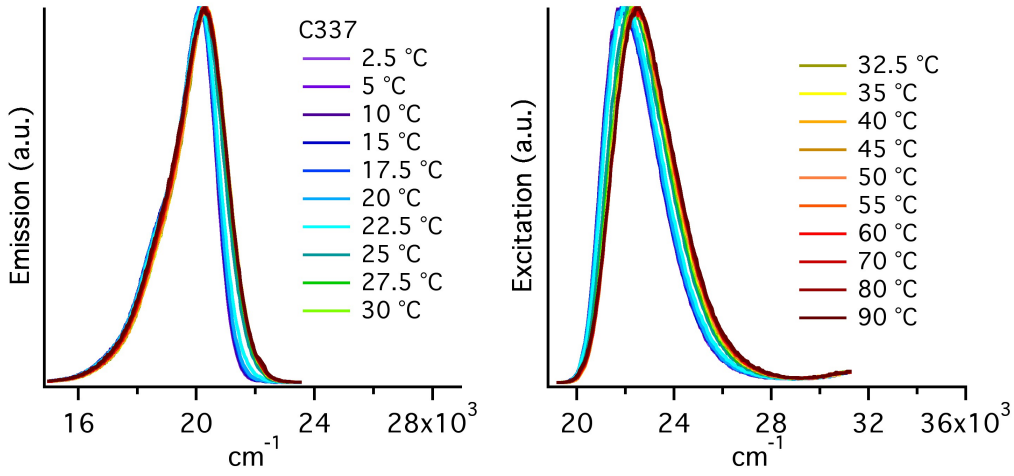

Figure 5.20: Temperature dependence of normalized emission and excitation spectra of C337 in 25 w/v% Pluronic F88. Temperatures range from 2.5 to 90 °C.

is solubilized inside the hydrophobic core. The fluorescence time constant of coumarin 153 is known to be extremely sensitive to the presence of single water molecules, and the large shift in fluorescence time constants upon micellization formation reflects this quality.[38]

Coumarin 102 Fluorescence Dynamics

The fluorescence time constants of C102 in 25 w/v% F88 solution as shown in Figure 5.32 consist of three individual time constants. All three time constants experience a change at 22.5 to 25 °C. The smallest time constants at 50 ps and at 1.5 ns merge to become approximately 200 ps as small populations of C102 are solubilized outside of the micelle, in the more polar bulk water solvent environment. The fractional amplitudes of both of the smaller time constants decreases as C102 is solubilized by the F88 micelles. The majority of the C102 population at low temperatures is loosely associated with F88 unimers and is then solubilized inside the micellar PEG and PPO environments at higher temperatures. According to the fractional amplitudes of C102 fluorescence time constants, the majority of the C102 population in solution has a fluorescence time constant around 6 ns when associated with the PPO of the F88 unimers in solution. When the polymer aggregates, the 6 ns time constant shifts to 5 ns as C102 is most

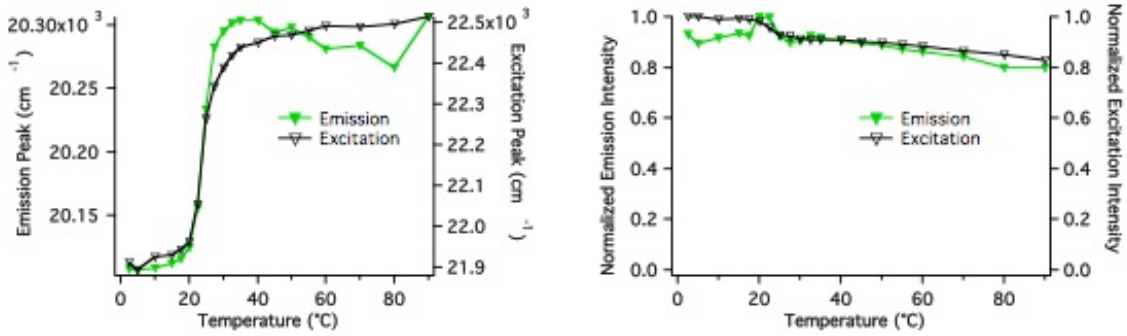

Figure 5.21: Temperature dependence of C337 emission and excitation peak frequency and normalized peak amplitude demonstrating the ability for C337 to detect the unimer-to-micelle phase transition of F88.

likely solvating in the PEG corona as well as the PPO core of F88 micelles. As more C102 molecules are encapsulated by polymer micelles, the fractional amplitude of the 5 ns time constant increases.

Coumarin 152 Fluorescence Dynamics

Coumarin 152 is found to have a distribution of four individual fluorescence time constants over the selected temperature range in Pluronic F88 solution. These time constants range from 6 ps to over 5 ns with the highest amplitudes concentrated at around 25 ps and 700 ps. As the polymer forms micelles, it is clear that C152 fluorescence time constants change with polymer aggregation. Two larger time constants appear at 2.5 and 4 ns at 22.5 °C. The fluorescence time constant at 700 ps with high fractional amplitude shifts up to approximately 1 ns and then decreases gradually with heating. The C152 population is distributed across more than one microenvironment within the polymer solution and most of these microenvironments change with micellization of the polymer. Changes in microenvironmen are is apparent by shifts in each individual time constant. Coumarin 152 is only a moderately hydrophobic molecule in comparison to C314T and C153. The intermediate polarity of C152 makes is moderately soluble in water, PEG and PPO too. C152 samples many microenvironments of the A-B-A triblock copolymer solution no matter what aggregation state the polymer may be forming, but the large changes in distribution of C152 in these microenvironments

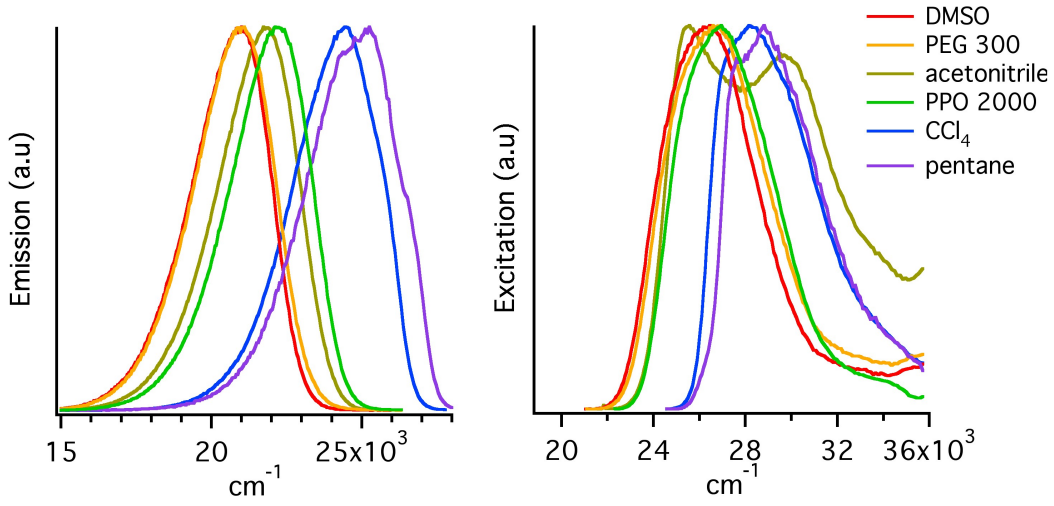

Figure 5.22: Emission and excitation spectra of C151 in 6 solvents ranging in polarity: DMSO (red), PEG 300 (orange), acetonitrile (yellow), PPO 2000 (green), CCl_4 (blue), and 1-pentane (purple).

indicates the micellization of F88.

Coumarin 337

The fluorescence time constants of C337 shown in Figure 5.34 indicate three microenvironments of this intermediately water-soluble coumarin. The smallest two time constants have small fractional amplitudes and are scattered across the temperature range at approximately 20 ps and 200 ps. The shift at micellization temperature of the polymer is not apparent for either of these time constants, but can be seen. The third, larger time constant has high fractional amplitude and is constant at all temperatures at 4.5 ns. The high fractional amplitude accounts for a high population of the C337 present in the PEG corona of the micelle solution and C337 associated with PEG environments in unimer solution. Because C337 has a nitrile group acting as a hydrogen bond acceptor, it is soluble in water, PEG and PPO and so the local environment distribution will not change significantly upon aggregation of the polymer.

Coumarin 151

The fluorescence time constants of C151 show three distinct microenvironments within the F88 polymer solution at all temperatures measured. The fluorescence time

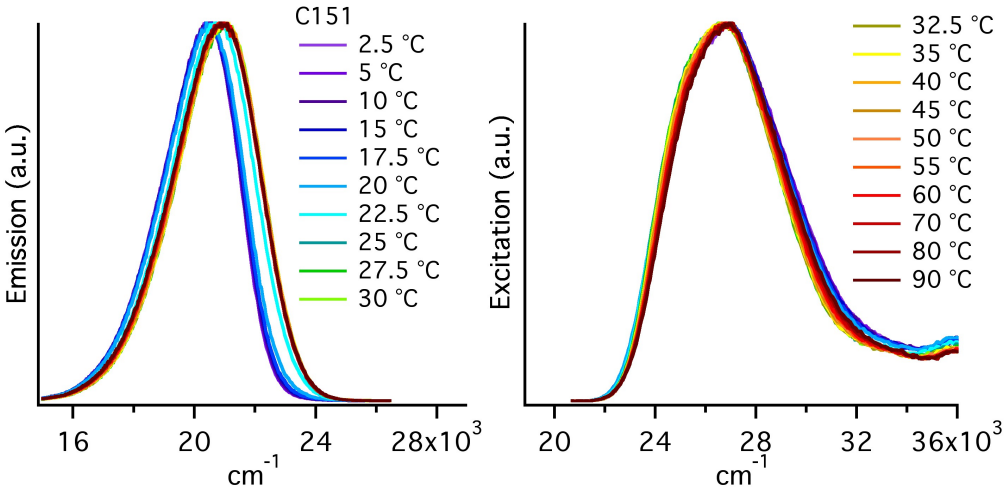

Figure 5.23: Temperature dependence of normalized emission and excitation spectra of C151 in 25 w/v% Pluronic F88. Temperatures range from 2.5 to 90 °C.

constants and fractional amplitudes are displayed in Figure 5.35. The smallest time constant at low temperatures begins at approximately 80 ps and decreases to 40 ps at polymer micellization. The second time constant begins at 310 ps and increases to 630 ps as F88 forms micelles. The third fluorescence time constant with the highest fractional amplitude shifts slightly from 5 to 6 ns when F88 forms micelles in solution.

It is clear that during micelle formation, some C151 is solubilized in bulk water solution instead of associating with single polymeric unimers such as may be the case at low temperatures. Because C151 is water-soluble, the association of C151 with the polymer aggregates is minimal. There is some association of C151 with F88 unimers and micelles as indicated by shifts in the fluorescence time constants.

Coumarin $343^{-}/Na^{+}$

The fluorescence time constants of $C343^{-}/Na^{+}$ reveal two distinct populations of the coumarin in different microenvironments. The fluorescence time constants and fractional amplitudes of $C343^{-}/Na^{+}$ in F88 solution are shown in Figure 5.36. The smaller of the two time constants is 1 ns at low temperatures and decreases to 200 ps at 22.5 °C. This shift in time constant indicates that population of $C343^{-}$ is moving to a more polar environment as micelles are formed. These coumarin molecules are

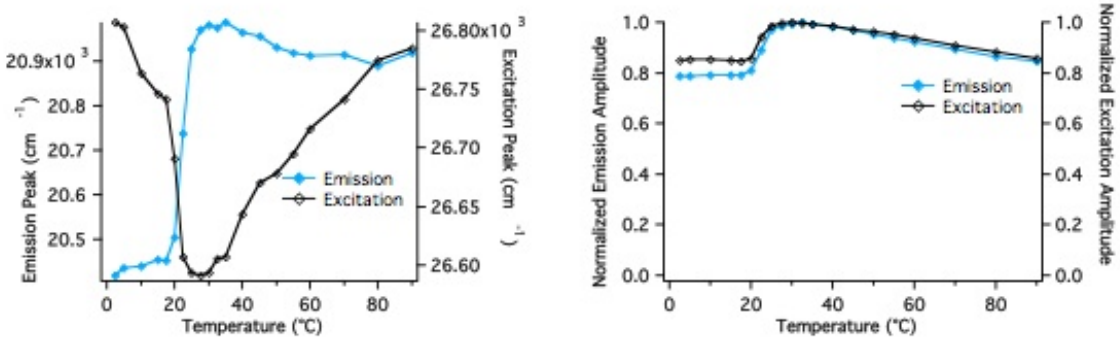

Figure 5.24: Temperature dependence of C151 emission and excitation peak frequency and normalized peak amplitude demonstrating the ability for C151 to detect the unimer-to-micelle phase transition of F88.

most likely weakly associated with polymeric unimers at low temperatures and are solubilized in bulk water solution at high temperatures. The predominant time constant of $C343^-/Na^+$ is 3.9 ns at all temperatures measured, indicating that most of the $C343^-$ is located in the bulk water of the solution and the microenvironment does not change when micelles are formed.[12, 32]

The average time constants show the general trend of the fluorescence time constants of each coumarin molecular probe and are plotted in Figure 5.37. It is clear from this graph that C152 has the largest change in average time constant from 1 ns to almost 3 ns over the micellization of the F88 polymer. C153 also has a large jump from under 3 ns to 4.6 ns between unimer and micelle solution. Intermediately soluble coumarin fluorophores 151, C337, and C102 show very little change, although small jumps in fluorescence time constants are present at 22.5 °C. The average fluorescence time constant of $C343^-/Na^+$ shows no transiton because it is not sampling the change in polarity from within the hydrophobic core of F88 micelles.[12]

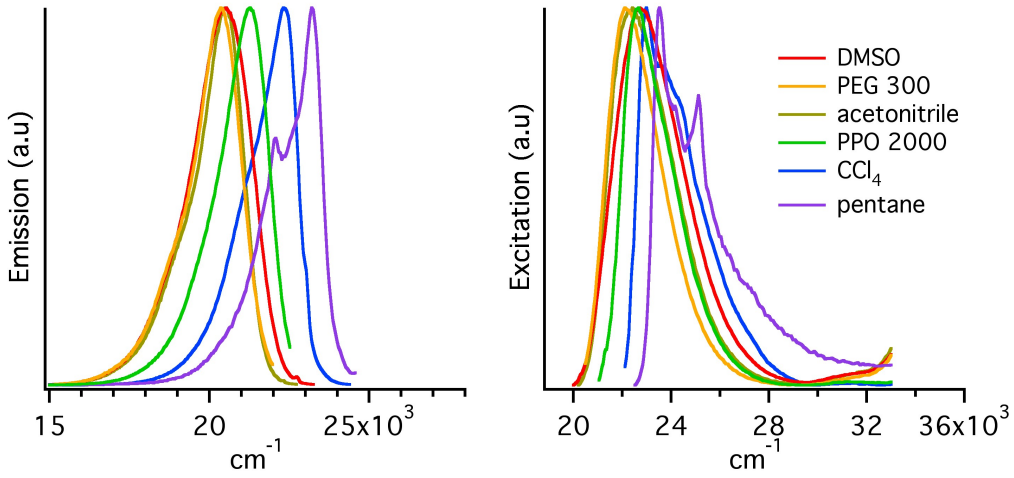

Figure 5.25: Emission and excitation spectra of $C343^-/Na^+$ in 6 solvents ranging in polarity: DMSO (red), PEG 300 (orange), acetonitrile (yellow), PPO 2000 (green), CCl_4 (blue), and 1-pentane (purple).

5.2.4 Local Friction From Fluorescence Anisotropy

Fluorescence Polarization Anisotropy

The temperature-dependence of the polarization anisotropy parameters were measured in both the steady-state and in the time-domain for each coumarin fluorophore in F88. Figure 5.38 shows the steady-state r values and Figure 5.39 shows the r_0 found in from the time-dependent fluorescence anisotropy decays, r(t). In the steady-state, r increases at the micellization temperature of the F88 solution for all of the coumarin molecules accept for $C343^-/Na^+$, which shows no change in reorientation properties. The limiting anisotropies (r_0) found from TCSPC fluorescence transientsare all near the 0.4 maximum limit for r_0, meaning that all seven of the coumarins are not highly depolarized and have larger reorientation time constants in viscous polymer solution than in fluid solvents such as water. The individual r_j values of each coumarin and the corresponding reorientation time constants in the next subsection show the real changes in reorientation properties.

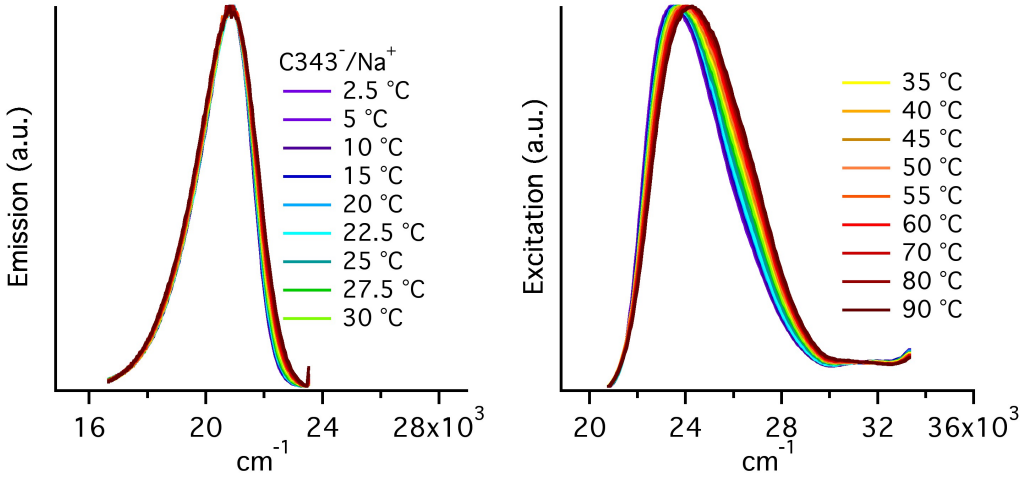

Figure 5.26: Temperature dependence of normalized emission and excitation spectra of $C343^{-}/Na^{+}$ in 25 w/v% Pluronic F88. Temperatures range from 2.5 to 90 °C.

Reorientation Time Constants

The polarization anisotropy decay r(t) was found for each coumarin in 25 w/v% F88 at each experimental temperature. These depolarization anisotropy decays were fit to a sum of two exponential equations revealing two reorientation time constants for each coumarin. From r(t), the values of $r_{rot,1}$, $r_{rot,2}$, $\theta_{rot,1}$, and $\theta_{rot,2}$ are calculated and plotted in Figure 5.40. While the $r_{rot,j}$ individual anisotropies are regarded as % amplitudes for the respective individual reorientation time constants, $\theta_{rot,j}$, the time constants themselves give a quantitative measurement of the reorientational motions of each coumarin in polymeric unimer, micelle, and gel solution.

The reorientation time constants shift at the micellization temperature of 22.5 °C in this solution of F88 polymer. The local friction of each coumarin is increasing corresponding to the increase in reorientation time constant, with the exception of $C343^{-}/Na^{+}$ in which case the reorientational motions report no change in local friction besides a shallow decrease as expected from thermal motions. The increase in reorientational motion of the other six coumarins from approximately 0 to 2 ns at low temperatures to 4 to 9 ns at polymeric micelle formation and the increase from 200 to 800 ps at low temperatures to 350 ps to 1 ns at micelle formation show that

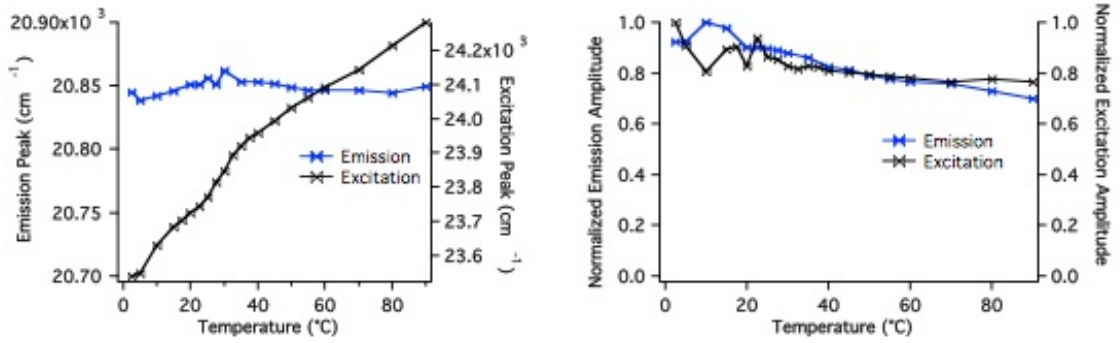

Figure 5.27: Temperature dependence of $C343^{-}/Na^{+}$ emission and excitation peak frequency and normalized peak amplitude demonstrating the lack of change in local polarity of $C343^{-}/Na^{+}$ during unimer-to-micelle phase transition of F88.

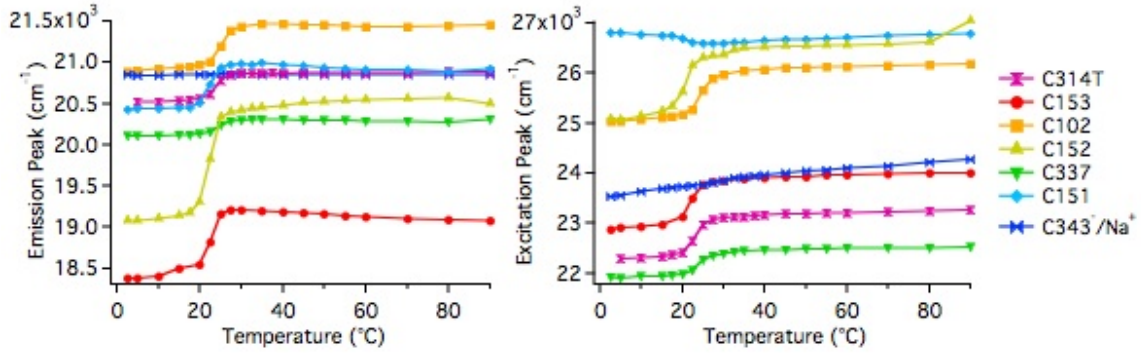

Figure 5.28: Temperature dependence of peak emission and excitation frequency of 7 coumarins in 25 w/v%Pluronic F88 solution.

both populations of reorienting species within each coumarin sample are changing in solvent environment microviscosity.[12] The smaller of the two reorientation time constants is most likely a population of each coumarin outside the immediate PPO core (either in the PEG or PEG-water micellar corona environment) and the larger of the two reorientation time constants is most likely a population of each coumarin inside or nearer to the hydrophobic PPO core of F88 micelles. The fractional amplitudes of each time constant are also revealing. The smaller time constant shows a sharp decrease in fractional amplitude ($r_{rot,1}$), meaning that the relative of coumarins in the PEG or PEG-water environment are decreasing. This is consistent with the hypothesis that at

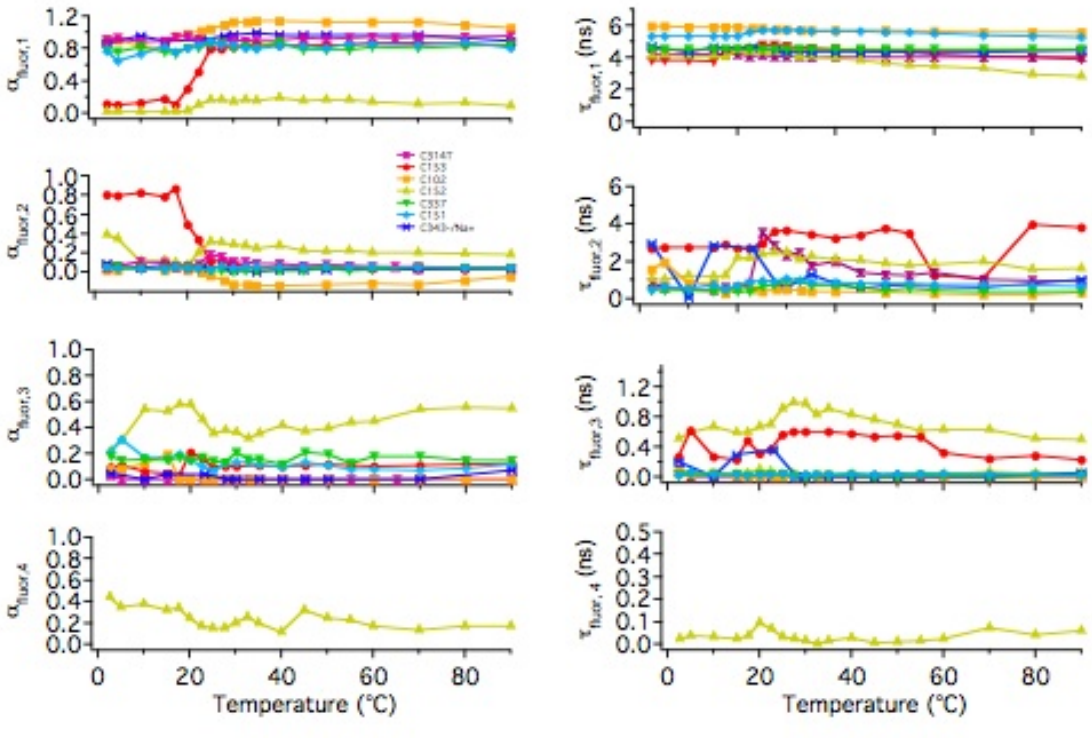

Figure 5.29: Temperature dependence of fluorescence time constant relative amplitudes (left) and individual time constants (right) for 7 coumarins in 25 w/v%Pluronic F88 solution.

higher temperatures, the PPO environment dehydrates, forming the hydrogel.[32] This dehydration would cause the population of hydrophobic coumarins in the more fluid (water-rich) environment to decrease while the population in the more viscous PPO core increases.

With the exception of the water-soluble $C343^{-}$ salt, the average reorientation time constant for each coumarin in 25 w/v% A-B-A triblock copolymer solution clearly indicates a change in local friction at the micellization temperature of the polymer. The temperature dependence of the reorientation time constants of all seven coumarins are shown in Figure 6.7. Coumarins 314t, C153, and C152 have the largest reorientation time constants corresponding to high local friction in the PPO core of F88 micelles. The reorientation time constants of the intermediately soluble coumarins (C102, C337, and C151) indicate a smaller change in local friction than the more hydrophobic coumarins.

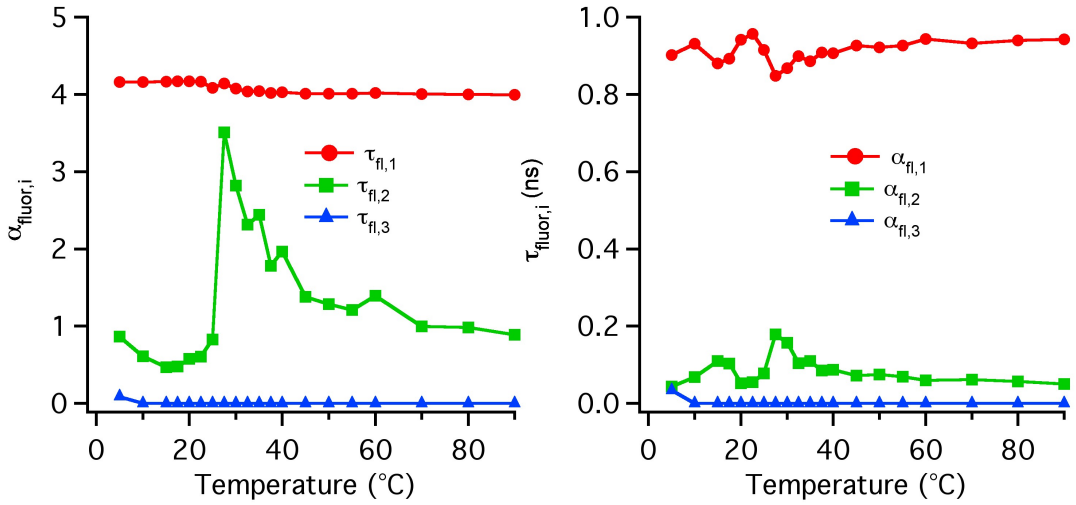

Figure 5.30: Temperature dependence of fractional amplitudes ($\alpha_{i,fl}$) (left) and individual fluorescence time constants ($\tau_{i,fl}$) (right) for C314T in 25 w/v%Pluronic F88 solution.

$C343^{-}$ has no sharp change in reorientation time constant with increasing temperature because most of the $C343^{-}$ population is not encapsulated by triblock copolymer.

Local Friction

Reorientation time constants can be related directly to the local viscosity the immediate environment of C153 using the equation: $\langle\theta_{rot}\rangle_{polar} = (58.1 \pm 1.6)\,\eta^{(0.96\pm0.03)}$ for a polar solvent and the equation: equation $\langle\theta_{rot}\rangle_{non-polar} = (34.8 \pm 4.1)\,\eta^{(0.63\pm0.02)}$ for a non-polar solvent.[29] These equations are used for coumarin 153 specifically.[29, 32, 35]

Reorientational Volumes from Stokes-Einstein-Debye Hydrodynamics

From S-E-D hydrodynamic theory the effective volumes of reorientational motion may be calculated using the reorientation time constants found from time-correlated single photon counting measurements of each coumarin. The viscosity of Pluronic F88 solution may be measured up until its gelation temperature and then be considered constant at approximately 5x10^7 cP as a gel. While this may not be the true value of the gel's viscosity, the flow is too slow to measure on a reasonable time scale and not possible using the instruments available to our labs. The bulk viscosity values used in this work

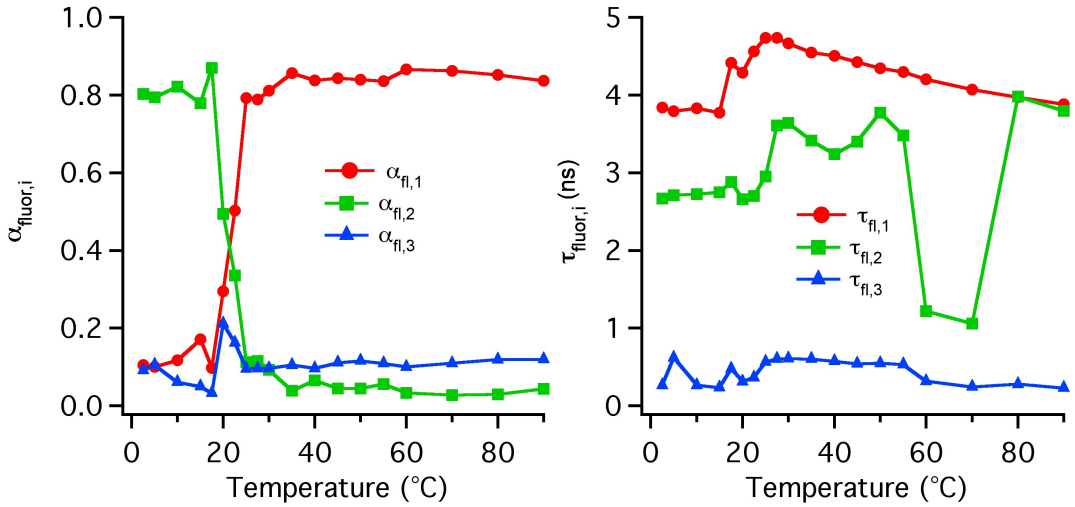

Figure 5.31: Temperature dependence of fractional amplitudes ($\alpha_{i,fl}$) (left) and individual fluorescence time constants ($\tau_{i,fl}$) (right) for C153 in 25 w/v%Pluronic F88 solution.

are taken from Grant, et. al.[32] The equation for S-E-D reorientational diffusion can be found in Chapter 2.

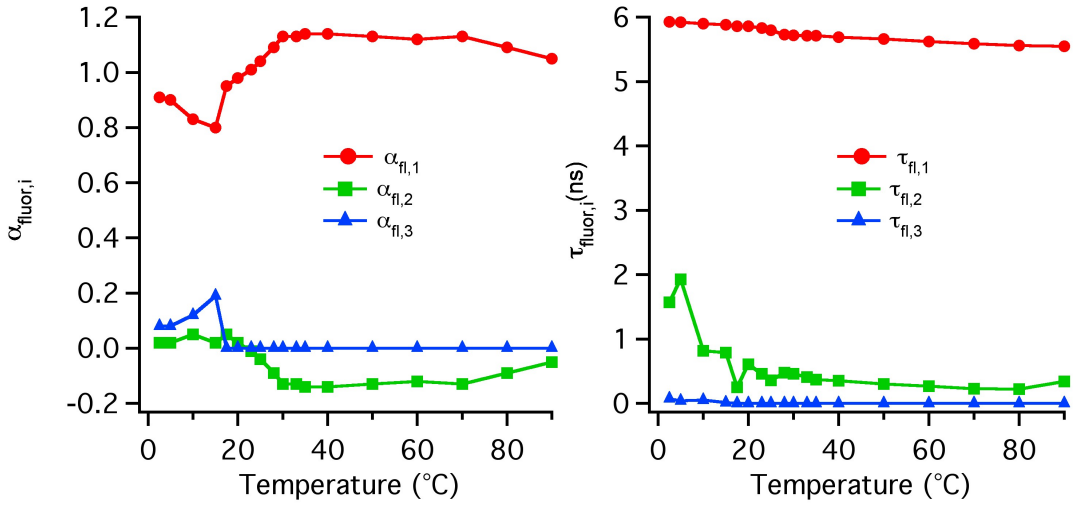

Figure 5.32: Temperature dependence of fractional amplitudes ($\alpha_{i,fl}$) (left) and individual fluorescence time constants ($\tau_{i,fl}$) (right) for C102 in 25 w/v%Pluronic F88 solution.

5.3 Conclusions

The changes in local solvent environment for each coumarin solvatochromic probe were observed by measurements of the steady-state and time-resolved fluorescence spectroscopy of each coumarin. Shifts in peak emission energy to higher energies indicated that fluorophores such as coumarin 314T, 153, and 102 localized inside the polymer micelle once the micelle was formed at its critical micellization temperature. Intermediately soluble coumarins showed similar but less drastic shifts in steady-state emission towards shorter wavelengths, indicating that a population of fluorophores such as coumarin 152, 337 and 151 were localized both in the core, corona, and interfacial regions of the polymer micelle and possibly in the bulk water solvent environment. The most hydrophilic coumarin probe, $C343^{-}/Na^{+}$ localized in the bulk water environment of the polymer solution at all temperatures and fluorescence spectra indicate no change in local environment during the unimer-to-micelle phase transition of the polymer. Analysis of the emission spectrum of $C343^{-}/Na^{+}$ shows that the fluorescence shifts little in peak frequency, but the distribution of local environments changes from two very narrow distributions to a wide variation distributed local environments as the A-B-A triblock

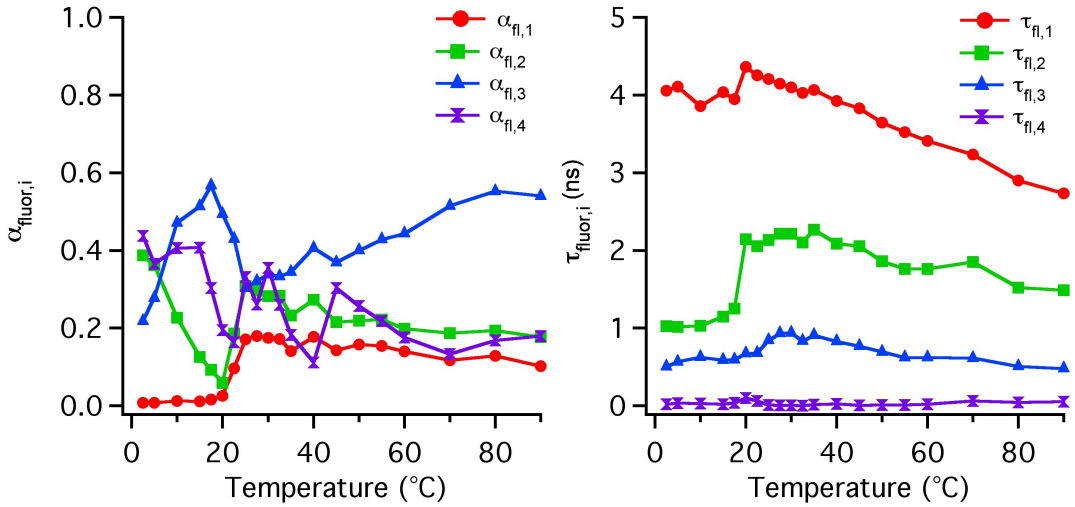

Figure 5.33: Temperature dependence of fractional amplitudes ($\alpha_{i,fl}$) (left) and individual fluorescence time constants ($\tau_{i,fl}$) (right) for C152 in 25 w/v%Pluronic F88 solution.

copolymer forms micelles.

Local polarity was characterized by the temperature dependence of the fluorescence time constants of each coumarin fluorophore. Since the time constants decrease with decreasing solvent polarity, the hydrophobic coumarins showed a decrease in time constant with increasing temperature as they localized inside the non-polar micelle core. Intermediately soluble coumarin fluorophores also showed a decrease in fluorescence time constant and even showed a small increase in the smaller time constant of every coumarin. This indicates that a small population of each coumarin was localized outside of the micelle in the bulk water once the polymer aggregates were formed. The increasing smaller time constant shows that a small population is going from a more non-polar to a more polar solvent environment. The dominating time constant around 4 to 5 ns for each of these intermediately soluble coumarins is decreasing, which indicates the unimer-to-micelle phase transition. The coumarins with intermediate solubility are solubilized in multiple regions of the core and the corona of the polymer aggregates.

The most hydrophilic coumarin $343^{-}/Na^{+}$ shows a predominant time constant at 4.5 ns which is unchanging with micellization of the polymer, however, there is a small

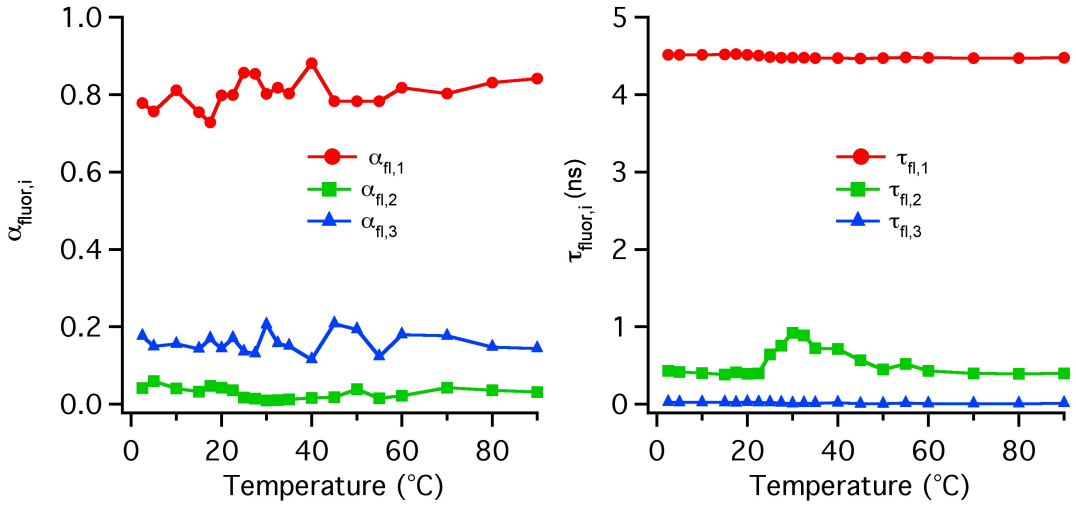

Figure 5.34: Temperature dependence of fractional amplitudes ($\alpha_{i,fl}$) (left) and individual fluorescence time constants ($\tau_{i,fl}$) (right) for C337 in 25 w/v%Pluronic F88 solution.

population that shows a decrease in a small time constant of 1 ns, indicating that some of the coumarin $343^{-}/Na^{+}$ is seeing the change associated with the micellization transition, perhaps in the corona of the micelle. All seven coumarins show a shift in fluorescence time constant at the micellization temperature of 22.5 °C indicating a shift in local polarity whether it be moving inside or outside the polymer aggregate. This shift is dependent on the solubility of the coumarin probe molecule.

Reorientation time constants and depolarization anisotropy values were found for each coumarin fluorophore at approximately 20 temperatures from 2.5 to 90.0 °C by time-correlated single photon counting techniques and time-dependent fluorescence polarization anisotropy measurements. This shows that the reorientation time scales of C153 were the largest, indicating that C153 is most rigidly solubilized within the hydrophobic core of F88 micelles. Coumarin C153, C152, and C314T all had similar average volumes of reorientation around approximately 30 $Å^3$ while the molecular volumes of each of the coumarins is approximately 175 to 356 $Å^3$.

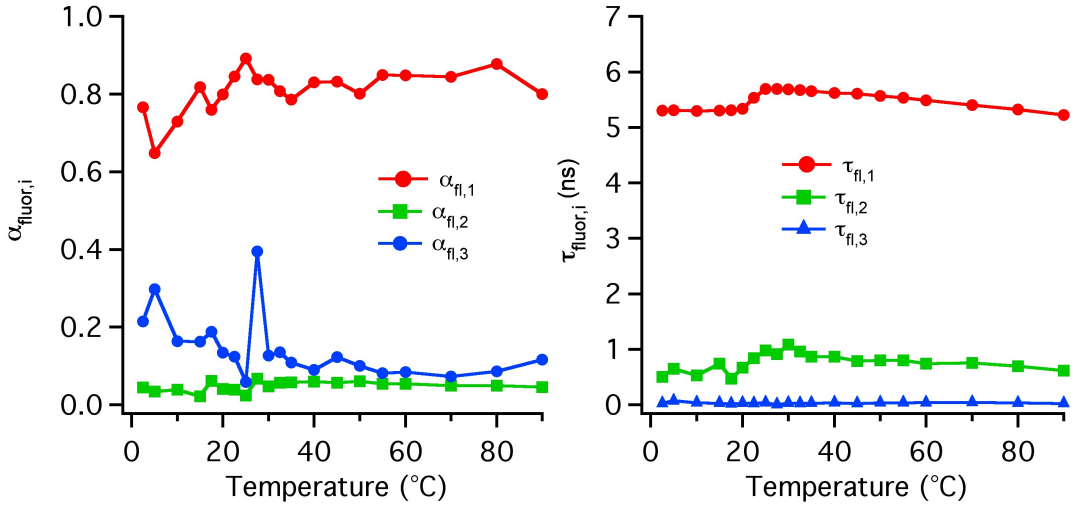

Figure 5.35: Temperature dependence of fractional amplitudes ($\alpha_{i,fl}$) (left) and individual fluorescence time constants ($\tau_{i,fl}$) (right) for C151 in 25 w/v%Pluronic F88 solution.

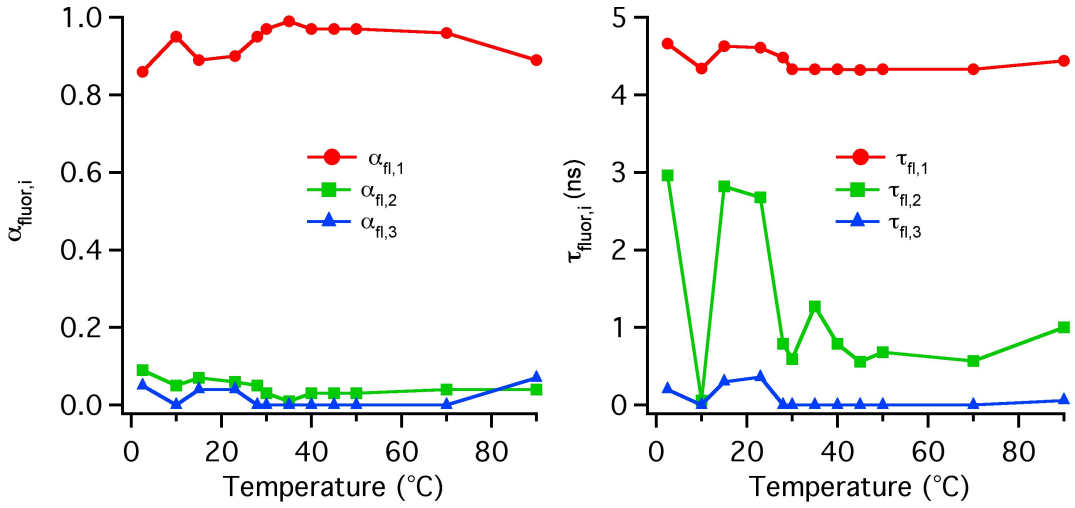

Figure 5.36: Temperature dependence of fractional amplitudes ($\alpha_{i,fl}$) (left) and individual fluorescence time constants ($\tau_{i,fl}$) (right) for $C343^{-}/Na^{+}$ in 25 w/v%Pluronic F88 solution.

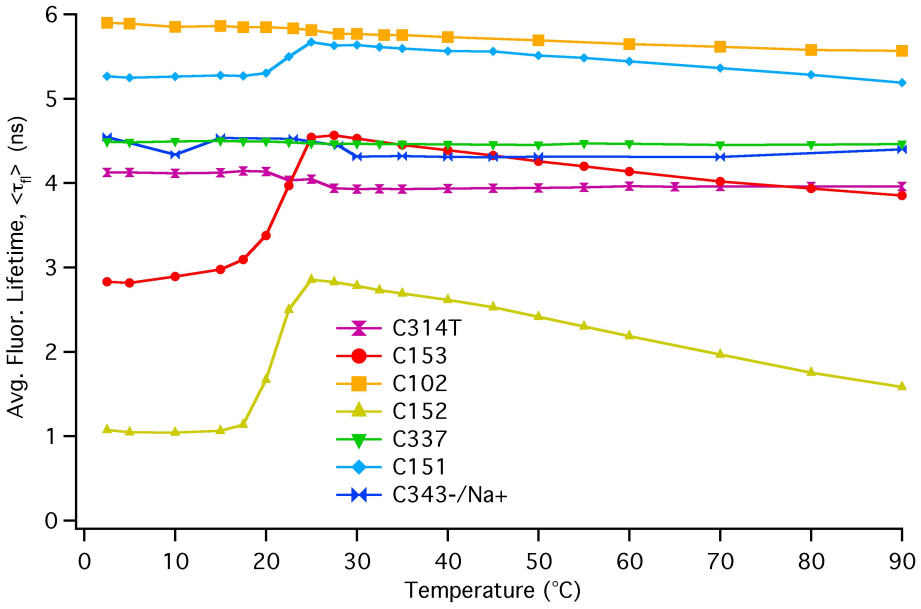

Figure 5.37: Temperature dependence of intensity-weighted average fluorescence time constants, ($\langle\tau_{fluor}\rangle$) for 7 coumarins in 25 w/v%Pluronic F88 solution.

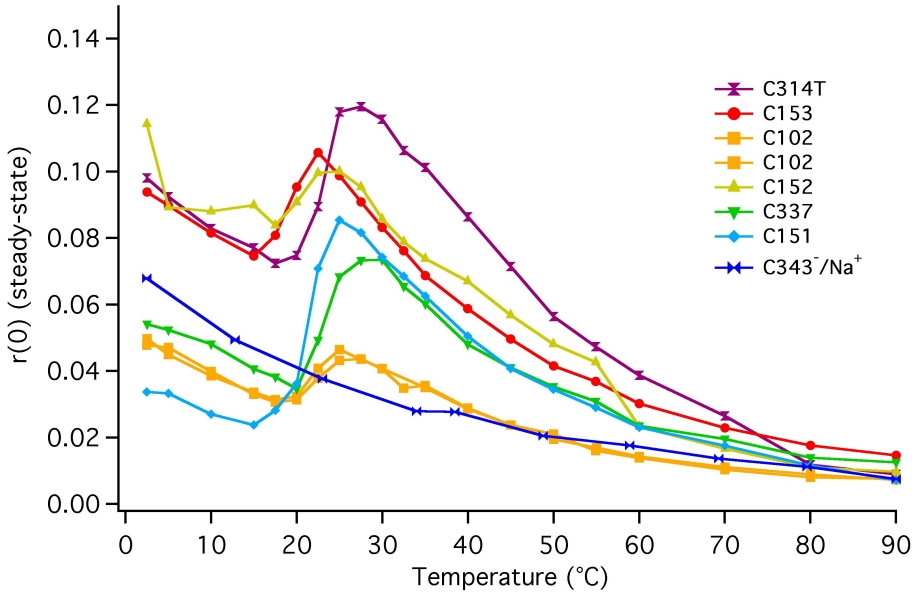

Figure 5.38: Temperature dependence of steady-state depolarization anisotropy, r_0, for 7 coumarins in 25 w/v%Pluronic F88 solution.

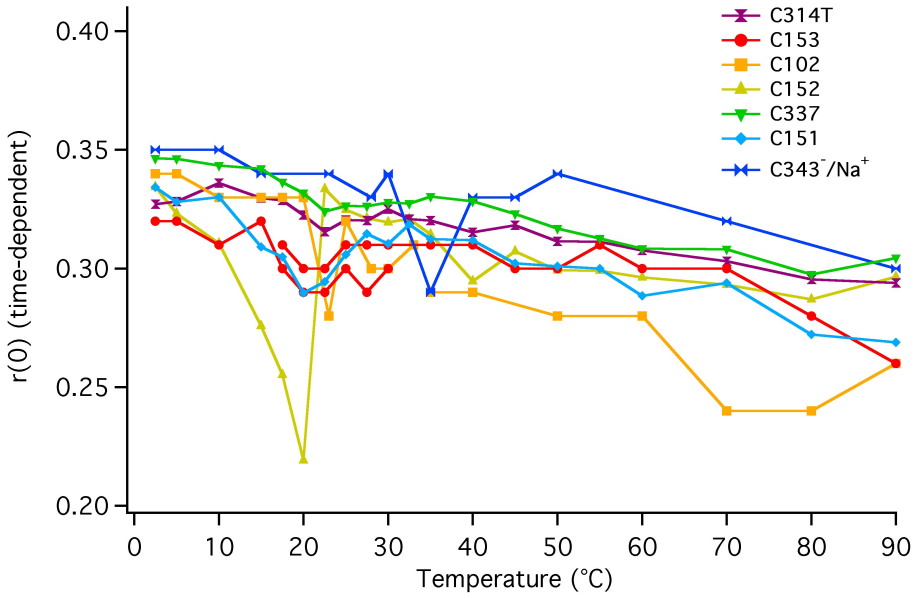

Figure 5.39: Temperature dependence of time-dependent depolarization anisotropy, r_0, for 7 coumarins in 25 w/v%Pluronic F88 solution.

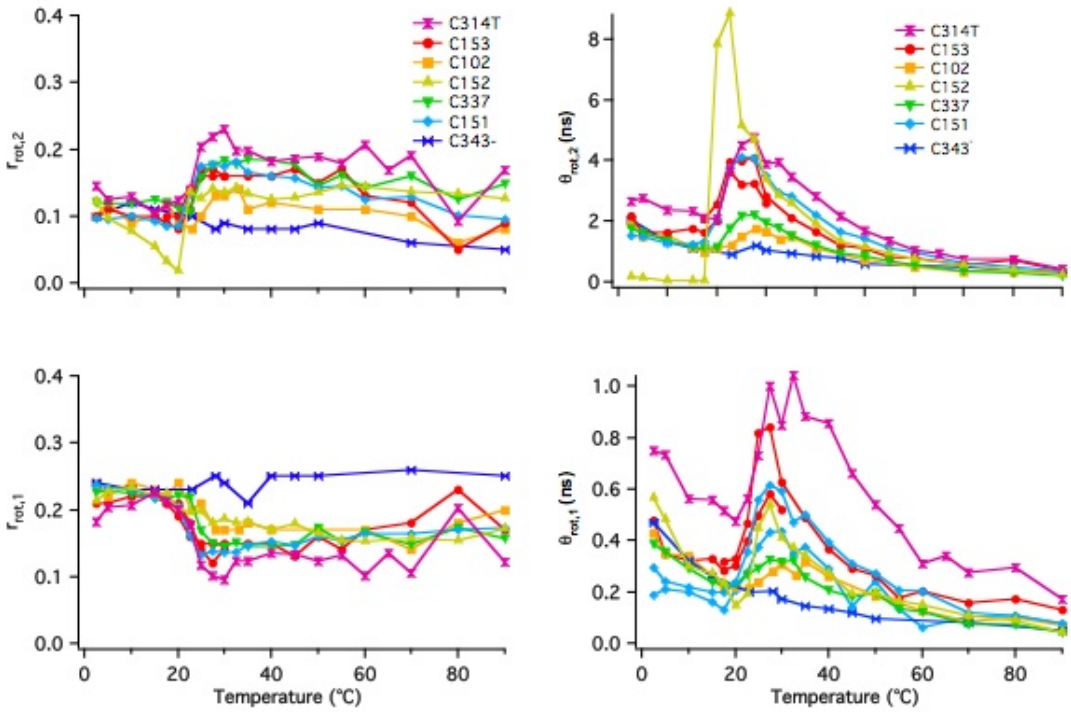

Figure 5.40: Temperature dependence of individual anisotropies ($r_{rot,j}$) (left) and reorientation time constants ($\theta_{rot,j}$) (right) for 7 coumarins in 25 w/v%Pluronic F88 solution.

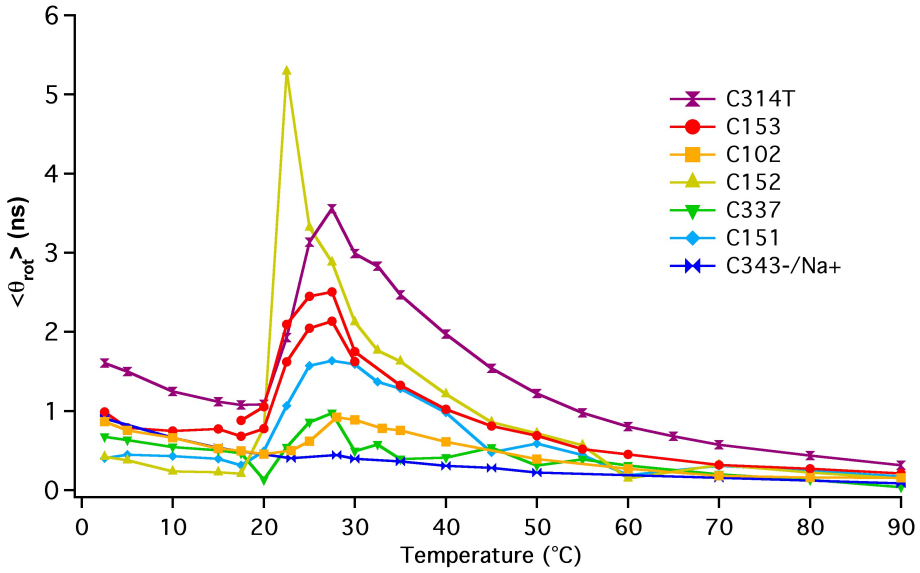

Figure 5.41: Temperature dependence of amplitude-weighted average reorientation time constants ($\langle\theta_{rot}\rangle$) for 7 coumarins in 25 w/v%Pluronic F88 solution.

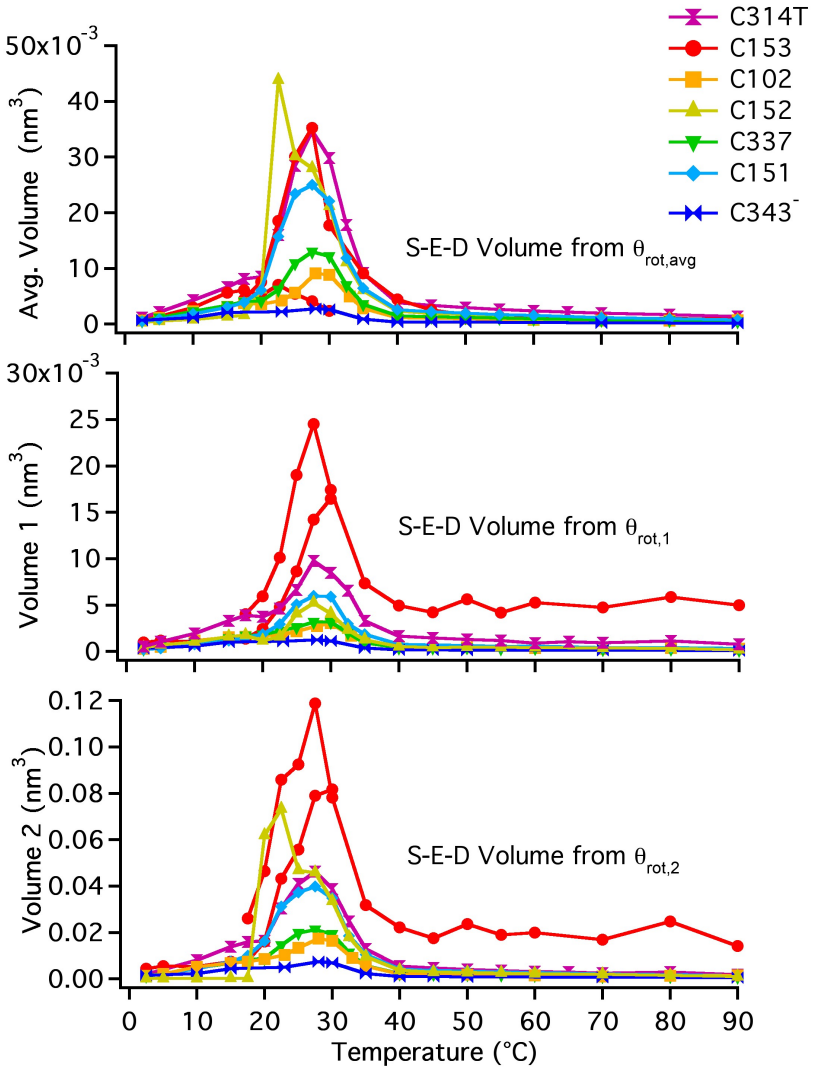

Figure 5.42: Temperature dependence of S-E-D hydrodynamic volumes deduced from reorientation time constants of 7 coumarins in 25 w/v%Pluronic F88 solution.

References

[1] D. Chandler; Interfaces and the driving force of hydrophobic assembly; *Nature* **2005**, *437*, 640–647.

[2] H. R. Allcock, F. W. Lampe, and J. E. Mark *Contemporary Polymer Chemistry;* Pearson Education, Inc.: Upper Saddle River, New Jersey, third edition ed., 2003.

[3] A. V. Kabanov *et al.;* Micelle formation and solubilization of fluorescent probes in poly(oxyethylene-b-oxypropylene-b-oxyethylene) solutions.; *Macromolecules* **1995**, *28*, 2303–14.

[4] A. V. Kabanov, E. V. Batrakova, and V. Y. Alakhov; Pluronic block copolymers as novel polymer therapeutics for drug and gene delivery.; *Journal of Controlled Release* **2002**, *82*, 189–212.

[5] N. Y. Rapoport, J. N. Herron, W. G. Pitt, and L. Pitina; Micellar delivery of doxorubicin and its paramagnetic analog, ruboxyl, to hl-60 cells: effect of micelle structure and ultrasound on the intracellular drug uptake.; *J. Controlled Release* **1999**, *58*, 153–162.

[6] M. Muniruzzaman *et al.;* Intracellular uptake of pluronic copolymer: effects of the aggregation state.; *Colloids Surf., B* **2002**, *25*, 233–241.

[7] E. V. Batrakova, S. Li, D. W. Miller, and A. V. Kabanov; Pluronic p85 increases permeability of a broad spectrum of drugs in polarized bbmec and caco-2 cell monolayers.; *Pharmaceutical Research* **1999**, *16*, 1366–1372.

[8] N. J. Jain, V. K. Aswal, P. S. Goyal, and P. Bahadur; Micellar structure of an ethylene oxide-propylene oxide block copolymer: a small-angle neutron scattering study.; *Journal of Physical Chemistry B* **1998**, *102*, 8452–8458.

[9] B. Valeur *Molecular Fluorescence: Principles and Applications;* Wiley-VCH, 2002.

[10] J. R. Lakowicz *Principles of Fluorescence Spectroscopy;* Kluwer Academic/ Plenum Publishers, 2nd ed., 1999.

[11] C. A. Lipinski; Drug-like properties and the causes of poor solubility and poor permeability; *Journal of Pharmacological and Toxicological Methods* **2000**, *44*, 235–249.

[12] C. D. Grant *et al.;* Fluorescence probing of interior, interfacial, and exterior regions in solution aggregates of poly(ethylene oxide)- poly(propylene oxide)-poly(ethylene oxide) triblock copolymers.; *Langmuir* **2005**, *21*, 1745–1752.

[13] R. J. Cave and E. W. Castner Jr.; Time-dependent density functional theory investigation of the ground and excited states of coumarins 102, 152, 153, and 343.; *Journal of Physical Chemistry A* **2002**, *106*, 12117–12123.

[14] R. J. Cave, K. Burke, and E. W. Castner Jr.; Theoretical investigation of the ground and excited states of coumarin 151 and coumarin 120.; *Journal of Physical Chemistry A* **2002**, *106*, 9294–9305.

[15] P. K. McCarthy and G. J. Blanchard; Am1 study of the electronic structure of coumarins; *Journal of Physical Chemistry* **1993**, *97*(47), 12205–12209.

[16] J. Ridley and M. Zerner; An intermediate neglect for differential overalap technique for spectroscopy: Pyrrole and the azines; *Theoretical Chemistry Accounts* **1973**, *32*, 111–134.

[17] M. C. Zerner, G. H. Loew, R. F. Kirchner, and U. T. Mueller-Westerhoff; An intermediate neglect of differential overlap technique for spectroscopy of transition-metal complexes. ferrocene.; *Journal of the American Chemical Society* **1980**, *102*, 589–99.

[18] M. C. Zerner *Semiempirical Molecular Orbital Methods in Reviews in Computational Chemistry*, Vol. 8; VCS Publishers Inc., 1991.

[19] M. A. Thompson and M. C. Zerner; A theoretical examination of the electronic structure and spectroscopy of the photosynthetic reaction center from rhodopseudomonas viridis.; *Journal of the American Chemical Society* **1991**, *113*, 8210–15.

[20] Arguslab version 4.0. M. A. Thompson Planaria Software LLC, Seattle, WA., **1996-2003**.

[21] N. J. Turro *Modern Molecular Photochemistry v. 2;* University Science Books, 1991.

[22] P. Suppan; Invited review. solvatochromic shifts. the influence of the medium on the energy of electronic states.; *Journal of Photochemistry and Photobiology, A: Chemistry* **1990**, *50*, 293–330.

[23] L. Reynolds *et al.;* Dipole solvation in nondipolar solvents: Experimental studies of reorganization energies and solvation dynamics.; *Journal of Physical Chemistry* **1996**, *100*, 10337–10354.

[24] M. L. Horng, J. A. Gardecki, A. Papazyan, and M. Maroncelli; Subpicosecond measurements of polar solvation dynamics: Coumarin 153 revisited.; *Journal of Physical Chemistry* **1995**, *99*, 17311–37.

[25] D. Ben-Amotz and J. M. Drake; The solute size effect in rotational diffusion experiments: A test of microscopic friction theories; *The Journal of Chemical Physics* **1988**, *89*(2), 1019–1029.

[26] G. Wanka, H. Hoffmann, and W. Ulbricht; Phase diagrams and aggregation behavior of poly (ox yethy1ene)-poly (oxypropylene) -poly(oxyet hylene) triblock copolymers in aqueous solutions; *Macromolecules* **1994**, *27*, 4145–4159.

[27] G. Jones II, W. R. Jackson, C. Y. Choi, and W. R. Bergmark; Solvent effects on emission yield and lifetime for coumarin laser dyes. requirements for a rotatory decay mechanism.; *Journal of Physical Chemistry* **1985**, *89*, 294–300.

[28] M. Maroncelli and G. R. Fleming; Picosecond solvation dynamics of coumarin 153: the importance of molecular aspects of solvation.; *Journal of Chemical Physics* **1987**, *86*, 6221–39.

[29] M.-L. Horng, J. A. Gardecki, and M. Maroncelli; Rotational dynamics of coumarin 153: Time-dependent friction, dielectric friction, and other nonhydrodynamic effects.; *Journal of Physical Chemistry A* **1997**, *101*, 1030–1047.

[30] H. Shirota and E. W. Castner Jr.; Solvation in highly nonideal solutions: A study of aqueous 1-propanol using the coumarin 153 probe.; *Journal of Chemical Physics* **2000**, *112*, 2367–2376.

[31] D. V. Matyushov and M. D. Newton; Understanding the optical band shape: Coumarin-153 steady-state spectroscopy.; *Journal of Physical Chemistry A* **2001**, *105*, 8516–8532.

[32] C. D. Grant, K. E. Steege, M. R. Bunagan, and E. W. Castner Jr.; Microviscosity in multiple regions of complex aqueous solutions of poly(ethylene oxide)-poly(propylene oxide)-poly(ethylene oxide).; *Journal of Physical Chemistry B* **2005**, *109*, 22273–22284.

[33] F. Ingrosso and B. M. Ladanyi; Solvation dynamics of c153 in supercritical fluoroform: A simulation study based on two-site and five-site models of the solvent.; *Journal of Physical Chemistry B* **2006**, *110*, 10120–10129.

[34] F. Ingrosso, B. M. Ladanyi, B. Mennucci, and G. Scalmani; Solvation of coumarin 153 in supercritical fluoroform.; *Journal of Physical Chemistry B* **2006**, *110*, 4953–4962.

[35] K. E. Steege, J. Wang, K. E. Uhrich, and E. W. Castner Jr.; Local polarity and microviscosity in the hydrophobic cores of amphiphilic star-like and scorpion-like macromolecules; *Macromolecules* **2007**, *40*, 3739–3748.

[36] M. J. Kamlet, J. L. Abboud, and R. W. Taft; The solvatochromic comparison method. 6. the π^* scale of solvent polarities.; *Journal of the American Chemical Society* **1977**, *99*, 6027–6038.

[37] clogp calculator www.daylight.com.

[38] B. A. Pryor, P. M. Palmer, Y. Chen, and M. R. Topp; Identification of dual conformers of coumarin 153 under jet-cooled conditions.; *Chemical Physics Letters* **1999**, *299*, 536–544.

Chapter 6

Future Directions

6.1 Overview

Fluorescence spectroscopy is a key tool used for the detection of molecular probes in both uniform and complex solvent environments. The investigation of the trends in fluorescence spectral shifts, time constants, and reorientational motions for fluorophores such as rilpivirine can also be applied to historically well-characterized solvatochromic probe molecules like 7-aminocoumarins to investigate various regions of complex solutions such as A-B-A triblock copolymer micelles. Rilpivirine is a newly characterized molecule in the area of fluorescence spectroscopy. The possibilities for meaningful research utilizing this physical characteristic of the HIV inhibitor are many and exciting.

6.2 Background of Emerging Fields

The characterization of the local solvent environment of dissolved coumarin probes, and the HIV inhibitor, rilpivirine in various solvent environment including aggregated polymer micelles in solution, combine the fields of polymer science, drug delivery, fluorescence spectroscopy, and electronic structure. At the interface between these emerging fields is the methodologies of fluorescence spectroscopy to physically characterize the state of complex drug delivery solutions for improvement of both polymeric nanocarriers and drug molecules themselves. Presented here is an overview of the background of developments in HIV treatments by DAPY non-nucleoside reverse transcriptase inhibitors (NNRTIs) and some information on the use of amphiphilic polymers for applications in drug delivery.

6.2.1 DAPYs for Treatment of HIV

The development of new and effective HIV inhibitors involves the goal of finding molecules that are easily adaptable to mutations in the reverse transcriptase protein to which they bind.[1] Diarylpyrimidines (DAPYs) posses this characteristic, making the group of NNRTIs effective in the inhibition of HIV replication.[2, 3] Rilpivirine, a DAPY molecule found to have EC_{50} values under 0.1 nM[3, 4] for the inhibition of HIV replication, is also a self-reporter of local environment; a helpful trait for the investigation of drug delivery formulations and solutions containing this molecule.[5]

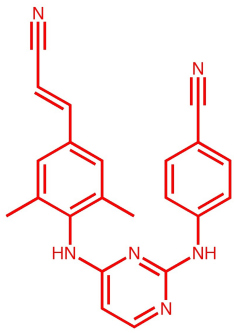

Figure 6.1: Structure of the rilpivirine (TMC 278, R278474), an NNRTI of HIV-1.

In comparison to two FDA-approved NNRTIs, efavirenz and nevirapine, rilpivirine was found to have 4 times the potency of efavirenz in wild-type HIV-1 and over 200 times the potency of nevirapine in cell-based assays.[3] In assays of single and double-point mutation forms of HIV-1, rilpivirine was found to be up to 10,000 times more potent than nevirapine and almost 3,000 times more potent than efavirenz.[3] Because HIV mutations are a major cause of drug resistance in HIV patients, rilpivirine may be a solution to a significant problem in HIV treatment.[3, 2, 1] The ability of the effectiveness of rilpivirine to withstand mutations in the binding site of RT is attributed to its loose fit in the RT hydrophobic binding pocket.[1, 6]

Recent work on DAPYs (and some diaryltriazines, DATAs) dissolved in aqueous buffer solutions, co-solvated with DMSO, PEG, or the surfactant, tylaxopol, has led to the discovery that rilpivirine, like most DAPYs and DATAs, form nanoparticle aggregates in the described solutions.[4] The average size of the aggregates varies with

concentration and pH; two important parameters in the bioavailability of a formulated solution.[4] The detection of the local solvent environment of rilpivirine and the presence of aggregates in solution is an important application of the fluorescence spectroscopy of DAPYs.

6.2.2 Amphiphilic Polymers for Applications in Drug Delivery

Amphiphilic block copolymers have been widely used for drug solublization and delivery applications.[7, 8, 9, 10, 11, 12, 13, 14, 15, 16, 17, 18, 19] The aqueous solubility, biocompatibility, and non-toxic nature of poly(ethylene glycol) (PEG) make this polymer a key component in many biomaterials.[20, 21, 22] Pluronics F88 is an A-B-A triblock copolymer that consist ofs poly(ethylene oxide)$_{109}$-poly(propylene oxide)$_{41}$-poly(ethylene oxide)$_{109}$ (PEO$_{109}$-PPO$_{41}$-PEO$_{109}$). The amphiphilic nature of the F88 polymer causes it to form spherical micelles and ccb hydrogels in aqueous solution, varying with concentration and temperature.[23, 24] The micelles formed from aqueous F88 are useful for the encapsulation and solubilization of small hydrophobic molecules.[23]

6.3 Key Findings

There are several connected themes to the conclusions drawn from the preceding chapters. Fluorescence spectroscopy is the tool used to investigate the local environments of several chemical systems. This tool can be used to explore the differences between local regions in solutions of amphiphilic polymers in the various phases of polymer aggregation. Fluorescence spectroscopy can also be used to identify the polarity and local friction of an unknown solvent environment of a fluorophore, whether it be a model drug molecule such as a coumarin, or an HIV-1 inhibitor such as rilpivirine. The fluorescence of rilpivirine has been found to be an easy method of detection and aggregate identification for this highly potent drug.

6.3.1 Fluorescence Spectroscopy of Rilpivirine

The instigation of the research presented here was the discovery that rilpivirine is a fluorescent molecule and the fact that rilpivirine is very hydrophobic presents challenges

for efficient biological delivery. Recent work on the formation of rilpivirine aggregates in solution also presented a challenge in terms of the spectroscopy of the rilpivirine in solution. Fluorescence properties of unimer molecules and aggregated fluorophores in solution are usually different from one another and rilpivirine is no exception.[25]

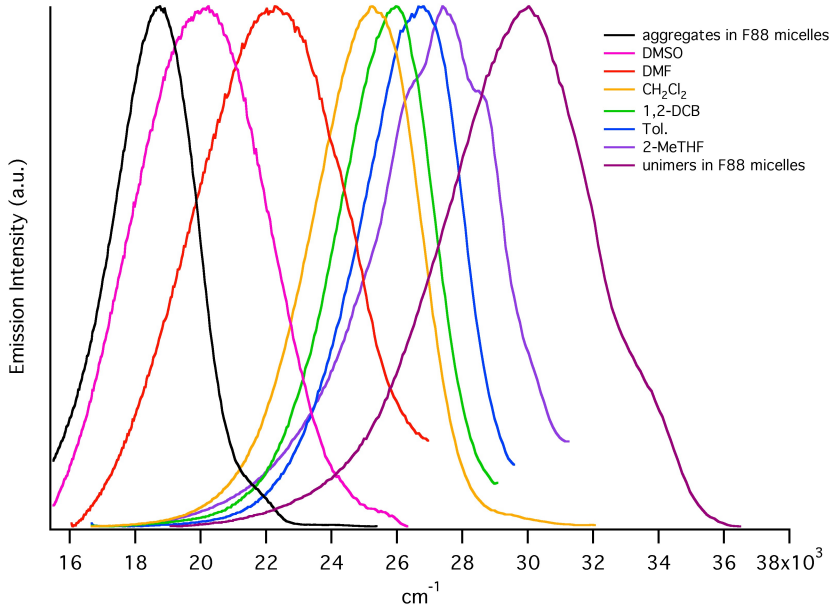

Figure 6.2: Emission of rilpivirine in some selected solvents. (DMSO, DMF, CH_2Cl_2, 1,2-DCB, toluene, and 2-MeTHF) as well as 1 and 84 μM concentrations of rilpivirine in aqueous solutions of A-B-A triblock copolymer F88 micelles

By dissolving rilpivirine in a variety of common solvents ranging in polarity, an empirical scale is created for the fluorescence emission spectral energies, fluorescence time constants, and reorientational dynamics. Figure 6.2 shows the emission spectra of rilpivirine dissolved in DMSO, DMF, dichloromethane, 1,2-dichlorobenzene, and 2-methyltetrahydrofuran. The rilpivirine emission spectrum in aqueous solution of 25 w/v% A-B-A triblock copolymer Pluronic F88 is presented for two concentrations of rilpivirine: 1 μM where rilpivirine is in unimer form, and 84 μM where rilpivirine is aggregate form. The emission of the rilpivirine unimers shows that the core environment of F88 polymer micelles is less polar than 2-methyltetrahydrofuran. The peak of emission from rilpivirine aggregates is characteristic of only aggregates present in solution and not of rilpivirine unimers in solution. This is an important discovery for the next

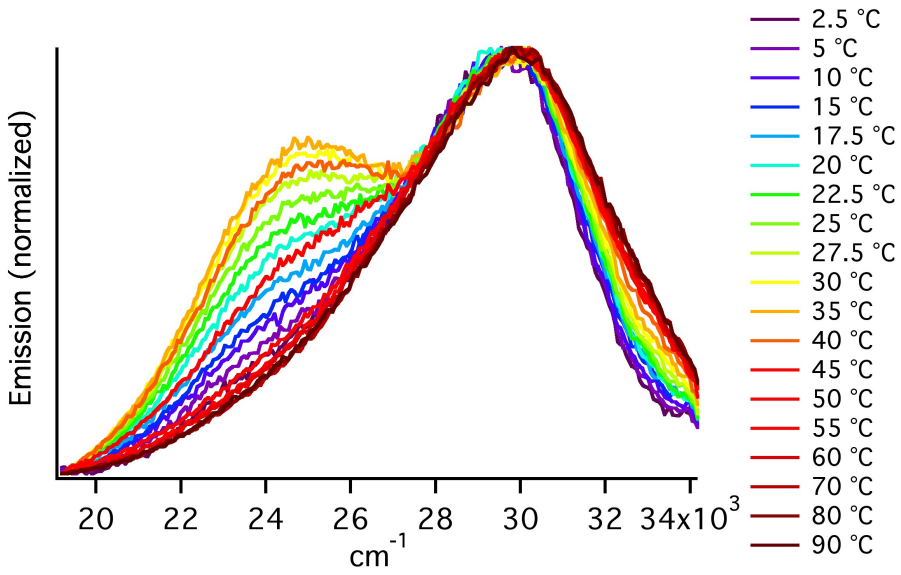

Figure 6.3: Normalized emission spectra of 5.8 μM rilpivirine in 25 w/v% Pluronic F88 in aqueous solution with changing temperature.

investigation of rilpivirine in different aqueous phases of A-B-A triblock copolymer F88.

The local solvent polarity is not the only property of rilpivirine that is readily detectable by fluorescence spectroscopy. Because the aggregate form of rilpivirine fluoresces at a lower energy than the unimer form of rilpivirine in solution, a second peak is visible in the emission spectrum when both forms are present. In the temperature-dependent emission spectrum of rilpivirine in Pluronic F88 solution, it is possible to see the change in aggregation of the drug when the polymer is in unimer, micelle, and hydrogel form in aqueous solution.

6.3.2 Hydrophobic Cores of Amphiphilic Star-like and Scorpion-like Macromolecules

Amphiphilic star-like macromolecules (ASMs) are composed of four macromolecules composed of an acylated mucic acid hydrophobic block and a polyethylene glycol (PEG) hydrophilic block, covalently bonded at the core. NC6P5 and NC12P5, two ASM molecules form macromolecular aggregates in aqueous solution above 1x10^{-7} mol/L at 37 °C. Amphiphilic scorpion-like macromolecules (AScMs) are single diblock molecules

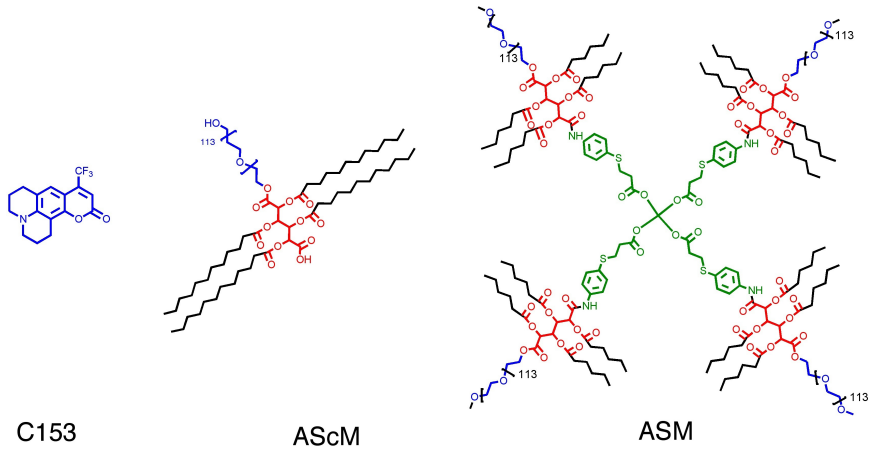

Figure 6.4: From Left to Right: Coumarin 153, M12P5, an amphiphilic scorpion-like macromolecule, and NC6P5, an amphiphilic star-like macromolecule.

composed of the same acylated mucic acid block and PEG block. M12P5, an AScM, forms micelles in aqueous solution at the same concentration and temperature. M12P5 and NC6P5 strucutres, along with the structure of fluorescence probe, coumarin 153 are shown in Figure 6.4.

The solvatochromic probe, C153 has fluorescence properties that are sensitive to changes in local environment.[26, 27, 28, 23] These properties include emission wavelength, fluorescence time constants, polarization anisotropies, and reorientation time constants. By using these spectroscopic properties, the local polarity and friction of the hydrophobic cores of ASMs and AScMs are compared. The AScM M12P5 forms micelles of approximately 20 nm in diameter while the ASMs NC6P5 and NC12P5 form macromolecular aggregates of approximately 30 and 40 nm in diameter, respectively. The fluorescence emission of C153 dissolved in solutions of each of the three polymers reports that the ASM aggregate cores are less polar than the flexible core of M12P5 micelles. Reorientational dynamics of C153 report that the local friction of the solvent environment inside AScM aggregate cores is higher than the local friction inside the AScM micellar core. Using Stokes-Einstein-Debye hydrodynamics, the effective local friction is calculated for C153 in each polymer solution and these values are plotted in Figure B-15. If a drug needs improved solubility and longer circulation time inside a

biological system, the ASM polymers are more suitable than AScM micelles. If a drug molecule need improved solubility, higher concentration, and a shorter release time, AScM micelles may be the more appropriate choice.

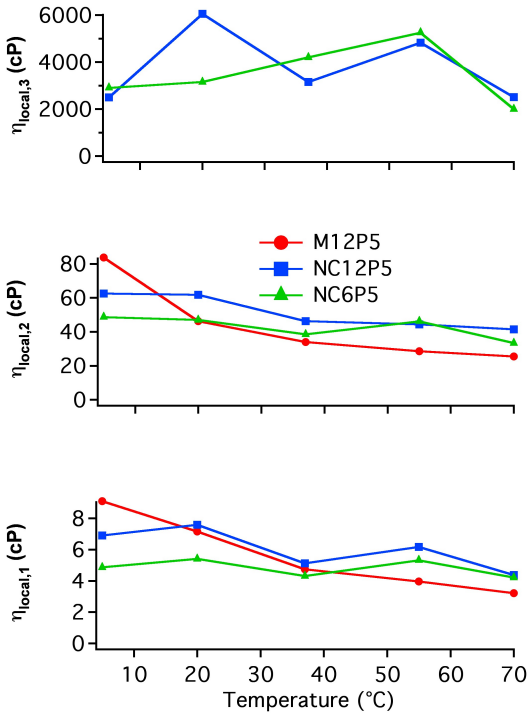

Figure 6.5: Local frictions from $\theta_{rot,j}$'s.

6.3.3 Probing Regions of Aqueous A-B-A Triblock Copolymer Micelles

Seven 7-aminocoumarin fluorescence probe molecule were each dissolved in aqueous solutions of 25 w/v% A-B-A triblock copolymer F88. These coumarins, in order of increasing aqueous solubility are: C314T, C153, C102, C152, C337, C151, and $C343^{-}/Na^{+}$. Figure 6.6 depicts the various regions for which each coumarin is most dissolved in aqueous F88 micelles. In the temperature range from 2.5 to 90 °C, the polymer changes phase from unimers (below 22.5 °C) to micelles (above 22.5 °C) to hydrogels (above 38 °C). Using coumarin dyes of various polarities, the polarity and local friction of different regions of these polymer phases in solution are measured and compared. While the

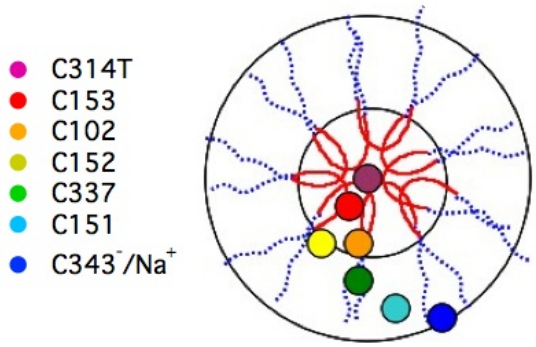

Figure 6.6: Representation of local distribution of 7 coumarin fluorescence probes in various regions of an amphiphilic A-B-A triblock copolymer micelle where red strands are the PPO core and blue strands are the PEO corona.

intermediately water-soluble coumarin molecules are distributed across all solubility regions of the micellar phase, the most hydrophobic coumarin dyes are located primarily in the PPO core and $C343^{-}/Na^{+}$ is completely soluble in the aqueous phase of the solution. Figure 6.7 displays the average reorientation time constant of each coumarin with the change in temperature of F88 solution. At exactly 22.5 °C, as micelles are formed, the reorientation time constants of the coumarins dissolved in the micellar core increase considerably. This slowing of reorientational motion is due to a change in local friction as reported by each coumarin probe. The $C343^{-}/Na^{+}$, which is not dissolved inside the micellar core, reports no change in local friction over the measured temperature range.

6.4 Future Directions

6.4.1 Rilpivirine and other Diarylpyrimidines

The findings presented here on the spectroscopy of rilpivirine can be utilized for various applications. The development of medicinal formulations for rilpivirine are not yet fully realized and the delivery mechanism for rilpivirine aggregates is not specifically known.[3, 4, 6] The application of fluorescence spectroscopy methods, as described in the preceding chapters may be useful in tracking aggregates, size scales and the local environment of rilpivirine molecules directly.

There are several directions in which research could be based from the studies of

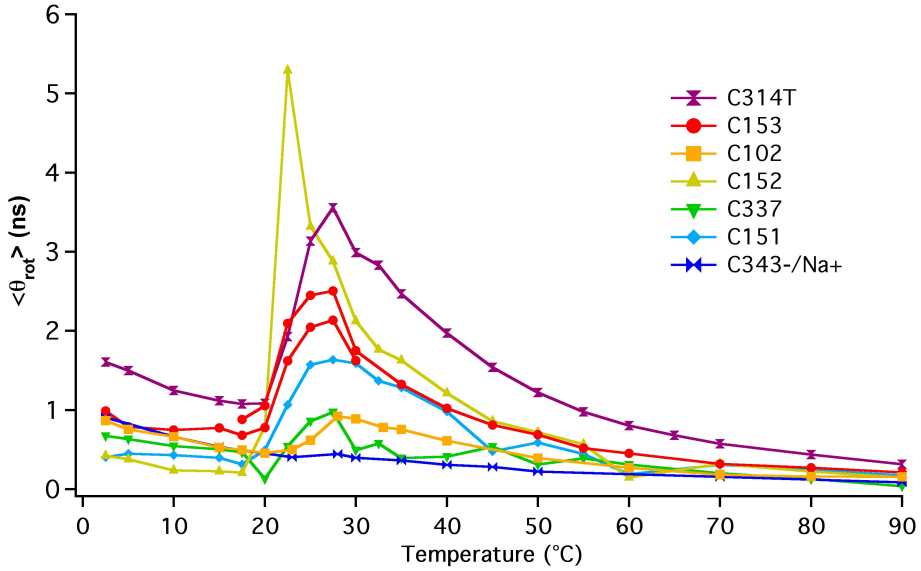

Figure 6.7: Temperature dependence of amplitude-weighted average reorientation time constants ($\langle\theta_{rot}\rangle$) for 7 coumarins in 25 w/v%Pluronic F88 solution.

rilpivirine presented here. Unfortunately, the absorption and fluorescence of rilpivirine completely overlap with that of tryptophan. There are approximately 30 tryptophan residues in the RT protein that saturate the fluorescence signal detected from a rilpivirine-bound RT solution. One solution to this problem would be to use a different DAPY molecule that absorbs and emits at shorter wavelengths than rilpivirine and tryptophan. If such a DAPY was bound to HIV-1 RT and this solution was measured using fluorescence emission and polarization anisotropy, the polarity and local friction of the RT binding pocket could be directly measured. This may provide insight into the loose fitting of DAPYs in the binding pocket which gives this set of drugs good resistance to mutations.[1] Other DAPYs and some diaryltriazines (DATAs) include R165335 (TMC 125), R147681 (TMC 120), and R152929.[4] All of these molecules have activity as HIV inhibitors, but the spectroscopy has not yet been fully characterized.

A second experiment that could result from the fluorescence spectroscopy of rilpivirine is the fluorescence microscopy and fluorescence lifetime imaging microscopy (FLIM) of rilpivirine aggregates. Measurements of rilpivirine in aqueous buffer solutions confirm that with UV optical fitlers, fluorescence microscopy has the ability to detect and image

rilpivirine aggregates. Unfortunately, the tools were not available to take full advantage of this novel experiment. Confocal fluorescence microscopy utilizes pinholes to focus the plane of an image and fluorescence detection while increasing the contrast between the image and the background. A confocal microscope with UV filters and UV-visible wavelength sensitive detectors would be extremely useful for undertaking the study of the interaction of rilpivirine aggregates with cells. Both the emission spectrum and the fluorescence time constants of rilpivirine aggregates could be imaged if the method of FLIM was used. Since rilpivirine aggregates have shorter fluorescence time constants than the unimer form of rilpivirine, the contrast is hypothesized to be significant.

6.4.2 Amphiphilic Polymers for Applications in Drug Delivery

The development of drug delivery vehicles is widely expanding in the fields of synthetic polymer chemistry and biomaterials.[29, 14, 8, 10, 11] The development of new polymers with various core structures provides the need for methods to characterize the differences between these molecules. By fluorescence spectroscopy of solvatochromic probes encapsulated in these nanocarriers as model drugs, the differences in core structure, dynamics, polarity, and flexibility can be directly compared.

Future directions of this research involve the characterization of a variety of novel ASMs and AScMs. The development of new polymeric nanocarriers for specific drug molecules and delivery properties is changing both the properties of the hydrophobic cores and the PEG coronas as well.[30, 31] Functionalized PEG chains, branched PEG chains, and charged molecules incorporated into the ASM and AScM structures inevitably change the core and corona structure and solubility properties of the macromolecule aggregates and micelles.[32] The ability to compare these changes will be helpful in characterizing the maximum potential for each of these nanocarrier polymers.

6.5 Summary

The HIV epidemic will not be cured overnight. Much hard work and research will continue to go into the understanding and development of better methods and mechanisms for the inhibition of HIV replication. The non-nucleoside reverse transcriptase inhibitor rilpivirine is a promising drug that has potent activity against HIV and is effective despite the high mutation rate of the virus and is also a self-reporter of local solvent environment and aggregation state. Fluorescence spectroscopy methods are used to detect local solvent polarity of rilpivirine. In aqueous solutions of A-B-A triblock copolymer Pluronic F88, the unimer and the aggregate form of the drug are both identified in solution by fluorescence anisotropy measurements. The temperature dependence of F88 polymer phase is detected by rilpivirine and the formation of rilpivirine aggregates as measured by the fluorescence spectrum. Analysis of time-resolved emission spectra report that the solvent relaxation rates in the aggregate state occur within the first 1 ns of the electronic excitation. The solvent relaxation with respect to the unimer form of rilpivirine is slower, over 10 ns after excitation of rilpivirine.

The development of novel amphiphilic drug delivery polymers ASMs and AScMs provide the need to characterize the differences in the encapsulated drug environment for each macromolecular aggregate. AScM M12P5 micelles have a relatively polar, flexible core while NC12P5 and NC6P5 ASMs have non-polar, rigid core environments in which hydrophobic drugs would be encapsulated. These differences were measured by the solvatochromic emission shift of coumarin 153 fluorescence from inside the core of each nanocarrier in solution.

A selection of 7 solvatochromic coumarin fluorescence probes were dissolved in 25 w/v% solutions of Pluronic F88. The fluorescence peak wavelength of each coumarin shifts in relation to the local solvent polarity of the fluorophore. The most hydrophobic coumarins, C314T, C153, and C102 display large shifts in temperature-dependent emission spectrum at 22.5 °C, the temperature at which F88 aggregates to form micelles, indicating that these coumarins are encapsulated in the poly(propylene oxide) core of the micelles. The intermediately water-soluble coumarins, C152, C337, and

C151 dissolved in multiple regions of the micelle core and corona, as shown by shifts in emission peak wavelength and broad spectral widths. $C343^{-}/Na^{+}$, the most water soluble coumarin of seven is completely soluble in the aqueous solvent environment of the micelle solution and since the local solvent environment of the water does not change with micelle formation, there is no shift in emission peak wavelength of $C343^{-}/Na^{+}$. The fluorescence time constants of the more hydrophobic coumarins follow the same trend, shifting to larger time constants upon micellization of F88, while the time constants of $C343^{-}/Na^{+}$ do not shift. Reorientation time constants of the seven coumarins report changes in local friction at the micellization temperature as well. The solubility properties of each coumarin determine the distribution of regions in F88 micelle solutions in which the coumarins are localized. The local solvent polarity and microviscosity of the various regions of aqueous solutions of A-B-A triblock copolymer F88 unimers, micelles, and hydrogels were characterized in each of these regions. This is a model for characterizing the encapsulation environments in other polymeric nanocarriers.

When drug solubility and delivery formulations are directed at specific properties such as aggregation state and retention time, the local environment of the encapsulated drug is an important factor in effective design of the delivery system. The characterization of rilpivirine unimers and aggregates, as well as the fundamental spectroscopy and structure of rilpivirine are applicable to characterization of the functionality of the drug in biological systems. The methods of characterization of polymer phase and local solvent regions of each phase are applied to polymers designed for hydrophobic drug delivery. Using fluorescence methods, important differences in the core regions of drug nanocarriers and the local environment and aggregations state of drug molecules such as rilpivirine can be physically characterized on molecular length scales.

References

[1] K. Das, P. J. Lewi, S. H. Hughes, and E. Arnold; Crystallography and the design of anti-aids drugs: conformational flexibility and positional adaptability are important in the design of non-nucleoside hiv-1 reverse transcriptase inhibitors.; *Progress in Biophysics & Molecular Biology* **2005**, *88*, 209–231.

[2] S. G. Sarafianos, K. Das, S. H. Hughes, and E. Arnold; Taking aim at a moving target: designing drugs to inhibit drug-resistant hiv-1 reverse transcriptases; *Current Opinion in Structural Biology* **2004**, *14*(6), 716–730.

[3] P. A. J. Janssen *et al.;* In search of a novel anti-hiv drug: Multidisciplinary coordination in the discovery of 4-[[4-[[4-[(1e)-2-cyanoethenyl]-2,6-dimethylphenyl]amino]-2- pyrimidinyl]amino]benzonitrile (r278474, rilpivirine).; *Journal of Medicinal Chemistry* **2005**, *48*, 1901–1909.

[4] Y. V. Frenkel *et al.;* Concentration and ph dependent aggregation of hydrophobic drug molecules and relevance to oral bioavailability.; *Journal of Medicinal Chemistry* **2005**, *48*, 1974–1983.

[5] K. E. Steege *et al.;* Spectroscopy, solvatochromism, and structure of rilpivirine, a potent non-nucleoside reverse transcriptase inhibitor; **2008**, page to be published.

[6] K. Das *et al.* submitted to PNAS, **2007**.

[7] V. P. Torchilin; Targeted polymeric micelles for delivery of poorly soluble drugs.; *Cellular and Molecular Life Sciences* **2004**, *61*, 2549–2559.

[8] G. S. Kwon; Polymeric micelles for delivery of poorly water-soluble compounds.; *Critical Reviews in Therapeutic Drug Carrier Systems* **2003**, *20*, 357–403.

[9] G. S. Kwon and M. L. Forrest; Amphiphilic block copolymer micelles for nanoscale drug delivery.; *Drug Development Research* **2006**, *67*, 15–22.

[10] R. Duncan; The dawning era of polymer therapeutics.; *Nature Reviews Drug Discovery* **2003**, *2*, 347–360.

[11] V. P. Torchilin; Micellar nanocarriers: Pharmaceutical perspectives.; *Pharmaceutical Research* **2007**, *24*, 1–16.

[12] H. Liu, A. Jiang, J. Guo, and K. E. Uhrich; Unimolecular micelles: synthesis and characterization of amphiphilic polymer systems.; *Journal of Polymer Science, Part A: Polymer Chemistry* **1999**, *37*, 703–711.

[13] V. Alakhov *et al.;* Block copolymer-based formulation of doxorubicin. from cell screen to clinical trials.; *Colloids and Surfaces, B: Biointerfaces* **1999**, *16*, 113–134.

[14] L. Tian *et al.;* Amphiphilic scorpion-like macromolecules: Design, synthesis, and characterization.; *Macromolecules* **2004**, *37*, 538–543.

[15] J. Djordjevic, M. Barch, and K. E. Uhrich; Polymeric micelles based on amphiphilic scorpion-like macromolecules: Novel carriers for water-insoluble drugs.; *Pharmaceutical Research* **2005**, *22*, 24–32.

[16] C. Rijcken, O. Soga, W. Hennink, and C. v. Nostrum; Triggered destabilisation of polymeric micelles and vesicles by changing polymers polarity: An attractive tool for drug delivery; *Journal of Controlled Release* **2007**, *120*(3), 131–148.

[17] K. T. Oh, T. K. Bronich, and A. V. Kabanov; Micellar formulations for drug delivery based on mixtures of hydrophobic and hydrophilic pluronic block copolymers.; *Journal of Controlled Release* **2004**, *94*, 411–422.

[18] X. Xiong, K. Tam, and L. Gan; Release kinetics of hydrophobic and hydrophilic model drugs from pluronic f127/poly(lactic acid) nanoparticles; *Journal of Controlled Release* **2005**, *103*(1), 73–82.

[19] V. P. Torchilin; Multifunctional nanocarriers.; *Advanced Drug Delivery Reviews* **2006**, *58*, 1532–1555.

[20] J. Khandare and T. Minko; Polymer-drug conjugates: Progress in polymeric prodrugs.; *Progress in Polymer Science* **2006**, *31*, 359–397.

[21] P. Krsko and M. Libera; Biointeractive hydrogels.; *Materials Today (Oxford, United Kingdom)* **2005**, *8*, 36–44.

[22] P. Alexandridis; Polymers and nanomaterials.; *Current Opinion in Colloid & Interface Science* **2003**, *8*, 62–63.

[23] C. D. Grant *et al.;* Fluorescence probing of interior, interfacial, and exterior regions in solution aggregates of poly(ethylene oxide)- poly(propylene oxide)-poly(ethylene oxide) triblock copolymers.; *Langmuir* **2005**, *21*, 1745–1752.

[24] N. J. Jain, V. K. Aswal, P. S. Goyal, and P. Bahadur; Micellar structure of an ethylene oxide-propylene oxide block copolymer: a small-angle neutron scattering study.; *Journal of Physical Chemistry B* **1998**, *102*, 8452–8458.

[25] J. R. Lakowicz *Principles of Fluorescence Spectroscopy;* Kluwer Academic/ Plenum Publishers, 2nd ed., 1999.

[26] M. L. Horng, J. A. Gardecki, A. Papazyan, and M. Maroncelli; Subpicosecond measurements of polar solvation dynamics: Coumarin 153 revisited.; *Journal of Physical Chemistry* **1995**, *99*, 17311–37.

[27] M.-L. Horng, J. A. Gardecki, and M. Maroncelli; Rotational dynamics of coumarin 153: Time-dependent friction, dielectric friction, and other nonhydrodynamic effects.; *Journal of Physical Chemistry A* **1997**, *101*, 1030–1047.

[28] C. D. Grant, K. E. Steege, M. R. Bunagan, and E. W. Castner Jr.; Microviscosity in multiple regions of complex aqueous solutions of poly(ethylene oxide)-poly(propylene oxide)-poly(ethylene oxide).; *Journal of Physical Chemistry B* **2005**, *109*, 22273–22284.

[29] L. Tian *et al.;* Core crosslinkable polymeric micelles from peg-lipid amphiphiles as drug carriers.; *Journal of Materials Chemistry* **2004**, *14*, 2317–2324.

[30] J. Wang, L. Tian, A. Argenti, and K. E. Uhrich; Nanoscale amphiphilic star-like macromolecules with carboxy-methoxy- and amine-terminated chain ends.; *J. Bioact. Compat. Polym.* **2006**, *21*, 297–313.

[31] J. Wang, L. Del Rosario, and K. E. Uhrich; The influence of branched peg chains on polymer micelles: how to build a better drug delivery system.; *Polym. Prepr. (Am. Chem. Soc., Div. Polym. Chem.)* **2007**, *48*, 225–226.

[32] J. Wang *et al.;* Development of reliable aqueous solubility models and their application in druglike analysis; *Journal of Chemical Information and Modeling* **2007**, *47*(4), 1395–1404.

Appendix A

Spectroscopy, Solvatochromism, and Electronic Structure of Rilpivirine: a Potent Non-Nucleoside Reverse Transcriptase Inhibitor

A:1 Fluorescence Quantum Yield

Fluorescence quatum yields of rilpivirine were obtained by comparing the emission to a quantum yield standard sample, quinine sulfate in 0.1 M aqueous sulfuric acid. The emission spectra were measured for rilpivirine in dichloromethane, dimethyl sulfoxide, 1,2-dichlorobenzene, and 1-pentane and for the quinine sulfate solution. These spectrum were measured in wavelength units of nm and the integral of each spectrum was converted to reduced frequency by using $I(\tilde{\nu}) = \lambda^2 I(\lambda)$ where $I(\tilde{\nu})$ is the integral of the spectrum in reduced frequency untis of cm^{-1} and $I(\lambda)$ is the integral of the spectral intensity (in nm).[1, 2] The quantum yield for rilpivirine in each solvent was then found by Eq. A-1 where A is the absorbance, n is the solvent refractive index, and R denotes the corresponding properties for the reference standard, quinine sulfate.[1, 2]

$$\phi_F = \phi_{FR} \frac{\int I(\tilde{\nu}) d\tilde{\nu}}{\int I_R(\tilde{\nu}) d\tilde{\nu}} \frac{A_R}{A} \frac{n^2}{n_R^2} \tag{A-1}$$

The fluorescence quantum yields ϕ_F were calculated from Equation A-1 where $\int \mathrm{I}(\tilde{\nu}) \mathrm{d}\tilde{\nu}$ is the integral of the spectrum measured in units of cm^{-1}, A is the absorbance value, n is the refractive index of the solvent, and R denotes the corresponding properties for the reference standard which, in this case, is quinine sulfate in 0.1 M sulfuric acid solution.[1, 2]

Quantum yield measurements were performed using a comparison with the standard, quinine sulfate in 0.1 M sulfuric acid (aq), in DMSO, in dichloromethane, and in

Table A-1: Fluorescence quantum yields (ϕ_F) measured using 268, 310, and 350 nm excitation for measured emission in comparison with the standard fluorophore, quinine sulfate.[1, 2]

Fluorophore	Solvent	n	ϕ_F	λ_{ex} (nm)
quinine sulfate	0.1 M H_2SO_4 (aq)	1.333	0.548	350
rilpivirine	DMSO	1.479	0.084	310
rilpivirine	dichloromethane	1.424	0.122	350
rilpivirine	1,2-dichlorobenzene	1.551	0.366	350
rilpivirine	1-pentane	1.358	0.115	268

1-pentane and are presented in Table A-1. Depending on solvent and excitation wavelength, the quantum yield of rilpivirine has a maximum of 0.366 in 1,2-dichlorobenzene using 350 nm excitation. The average quantum yield found from these experiments is approximately 0.172 (or 17.2%).

A:2 ZINDO Calculations of Rilpivirine: Dipole Moments and Energies of S_0 →S' and S"

The spectroscopy parameters found from ZINDO calculations of three structural conformations of rilpivirine are presented in Tables A-2, A-3, and A-4. Each table presents ground and excited state dipole moments, energies of transitions from the ground state to the first two excited states, and oscillator strengths for the corresponding transtions. Table A-2 includes the aforementioned parameters for the conformation of rilpivirine found from the anhydrous crystal structure.[3] Table A-3 includes the data for the conformation of rilpivirine found from the crystal structure of anhydrous rilpivirine crystal co-crystallized with DMSO and Table A-4 includes the same data for the conformation of rilpivirine found from the x-ray diffraction of the drug bound to HIV-1 reverse transcriptase.[4] The more polar solvents have larger dipole moments that interact with the dipole moment of rilpivirine in solution, making the dipole moment slightly larger. This dipole-dipole interaction is a significant cause of solvatochromic shift in rilpivirine absorption and fluorescence.[1, 2, 5] This solvatochromic shift is evident in the transition energies from the ground to the first two excited states, analogous to absorption energies. In more polar solvents, the absorption energy of the rilpivirine molecule is generally lower than the absorption of rilpivirine in non-polar solvents.

Table A-2: Dipole moments in D, ground and excited state energies (S_0, S', and S") in cm^{-1}, and oscillator strengths for rilpivirine by ZINDO-SCRF methods modeling 15 solvents, solvent cavity radii in $Å^3$ for the structure of anhydrous rilpivirine.

Solvent	r_{cav}	μ (S_0)	μ (S')	μ (S")	E (S_0→S')	E (S_0→S")	f (S_0 →S')	f (S_0 →S")
CCl_4	5.16	16.13	39.62	34.17	40429	40452	0.26	0.52
1,2-DCB	5.26	19.14	48.42	43.16	36772	37469	0.12	0.35
ethyl acetate	5.95	16.50	40.91	35.47	40115	40162	0.23	0.49
toluene	6.02	15.20	36.07	30.59	41057	41115	0.33	0.57
methanol	6.20	16.84	42.06	36.65	39781	39870	0.21	0.47
CH_2Cl_2	5.22	19.13	48.38	43.12	36800	37491	0.12	0.35
DMF	5.85	17.70	44.73	39.37	38795	39057	0.17	0.42
ethylene glycol	5.53	18.77	47.55	42.27	37328	37901	0.13	0.37
formamide	5.50	19.12	48.37	43.11	36803	37493	0.12	0.35
DMSO	5.56	18.75	47.48	42.20	37370	37934	0.13	0.37
water	5.74	18.15	45.98	40.65	38205	38588	0.15	0.40

Table A-3: Dipole moments in D, ground and excited state energies (S_0, S', and S") in cm^{-1}, and oscillator strengths for rilpivirine by ZINDO-SCRF methods modeling 15 solvents, solvent cavity radii in $Å^3$ for the structure of anhydrous rilpivirine with 2 DMSO.

Solvent	r_{cav}	μ (S_0)	μ (S')	μ (S")	E (S_0→S')	E (S_0→S")	f (S_0 →S')	f (S_0 →S")
CCl_4	5.16	15.14	37.67	34.36	40101	42116	0.37	0.31
1,2-DCB	5.26	18.00	47.25	42.18	37294	38560	0.14	0.22
ethyl acetate	5.95	15.49	39.22	35.46	39957	41692	0.32	0.30
toluene	6.02	14.25	33.06	31.62	40145	43267	0.51	0.31
methanol	6.20	15.82	40.58	36.47	39758	41295	0.28	0.29
CH_2Cl_2	5.22	17.99	47.21	42.14	37319	38583	0.14	0.22
DMF	5.85	16.64	43.50	38.85	39028	40297	0.21	0.26
ethylene glycol	5.54	17.66	46.39	41.40	37784	39017	0.15	0.23
formamide	5.50	17.99	47.20	42.14	37321	38585	0.14	0.22
DMSO	5.56	17.63	46.32	41.33	37821	39052	0.15	0.23
water	5.74	17.08	44.81	39.97	38541	39765	0.18	0.25

Table A-4: Dipole moments in D, ground and excited state energies (S_0, S', and S") in cm^{-1}, and oscillator strengths for rilpivirine by ZINDO-SCRF methods modeling 15 solvents, solvent cavity radii in $Å^3$ for the structure of rilpivirine in the RT binding pocket .

Solvent	r_{cav}	μ (S_0)	μ (S')	μ (S")	E (S_0→S')	E (S_0→S")	f (S_0 →S')	f (S_0 →S")
CCl_4	5.16	15.59	37.27	32.27	42976	38256	0.08	0.51
1,2-DCB	5.26	17.86	42.21	43.48	39588	38726	0.15	0.22
ethyl acetate	5.95	15.49	37.09	31.83	43110	38262	0.08	0.52
toluene	6.02	14.31	35.09	27.23	44453	38579	0.08	0.61
methanol	6.20	15.78	34.51	37.44	43	50804	0.541	0.07
CH_2Cl_2	5.22	17.51	41.76	41.16	44488	47886	0.36	0.11
DMF	5.85	16.45	37.30	38.75	43483	49680	0.48	0.08
ethylene glycol	5.53	17.25	40.70	40.56	44301	48327	0.39	0.10
formamide	5.50	17.51	41.76	41.16	44487	47888	0.36	0.11
DMSO	5.56	17.23	40.62	40.51	44284	48363	0.39	0.10
water	5.74	16.79	38.75	39.50	43872	49107	0.44	0.09

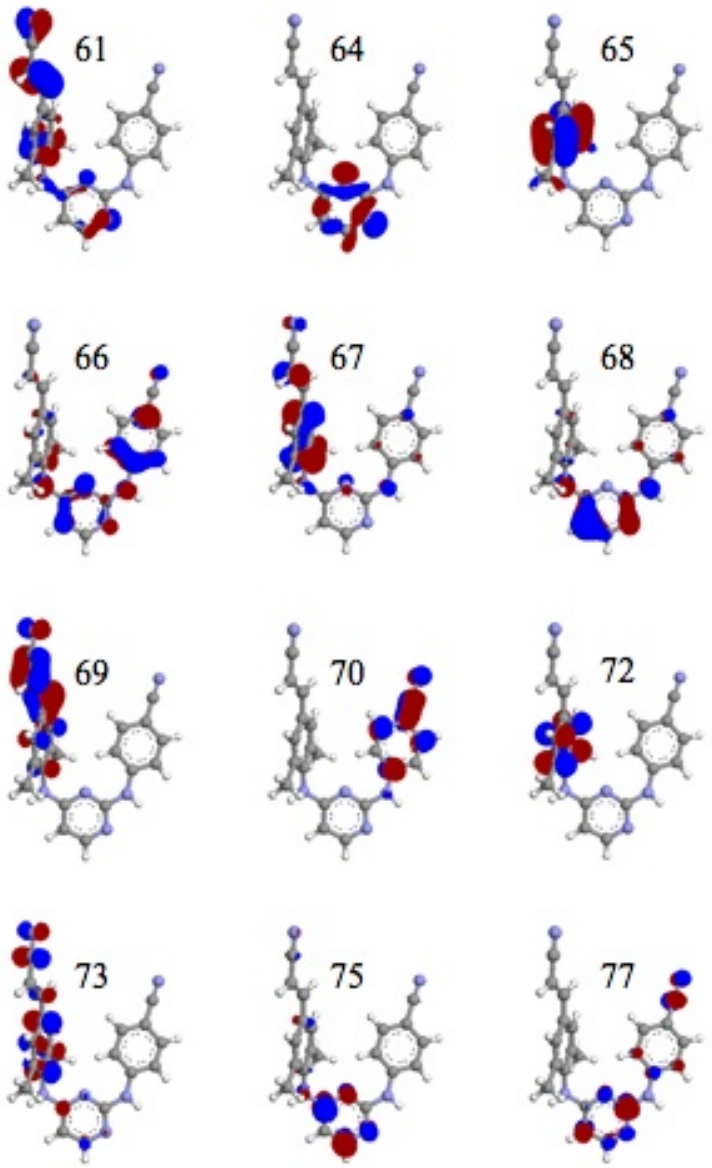

Figure A-1: Molecular orbital surface plots of rilpivirine from ZINDO[6] calculations of the anhydrous crystal conformation with DMSO solvent dielectric in the electronic states of orbitals contributing to the $S_0 \rightarrow$S' and $S_0 \rightarrow$S" transitions.

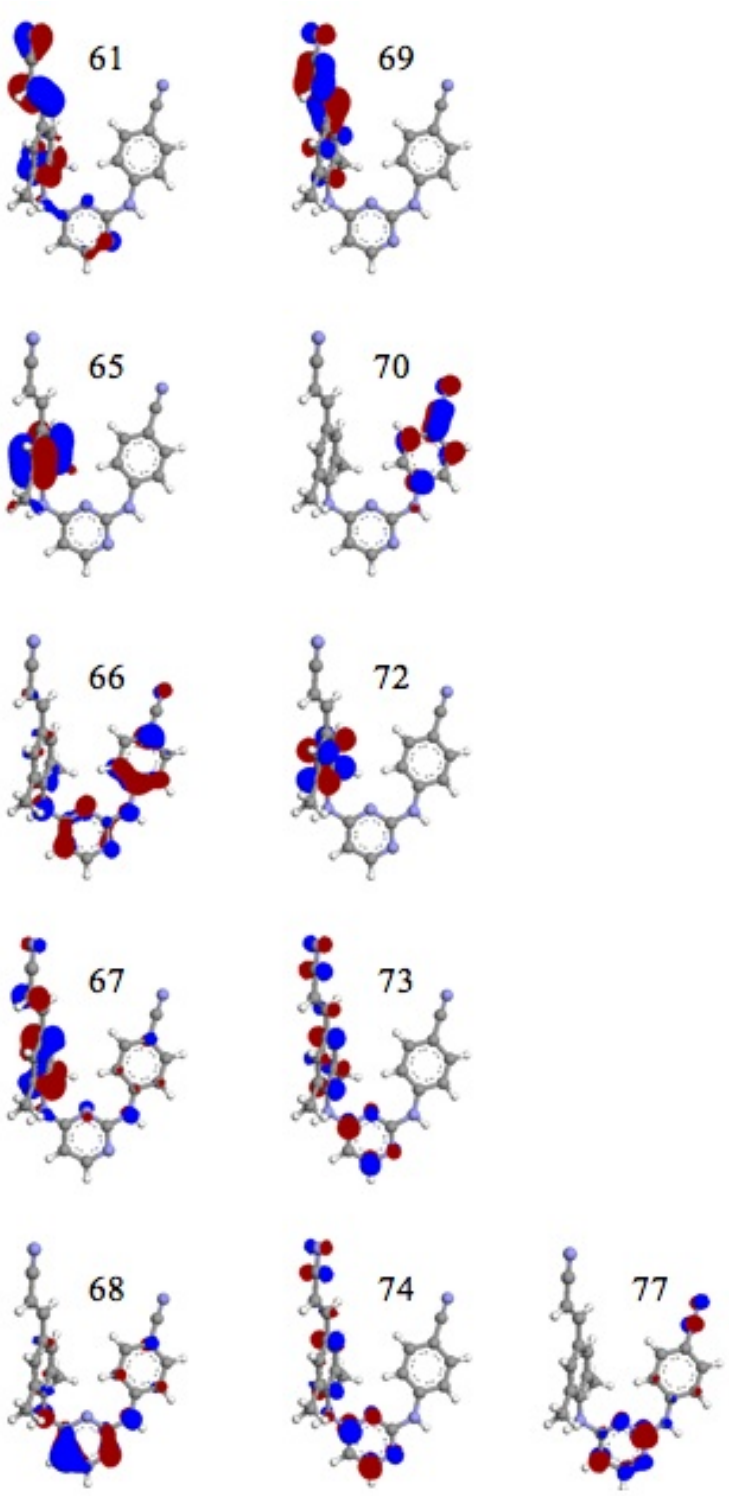

Figure A-2: Molecular orbital surface plots of rilpivirine from ZINDO[6] calculations of the anhydrous crystal conformation with water solvent dielectric in the electronic states of orbitals contributing to the $S_0 \rightarrow$S' and $S_0 \rightarrow$S" transitions.

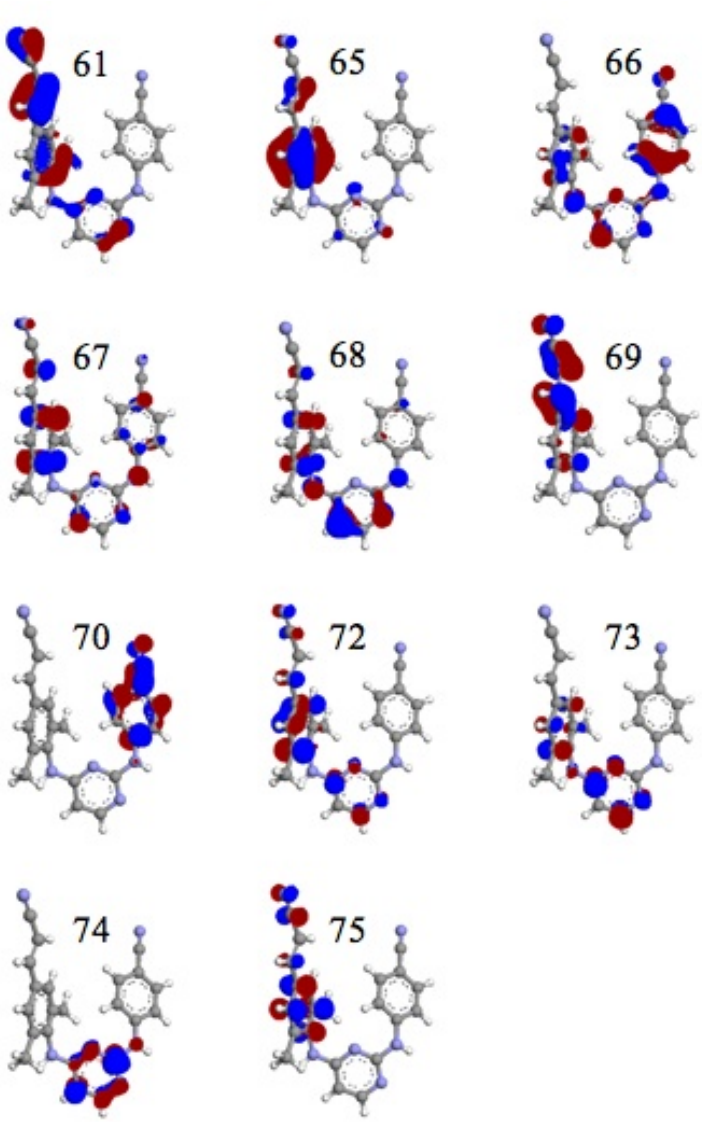

Figure A-3: Molecular orbital surface plots of rilpivirine from ZINDO[6] calculations of the anhydrous ·2 DMSO crystal conformation with 2-MeTHF solvent dielectric in the electronic states of orbitals contributing to the $S_0 \rightarrow$S' and $S_0 \rightarrow$S" transitions.

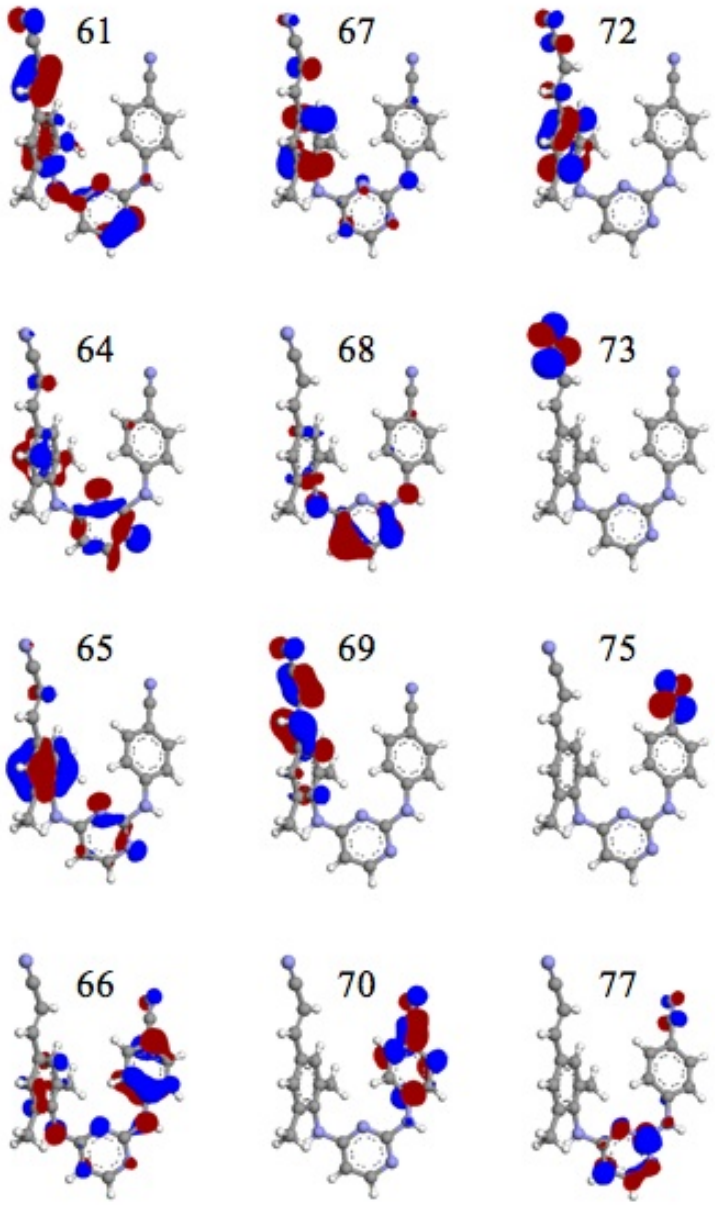

Figure A-4: Molecular orbital surface plots of rilpivirine from ZINDO[6] calculations of the anhydrous ·2 DMSO crystal conformation with DMSO solvent dielectric in the electronic states of orbitals contributing to the $S_0 \rightarrow$S' and $S_0 \rightarrow$S" transitions.

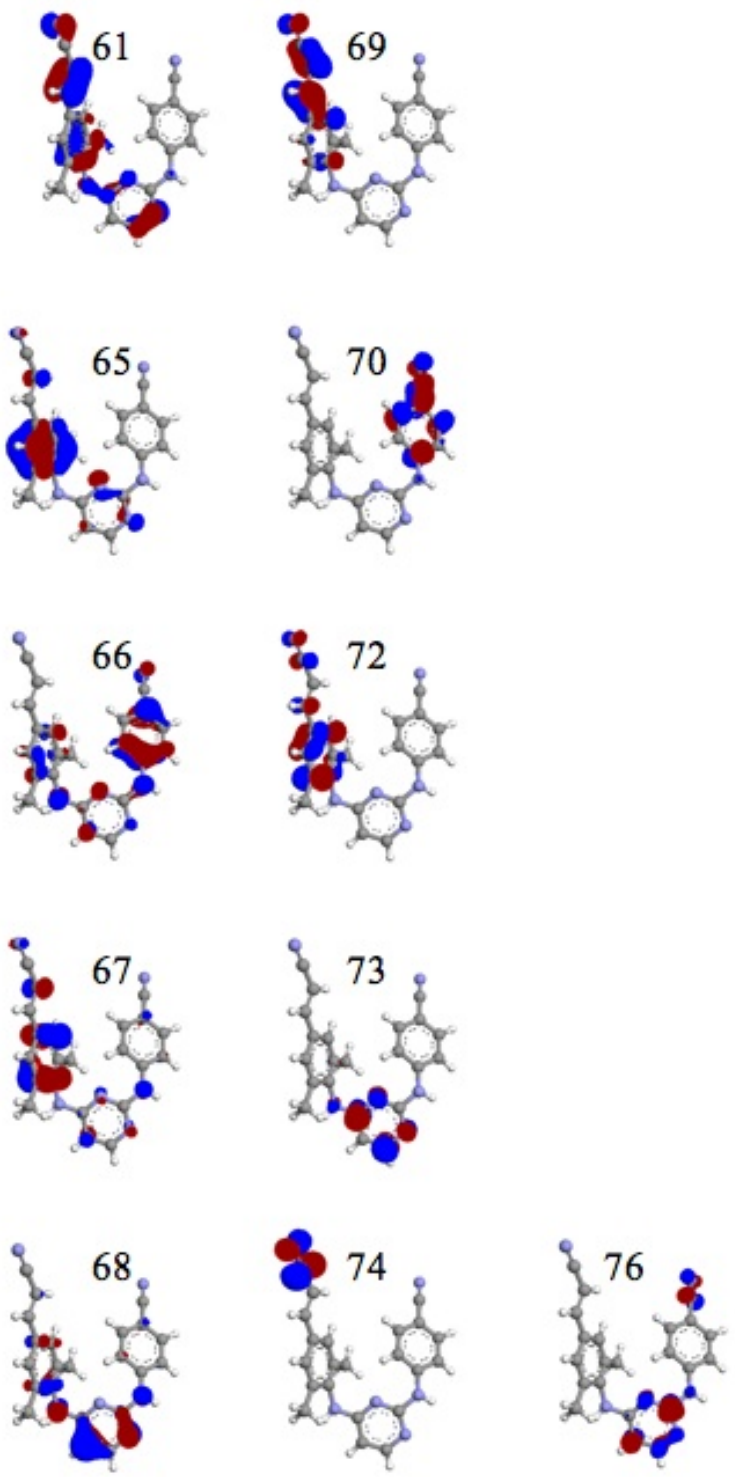

Figure A-5: Molecular orbital surface plots of rilpivirine from ZINDO[6] calculations of the anhydrous ·2 DMSO crystal conformation with water solvent dielectric in the electronic states of orbitals contributing to the $S_0 \rightarrow$S' and $S_0 \rightarrow$S" transitions.

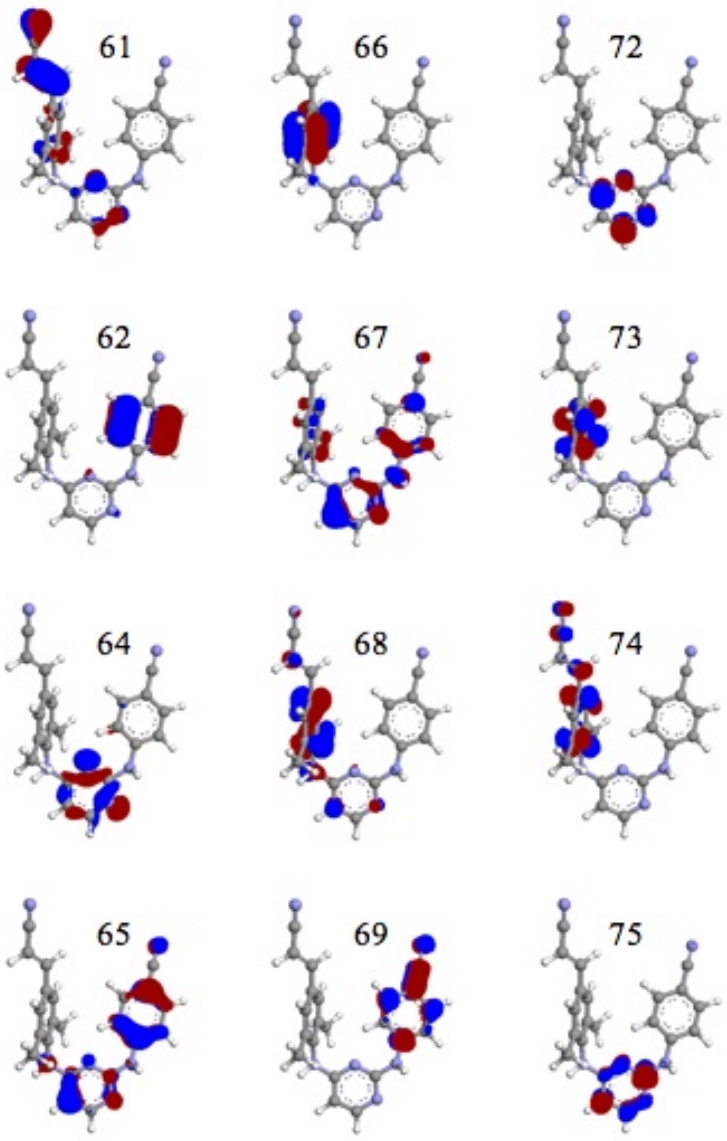

Figure A-6: Molecular orbital surface plots of rilpivirine from ZINDO[6] calculations of the anhydrous ·2 DMSO crystal conformation with 2-MeTHF solvent dielectric in the electronic states of orbitals contributing to the $S_0 \rightarrow$S' and $S_0 \rightarrow$S" transitions.

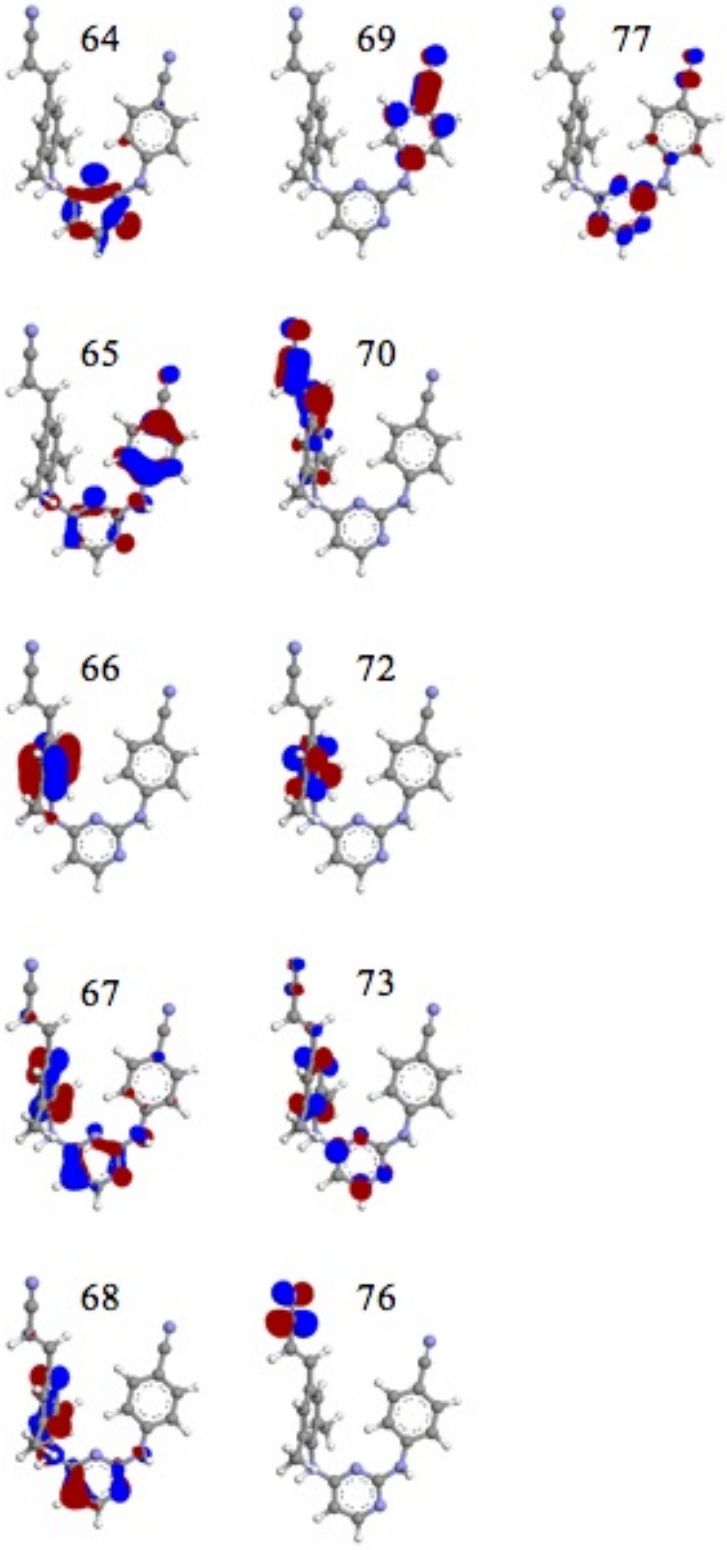

Figure A-7: Molecular orbital surface plots of rilpivirine from ZINDO[6] calculations of the anhydrous ·2 DMSO crystal conformation with DMSO solvent dielectric in the electronic states of orbitals contributing to the $S_0 \rightarrow$S' and $S_0 \rightarrow$S" transitions.

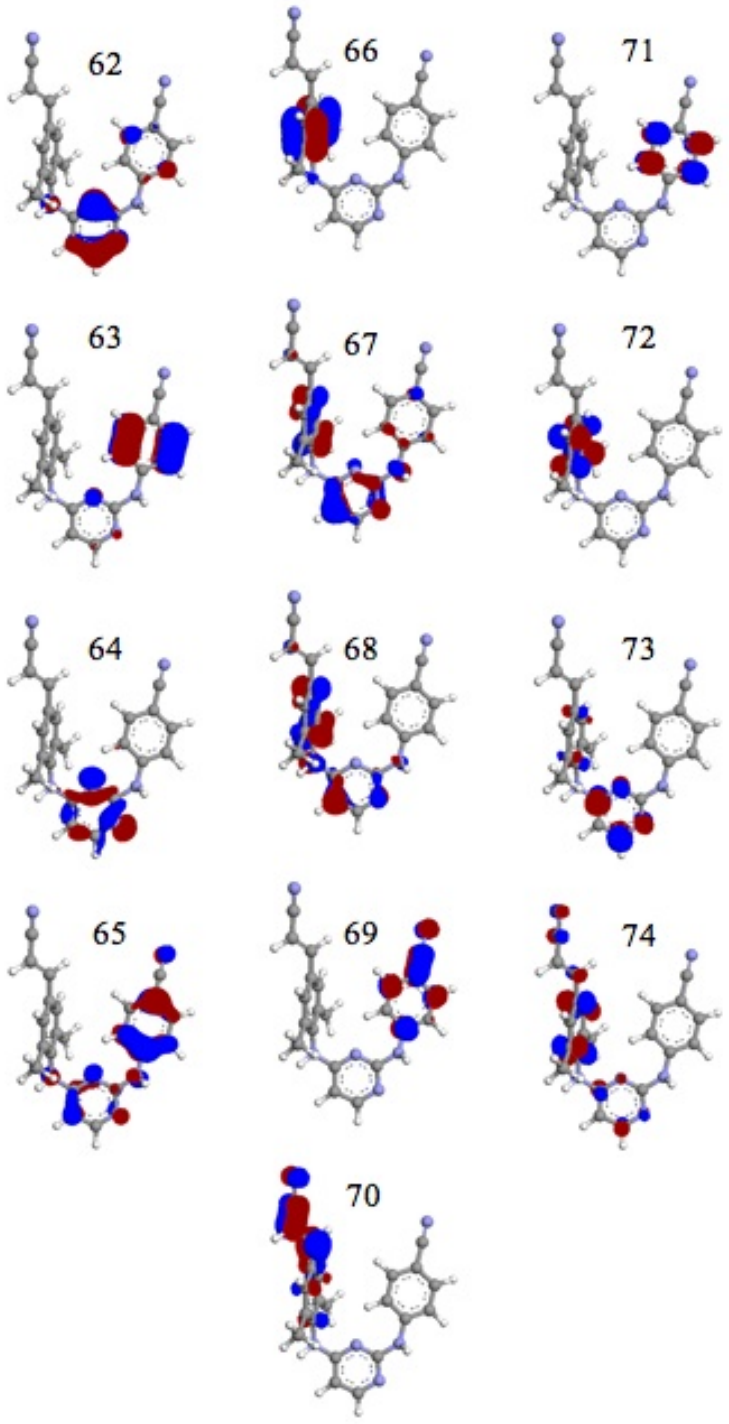

Figure A-8: Molecular orbital surface plots of rilpivirine from ZINDO[6] calculations of the anhydrous ·2 DMSO crystal conformation with water solvent dielectric in the electronic states of orbitals contributing to the $S_0 \rightarrow$S' and $S_0 \rightarrow$S" transitions.

Table A-5 describes the contribution of each orbital configuration to the ground to excited state transition using normalized coefficients ($c_{i,j}$) for the anhydrous crystal structure conformation of rilpivirine .

Table A-6 describes the contribution of each orbital configuration to the ground to excited state transition using normalized coefficients ($c_{i,j}$) for the anhydrous/ 2 DMSO crystal structure (with 1 rilpivirine:2 DMSO ratio) conformation of rilpivirine . The 65→69 orbital configuration interaction is the largest contributor to the S_0 →S' transition and the 67→69 orbital configuration interaction is the largest contributor to the S_0 →S" transition.

Table A-7 describes the contribution of each orbital configuration to the ground to excited state transition using normalized coefficients ($c_{i,j}$) for the conformation of rilpivirine found from the crystal structure of the drug bound to HIV-1 RT.

The HOMO to LUMO transition, as assigned by ZINDO methods, is the configuration orbital transition 68→69. The normalized coefficients of this configuration in the S_0 →S' transition to the excited state reflect that 68→69 is not the orbital configuration that contributes the most to the electronic transition. In fact, for the examples listed in the the tables A-5, A-6, and A-7, the coefficients for the 68→69 configuration are 0.047, 0.324, 0.317, 0.053, and 0.018 for various conformations of rilpivirine and SCRF solvent parameters. In some cases, the 68→69 orbital configuration has negligible contribution and so is not listed.

Table A-5: Orbitals that contribute to 90% of the $S_0 \rightarrow$S' and the $S_0 \rightarrow$S" transitions, with corresponding coefficients ($c_{i,j}$) from ZINDO-SCRF calculations of the anhydrous crystal structure conformation of rilpivirine in 2-MeTHF ($\epsilon = 6.97$, $n = 1.405$, and $r_{cavity} = 6.046$ Å), DMSO ($\epsilon = 46.71$, $n = 1.478$, and $r_{cavity} = 5.556$ Å), water ($\epsilon = 80.00$, $n = 1.333$, and $r_{cavity} = 5.742$ Å) solvent dielectric fields, and no solvent.

Solvent	orbitals for $S_0 \rightarrow$S'	$c_{i,j}$	orbitals for $S_0 \rightarrow$S"	$c_{i,j}$
2-MeTHF	67→69	0.234	68→70	0.451
	68→69	0.190	67→ 69	0.139
	65→69	0.121	67→ 70	0.122
	68→73	0.105	68→ 69	0.066
	68→70	0.066	66→ 70	0.058
	68→70	0.066	68→ 75	0.048
	67→72	0.052	68→ 73	0.009
	67→73	0.039	68→ 72	0.009
	66→72	0.026	65→ 70	0.007
DMSO	67→69	0.452	68→70	0.541
	68→69	0.296	66→70	0.116
	68→70	0.066	67→70	0.091
	68→73	0.041	67→69	0.078
	68→75	0.024	68→77	0.055
	66→70	0.017	68→69	0.047
	66→69	0.013	68→75	0.008
	67→70	0.013	62→71	0.007
water	67→ 69	0.445	68→70	0.509
	68→ 69	0.279	66→70	0.105
	68→ 70	0.069	67→70	0.0989
	68→ 73	0.060	67→69	0.089
	66→ 70	0.017	68→77	0.055
	67→ 70	0.015	68→69	0.046
	65→ 69	0.014	68→ 71	0.008
	66→ 69	0.014	66→ 71	0.008
	66→ 73	0.011	62→ 70	0.008
	68→ 74	0.010	68→ 74	0.007
none	68→69	0.221	67→ 69	0.336
	68→71	0.201	68→ 69	0.177
	67→69	0.194	68→ 71	0.155
	65→71	0.121	68→ 70	0.087
	68→70	0.107	65→ 71	0.050
	67→70	0.046	65→ 74	0.0246
	63→71	0.015	67→ 70	0.024
	67→71	0.011	62→ 71	0.018
	65→74	0.009	68→ 74	0.015
	59→74	0.009	67→ 71	0.014

Table A-6: Orbitals that contribute to 90% of the $S_0 \rightarrow$S' and the $S_0 \rightarrow$S" transitions, along with corresponding coefficients ($c_{i,j}$) from ZINDO-SCRF calculations of the anhydrous crystal structure (with 2 DMSO) conformation of rilpivirine in 2-MeTHF, DMSO, and water solvent dielectric fields.

Solvent	$S_0 \rightarrow$S'	$c_{i,j}$	$S_0 \rightarrow$S"	$c_{i,j}$
2-MeTHF	65→ 69	0.393	67→ 69	0.320
	67→ 73	0.194	68→ 69	0.301
	68→ 73	0.082	65→ 69	0.073
	65→ 75	0.071	68→ 72	0.058
	67→ 69	0.059	68→ 73	0.047
	68→ 69	0.047	68→ 70	0.031
	68→ 72	0.020	66→ 72	0.023
	65→ 74	0.015	67→ 73	0.021
	67→ 72	0.014	66→ 69	0.016
	66→ 73	0.008	67→ 70	0.015
			67→ 72	0.015
DMSO	67→69	0.482	65→69	0.545
	68→69	0.324	67→72	0.242
	68→73	0.051	65→73	0.084
	68→70	0.030	68→72	0.065
	68→75	0.017	65→75	0.025
	66→70	0.012	66→72	0.011
	66→69	0.009	67→69	0.004
water	67→69	0.464	65→69	0.521
	68→69	0.317	67→72	0.242
	68→73	0.071	65→74	0.073
	68→70	0.031	68→72	0.073
	66→70	0.012	65→73	0.036
	66→73	0.012	66→72	0.011
	66→69	0.009	67→69	0.010
	67→70	0.008		
none	68→69	0.640	67→71	0.158
	67→69	0.066	68→69	0.146
	66→71	0.040	68→71	0.141
	68→71	0.038	66→71	0.108
	67→71	0.036	67→70	0.056
	68→73	0.028	63→71	0.051
	68→75	0.026	68→73	0.047
	67→70	0.019	65→71	0.042
	65→69	0.012	67→69	0.039
	65→71	0.008	68→70	0.023
	66→69	0.008	65→69	0.021
	65→73	0.006	66→74	0.017

Table A-7: Orbitals that contribute to 90% of the $S_0 \rightarrow$S' and the $S_0 \rightarrow$S" transitions, along with corresponding coefficients ($c_{i,j}$) from ZINDO-SCRF calculations of the HIV RT-bound crystal structure conformation of rilpivirine in 2-MeTHF, DMSO, and water solvent dielectric fields.

Solvent	$S_0 \rightarrow$S'	$c_{i,j}$	$S_0 \rightarrow$S"	$c_{i,j}$
2-MeTHF	66→69	0.323	64→73	0.759
	67→72	0.312	67→73	0.062
	66→74	0.150	65→73	0.060
	68→72	0.070	59→86	0.030
	67→69	0.035	63→73	0.028
	67→74	0.032	64→74	0.024
	66→72	0.029	64→75	0.005
DMSO	67→69	0.295	67→69	0.180
	66→69	0.151	66→69	0.169
	67→72	0.131	68→70	0.147
	66→73	0.062	67→72	0.124
	68→69	0.053	68→69	0.066
	67→73	0.051	65→70	0.040
	65→69	0.048	66→73	0.039
	66→72	0.043	68→72	0.030
	68→70	0.039	65→73	0.023
	68→73	0.019	66→72	0.020
	68→72	0.014	67→70	0.018
	65→70	0.012	68→76	0.017
water	66→69	0.281	67→69	0.282
	67→72	0.228	68→70	0.199
	67→69	0.132	68→69	0.086
	66→73	0.108	66→69	0.070
	67→73	0.051	65→70	0.060
	66→72	0.048	67→72	0.051
	68→72	0.0.035	68→74	0.038
	68→69	0.018	67→70	0.028
	65→69	0.013	66→73	0.017
	68→73	0.013	68→73	0.016
	68→70	010	68→72	0.015
	66→74	0.010	68→71	0.012
			65→73	0.010
			63→70	0.009
			64→69	0.009
			65→71	0.008
			62→70	0.006

A:3 Fluorescence Dynamics

The rilpivirine fluorescence time constant is composed of multiple time constants. The fluorescence transients of rilpivirine are consistently fit to a sum of four, five, or six exponentials, and therefore has four, five or six component fluorescence lifetimes. In actuality, the fluorescence lifetimes of rilpivirine are not only dependent on solvent properties such as polarity or dielectric constant values. Figure A-9 and table A-8 shows the component relative amplitudes and the component tim constants of rilpivirine plotted against the polarity of the solvent using the π^* empirical polarity scale.[7, 8]

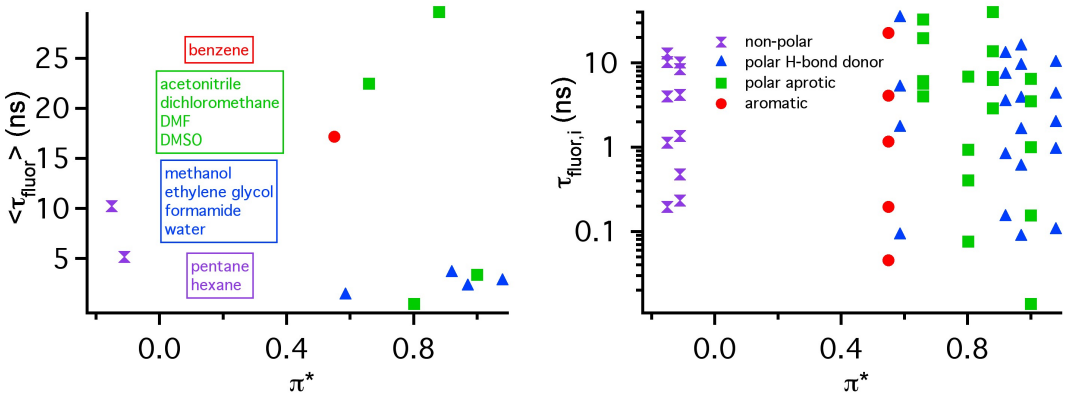

Figure A-9: Fluorescence time constants of rilpivirine versus solvent polarity in the π^* empirical polarity scale. Plotted are the intensity-weighted averages (left) and individual lifetimes from multi-exponential decays (right).

Table A-8: Fluorescence time constants ($\tau_{fl,i}$) and relative amplitudes ($\alpha_{fl,i}$) of rilpivirine in various solvents. (See Eq. 1.)

Solvent	$\alpha_{fl,1}$	$\alpha_{fl,2}$	$\alpha_{fl,3}$	$\alpha_{fl,4}$	$\alpha_{fl,5}$	$\alpha_{fl,6}$	$\tau_{fl,1}$	$\tau_{fl,2}$	$\tau_{fl,3}$	$\tau_{fl,4}$	$\tau_{fl,5}$	$\tau_{fl,6}$
1-pentane	0.11	0.57	0.12	0.08	0	0.12	13.00	10.25	4.02	1.13	0	0.20
1-hexane	0.03	0.07	0.16	0.35	0.31	0.08	10.09	8.42	4.17	1.36	0.48	0.23
CH_2Cl_2	< 0.01	0	0.06	0.31	0.63	0	6.90	0	0.93	0.40	0.08	0
DMSO	< 0.01	0.33	0.07	0.08	0.51	0	6.48	3.51	1.00	0.16	0.01	0
benzene	0.08	0.08	0.25	0.03	0.56	0	22.72	4.11	1.17	0.20	0.05	0
methanol	< 0.01	0	< 0.01	0.02	0	0.98	33.80	0	5.11	1.69	0	0.09
acetonitrile	0.94	0.83	0.51	0.21	2.76	-4.26	5.66	6.09	4.01	0.98	0.26	0.18
DMF	0.18	0.218	0.11	0	0.18	0.32	6.29	6.80	2.88	0	0.36	0.15
E.G.	< 0.01	0.01	0.01	0.03	0	0.95	12.76	7.23	3.40	0.80	0	0.15
formamide	< 0.01	< 0.01	< 0.01	0.02	0.02	0.95	15.58	9.17	3.73	1.59	0.59	0.09
water	0	0.02	0.11	1.13	0.41	-0.67	0	9.96	4.20	1.93	0.93	0.10

References

[1] B. Valeur *Molecular Fluorescence: Principles and Applications;* Wiley-VCH, 2002.

[2] J. R. Lakowicz *Principles of Fluorescence Spectroscopy;* Kluwer Academic/ Plenum Publishers, 2nd ed., 1999.

[3] Y. V. Frenkel, T. Emge, and E. Arnold unpublished, **2008**.

[4] Y. V. Frenkel *et al.;* Concentration and ph dependent aggregation of hydrophobic drug molecules and relevance to oral bioavailability.; *Journal of Medicinal Chemistry* **2005**, *48*, 1974–1983.

[5] N. Mataga, Y. Kaifu, and M. Koizumi; Sovent effects upon fluorescence spectra and the dipole moments of excited molecules; *Bulletins of the Chemical Society of Japan* **1956**, *29*, 465.

[6] Arguslab version 4.0. M. A. Thompson Planaria Software LLC, Seattle, WA., **1996-2003**.

[7] M. J. Kamlet, J. L. Abboud, and R. W. Taft; The solvatochromic comparison method. 6. the π^* scale of solvent polarities.; *Journal of the American Chemical Society* **1977**, *99*, 6027–6038.

[8] C. Laurence *et al.;* The empirical treatment of solvent-solute interactions: 15 years of π^*; *Journal of Physical Chemistry* **1994**, *98*, 5807–5816.

Appendix B

Local Polarity and Microviscosity in the Hydrophobic Cores of Amphiphilic Star-like and Scorpion-like Macromolecules

B:1 Particle Size Analysis of Polymer Aggregates

B:1.1 Polymer Concentration Dependence

Dynamic light scattering measurements were made with a Nicomp 380 Particle Sizing System as described in detail in the 'Materials and Methods' section. Aqueous solutions of M12P5, NC12P5 and NC6P5 were measured using DLS for polymer concentrations ranging from 1x10^{-9} M to1x10^{-3} M at 37°C. The volume-weighted distributions of these concentration-dependent particle diameters are shown for M12P5 in Figure B-1, for NC12P5 in Figure B-2, and for NC6P5 in Figure B-3.

B:1.2 Temperature Dependence

Temperature-dependent particle sizes of each polymer were also measured using DLS. A solution of 2x10^{-4} M M12P5, a solution of 5x10^{-5} M NC12P5 and a solution of 5x10^{-5} M NC6P5 were measured with DLS at 5°C, 10°C, 20°C, 30°C, 37°C, 45°C, and 55°C. The volume-weighted distributions of these temperature-dependent particle diameters are shown for M12P5 in Figure B-4, for NC12P5 in Figure B-5, and for NC6P5 in Figure B-6.

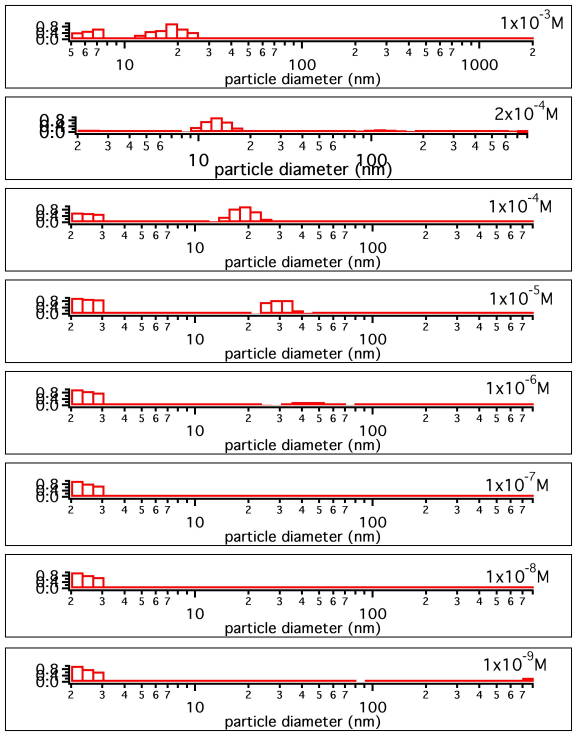

Figure B-1: Volume-weighted particle diameters at varied concentrations of M12P5 solutions at 37°C.

B:2 Solution Viscosity

Shear viscosities of M12P5, NC12P5 and NC6P5 aqueous solutions were measured at 0.001 M polymer concentrations and the concentrations used for fluorescence measurements (2x10^{-4} M M12P5, 5x10^{-5} M NC12P5, and 5x10^{-5} M NC6P5.) over a temperature range of 5 to 70 °C. These temperature-dependent viscosities of the three polymer solutions are shown in Figure S-7. The viscosity of pure water with various temperatures is also plotted.[1] Notice that the solutions with polymer concentrations used for fluorescence measurements have shear viscosities close to that of pure water because the solutions are dilute.

B:3 Steady State Emission Spectral Linewidth

The steady state emission spectra of C153 in each of the three polymer solutions is broader than in a single solvent solution as shown by Shirota and Castner[2] and by

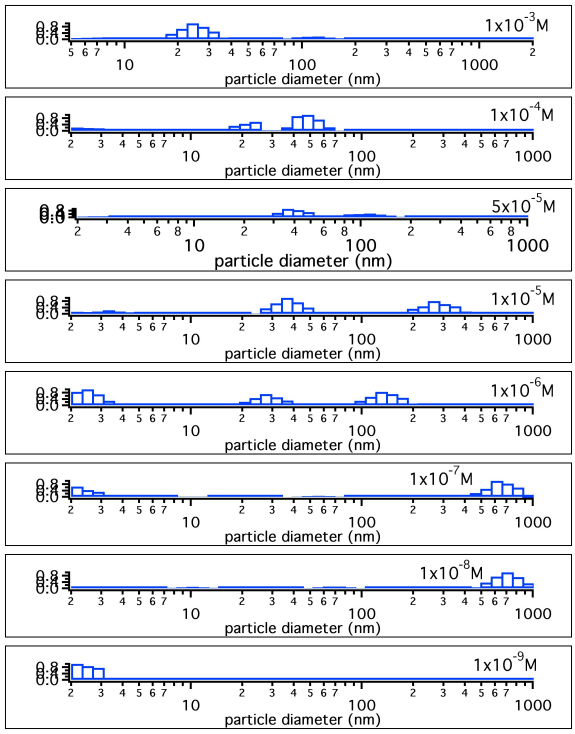

Figure B-2: Volume-weighted particle diameters at varied concentrations of NC12P5 solutions at 37°C.

Matyushov and Newton[3]. The broader spectral linewidth indicates that C153 is localized in multiple environments within each nanocarrier and with a range of polarities. This is especially true in the solution of NC12P5 star-like macromolecule. The full spectral line-widths at half-maximum (FWHM) are plotted for C153 in each polymer solution, in nm and cm^{-1} versus sample temperature in Figure B-8.

The broad frequency-width at half the maximum of the emission spectra of C153 in both NC12P5 and NC6P5 suggest that C153 may be in a range of non-polar environments within the hydrophobic cores of the two star-like macromolecules.[3]

B:4 Effective polarity of C153 local environment in ASM and AScM cores using the π^* scale

Using the π^* polarity scale[4], and work done by Horng, et.al.[5], the local solvent polarity of C153 in each polymer solution can be calculated and compared to the polarity of several common solvents. Horng, et.al. established a strong linear correlation between

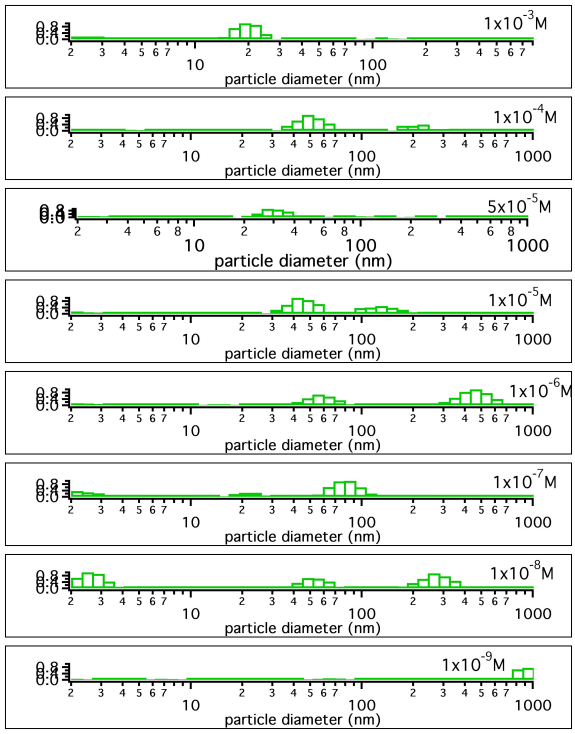

Figure B-3: Volume-weighted particle diameters at varied concentrations of NC6P5 solutions at 37°C.

the π^* solvent polarity scale and the peak fluorescence emission frequency via the relation $\widetilde{\nu}_{em}[10^{-3}\ \mathrm{cm}^{-1}] = 21.217 - 3.505\pi^*$.[5] C153 emission spectra in aqueous ASM and AScM solutions can thus be compared directly with solvent polarities. According to the π^* scale, C153 is in a local environment in the M12P5 micelles with polarity similar to that of dichloromethane ($\pi^* = 0.73$) or chloroform ($\pi^* = 0.76$).[4, 5] Inside the NC6P5 macromolecule, C153 experiences a solvent ranging in polarity from ethyl acetate($\pi^* = 0.55$) to tetrahydrofuran ($\pi^* = 0.58$) or benzene ($\pi^* = 0.59$).[4, 5] C153 encapsulated inside the NC12P5 macromolecule has a solvent environment with polarity similar to ethyl acetate or dimethyl carbonate ($\pi^* = 0.47$).[4] This supports our findings that the core of the scorpion-like M12P5 micelles is relatively polar compared to that of the two ASMs. π^* values are shown in Figure B-9.

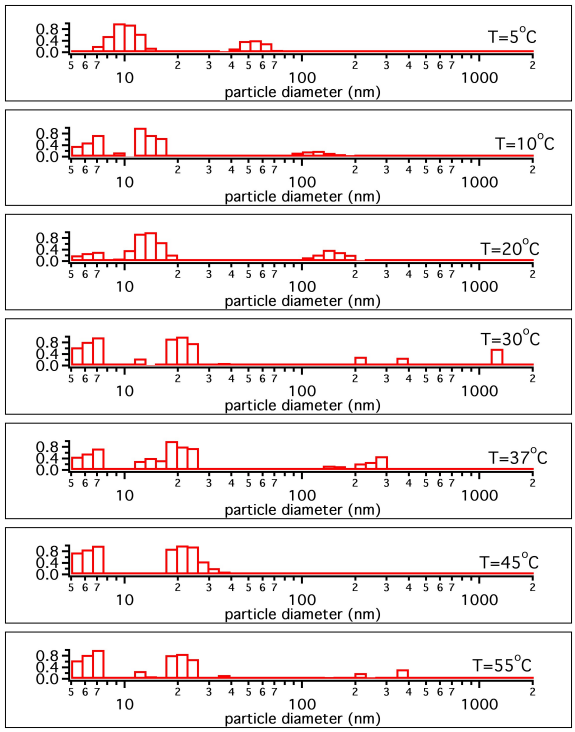

Figure B-4: Volume-weighted particle diameters at varied temperatures of 2x10^{-4} M M12P5 aqueous solutions.

B:5 Fluorescence Dynamics

The time-resolved fluorescence emission decay at 530 nm of C153 in M12P5 was measured over a 70 ns TCSPC time window. The decay transients measured at magic angle polarization were fit to a three-exponential equation. The average fluorescence time constant was calculated using intensity weighting, $\langle \tau_{fluor} \rangle$, as expressed in Equation B-1.[6, 7]

$$\langle \tau_{fluor} \rangle = \sum_{i=1}^{n} \frac{\alpha_i \tau_i^2}{\alpha_i \tau_i} \tag{B-1}$$

The fluorescence decay transients of C153 in each polymer solution detected at polarization angle of 54.7° (VM) relative to vertical polarization (90°)were fit to multi-exponential equations yielding exponential components in M12P5 solution and four exponential components in each of the ASM solutions. The intensity-weighted average of the time constants, $\langle \tau_{fluor} \rangle$ from each of these exponential components is plotted in

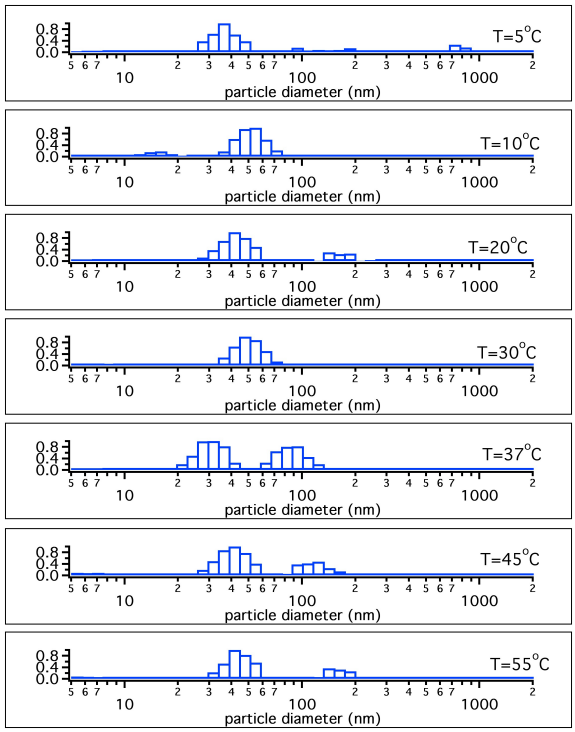

Figure B-5: Volume-weighted particle diameters at varied temperatures of 5x10^{-5} M NC12P5 aqueous solutions.

Figure B-10 (details discussed in 'Results and Discussion'). The amplitudes expressed in percent of total amplitude for each component time constant is shown in Figure B:5. The individual $\tau_{i,fluor}$ are plotted in Figure B-12. With regard to multiple fluorescence time constants, the distribution of C153 time constants correlates to the multiple environments of C153 solubilization within each polymeric nanocarrier.[6] C153 has a time constant that ranges with both solvent polarity and viscosity.[8] A range of local polarity and friction is experienced by C153 in all three nanocarriers, as shown by the individual component fluorescence time constants.

Fluorescence transients for C153 in both NC12P5 and NC6P5 were measured at 510 nm and these decay transients were fit to a four-exponential equation. The values of $\langle\tau_{fluor}\rangle$ from 5 to 70 °C for C153 in the M12P5 AScM ranged from 4.6 to 4.0 ns. The values of $\langle\tau_{fluor}\rangle$ from 5 to 70 °C for C153 in the NC12P5 star-like macromolecule ranged from 5.6 to 5.1 ns. The values of $\langle\tau_{fluor}\rangle$ from 5°C to 70°C for C153 in NC6P5

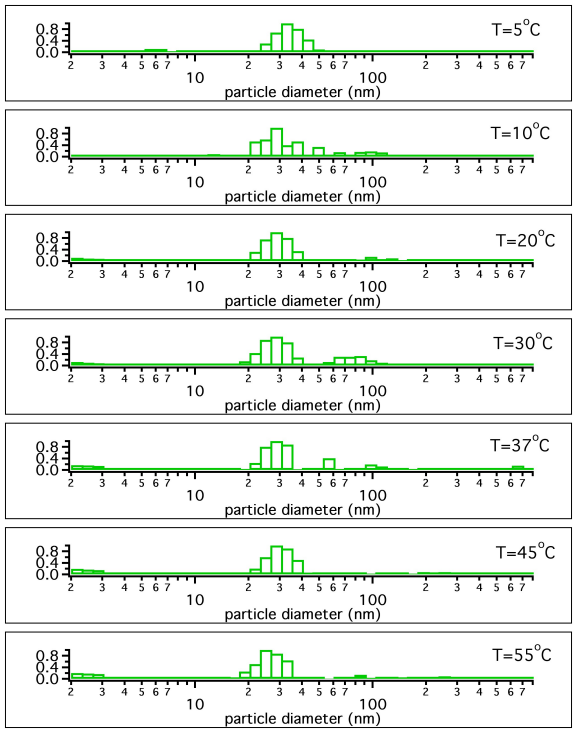

Figure B-6: Volume-weighted particle diameters at varied temperatures of 5x10^{-5} M NC6P5 aqueous solutions.

solution ranged from 5.5 to 4.1 ns.

The solvatochromic behavior of C153 in solvents representing a range of polarities and solvent viscosities is detailed in other articles.[8, 9, 10] In one previous study,[10] the fluorescence time constant of C153 in a polar (water-PEG) environment was measured and shown to be different than the time constant of C153 in a water-free, hydrophobic micelle core environment. In this study of ABA triblock copolymer Pluronic F88, the fluorescence time constant of C153 was shown to shift from 2.8 ns in a polar, water-like environment to approximately 4.6 ns in the hydrophobic, non-polar core of an ABA triblock copolymer micelle.[10] From the comparison of intensity-weighted average fluorescence time constants of C153 in the three drug delivery polymers in the present discussion, M12P5 shows a relatively non-polar core environment while NC12P5 has a more extremely non-polar environment. The fluorescence time constants show that

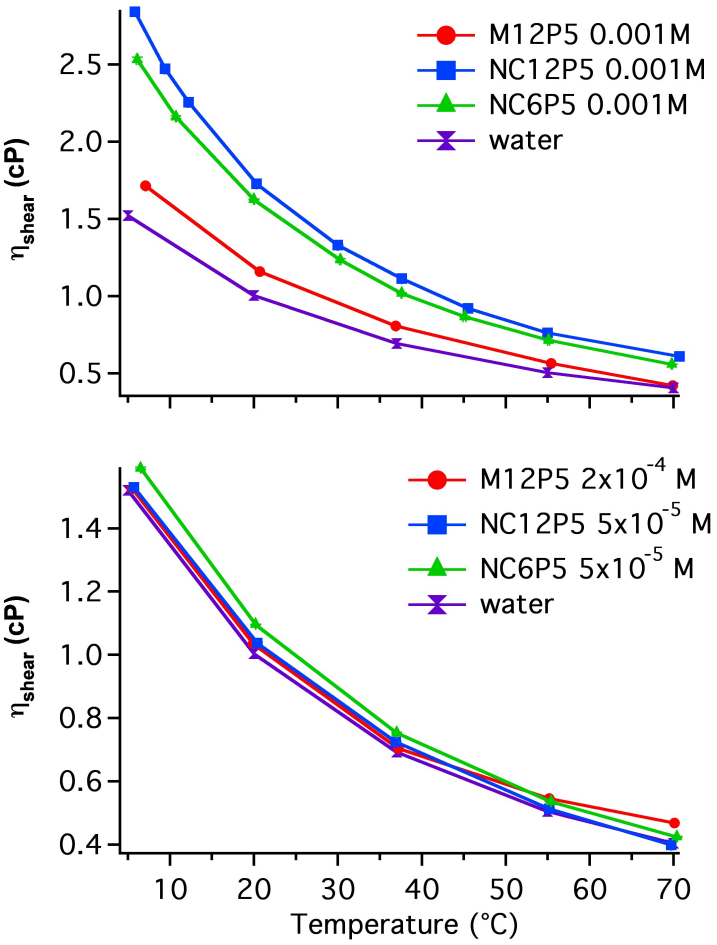

Figure B-7: Shear viscosities of M12P5, NC12P5 and NC6P5 in aqueous solutions at concnetrations of 0.001M (top) and 2x10^{-4} M (AScM) and 5x10^{-5} M ASMs (bottom).

C153 is in a more polar environment in the M12P5 micelle than in the NC12P5 aggregate. The NC6P5 unimolecular micelle aggregate core polarity, according to C153 lifetimes lays somewhere between the relatively polar M12P5 micelle core and the non-polar core of the NC12P5 aggregate. This may result because NC6P5 has 96 fewer aliphatic carbons in the core relative to the NC12P5 star-like macromolecule. The fluorescence lifetimes of C153 correlate well with steady-state fluorescence measurements corresponding to local polarity of C153.

Graphs of the fluorescence time constants versus temperature for C153 in aqueous solutions of M12P5, NC12P5, and NC6P5 are plotted here, along with plots of the

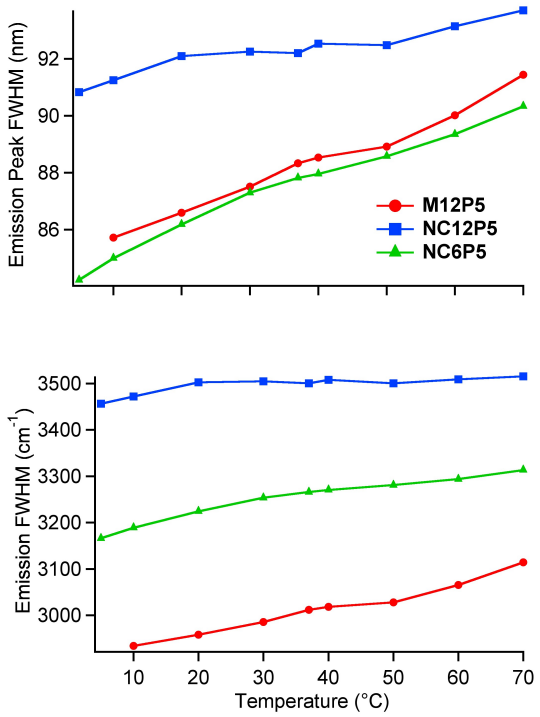

Figure B-8: Steady state emission spectral fwhm in nm (top) and in cm^{-1} of C153 in M12P5, NC12P5, and NC6P5 solutions.

component amplitudes, α_i, time constants, $\tau_{i,fluor}$, and the intensity-weighted average time constants, $\langle\tau_{fluor}\rangle$.

B:6 Predicted θ_{rot} for each unimer from SED and Van der Waals volumes.

Stokes-Einstein-Debye hydrodynamics (Equation 9) relates the fluorophore reorientation time constant to the effective volume of reorientation.[6, 11] The estimated incremental Van der Waals volumes of each polymeric unimer are used to predict the reorientation of each single unimer.[12, 11] These predicted time constants are plotted in Figure B:6 and lie between the second and third longest time constants of C153 as measured by TCSPC methods.

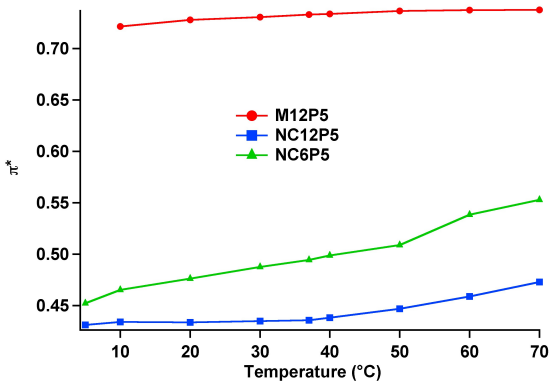

Figure B-9: Effective π^* solubility scale of C153 local environment in M12P5, NC12P5 and NC6P5 solutions.

B:7 Effective Diameters for C153 Reorientation

If the C153 were tightly associated with the M12P5, NC6P5, or NC12P5 unimers or aggregates, then each reorientation time constant might be identified with an effective volume (or diameter) for the particles. If this assumption holds true, then this leads to two and three effective volumes of reorientation for M12P5, and for NC6P5 and NC12P5 respectively. The effective diameters derived from these volumes assuming spherical dimensions are plotted in Figure 4.11 . With regard to the fastest motion of C153 measured with time-resolved fluorescence anisotropy, similar reorientation time scales are present in each of the polymer solutions.

B:8 Local Frictions

Using the equation $\langle\theta_{rot}\rangle_{polar} = (58.1 \pm 1.6)\eta^{(0.96\pm0.03)}$ where θ_{rot} is the time constant in ps and η is local viscosity in cP, we calculated the local friction of C153 in each polymeric nanocarrier.[13] We also find that the bulk viscosity of all three dilute solutions is that of pure water and the local viscosity of C153 solvent environment is on the order of ten to ten thousand times the viscosity of water .[13] These large local viscosities are due to the dielectric friction of C153 with solvent molecules surrounding the fluorophore.[13] The estimated local frictions found using $\theta_{1,rot}$, $\theta_{2,rot}$, and $\theta_{3,rot}$ are plotted in Figure B-15.

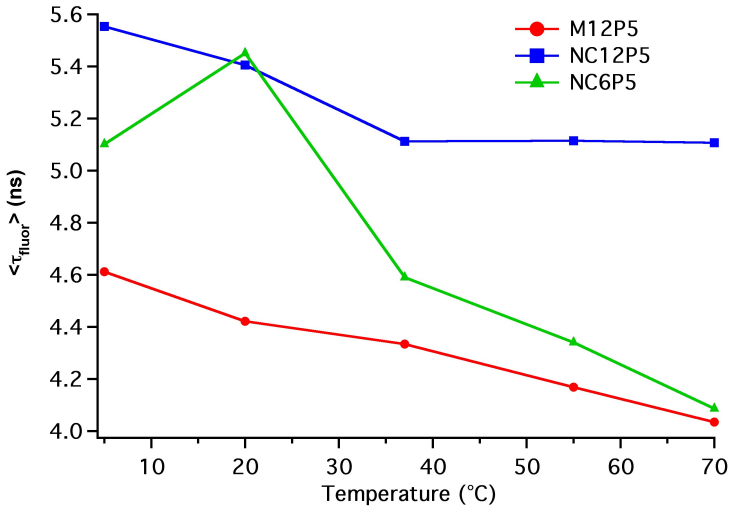

Figure B-10: Intensity-weighted average fluorescence time constants of coumarin 153 in M12P5, NC12P5, and NC6P5 solutions.

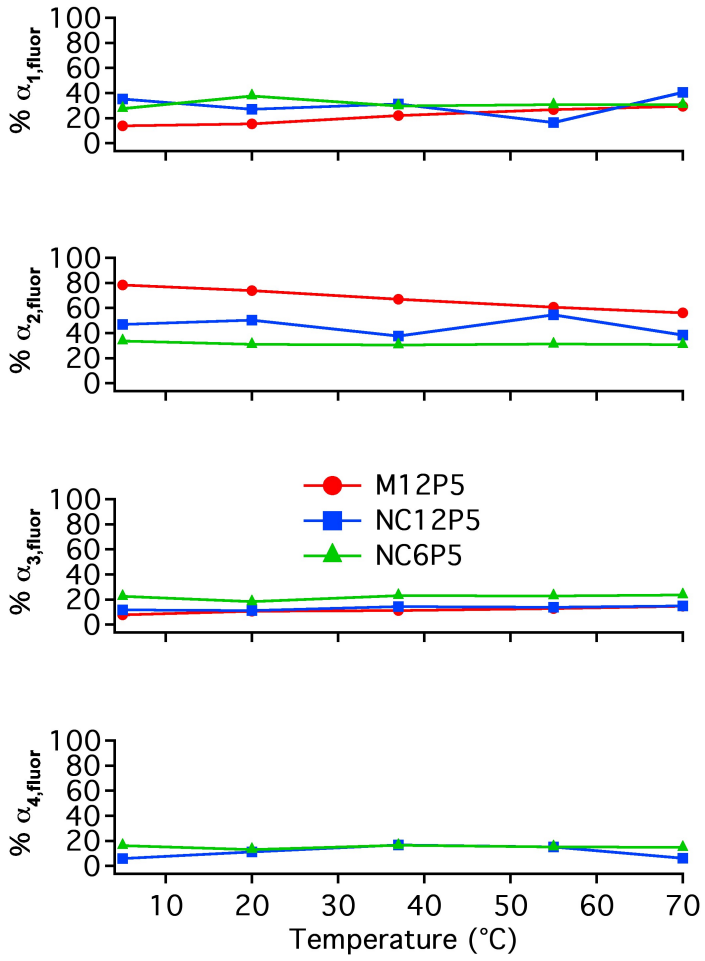

Figure B-11: Percent amplitudes ($\%\alpha_{i,fluor}$) of each component C153 fluorescence time constant, ($\tau_{i,fluor}$), in M12P5, NC12P5, and NC6P5 solutions.

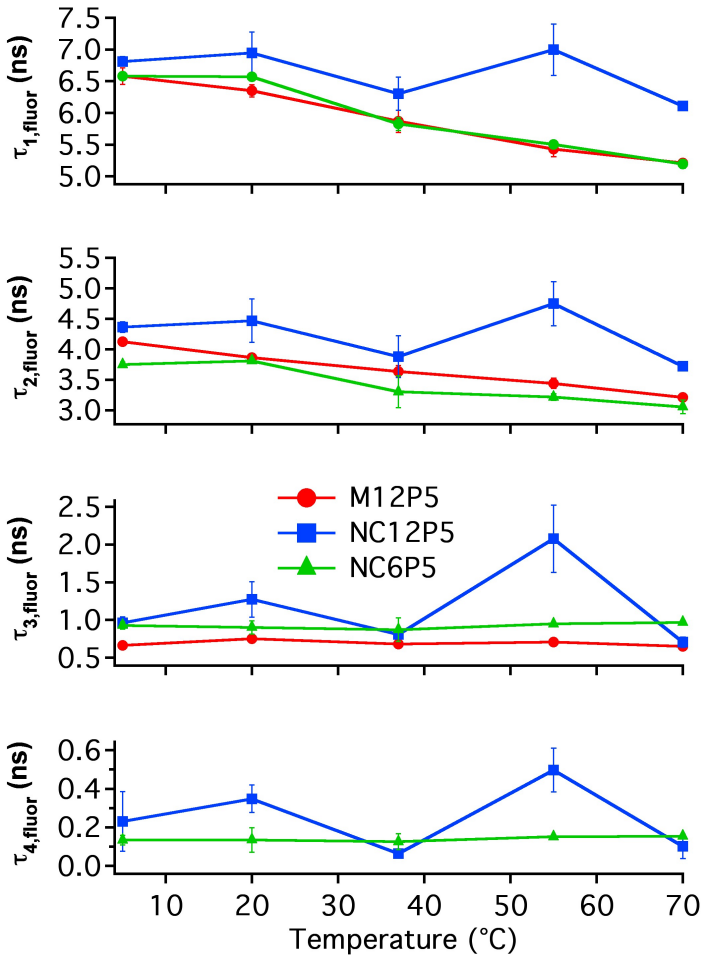

Figure B-12: Component C153 fluorescence time constants ($\tau_{i,fluor}$) in M12P5, NC12P5, and NC6P5 solutions.

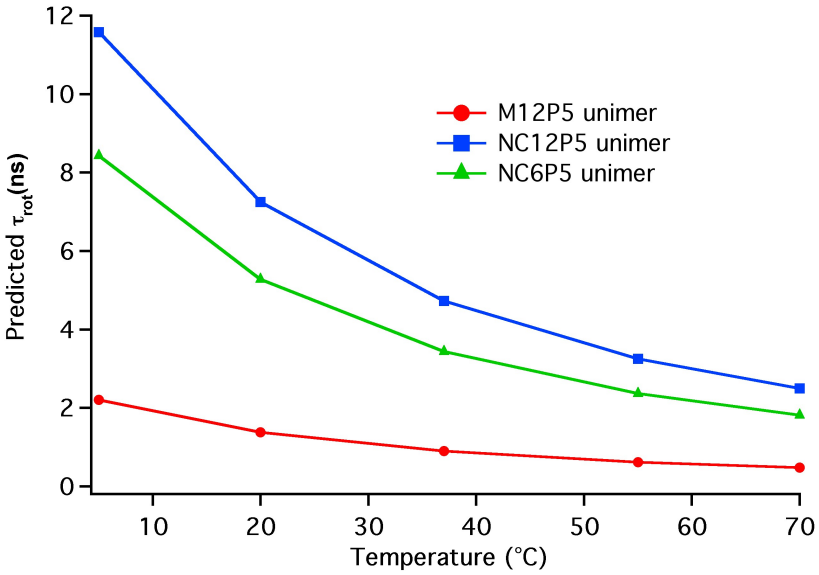

Figure B-13: Predicted θ_{rot} for each unimer from SED and Van der Waals volumes.

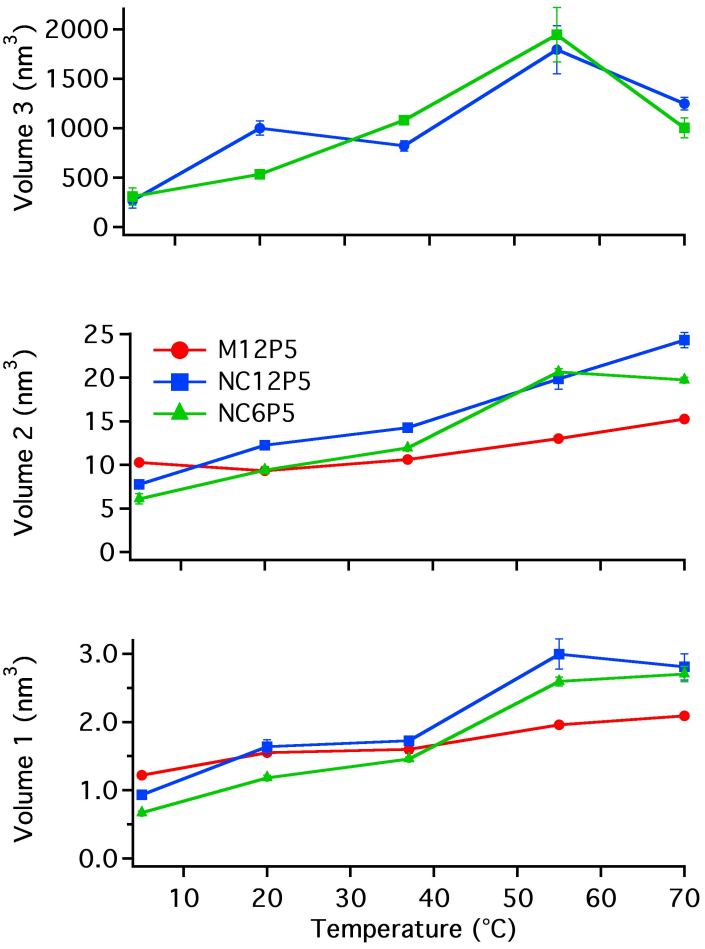

Figure B-14: Volumes of C153 Reorientation Calculated from S-E-D hydrodynamics and θ_{rot}.

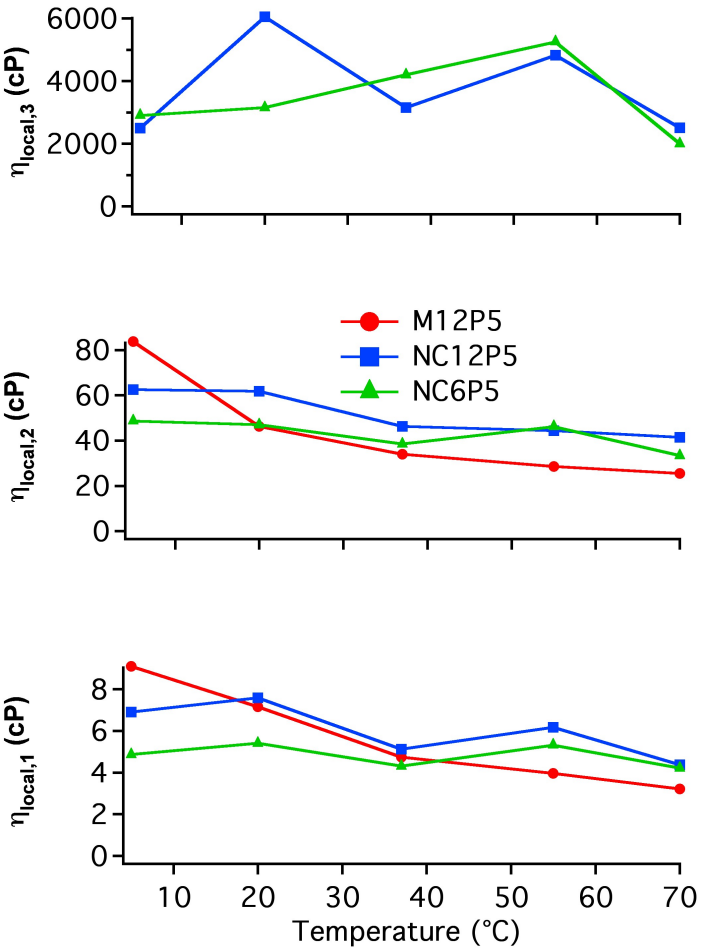

Figure B-15: Local frictions from $\theta_{rot,j}$'s.

References

[1] R. C. Weast and M. J. Astle, Eds. *CRC Handbook of Chemistry and Physics;* CRC Press, Inc., 61 ed., 1980.

[2] H. Shirota and E. W. Castner Jr.; Solvation in highly nonideal solutions: A study of aqueous 1-propanol using the coumarin 153 probe.; *Journal of Chemical Physics* **2000**, *112*, 2367–2376.

[3] D. V. Matyushov and M. D. Newton; Understanding the optical band shape: Coumarin-153 steady-state spectroscopy.; *Journal of Physical Chemistry A* **2001**, *105*, 8516–8532.

[4] M. J. Kamlet, J. L. Abboud, and R. W. Taft; The solvatochromic comparison method. 6. the π^* scale of solvent polarities.; *Journal of the American Chemical Society* **1977**, *99*, 6027–6038.

[5] M. L. Horng, J. A. Gardecki, A. Papazyan, and M. Maroncelli; Subpicosecond measurements of polar solvation dynamics: Coumarin 153 revisited.; *Journal of Physical Chemistry* **1995**, *99*, 17311–37.

[6] J. R. Lakowicz *Principles of Fluorescence Spectroscopy;* Kluwer Academic/ Plenum Publishers, 2nd ed., 1999.

[7] B. Valeur *Molecular Fluorescence: Principles and Applications;* Wiley-VCH, 2002.

[8] G. Jones II, W. R. Jackson, C. Y. Choi, and W. R. Bergmark; Solvent effects on emission yield and lifetime for coumarin laser dyes. requirements for a rotatory decay mechanism.; *Journal of Physical Chemistry* **1985**, *89*, 294–300.

[9] L. Reynolds *et al.;* Dipole solvation in nondipolar solvents: Experimental studies of reorganization energies and solvation dynamics.; *Journal of Physical Chemistry* **1996**, *100*, 10337–10354.

[10] C. D. Grant *et al.;* Fluorescence probing of interior, interfacial, and exterior regions in solution aggregates of poly(ethylene oxide)- poly(propylene oxide)-poly(ethylene oxide) triblock copolymers.; *Langmuir* **2005**, *21*, 1745–1752.

[11] J. T. Edward; Molecular volumes and the stokes-einstein equation; *Journal of Chemical Education* **1970**, *47*(4), 261–270.

[12] A. Bondi; van der waals volumes and radii; *Journal of Physical Chemistry* **1964**, *68*, 441–51.

[13] M.-L. Horng, J. A. Gardecki, and M. Maroncelli; Rotational dynamics of coumarin 153: Time-dependent friction, dielectric friction, and other nonhydrodynamic effects.; *Journal of Physical Chemistry A* **1997**, *101*, 1030–1047.

Appendix C

Fluorescence Probing of Aqueous Copolymer Solutions

C:1 Solubilities and Molecular Volumes of Coumarins

The solublity of coumarin dyes can be calculated using the clogP or calculated water/octanol partition coefficient. A high clogP value denotes that the molecule is water insoluble while a value closer to zero denotes water-solubility.[1]

Table C-1: Calculated logP (clog) and molecular volumes (V_m) of seven coumarin molecules.[2, 3, 1, 4, 5]

Coumarin	V_m (Å^3)	clogP
C314T	355.9	5.77
C153	245.5	4.08
C102	232.9	3.67
C152	209.9	2.99
C337	226.1	2.64
C151	174.8	1.94
C343$^-$	239.7	-1.08

C:2 Spectral Lineshape Analysis

The lineshape of the fluorescence spectra of coumarins is indicative of the distribution of local environments in which a coumarin is solubilized.[3] Populations of coumarin probes in multiple local environments within a micelle solution will shift to either more hydrophobic polymer regions or to more water-rich regions. By looking at the fwhm of the emission or excitation spectrum, we can make some conclusions about the distributions of coumarin populations and whether the distribution in a particular environment is becoming broader or more narrow upon micellization of F88.[3] Figure C-1 gives the temperature dependence of the fwhm of the emission and excitation spectrum for each coumarin fluorophore. The broadening of the emission spectrum of all of the coumarins

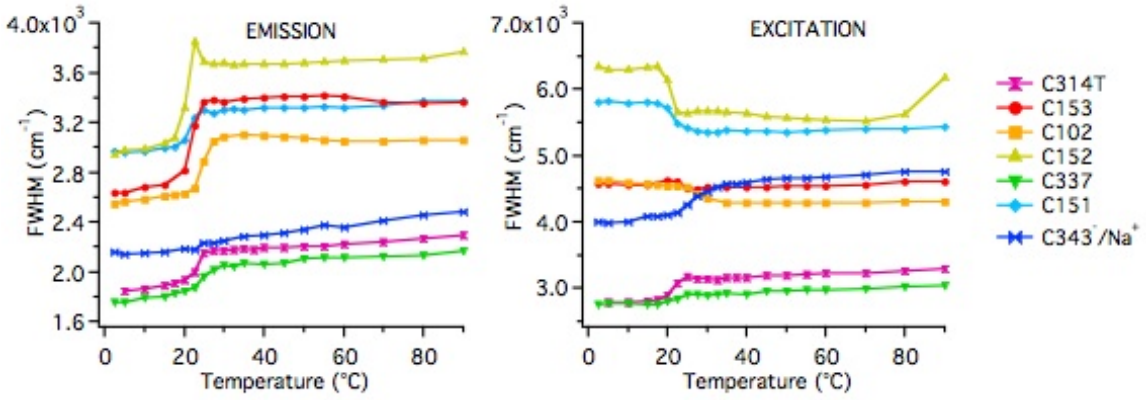

Figure C-1: Temperature dependence of emission (left) and excitation (right) spectral fwhm of 7 coumarins in 25 w/v%Pluronic F88 solution displaying changes in population distribution upon F88 aggregation.

is indicative that all of the fluorophores are located in multiple environments and the number of local environments is increasing upon F88 aggregation. The emission spectra of C153, C102, and C152 broaden the most at the micellization temperature displaying that these three coumarins are sampling both core, corona and interfacial regions of F88 micelles in solution.

C:3 Spectral Energies From Fluorescence

In Chapter 5, the emission and excitation spectral peaks were plotted at approximately 20 temperatures in the range of 2.5 to 90 °C. These values the spectra of all seven coumarins in aqueous solution of 25 w/v% Pluronic F88 are listed in Tables C-2, C-3, C-4,C-5, C-6, C-7, and C-8. The spectral energies are presented in both wavelength (nm) and reduced frequency (cm^{-1}) units.

Table C-2: Temperature dependence of emission and excitation peak energies of C314T from fluorescence spectra in aqueous solution of 25 w/v% Pluronic F88.

Temp (°C)	λ_{ex} (nm)	$\tilde{\nu}_{ex}$ (cm^{-1})	λ_{em} (nm)	$\tilde{\nu}_{em}$ (cm^{-1})
5.0	449	22282	487	20516
10.0	448	22300	487	20523
15.0	448	22329	487	20531
17.5	447	22354	487	20539
20.0	446	22404	487	20552
22.5	442	22632	485	20613
25.0	435	22973	481	20777
27.5	434	23064	480	20851
30.0	433	23094	479	20857
32.5	433	23117	479	20866
35.0	432	23130	479	20865
37.5	432	23146	479	20868
40.0	432	23153	479	20866
45.0	432	23171	479	20872
50.0	431	23180	479	20872
55.0	431	23198	479	20870
60.0	431	23206	479	20868
70.0	430	23229	479	20872
80.0	430	23249	479	20883
90.0	430	23267	479	20889

C:4 Polarity of C153 Local Environment

The steady-state emission peak frequency, ν_{em}, can be assigned to a value on the π^* empirical polarity scale using equations derived from experiments by Horng, et.al. Equation C-1 uses the peak emission frequency of C153 (in 10^3 cm^{-1}), the π^* value of the C153 local environment can be estimated. From Equation C-2, using the peak excitation frequency (in 10^3 cm^{-1}), the C153 local environment can also be assigned to a value on the π^* empirical polarity scale..[6, 7, 8, 9] The calculated π^* values are listed in Table C-9 for temperatures from 2.5 to 90 °C.

$$\nu_{em} = 21.217 - 3.505\pi^* \tag{C-1}$$

$$\nu_{abs} = 25.774 - 2.066\pi^* \tag{C-2}$$

A transition in the local polarity environment of C153 occurs at 22.5 °C, the same

Table C-3: Temperature dependence of emission and excitation peak energies of C153 from fluorescence spectra in aqueous solution of 25 w/v% Pluronic F88.

Temp (°C)	λ_{ex} (nm)	$\tilde{\nu}_{ex}$ (cm^{-1})	λ_{em} (nm)	$\tilde{\nu}_{em}$ (cm^{-1})
2.5	437	22871	544	18379
5.0	437	22906	544	18383
10.0	436	22926	543	18406
15.0	435	22974	541	18493
20.0	432	23131	539	18550
22.5	426	23485	531	18815
25.0	421	23763	522	19155
27.5	420	23821	521	19204
30.0	420	23837	521	19202
35.0	419	23881	521	19192
40.0	418	23905	521	19179
45.0	418	23923	522	19173
50.0	418	23930	522	19160
55.0	417	23953	523	19135
60.0	417	23965	523	19119
70.0	417	23972	524	19097
80.0	417	24000	524	19092
90.0	417	24007	524	19080

Table C-4: Temperature dependence of emission and excitation peak energies of C102 from fluorescence spectra in aqueous solution of 25 w/v% Pluronic F88.

Temp (°C)	λ_{ex} (nm)	$\tilde{\nu}_{ex}$ (cm^{-1})	λ_{em} (nm)	$\tilde{\nu}_{em}$ (cm^{-1})
2.5	400	25024	479	20887
5.0	399	25040	479	20897
10.0	399	25072	478	20917
15.0	398	25107	478	20935
17.5	399	25129	477	20944
20.0	397	25169	477	20963
22.5	396	25270	476	21004
25.0	390	25665	472	21188
27.5	386	25893	468	21377
30.0	385	25977	467	21428
35.0	384	26051	466	21465
40.0	386	26076	466	21461
45.0	383	26097	466	21453
50.0	383	26108	466	21448
55.0	383	26119	466	21441
60.0	383	26127	467	21431
70.0	383	26142	467	21431
80.0	382	26156	466	21437
90.0	382	26178	466	21451

Table C-5: Temperature dependence of emission and excitation peak energies of C152 from fluorescence spectra in aqueous solution of 25 w/v% Pluronic F88.

Temp (°C)	λ_{ex} (nm)	$\tilde{\nu}_{ex}$ (cm^{-1})	λ_{em} (nm)	$\tilde{\nu}_{em}$ (cm^{-1})
2.5	399	25067	524	19080
5.0	399	25052	524	19082
10.0	398	25138	523	19104
15.0	396	25231	523	19137
17.5	395	25318	522	19167
20.0	390	25627	518	19301
22.5	383	26142	504	19822
25.0	380	26299	492	20334
27.5	380	26334	490	20391
30.0	379	26359	490	20414
32.5	378	26454	490	20431
35.0	377	26500	489	20447
40.0	377	26516	489	20447
45.0	377	26530	488	20502
50.0	377	26541	488	20517
55.0	376	26560	487	20529
60.0	376	26562	487	20546
70.0	376	26577	487	20550
80.0	376	26605	486	20565
90.0	370	27042	488	20490

Table C-6: Temperature dependence of emission and excitation peak energies of C337 from fluorescence spectra in aqueous solution of 25 w/v% Pluronic F88.

Temp (°C)	λ_{ex} (nm)	$\tilde{\nu}_{ex}$ (cm^{-1})	λ_{em} (nm)	$\tilde{\nu}_{em}$ (cm^{-1})
2.5	456	21913	497	20107
5.0	457	21894	497	20107
10.0	456	21925	497	20108
15.0	456	21929	497	20111
17.5	456	21943	497	20115
20.0	455	21963	497	20124
22.5	453	22055	497	20156
25.0	449	22263	496	20233
27.5	448	22344	494	20283
30.0	447	22389	493	20295
32.5	446	22420	493	20301
35.0	446	22440	493	20304
40.0	445	22451	493	20304
45.0	445	22466	493	20294
50.0	445	22469	493	20298
55.0	445	22479	493	20290
60.0	445	22491	493	20281
70.0	445	22489	493	20284
80.0	445	22495	493	20266
90.0	444	22514	492	20307

Table C-7: Temperature dependence of emission and excitation peak energies of C151 from fluorescence spectra in aqueous solution of 25 w/v% Pluronic F88.

Temp (°C)	λ_{ex} (nm)	$\tilde{\nu}_{ex}$ (cm^{-1})	λ_{em} (nm)	$\tilde{\nu}_{em}$ (cm^{-1})
2.5	373	26807	490	20419
5.0	373	26802	489	20436
10.0	374	26764	489	20439
15.0	374	26746	489	20454
17.5	374	26742	489	20452
20.0	375	26691	488	20504
22.5	376	26607	482	20737
25.0	376	26594	478	20927
27.5	376	26592	477	20969
30.0	376	26594	477	20981
32.5	376	26606	477	20974
35.0	376	26607	476	20986
40.0	375	26643	477	20963
45.0	375	26670	477	20954
50.0	375	26678	478	20929
55.0	375	26694	478	20917
60.0	374	26716	478	20911
70.0	374	26742	478	20914
80.0	373	26774	479	20889
90.0	373	26785	478	20918

Table C-8: Temperature dependence of emission and excitation peak energies of $C343^{-}/Na^{+}$ from fluorescence spectra in aqueous solution of 25 w/v% Pluronic F88.

Temp (°C)	λ_{ex} (nm)	$\tilde{\nu}_{ex}$ (cm^{-1})	λ_{em} (nm)	$\tilde{\nu}_{em}$ (cm^{-1})
2.5	425	23539	480	20845
5.0	425	23548	480	20839
10.0	423	23630	480	20842
15.0	422	23683	480	20845
20.0	422	23724	480	20851
22.5	421	23743	480	20851
25.0	421	23769	479	20856
27.5	420	23813	480	20851
30.0	419	23846	479	20862
35.0	418	23920	480	20853
40.0	417	23959	480	20853
45.0	417	23993	480	20852
50.0	416	24032	480	20849
55.0	416	24062	480	20846
60.0	415	24091	480	20846
70.0	414	24144	480	20846
80.0	413	24215	480	20845
90.0	412	24282	480	20849

temperature at which F88 forms micelles in aqueous solution. C153 fluorescence excitation and emission are both reporting on the local solvent polarity of the PPO cores of aqueous F88 micelles

Table C-9: Temperature dependence of calculated π^* values of C153 local environment from steady-state emission and excitation peak frequencies in aqueous solutions of Pluronic F88.[6]

Temperature (°C)	π^* (emission)	π^* (excitation)
2.5	0.809708	1.40501
5.0	0.808551	1.38827
10.0	0.80189	1.37861
15.0	0.777223	1.35541
20.0	0.760878	1.27928
22.5	0.685298	1.10811
25.0	0.58844	0.973589
27.5	0.574271	0.945369
30.0	0.574797	0.937399
35.0	0.577847	0.916458
40.0	0.581417	0.904853
45.0	0.583201	0.895996
50.0	0.586764	0.892394
55.0	0.593877	0.881573
60.0	0.598574	0.875461
70.0	0.604929	0.872124
80.0	0.606385	0.858478
90.0	0.609815	0.855411

References

[1] clogp calculator www.daylight.com.

[2] C. D. Grant, K. E. Steege, M. R. Bunagan, and E. W. Castner Jr.; Microviscosity in multiple regions of complex aqueous solutions of poly(ethylene oxide)-poly(propylene oxide)-poly(ethylene oxide).; *Journal of Physical Chemistry B* **2005**, *109*, 22273–22284.

[3] C. D. Grant *et al.;* Fluorescence probing of interior, interfacial, and exterior regions in solution aggregates of poly(ethylene oxide)- poly(propylene oxide)-poly(ethylene oxide) triblock copolymers.; *Langmuir* **2005**, *21*, 1745–1752.

[4] J. T. Edward; Molecular volumes and the stokes-einstein equation; *Journal of Chemical Education* **1970**, *47*(4), 261–270.

[5] A. Bondi; van der waals volumes and radii; *Journal of Physical Chemistry* **1964**, *68*, 441–51.

[6] M. L. Horng, J. A. Gardecki, A. Papazyan, and M. Maroncelli; Subpicosecond measurements of polar solvation dynamics: Coumarin 153 revisited.; *Journal of Physical Chemistry* **1995**, *99*, 17311–37.

[7] K. E. Steege, J. Wang, K. E. Uhrich, and E. W. Castner Jr.; Local polarity and microviscosity in the hydrophobic cores of amphiphilic star-like and scorpion-like macromolecules; *Macromolecules* **2007**, *40*, 3739–3748.

[8] C. Laurence *et al.;* The empirical treatment of solvent-solute interactions: 15 years of π^*; *Journal of Physical Chemistry* **1994**, *98*, 5807–5816.

[9] M. J. Kamlet, J. L. Abboud, and R. W. Taft; The solvatochromic comparison method. 6. the π^* scale of solvent polarities.; *Journal of the American Chemical Society* **1977**, *99*, 6027–6038.

Curriculum Vita

Karen E. Steege

Education

2008 Ph. D. in Chemistry and Chemical Biology, Rutgers, The State University of New Jersey

2003 B. S. in Chemistry from the University of Rhode Island, Kingston, RI

1998 Graduated from Mount Olive High School, Flanders, NJ

Employment

2007- Fluorescence Applications Scientist, Horiba Jobin Yvon, Edison, NJ

2006-7 Graduate Assistant, Department of Chemistry and Chemical Biology, Rutgers, The State University of New Jersey, GAANN Fellowship

2006 Teaching assistant, Department of Chemistry and Chemical Biology, Rutgers, The State University of New Jersey, Physical Chemistry Laboratory

2005 Summer Intern, Pharmaceutical Research Institute, Bristol-Myers Squibb Company, New Brunswick, NJ

2004-6 Graduate Trainee, Department of Chemistry and Chemical Biology and Biomedical Engineering, Rutgers, The State University of New Jersey, NSF-IGERT

2002-4 Teaching assistant, Department of Chemistry and Chemical Biology, Rutgers, The State University of New Jersey, General Chemistry Laboratory

Publications

2008 **Steege, Karen E.**, Kodali, Goutham; Lee, Benjamin J.; Frenkel, Yulia Volovik; Stanley, Robert J.; Arnold, Eddy; Castner, Edward W., Jr. "Spectroscopy, Solvatochromism, and Structure of Rilpivirine, a Potent Non-Nucleoside Reverse Transcriptase Inhibitor." *submitted* (2008)

2007 **Steege, Karen E.**; Wang, Jinzhong; Uhrich, Kathryn E.; Castner, Edward W., Jr. "Local Polarity and Microviscosity in the Hydrophobic Cores of Amphiphilic Star-like and Scorpion-like Macromolecules." *Macromolecules.* (2007) 40, 3739-3748.

2005 Grant, Christian D.; **Steege, Karen E.**; Bunagan, Michelle R.; Edward W. Castner, Jr. "Microviscosity in Multiple Regions of Complex Aqueous Solutions of Poly(ethylene oxide)-Poly(propylene oxide)-Poly(ethylene oxide)." *Journal of Physical Chemistry B.* (2005) 109, 22273-22284.

2005 Grant, Christian D.; DeRitter, Michelle R.; **Steege, Karen E.**; Fadeeva, Tatiana A.; Castner, Edward W., Jr. "Fluorescence Probing of Interior, Interfacial, and Exterior Regions in Solution Aggregates of Poly(ethylene oxide)- Poly(propylene oxide)-Poly(ethylene oxide) Triblock Copolymers." *Langmuir.* (2005) 12, 1745-1752.